Towards High Throughput Single Crystal Neutron Diffraction of Hydrogen Bonded Molecular Complexes

Jones, Andrew

Award date:
2012

Awarding institution:
University of Bath

Towards High Throughput Single Crystal Neutron Diffraction of Hydrogen Bonded Molecular Complexes

Andrew Owen Fletcher Jones

A thesis submitted for the degree of Doctor of Philosophy

University of Bath

Department of Chemistry

September 2012

Supervisor: Prof. Chick Wilson

Table of Contents

List of Figures v
List of Tables xvi
Acknowledgements xx
Abstract xxi
List of Abbreviations xxii

1. Introduction 1
1.1 Preamble 1
1.2 Hydrogen Bonding 1
1.2.1 Strong Hydrogen Bonds 4
1.2.2 Moderate Hydrogen Bonds 5
1.2.3 Weak Hydrogen Bonds 5
1.2.4 Bifurcated Hydrogen Bonds 6
1.3 Other Intermolecular Interactions 7
1.3.1 Halogen Bonding 7
1.3.2 π Interactions 8
1.4 Crystal Engineering 8
1.5 Polymorphism 12
1.6 Proton Transfer 12
1.7 Proton Migration 13
1.8 Proton Disorder 18
1.9 Urea and its Derivatives 21
1.10 DMAN 24

2. Theory 26
2.1 Crystallography 26
2.1.1 The Lattice and Unit Cell 26
2.2 Diffraction 27
2.2.1 History 27
2.2.2 Diffraction of X-rays, Neutrons and Electrons 28
2.2.3 The Laue Equations 29
2.2.4 Bragg's Law 30
2.2.5 Reciprocal Space and the Ewald Sphere 30
2.2.6 Fourier Synthesis 32
2.2.7 Structure Solution 33
2.2.7.1 The Phase Problem 33
2.2.7.2 Patterson Method 34
2.2.7.3 Direct Methods 34
2.2.7.4 Charge Flipping[130,131] 36
2.2.8 Structure Refinement 36
2.2.9 Fourier Difference Maps 37
2.3 Neutron Diffraction 38
2.4 Computational Chemistry 40
2.4.1 Molecular Mechanics 40
2.4.2 Quantum Mechanical Calculations 41

2.4.1.1 The Born-Oppenheimer Approximation 41
2.4.1.2 Hartree-Fock Theory 42
2.4.1.3 Polarisation and Diffuse Functions 42
2.4.2 Density Functional Theory 43
2.4.2.1 Plane-waves and Pseudopotentials 44
2.4.3 Computational Simulations 45
2.4.3.1 Geometry Optimisation 45
2.4.3.2 Molecular Dynamics 46
2.5 Solid-state Vibrations 47

3. Techniques and Instrumentation 48
3.1 Sample Preparation 48
3.1.1 Crystallisation 48
3.1.2 Sample Characterisation and Screening 51
3.2 Single Crystal X-ray Diffraction 51
3.2.1 Unit Cell Determination by Indexing of Peaks 52
3.2.2 Data Collection 53
3.2.3 Structure Solution and Refinement 53
3.2.4 Variable Temperature Measurements 54
3.3 X-ray Powder Diffraction 54
3.4 Single Crystal Neutron Diffraction 56
3.4.1 Neutron Sources 57
3.4.1.1 Spallation Sources 57
3.4.1.3 The ILL Reactor Source 59
3.4.2 SXD at ISIS 60
3.4.3 VIVALDI at ILL 61
3.4.3.1 Koala at the Bragg Institute 64
3.5 Data Reduction and Processing on VIVALDI 64
3.5.1 Sample Orientation and Indexing – LAUEGEN 66
3.5.2 Integration – ARGONNE_BOXES 68
3.5.3 Absorption Correction 69
3.5.4 Wavelength Normalisation – LAUENORM / LAUE4 69
3.5.5 Refinement 70
3.6 Computational Methods 70
3.6.1 CP2K and QUICKSTEP[165] 71
3.6.2 Methodology 71

4. Proton migration 73
4.1 Experimental 74
4.1.1 Crystallography 74
4.1.2 Computational 76
4.2 *N,N*-Dimethylurea Oxalic Acid (2:1)[167] 82
4.2.1 Crystallographic Data 82
4.2.2 Computational Data 89
4.3 *N,N'*-Dimethylurea Oxalic Acid (2:1)[167] 90
4.3.1 Crystallographic Data 90
4.3.2 Temperature Dependent Structural Effects 94

4.3.3 Computational Data....95
4.4 *N*-Methylurea Chloranilic Acid (2:1)....97
4.4.1 Crystallographic Data....97
4.4.2 Computational Data....100
4.5 *N*-Methylurea Bromanilic Acid (2:1)....102
4.6 Urea Bromanilic Acid (2:1)....105
4.7 Understanding and Designing Systems Which Display Proton Migration....109
4.8 Conclusions....113

5. Molecular Complexes of Dicarboxylic Acids with Urea and Methyl Substituted Ureas....116
5.1 Experimental....117
5.2 Complexes of Urea with Succinic and Fumaric Acid....127
5.2.1 Urea Succinic Acid (2:1) (US)....127
5.2.2 Urea Fumaric Acid (2:1) (UF)....128
5.3 Complexes of *N*-Methylurea with Succinic, Fumaric and Oxalic acid....130
5.3.1 *N*-Methylurea Succinic Acid (2:1) (MUS)....130
5.3.2 *N*-Methylurea Fumaric Acid (2:1) (MUF)....132
5.3.3 *N*-Methylurea Oxalic Acid (2:1) (MOX)....134
5.4 Complexes of *N,N*-Dimethylurea with Succinic and Fumaric Acid....135
5.4.1 *N*,*N*-Dimethylurea Succinic Acid (2:1) (DMUS)....135
5.4.2 *N*,*N*-Dimethylurea Fumaric Acid (2:1) (DMUF)....137
5.5 Structural Similarities....138
5.6 Short Strong Hydrogen Bonds in the Dicarboxylic Acid Complexes....142
5.7 Temperature Dependent Effects of the Crystal Packing....149
5.8 Conclusions....152

6. Proton Disorder....155
6.1 Experimental....158
6.2 2:2 Complex of 3,5-Dinitrobenzoic Acid and 4-Dimethylaminobenzoic Acid....163
6.3 3,5-Dinitrobenzoic Acid ($P2_1/c$ Polymorph)....171
6.4 3,5-Dinitrobenzoic Acid ($C2/c$ Polymorph)....175
6.5 Disorder in Benzoic Acid Dimers....181
6.6 Evolution of the 3,5-Dinitrobenzoic Acid Unit Cells with Temperature....185
6.7 Conclusions....186

7. Neutron Studies of Complexes of the Proton Sponge DMAN....189
7.1 Experimental....192
7.2 Molecular Complexes of DMAN and Halobenzoic Acids....194
7.2.1 DMAN 2-Fluorobenzoic Acid (1:2)....194
7.2.2 DMAN 2-Iodobenzoic Acid (1:2)....196
7.2.3 DMAN 4-Iodobenzoic Acid (1:2)....199
7.3 DMAN Chloranilic Acid (1:1)....201
7.4 DMAN 2,3-Dihydroxybenzoic Acid (1:1)....203
7.5 Hydrogen Atom Behaviour in DMAN-Acid Complexes....205
7.5.1 Over What Range is a Weak Hydrogen Bond Significant?....205
7.5.2 The Position of the Proton in the N-H···N Hydrogen Bond of $DMANH^+$....208

7.5.3 The Position of the Proton in the Charge-Assisted Hydrogen Bonds 212
7.6 Conclusions.....215

8. Other Complexes of Urea and Substituted Ureas with Organic Acids ..217
8.1 Experimental 218
8.2 2:1 Molecular Complex of Urea and Picolinic Acid Monohydrate 224
8.3 2:1 Molecular Complex of Urea and 4-Hydroxybenzoic Acid 226
8.4 7:4 Molecular Complex of Urea and Bromanilic Acid Monohydrate.....229
8.5 1:1 Molecular Complex of *N*-Methylurea and Picolinic Acid 234
8.6 2:1 Molecular Complex of *N*-Methylurea and 2,4-Dihydroxybenzoic Acid 236
8.7 1:1 Molecular Complex of *N*,*N*-Dimethylurea and Chloranilic Acid Monohydrate 239
8.8 2:1 Molecular Complex of *N*,*N*-Dimethylurea and Bromanilic Acid.....241
8.9 Conclusions.....244

9. Conclusions and Future Work 245
9.1 Strong Hydrogen Bonds 245
9.2 Moderate Hydrogen Bonds.....250
9.3 Weak Hydrogen Bonds 253
9.4 Crystal Engineering of Urea-Acid Complexes.....256
9.5 Variable Temperature Measurements 257
9.6 Complementarity of X-ray and Neutron Diffraction.....257
9.7 High Throughput Neutron Diffraction 258
9.8 Future Work 259

10. References.....261

List of Figures

Figure 1.1 Hydrogen bond potential energy surfaces showing: a single broad potential (left), an asymmetric double-well potential (centre) and a symmetric double-well potential (right).[6] 3

Figure 1.2 The strong intramolecular hydrogen bond in potassium hydrogen maleate.[12] ...4

Figure 1.3 An example of a DHAA bifurcated hydrogen bond (left), a DDHHA bifurcated hydrogen bond (centre) and a generalised schematic showing a three-centred hydrogen bond (right) with labelled bond distances (R_i) and angles (α_i).[2] 6

Figure 1.4 Examples of the three conformations of π···π stacking: sandwich conformation (a), T-shaped conformation (b) and parallel-displaced conformation (c); and a cation···π interaction (d). 8

Figure 1.5 Examples of hydrogen bonded architectures, from top to bottom: a 0-D dimer motif in benzoic acid,[39] a 1-D chain motif in a 1:1 complex of 4,4'-biphenol and 4,4'-bipyridine,[40] a 2-D sheet motif in the 2:1 complex of isonicotinamide and fumaric acid[41] and a 3-D motif in a 1:1 complex of carbamazepine and adamantane-1,3,5,7-tetracarboxylic acid.[42] 10

Figure 1.6 The O-H···N hydrogen bond in the complex of pentachlorophenol and 4-methylpyridine showing the hydrogen atom migrating across the hydrogen bond as the temperature is varied.[60] 14

Figure 1.7 The evolution of the short, strong hydrogen bond with temperature in the complex of urea and phosphoric acid.[62] 15

Figure 1.8 The PES of the short, strong hydrogen bond in urea phosphoric acid (black curve). The lower blue curve shows the ground state wavefunction of the hydrogen atom (n = 0) while the upper red curve shows the first excited state (n = 1).[69] 17

Figure 1.9 The 4-dimethylaminobenzoic acid dimer, a system known to show proton disorder, showing the inversion centre in the dimer (black dot). 19

Figure 1.10 A disordered dimer of benzoic acid at 175 K.[77] 20

Figure 1.11 From left to right: urea, N-methylurea, N,N-dimethylurea and N,N'-dimethylurea. 21

Figure 1.12 The structure of urea showing the tape motif which involves bifurcated hydrogen bonds.[110] 22

Figure 1.13 The structures of N-methylurea (top),[113] N,N-dimethylurea (centre)[114] and the Cc polymorph of N,N'-dimethylurea (bottom).[115] 23

Figure 1.14 Unprotonated (left) and protonated (right) DMAN molecules. 24

Figure 2.1 Diffraction from a one-dimensional array of atoms. 29

Figure 2.2 Diagram of Bragg's law and the difference in path length between two diffracted beams. 30

Figure 2.3 Ewald sphere showing diffraction from parallel planes. 31

Figure 2.4 Ewald sphere for Laue diffraction: all reciprocal lattice points located between the λ_{min} and λ_{max} spheres will be collected in one image. 31

Figure 2.5 X-ray scattering factors (dotted line) compared with those for neutrons (top) and an expanded view of neutron scattering factors (bottom). 39

Figure 2.6 The improved hydrogen molecular orbital model when the higher angular momentum 2p orbital is included. 43

Figure 3.1 Photographs of the temperature controlled hotplates (left) and the ReactArray Microvate (right) used in sample preparation. 50

Figure 3.2 Photographs of the Rigaku R-AXIS / RAPID diffractometer. 52

Figure 3.3 A photograph of the D8 powder diffractometer (left) and a typical powder diffraction pattern (right). 56

Figure 3.4 Schematic layout of ISIS. SXD is located at target station 1.[144] 58

Figure 3.5 Diagram of the ILL reactor core showing: 1. Safety rod; 2. Neutron guide pool; 3. Reflector tank; 4. Double neutron guide; 5. Vertical cold source; 6. Reactor core; 7. Horizontal cold source; 8. Control rod.[148] 59

Figure 3.6 SXD viewed from above (left) and diagram of the detector layout with the direction of the neutron beam shown (right).[143] 61

Figure 3.7 VIVALDI with orange cryostat mounted (left) and schematic diagram of the instrument (right).[147] 62

Figure 3.8 Plan view of VIVALDI from neutron guide to beam stop showing the cylindrical detector.[148] 62

Figure 3.9 Koala at the Bragg Institute.[145] 64

Figure 3.10 Flow diagram of the data processing and reduction steps for VIVALDI. 65

Figure 3.11 The LAUEGEN interface. 66

Figure 3.12 Typical diffraction pattern collected on VIVALDI showing the spots used to determine the orientation matrix circled and in red. The transmitted beam exits the detector through the hole in the middle. 67

Figure 3.13 VIVALDI diffraction pattern showing the areas over which reflections are integrated in the form of three ellipses; dark ellipses correspond to strong reflections and white ellipses to weaker ones. The two white circles mask off a scratch on the image plate. 68

Figure 4.1 Clockwise from top left: molecular structures of urea, N-methylurea, N,N-dimethylurea, N,N'-dimethylurea, chloranilic acid, bromanilic acid and oxalic acid. 74

Figure 4.2 Hydrogen bonded three molecule "DMU-A-DMU" units in the low- (top at 100 K) and high- (bottom at 200 K) temperature phases of the 2:1 complex of N,N-dimethylurea and oxalic acid, as refined from the X-ray data. 82

Figure 4.3 Three molecule "DMU-A-DMU" hydrogen bonded units assembled into a hydrogen bonded chain in the low temperature phase of the N,N-dimethylurea oxalic acid molecular complex (top) and layers of these units viewed along the b-axis (bottom), both from the 100 K X-ray data. 83

Figure 4.4 Variable temperature X-ray powder diffraction patterns showing a significant peak shift in the (1,1,-1) refection of the high temperature phase from its position at low temperature (indexed as (2,1,-1) reflecting the doubling of the a-axis) through the phase transition. To allow the shift to be seen more easily, the pink and green profiles represent the calculated patterns from single crystal diffraction data for the low and high temperature phases, respectively. The peak shift occurs between 120 and 130 K. 84

Figure 4.5 Three molecule "DMU-A-DMU" units in the low (left, at 100K) and high (right, at 200K) temperature phases of the N,N-dimethylurea oxalic acid molecular complex from the X-ray data. In the high temperature phase the unit is flatter and more symmetric. 85

Figure 4.6 Fourier difference maps showing the electron (left) and nuclear (right) density of the hydrogen atom in the short, strong hydrogen bond in the 2:1 complex of N,N-dimethylurea and oxalic acid. The acid oxygens are denoted with an asterisk (*). 87

Figure 4.7 A "DMU-A-DMU" molecular unit from the neutron structure of the 2:1 complex of N,N-dimethylurea and oxalic acid at 150 K. 88

Figure 4.8 The change in D-H and H···A distances in the short, strong hydrogen bond of the 2:1 complex of N,N-dimethylurea and oxalic acid determined by neutron diffraction as a function of temperature. 88

Figure 4.9 One "DMU-A-DMU" molecular unit of the molecular complex of N,N'-dimethylurea with oxalic acid, (top), the relative orientations of adjacent units (red and blue) looking along the c-axis (middle) and the DHAA bifurcated hydrogen bond and weaker interactions betwen molecular units (bottom), from the 100 K X-ray data. 91

Figure 4.10 Fourier difference maps showing the electron (left) and nuclear (right) density of the hydrogen atom in the short, strong hydrogen bond in the 2:1 complex of N,N'-dimethylurea and oxalic acid, at selected temperatures. The acid oxygen is denoted with an asterisk (*). 92

Figure 4.11 A "DMU-A-DMU" molecular unit from the neutron structure of the 2:1 complex of N,N'-dimethylurea and oxalic acid at 200 K. 93

Figure 4.12 The change in D-H and H...A distances in the short, strong hydrogen bond of the 2:1 complex of N,N'-dimethylurea and oxalic acid determined by neutron diffraction as a function of temperature. 93

Figure 4.13 Structural overlay of two adjacent three-molecule “DMU-A-DMU” units viewed along the c-axis in the molecular complex of N,N'-dimethylurea with oxalic acid, at 100 K (cyan) and 300 K (red). The structural overlay is optimised for the unit on the left and separation of the units occurs as a function of temperature, which can be seen in the unit to the right.....94

Figure 4.14 The potential energy surfaces of the short, strong hydrogen bond in the 2:1 complex of N,N’-methylurea and oxalic acid at 100 K (top) and 300 K (bottom), generated from the theoretical data. 96

Figure 4.15 Interactions between “MU-A-MU” units (unit highlighted in box in top image) in the same layer (top) and in different layers (bottom) in the 2:1 complex of N-methylurea and chloranilic acid at 100 K (X-ray). 98

Figure 4.16 Fourier difference maps showing the electron (left) and nuclear (right) density of the hydrogen atom in the short, strong hydrogen bond in the 2:1 complex of N-methylurea and chloranilic acid. Acid oxygens are marked with an asterisk (*). 99

Figure 4.17 An “MU-A-MU” molecular unit from the neutron structure of the 2:1 complex of N-methylurea and chloranilic acid at 200 K. 100

Figure 4.18 The potential energy surfaces of the short, strong hydrogen bond in the 2:1 complex of N-methylurea and chloranilic acid at 100 and 300 K, generated from the theoretical data. 101

Figure 4.19 Interactions between “MU-A-MU” units (unit highlighted in box in top image) in the same layer (top) and in different layers (bottom) in the 2:1 complex of N-methylurea and bromanilic acid at 100 K (X-ray). 103

Figure 4.20 Fourier difference maps showing the electron density of the hydrogen atom in the short, strong hydrogen bond in the 2:1 complex of N-methylurea and bromanilic acid. The acid oxygen is marked with an asterisk (*). 104

Figure 4.21 Interactions within a layer (top) and between layers (bottom) showing the different urea (orange, pink, red and purple) and bromanilic acid (blue and green) environments in the 2:1 complex of urea and bromanilic acid at 110 K (X-ray). In the top image the two subunits are highlighted in boxes while the short, strong hydrogen bond and transferred proton are circled in red and blue, respectively. 106

Figure 4.22 Fourier difference maps showing the electron density of the hydrogen atom in the short, strong hydrogen bond in the 2:1 complex of urea and bromanilic acid. The acid oxygens are marked with an asterisk (*). 108

Figure 5.1 Clockwise from top left, molecular structure diagrams of: urea, N-methylurea, N,N-dimethylurea, succinic acid, fumaric acid and oxalic acid.....116

Figure 5.2 The hydrogen bonded three molecule “U-A-U” unit in the 2:1 complex of urea and succinic acid at 100 K (X-ray). 127

Figure 5.3 One-dimensional zigzag molecular chain (left) and the different orientations of chains (right, red and blue) in the 2:1 complex of urea succinic acid at 100 K (X-ray). 127

Figure 5.4 Lateral hydrogen bonds between a molecular chain and adjacent chains in different orientations in the 2:1 complex of urea succinic acid at 100 K (X-ray). 128

Figure 5.5 The hydrogen bonded three molecule “U-A-U” unit in the 2:1 complex of urea and fumaric acid at 100 K (X-ray). 129

Figure 5.6 One-dimensional zigzag molecular chain (left) and the two different orientations of chains (right, red and blue) in the 2:1 complex of urea fumaric acid at 100 K (X-ray). 129

Figure 5.7 Lateral hydrogen bonds between a molecular chain and adjacent chains in different orientations in the 2:1 complex of urea fumaric acid at 100 K (X-ray). 130

Figure 5.8 The hydrogen bonded three molecule “MU-A-MU” unit in the 2:1 complex of N-methylurea and succinic acid at 100 K (X-ray). 131

Figure 5.9 One-dimensional zigzag molecular chain (left) and the two different orientations of chains (right, red and blue) in the 2:1 complex of N-methylurea succinic acid at 100 K (X-ray). 131

Figure 5.10 Lateral hydrogen bonds between a molecular chain and adjacent chains in different orientations in the 2:1 complex of N-methylurea succinic acid at 100 K (X-ray). 132

Figure 5.11 The hydrogen bonded three molecule “MU-A-MU” unit in the 2:1 complex of N-methylurea and fumaric acid at 100 K (X-ray). 132

Figure 5.12 One-dimensional zigzag molecular chain (left) and the two different orientations of chains (right, red and blue) in the 2:1 complex of N-methylurea fumaric acid at 100 K (X-ray). 133

Figure 5.13 Lateral hydrogen bonds between a molecular chain and adjacent chains in different orientations in the 2:1 complex of N-methylurea fumaric acid at 100 K (X-ray). 133

Figure 5.14 The hydrogen bonded three molecule “MU-A-MU” unit of the 2:1 complex of N-methylurea and oxalic acid at 200 K (X-ray). 134

Figure 5.15 The layered structure (left) and hydrogen bonds between three molecule units in a layer (right) of the 2:1 complex of N-methylurea and oxalic acid at 200 K (X-ray). 135

Figure 5.16 The hydrogen bonded three molecule “DMU-A-DMU” unit of the 2:1 complex of N,N-dimethylurea and succinic acid at 100 K (X-ray). 135

Figure 5.17 One-dimensional zigzag molecular chain (left) and the two possible orientations of chains (right, red and blue) in the 2:1 complex of N,N-dimethylurea succinic acid at 100 K (X-ray). 136

Figure 5.18 Lateral hydrogen bonds between a molecular chain and adjacent chains in different orientations in the 2:1 complex of N,N-dimethylurea succinic acid at 100 K (X-ray). 136

Figure 5.19 The hydrogen bonded three molecule “DMU-A-DMU” unit of the 2:1 complex of N,N-dimethylurea and fumaric acid at 100 K (X-ray). 137

Figure 5.20 One-dimensional chain of molecules (left) and interactions between chains in different orientations (right) in the 2:1 complex of N,N-dimethylurea and fumaric acid at 100 K (X-ray). 138

Figure 5.21 Overlayed unit cells of the **US** (red) and **UF** (blue) complexes (left) and the **MUS** (red) and **MUF** (blue) complexes (right) looking along the b-axes from the 100 K X-ray structures. 139

Figure 5.22 One dimensional chains of “DMU-A-DMU” units in the N,N-dimethylurea succinic acid (top) and N,N-dimethylurea fumaric acid (bottom) at 100 K (X-ray). 141

Figure 5.23 The D-H and H···A lengths as a function of the temperature from the neutron data (left) and a comparison of the X-ray and neutron D-H···A lengths for the short, strong O-H···O hydrogen bond in the 2:1 complex of N,N-dimethylurea and fumaric acid. 144

Figure 5.24 The hydrogen bonded “U-A-U” units in the neutron structures of, from top to bottom: **US**, **UF**, **MUS**, **DMUS** and **DMUF**. All images are taken from the 100 K data with the exception of that for **DMUS** which is taken from the 20 K neutron structure. 145

Figure 5.25 Fourier difference maps showing the electron (left) and nuclear (right) density of the hydrogen atom in the short, strong hydrogen bond in the 2:1 complex of N,N-dimethylurea and fumaric acid. For labelling scheme see **Figure 5.24**. 146

Figure 5.26 A structural overlay showing a shift in the molecular units relative to the neighbouring units viewed along the b- (left) and c-axes (right) taken from the **US** X-ray data at 100 (cyan) and 300 K (red). 150

Figure 5.27 A molecular unit viewed from above (top) and the side (bottom) showing the large anisotropic thermal parameters of the hydrogen atoms in the 300 K neutron structure of **MUS**. 151

Figure 6.1 Diagrams of 4-dimethylaminobenzoic acid (left), 3,5-dinitrobenzoic acid (centre) and 4,4’-bipyridine (right). 156

Figure 6.2 A disordered dimer of 4-DABA in form III of the native structure.[174] 156

Figure 6.3 The homodimers of 3,5-DNBA (top) and 4-DABA (middle) with the neighbouring stacks (bottom) of 3,5-DNBA (red) and 4-DABA (blue) dimers taken from the 30 K neutron data. 163

Figure 6.4 Fourier difference maps showing the electron (left)[76] and nuclear density (right) in the hydrogen bond linking the 4-DABA homodimers 165

Figure 6.5 A 4-DABA molecule in the form I native structure (top left)[76] and in the complex with 3,5-DNBA (bottom left) showing the methyl groups out of the plane of the aromatic ring and the close contact with a nitro group of 3,5-DNBA (right). 166

Figure 6.6 Weak lateral interactions with the 4-DABA acid dimers (left) and interactions to a 3,5-DNBA molecule in the layer above (right). 166

Figure 6.7 The evolution of the anisotropic displacement parameter of the hydrogen atom in the 3,5-DNBA homodimer in the complex. A single, localised position is observed at 30 K which moves to a more elongated central position as the temperature is increased, indicative of the inadequacy of the single, non-disordered hydrogen atom model employed in these initial refinements. 167

Figure 6.8 Fourier difference maps showing the electron (left)[76] and nuclear density (right) of the disordered hydrogen bond linking the 3,5-DNBA homodimers in the complex. 169

Figure 6.9 The 3,5-DNBA homodimers in the complex at 100 K (top) and 250 K (bottom) showing the split occupancy hydrogen atom. A gap is clearly visible between the disordered hydrogen displacement parameters at 100 K while at 250 K the displacement parameters are almost overlapping. 170

Figure 6.10 A dimer of 3,5-DNBA (top), a side-on view of a dimer showing the nitro and acid groups slightly out of the plane of the ring (middle) and short contacts between a 3,5-DNBA dimer (red) and surrounding molecules showing layers of dimers (bottom), all taken from the X-ray structure of the $P2_1/c$ polymorph at 100 K. 171

Figure 6.11 Fourier difference maps showing the electron density of the hydrogen atom within the hydrogen bond linking the 3,5-DNBA dimers in the $P2_1/c$ polymorph. 173

Figure 6.12 The 3,5-DNBA dimer in the $P2_1/c$ polymorph with the hydrogen atom modelled as disordered over two positions at 300 K. 174

Figure 6.13 A dimer of 3,5-DNBA (top), a side-on view of a dimer showing the nitro and acid groups out of the plane of the benzene ring (middle) and short contacts between a 3,5-DNBA molecule (red) and surrounding molecules showing layers of dimers (bottom) all from the structure of the C2/c polymorph at 100 K. 175

Figure 6.14 A dimer of 3,5-DNBA taken from the C2/c polymorph neutron structure at 300 K. 177

Figure 6.15 Fourier difference maps showing the electron (left) and nuclear (right) density of the hydrogen atom in the hydrogen bond linking the 3,5-DNBA dimers in the C2/c polymorph. 178

Figure 6.16 Disordered 3,5-DNBA dimers in the C2/c polymorph from the X-ray (left) and neutron (right) data at 300 K. 179

Figure 6.17 A dimer of 4-DABA (left, green) involved in asymmetric weak interactions and an isolated dimer of 3,5-DNBA (centre, blue) from the binary complex with a benzoic acid dimer (right, red) involved in symmetric weak interactions,[80] all at 100 K. 181

Figure 6.18 Schematic representations of the hydrogen bond double-well potentials for the 3,5-DNBA dimers in the polymorphs where the energy difference between the two possible position is significant (left), and in the complex with 4-DABA, where the two possible positions are close in energy (right).[6] 182

Figure 6.19 Overlayed dimers of 3,5-DNBA looking approximately along the c-axis in the P21/c (left) and C2/c (right) forms in cyan and red from the 100 and 300 K X-ray data, respectively.....186

Figure 7.1 A protonated $DMANH^+$ showing the intramolecular N-H···N hydrogen bond (left) and a benzoic acid dimer containing a charge-assisted short, strong hydrogen bond where a dimer oxygen is positioned above a $DMANH^+$ (right). 190

Figure 7.2 Clockwise from top left: molecular structures of DMAN, 2-fluorobenzoic acid, 2-iodobenzoic acid, 4-iodobenzoic acid, chloranilic acid and 2,3-dihydroxybenzoic acid…191

Figure 7.3 A protonated $DMANH^+$ molecule (left) and the $ACID^-$ dimer containing a charge-assisted, short strong hydrogen bond (right). Taken from the 200 K neutron structure of the 1:2 DMAN 2-FBA complex. 194

Figure 7.4 Weak interactions between $DMANH^+$ and a 2-FBA molecule viewed in two orientations. Taken from the 200 K neutron structure of the 1:2 DMAN 2-FBA complex. 195

Figure 7.5 Weak interactions between $ACID^-$ dimers (left) and stacked $DMANH^+$ molecules (right) in the 200 K neutron structure of the 1:2 DMAN 2-FBA complex.....195

Figure 7.6 A protonated $DMANH^+$ molecule (left) and the $ACID^-$dimer containing a charge-assisted, short strong hydrogen bond (right). Taken from the 200 K neutron structure of the 1:2 DMAN 2-IBA complex.....197

Figure 7.7 Weak interactions between $ACID^-$dimers (left) and weak interactions between a $DMANH^+$ molecule (blue) and surrounding $ACID^-$ dimers (right). Taken from the 200 K neutron structure of the 1:2 DMAN 2-IBA complex.....197

Figure 7.8 Weak interactions between $DMANH^+$ and a 2-IBA molecule viewed in two orientations in the 200 K neutron structure of the 1:2 complex of DMAN and 2-IBA.....198

Figure 7.9 The DMANH+ and $ACID^-$ dimer viewed from two orientations showing weak interactions to the bound proton and methyl groups of DMANH+ in the 200 K neutron structure of the 1:2 complex of DMAN and 4-IBA.....200

Figure 7.10 A zigzag chain of $ACID^-$ dimers (top) and interactions between $DMANH^+$ molecules (bottom) in the 200 K neutron structure of the 1:2 complex of DMAN and 4-IBA. 200

Figure 7.11 Interactions between protonated $DMANH^+$ molecules and a $ACID^{2-}$ dimer viewed in two orientations in the 200 K neutron structure of the 1:1 complex of DMAN and CLA. 201

Figure 7.12 Weak interactions between a CLA^- molecule and surrounding $DMANH^+$ molecules (left) and stacked $DMANH^+$ molecules (right) in the 200 K neutron structure of the 1:1 complex of DMAN and CLA. 202

Figure 7.13 A protonated $DMANH^+$ with an $ACID^{2-}$ dimer above viewed in two orientations in the 200 K neutron structure of the 1:1 complex of DMAN and 2,3-DOHBA. 204

Figure 7.14 Weak interactions between 2,3-$DOHBA^-$ and $DMANH^+$ molecules (left) and the displaced stacking of $DMANH^+$ molecules in red and blue (right) in the 200 K neutron structure of the 1:1 complex of DMAN and 2,3-DOHBA. 204

Figure 7.15 Interactions between the bound protons in $DMANH^+$ and the acid oxygens. Clockwise from top left: DMAN complexes with 2-FBA, 2-IBA, 4-IBA, 2,3-DOHBA and CLA. 206

Figure 7.16 Fourier difference maps of the DMANH+ N-H···N intramolecular hydrogen bond showing the hydrogen atom nuclear density in the complexes of DMAN with 2-FBA (top left), 2-IBA (top right), 4-IBA (centre left), CLA (centre right) and 2,3-DOHBA (bottom), taken from the 200 K neutron structures. 209

Figure 7.17 The distances between the $DMANH^+$ nitrogen atoms and the acid oxygen positioned above the $DMANH^+$ in the DMAN 2-FBA complex. Methyl groups have been removed for clarity. 210

Figure 7.18 A $DMANH^+$ molecule and a 4-IBA dimer containing a short, strong charge-assisted hydrogen bond with the **x** and **y** acid molecules labelled. 213

Figure 8.1 Top to bottom and left to right: urea, N-methylurea, N,N-dimethylurea, picolinic acid, 4-hydroxybenzoic acid, 2,3-dihydroxybenzoic acid, chloranilic acid and bromanilic acid. 217

Figure 8.2 Urea-picolinic acid-water chains (top) and three sets of chains (yellow, magenta and green) showing stacked sets of chains (yellow and magenta) and the tilted orientation of adjacent sets of chains (yellow/magenta vs. green) (bottom) in the 2:1 urea picolinic acid monohydrate complex at 100 K (X-ray). 225

Figure 8.3 The neutron structure of the 2:1 complex of urea picolinic acid monohydrate at 10 K, showing the hydrogen atoms of the urea molecules bent towards the hydrogen bond acceptor atoms. 226

Figure 8.4 Packing of urea and 4-OHBA molecules in a unit cell (top), hydrogen bonds between urea moieties (red and blue), showing the one-dimensional chain (blue) and bifurcated hydrogen bonds to other ureas (bottom left) and the two parallel planes of urea molecules in the chain (bottom right) in the 2:1 complex of urea and 4-OHBA at 100 K (from the X-ray determination). 227

Figure 8.5 Hydrogen bonds between urea moieties (red and blue) and the 4-OHBA molecule in the 100 K X-ray structure of the 2:1 complex of urea and 4-OHBA. 227

Figure 8.6 Weak hydrogen bonds involving the acid carbonyl oxygen in the 100 K X-ray structure of the 2:1 complex of urea and 4-OHBA. 228

Figure 8.7 Interactions in layer **a**, showing the subunits in boxes and the protonated urea molecules circled, in the 100 K X-ray structure of the 7:4 complex of urea and BRA monohydrate. 230

Figure 8.8 Interactions in layer **b**, showing the subunits in boxes and the protonated urea circled, in the 100 K X-ray structure of the 7:4 complex of urea and BRA monohydrate. Note: the light green urea molecule marked with an asterisk (*) is in the next layer **a**, in the layer above the rest of the molecules in the figure. 232

Figure 8.9 Interactions between layers in the 100 K X-ray structure of the 7:4 complex of urea and BRA monohydrate, viewed along the a-axis. 233

Figure 8.10 Fourier difference map of the short, strong O-H···O hydrogen bond in the 7:4 complex of urea and BRA, from the X-ray data at 100 K. 234

Figure 8.11 A layer of dimers (top) and interactions between dimers in different layers (bottom) in the 1:1 complex of N-methylurea and picolinic acid, from the 100 K X-ray data. 235

Figure 8.12 Fourier difference map of the short, strong O-H···O hydrogen bond in the 1:1 complex of N-methylurea and picolinic acid, from the X-ray data at 100 K. 235

Figure 8.13 One-dimensional acid-N-methylurea chains linked by tilted N-methylureas (top) and two layers of chains (bottom) in the 1:1 complex of N-methylurea and 2,4-DOHBA from the 300 K X-ray data. 237

Figure 8.14 Fourier difference maps of the short strong O-H···O hydrogen bonds linking the acid···amide dimers in the 1:1 complex of N-methylurea and 2,4-DOHBA, from the 300 K X-ray data. 239

Figure 8.15 Hydrogen bonds linking dimethylurea-CLA units showing the stacked units in the 100 K X-ray structure of the 1:1 complex of N,N-dimethylurea and CLA monohydrate. 240

Figure 8.16 Weak interactions linking adjacent molecular units (top) and layered units (bottom) in the 100 K (X-ray) structure of the 2:1 complex of N,N-dimethylurea and BRA. 242

Figure 8.17 A molecular unit of the 2:1 complex of N,N-dimethylurea and BRA in the 20 K neutron structure. 242

Figure 8.18 Fourier difference maps of the short strong O-H···O hydrogen bond in the 2:1 complex of N,N-dimethylurea and BRA from the X-ray and neutron data. 243

Figure 9.1 The short, strong hydrogen bonds in which protons undergo temperature dependent proton migration from the neutron diffraction data, showing the hydrogen bonded units in the complexes of N-methylurea and CLA (top), N,N-dimethylurea and oxalic acid (middle) and N,N'-dimethylurea and oxalic acid (bottom). 247

Figure 9.2 Disordered dimers of 3,5-DNBA in the molecular complex with 4-DABA at 100 K and 250 K (top and bottom, respectively). 251

Figure 9.3 A $DMANH^+$ molecule and a 4-IBA dimer containing a short, strong charge-assisted hydrogen bond.....254

Figure 9.4 A “U-A-U” hydrogen bonded unit in the complex of urea and succinic acid. This motif is observed in the structures of all urea-dicarboxylic acid complexes presented in this work.....256

List of Tables

Table 2.1 Unit cell types with possible lengths and angles and the possible Bravais lattices. 26

Table 4.1 X-ray and neutron data collection and refinement information for the 2:1 complex of N,N-dimethylurea and oxalic acid.[a] 77

Table 4.2 X-ray and neutron data collection and refinement information for the 2:1 complex of N,N'-dimethylurea and oxalic acid.[a] 78

Table 4.3 X-ray and neutron data collection and refinement information for the 2:1 complex of N-methylurea and chloranilic acid.[a] 79

Table 4.4 X-ray data collection and refinement information for the 2:1 complex of N-methylurea and bromanilic acid. 80

Table 4.5 X-ray data collection and refinement information for the 2:1 complex of urea and bromanilic acid. 81

Table 4.6 Lengths of the short, strong O-H···O hydrogen bond in the three molecule "DMU-A-DMU" units of the complex of N,N-dimethylurea with oxalic acid. 84

Table 4.7 Lengths of the short, strong O-H···O hydrogen bond in the three molecule "DMU-A-DMU" units in the high temperature phase of the complex of N,N-dimethylurea with oxalic acid from the neutron diffraction and theoretical data. 89

Table 4.8 Lengths of the short, strong O-H···O hydrogen bond in the three molecule "DMU-A-DMU" units of the complex of N,N'-dimethylurea with oxalic acid. 90

Table 4.9 Lengths of the short, strong O-H···O hydrogen bond in the three molecule "DMU-A-DMU" units in the high temperature phase of the complex of N,N'-dimethylurea with oxalic acid from the neutron diffraction and theoretical data. 95

Table 4.10 Lengths of the short, strong O-H···O hydrogen bond in the three molecule "MU-A-MU" units of the complex of N-methylurea with chloranilic acid. 97

Table 4.11 Lengths of the short, strong O-H···O hydrogen bond in the three molecule "MU-A-MU" units of the complex of N-methylurea with chloranilic acid from the neutron diffraction and theoretical data. 101

Table 4.12 Lengths of the short, strong O-H···O hydrogen bond in the three molecule "MU-A-MU" units of the complex of N-methylurea with bromanilic acid, from the X-ray data. 103

Table 4.13 Lengths of the short, strong O-H···O hydrogen bond in the complex of urea with bromanilic acid. 108

Table 4.14 ΔpK_a values and short, strong hydrogen bond distances from the 100 K X-ray data (110 K in the case of urea-BRA) for the proton migration complexes presented in this chapter. 111

Table 5.1 X-ray and neutron data collection and refinement information for the 2:1 complex of urea and succinic acid.[a] 120

Table 5.2 X-ray and neutron data collection and refinement information for the 2:1 complex of urea and fumaric acid. 121

Table 5.3 X-ray and neutron data collection and refinement information for the 2:1 complex of N-methylurea and succinic acid.[a] 122

Table 5.4 X-ray data collection and refinement information for the 2:1 complex of N-methylurea and fumaric acid. 123

Table 5.5 X-ray data collection and refinement information for the 2:1 complex of N-methylurea and oxalic acid. 124

Table 5.6 X-ray and neutron data collection and refinement information for the 2:1 complex of N,N-dimethylurea and succinic acid.[a] 125

Table 5.7 X-ray and neutron data collection and refinement information for the 2:1 complex of N,N-dimethylurea and fumaric acid.[a] 126

Table 5.8 Unit cell parameters for the seven complexes from the 200 K X-ray data. 139

Table 5.9 Lengths of the short, strong O-H···O hydrogen bond in the three molecule "U-A-U" units of the complexes of urea with succinic and fumaric acid from the X-ray and neutron data. 143

Table 5.10 Lengths of the short, strong O-H···O hydrogen bond in the three molecule "MU-A-MU" units of the complexes of N-methylurea with succinic, fumaric and oxalic acid from the X-ray and neutron data. 143

Table 5.11 Lengths of the short, strong O-H···O hydrogen bond in the three molecule "DMU-A-DMU" units of the complexes of N,N-dimethylurea with succinic and fumaric acid from the X-ray and neutron data. 144

Table 5.12 ΔpK_a values and short, strong hydrogen bond distances from the 200 K X-ray data for the seven complexes presented in this chapter and the two dimethylurea oxalic acid complexes presented in **Chapter 4**. 148

Table 5.13 Unit cell parameters of selected complexes from the 100 and 300 K X-ray data with contracting unit cell axes displayed in bold. 149

Table 6.1 Neutron data collection and refinement information for the 2:2 complex of 4-DABA and 3,5-DNBA.[a] 160

Table 6.2 X-ray data collection and refinement information for the $P2_1/c$ polymorph of 3,5-DNBA. 161

Table 6.3 X-ray and neutron data collection and refinement information for the C2/c polymorph of 3,5-DNBA.[a] 162

Table 6.4 Lengths of hydrogen bonds linking the 4-DABA and 3,5-DNBA homodimers in the complex from the neutron data. Where disorder is modelled in the 3,5-DNBA dimers, two values are given, (a) represents the major site and (b) the minor. 164

Table 6.5 Lengths of hydrogen bonds linking the 3,5-DNBA dimers in the P21/c polymorph from the X-ray data. Where disorder is modelled in the 3,5-DNBA dimers two values are given, (a) represents the major site and (b) the minor.....172

Table 6.6 Lengths of hydrogen bonds linking the 3,5-DNBA dimers in the C2/c polymorph from X-ray and neutron data. Where disorder is modelled in 3,5-DNBA dimers two values are given, (a) represents the major site and (b) the minor.....176

Table 6.7 Relative occupancies of the major and minor disordered proton sites in homodimers of 3,5-DNBA in the pure $P2_1/c$ and C2/c polymorphs, the binary complex[a], 4-DABA in the ternary complex and benzoic acid in its native structure from X-ray and neutron diffraction data. 180

Table 6.8 Evolution of the unit cell parameters of the two polymorphs of 3,5-DNBA with temperature showing the contraction of the b-axes with increasing temperature.....185

Table 7.1 Neutron data collection and refinement information for the DMAN-acid complexes.[a] 193

Table 7.2 Lengths of the intramolecular and intermolecular hydrogen bonds in $DMANH^+$ and linking the $ACID^-$ dimers in the 1:2 complex of DMAN and 2-FBA at 200 K from the X-ray[125] and neutron data. 196

Table 7.3 Lengths of the intramolecular and intermolecular hydrogen bonds in $DMANH^+$ and linking the $ACID^-$ dimers in the 1:2 complex of DMAN and 2-IBA at 200 K from the X-ray[125] and neutron data. 198

Table 7.4 Lengths of the intramolecular and intermolecular hydrogen bonds in DMAN and linking the 4-IBA dimers in the 1:2 complex of DMAN and 4-IBA at 200 K from the X-ray[125] and neutron data.....199

Table 7.5 Lengths of the intramolecular and intermolecular hydrogen bonds in $DMANH^+$ and linking the $ACID^{2-}$ dimers in the 1:1 complex of DMAN and CLA from the X-ray[125] and neutron data.[a] 202

Table 7.6 Lengths of the intramolecular and intermolecular hydrogen bonds in the 1:1 complex of DMAN and 2,3-DOHBA at 200 K from the X-ray and neutron data. 204

Table 7.7 Distances between the bound protons in $DMANH^+$ and the acid oxygens above the N-H···N hydrogen bond listed with the largest principal thermal parameters of the bound proton. The two values for the CLA and 2,3-DOHBA complexes correspond to the two oxygens which interact with the bound proton. 207

Table 7.8 Hydrogen bond distances for the intramolecular N-H···N bond in the $DMANH^+$ molecule in the DMAN acid complexes from the 200 K neutron structures. 210

Table 8.1 X-ray and neutron data collection and refinement information for the 2:1 complex of urea picolinic acid monohydrate.[a] 220

Table 8.2 X-ray data collection and refinement information for the 2:1 complex of urea and 4-OHBA, the 7:4 complex of urea and BRA monohydrate, the 1:1 complex of N-methylurea and picolinic acid and the 2:1 complex of N-methylurea and 2,4-DOHBA....221

Table 8.3 X-ray data collection and refinement information for the 1:1 complex of N,N-dimethylurea and CLA monohydrate.....222

Table 8.4 X-ray and neutron data collection and refinement information for the 2:1 complex of N,N-dimethylurea and BRA.[a] 223

Table 8.5 Lengths of hydrogen bonds linking the acid···amide dimer in the 1:1 complex of N-methylurea and picolinic acid, from the 100 K X-ray data.....236

Table 8.6 Lengths of hydrogen bonds linking the acid···amide dimers in the 1:1 complex of N-methylurea and 2,4-DOHBA, from the 300 K X-ray data. (a) represents one dimer environment and (b) the other.....238

Table 8.7 Lengths of the short strong O-H···O hydrogen bond in the 1:1 complex of N,N-dimethylurea and CLA monohydrate from the variable temperature X-ray data. 240

Table 8.8 Lengths of the short strong O-H···O hydrogen bond in the 2:1 complex of N,N-dimethylurea and BRA from the variable temperature X-ray and neutron data.....241

Table 9.1 Selected properties and experimental details of some of the urea-acid complexes presented in this work. A key is below the table. 246

Acknowledgements

I firstly have to thank Chick, for giving me this opportunity, and also for the endless positivity and patience regarding the project, even when for long periods it seemed as if I was getting nowhere. A huge thank you also has to go to Lynne for constant encouragement and guidance, and also for the painful task of reading the first drafts of my thesis chapters. At the time I may not have appreciated the return of a chapter covered in green or blue (thankfully not red) pen, but it was never as bad as it looked and my thesis is much improved for it so thank you.

I also have to thank Garry for all the help on VIVALDI during experiments and for teaching me how to get results out of the huge amount of neutron data collected over my time at ILL. I should also thank everyone at the ILL and in Grenoble who made my stay there so enjoyable. If I had it my way I would have stayed there much longer, but those two years were great, even though I never quite became fluent in French, I at least improved my Spanish.

A huge thank you must also go to Carole for all the help and support with the computational work. You certainly have a gift for explaining complex theory in an easy to understand manner and without your guidance I would have been completely lost. It's a shame the results didn't quite come out as we had hoped but I enjoyed my time in Edinburgh and it was nice to be able to learn about new techniques that I can hopefully make use of in the future.

Thanks to all the chicklets, both in Glasgow and Bath, for providing many a healthy distraction from work and for the company during conferences. It's probably for the best that we don't have to spend that much time together often, though it was certainly enjoyable at the time. I also have to thank the project students Niall and Hayleigh, who I was lucky enough to help supervise and who did a fantastic job of setting up many, many crystallisations (sorry about that).

Finally I have to thank the friends and family that supported me throughout the PhD and even more so when writing up. I especially have to thank my parents without whom none of this would have ever been possible. Your support and encouragement over the years always got me through and I will be forever grateful.

Abstract

This work presents findings from experiments carried out using the neutron Laue method in tandem with laboratory source X-ray diffraction to characterise a series of organic molecular complexes which exhibit interesting, and potentially "tunable", temperature dependent charge transfer effects, such as proton migration and proton disorder within hydrogen bonded networks. These subtle processes are studied by variable temperature neutron diffraction studies, allowing the positional and anisotropic displacement parameters of the hydrogen atoms to be refined accurately and their evolution with temperature followed. The hydrogen atom behaviour is found to be influenced by the local environment, including weak intermolecular interactions in the vicinity of the hydrogen bond under study.

Complexes of urea and methyl substituted ureas with small organic acids are presented, which show robust and reproducible structural motifs. In favourable circumstances, these contain short, strong hydrogen bonds (SSHBs) within which the proton may undergo temperature dependent migration. By synthesising a number of complexes containing SSHBs, potential routes to the design of proton migration complexes are found, which utilise crystal engineering principles and pK_a matching. Variable temperature studies conducted on these complexes also show unusual thermal expansion properties and phase transitions in urea-acid complexes which do not display proton migration.

Systems containing hydrogen bonded dimers of 3,5-dinitrobenzoic acid are also studied, and shown to contain temperature proton disorder within moderate strength hydrogen bonds linking the dimers. The presence and potential onset temperature of any disorder is found to be influenced by interactions around the acid dimers and potential routes to controlling proton disorder are discussed.

Complexes of the proton sponge, 1,8-bis(dimethylamino)napthalene (DMAN), with organic acids are also presented, in which the structures have been determined using neutron diffraction. DMAN readily accepts a proton from the acid co-molecules used in forming the complexes, forming a strong intramolecular SSHB within the protonated DMAN. Strong intermolecular hydrogen bonds are also induced between the acid molecules in many cases. The neutron studies presented here investigate the effect of weak interactions on the behaviour of hydrogen atoms located within these SSHBs, and also indicate over what distance such interactions significantly affect the hydrogen atom behaviour.

List of Abbreviations

2-FBA	2-Fluorobenzoic acid
2-IBA	2-Iodobenzoic acid
2,3-DOHBA	2,3-Dihydroxybenzoic acid
2,4-DOHBA	2,4-Dihydroxybenzoic acid
3,5-DNBA	3,5-Dinitrobenzoic acid
4-DABA	4-Dimethylaminobenzoic acid
4-IBA	4-Iodobenzoic acid
4-OHBA	4-Hydroxybenzoic acid
BIPY	4,4’-Bipyridine
BRA	Bromanilic acid
CLA	Chloranilic acid
DMAN	1,8-Bis(dimethylamino)napthalene
DMU	Dimethylurea
MU	Methylurea
PES	Potential energy surface
SSHB	Short, strong hydrogen bond
U	Urea

Chapter 1

1. Introduction

1.1 Preamble

This thesis concerns the exploration of hydrogen bonded networks in solid-state molecular complexes with a view to designing materials with interesting, and potentially useful, chemical and physical properties. Full structural characterisation of such materials is vital in their development and understanding and single crystal X-ray and neutron diffraction are the key techniques which have been used in this work. All general background theory will be described here including an in depth introduction to hydrogen bonding and the potentially tunable properties of certain categories of hydrogen bonds such as proton migration and proton disorder.

It should be noted that when describing structures solved using X-ray diffraction, the term hydrogen atom is used to refer to the electron density associated with the hydrogen which is not normally located at the same position as the nuclear density. This is not the case in structures determined using neutron diffraction where it is the nuclear density which is located from the diffraction experiment.

1.2 Hydrogen Bonding

The first use of the term hydrogen bond is thought to have first been in a paper by Pauling on the nature of the chemical bond in 1931; this was followed up in his book, *Nature of the Chemical Bond*, where hydrogen bonding is introduced when discussing the $[H:F:H]^-$ ion.[1] In the subsequent years, many papers on the nature of the hydrogen bond have been published alongside papers on the chemical and physical properties which are affected by hydrogen bonding. Jeffrey summarises much of the hydrogen bonding literature and also discusses the techniques used to study the hydrogen bond in his 1997 book, *An Introduction to Hydrogen Bonding*.[2]

As one of the most common interactions in chemistry, the hydrogen bond is important in many fields of research and also in day to day life; the relatively high boiling point of water is a classic example of the importance of the hydrogen bond. Hydrogen bonds are also key in many biological systems, playing a role in determining the shapes of folded proteins and in linking base-pairs in strands of DNA. There are many different types of hydrogen bond and their properties vary; the strongest hydrogen bonds can have strengths approaching those of covalent bonds while weak hydrogen bonds are little stronger than

van der Waal's interactions. The majority of hydrogen bonds fall somewhere between these two extremes.

The hydrogen bond can be described as a highly directional, attractive interaction involving a hydrogen atom covalently bonded to a donor atom, D, interacting with an acceptor atom, A. The donor atom is more electronegative than the hydrogen atom and is therefore an electron withdrawer, encouraging the partially unshielded proton to interact with the acceptor atom, while the acceptor usually has a lone-pair of electrons or polarisable π electrons which interact with the hydrogen atom. The most recent recommendation on the IUPAC definition of a hydrogen bond states that *"A typical hydrogen bond may be depicted as X-H···Y-Z, where the three dots denote the bond. X-H represents the hydrogen-bond donor. The acceptor may be an atom or an anion Y, or a fragment or a molecule Y-Z, where Y is bonded to Z. In specific cases X and Y can be the same with both X-H and Y-H bonds being equal. In any event, the acceptor is an electron-rich region such as, but not limited to, a lone pair in Y or a π-bonded pair in Y-Z."*[3,4] This is a slightly different wording to that used in the IUPAC gold book of 1997,[5] modified to include weaker hydrogen bonds (such as those to π electron acceptor groups).

Table 1.1 *The classification of strong, moderate and weak hydrogen bonds.*[2]

	Strong	**Moderate**	**Weak**
D-H···A interaction	Mostly covalent	Mostly electrostatic	Electrostatic
Bond lengths	D-H ≈ H···A	D-H < H···A	D-H < < H···A
H···A / Å	~1.2 - 1.5	~1.5 - 2.2	2.2 - 3.2
D-H···A / Å	2.2 - 2.5	2.5 - 3.2	3.2 - 4.0
Bond angles / °	175 - 180	130 - 180	90 - 150
Bond energy / kJ mol^{-1}	60 - 170	15 - 60	< 15

Hydrogen bonds can be classified in a number of ways, but in this work they will be classed according to three groups: strong, moderate and weak. Jeffrey[2] used this classification system to detail the bond energies and expected bond lengths and angles

associated with each class of hydrogen bond (**Table 1.1**). These classifications are not rigid and there are exceptions and intermediates to these classes. Each class of hydrogen bond is discussed further in **Sections 1.2.1 – 1.2.3**. There are also dynamic proton effects, such as proton migration and proton disorder, which may occur in specific classes of hydrogen bonds; these are discussed in **Sections 1.7** and **1.8**.

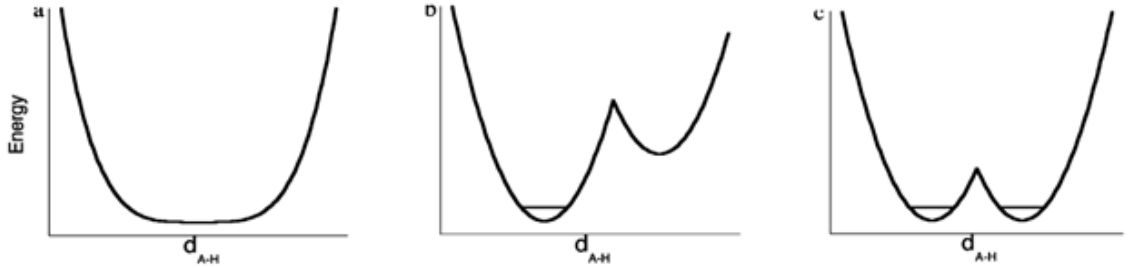

Figure 1.1 *Hydrogen bond potential energy surfaces showing: a single broad potential (left), an asymmetric double-well potential (centre) and a symmetric double-well potential (right).*[6]

In general, when a hydrogen bond forms in the solid-state, the hydrogen atom within it will reside in a symmetric or asymmetric double-well potential energy surface (PES), this differs depending on the class of hydrogen bond (**Figure 1.1**).[2] If the PES is a symmetric or asymmetric double-well, the hydrogen atom either resides on the parent molecule donor atom or is transferred across the bond and resides closer to the acceptor atom (see **Section 1.6**). The asymmetric double-well PES is the most common outcome of hydrogen bond formation, where there is a significant difference in energy between the two possible sites and the higher energy site is not normally occupied by the hydrogen atom, this is typical of weak and moderate strength hydrogen bonds. The symmetric double-well is a special case of the double-well PES which exhibits two possible hydrogen atom sites which are very close in energy; this may be observed in moderate strength hydrogen bonds. The small energy difference can lead to both sites being partially occupied and proton disorder is observed (see **Section 1.8**); this can also be influenced by the barrier height between the two wells, with a low barrier encouraging occupancy of the second site. It is also possible for a flat bottomed single well PES to form in short strong hydrogen bonds (SSHBs) which may allow the hydrogen atom to move along the hydrogen bond, this is known as proton migration and is discussed in **Section 1.7**. Clearly the shape of the PES affects the behaviour of the hydrogen atom, which can in turn affect the properties of the material.

1.2.1 Strong Hydrogen Bonds

Strong hydrogen bonds (**Table 1.1**), also known as low-barrier hydrogen bonds, can be thought of as three-centre, four-electron bonds which are quasi-covalent in nature *via* electron sharing.[7] The energy of these hydrogen bonds can be in excess of 170 kJ mol^{-1}, similar to the energies of some covalent bonds. The D···A distance is often linked to the hydrogen bond strength and strong hydrogen bonds will have the shortest D···A distances, possibly with the hydrogen atom located close to the centre of the hydrogen bond. Generally speaking, a hydrogen bond is considered strong if the D···A distance is less than ~2.5 - 2.55 Å, in the case of O-H···O hydrogen bonds, or 2.55 - 2.6 Å, in the case of N-H···N hydrogen bonds. Strong hydrogen bonds tend to be highly directional, with D-H···A bond angles close to 180°. As already mentioned, the PESs of strong hydrogen bonds are often, though not exclusively, regarded to be broad single wells,[8] in stark contrast to the typical double-well scenario of moderate and weak hydrogen bonds (**Figure 1.1**).

Strong hydrogen bonds most commonly form either when the donor group is electron poor or the acceptor group is electron rich; both cases lead to an increase in the charge separation between donor and acceptor groups and therefore strengthen the hydrogen bond interaction. Hydrogen bonds which are strong due to one, or both, of the donor or acceptor groups belonging to an ion are called charge-assisted hydrogen bonds.[9] Another situation which can favour the formation of strong hydrogen bonds is when neutral donor and acceptor atoms are connected by a system of π-conjugated double bonds; this is known as resonance-assisted hydrogen bonding.[7] Strong hydrogen bonds can also be formed when the donor and acceptor groups are forced close together due to the molecular configuration; this most often occurs in the form of intramolecular hydrogen bonds with an example being the strong hydrogen bond in potassium hydrogen maleate (**Figure 1.2**).[10-12]

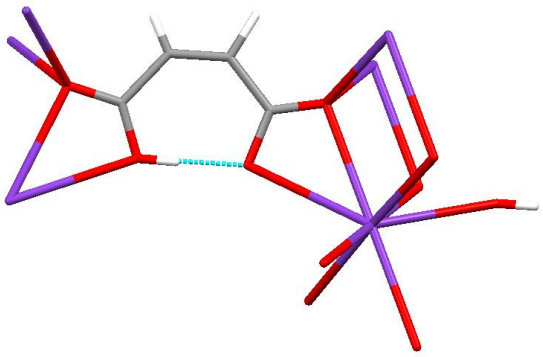

Figure 1.2 *The strong intramolecular hydrogen bond in potassium hydrogen maleate.*[12]

1.2.2 Moderate Hydrogen Bonds

Moderate hydrogen bonds (**Table 1.1**), also known as normal hydrogen bonds, are the most commonly occurring type of hydrogen bond in chemistry and are mainly electrostatic in nature. These most often occur between a neutral donor and a neutral acceptor atom. There is a certain degree of overlap in the definitions of strong and moderate hydrogen bonds, with moderate hydrogen bonds having D···A distances of the order of 2.5 – 3.2 Å. At their shortest, moderate hydrogen bonds can be quasi-covalent in character,[13] similar to strong hydrogen bonds, while longer moderate hydrogen bonds may have more van der Waals character, similar to weak hydrogen bonds.[14] The overlapping definitions mean that an O-H···O hydrogen bond ~2.5 Å in length may be classed as either strong or moderate which may lead to confusion when describing such hydrogen bonds around the limits between hydrogen bond types. Moderate strength hydrogen bonds tend to have a much more flexible geometric arrangement than strong hydrogen bonds, with D-H···A bond angles in the range of 130 – 180°. They typically have asymmetric double-well PESs with the hydrogen atom well localised on one side of the hydrogen bond. In favourable circumstances, moderate hydrogen bonds may form with a symmetric double-well potential which can lead to proton disorder (see **Section 1.8**). The ubiquitous nature of moderate hydrogen bonds means they play an important role in many biological systems. Despite not being the strongest form of hydrogen bonds, they are often one of the main drivers in determining how molecular architectures form in the solid-state.

1.2.3 Weak Hydrogen Bonds

Weak hydrogen bonds (**Table 1.1**) tend to have D···A distances greater than ~3.2 Å and also occur fairly commonly. They normally form between neutral donors and acceptors and are electrostatic in nature, though at longer D···A distances they become more like van der Waals interactions in a similar manner to longer moderate hydrogen bonds.[14] The PES of a weak hydrogen bond is an asymmetric double-well with a large energy barrier between the two possible proton sites; the hydrogen atom is well localised on one site. These bonds are even more flexible in their geometry than moderate hydrogen bonds and may have D-H···A bond angles as low as 90°.

As with the other classes of hydrogen bond, there may be some confusion as to what constitutes a weak hydrogen bond, particularly regarding where the boundary between a weak hydrogen bond and a van der Waals interaction is placed. Generally, weak hydrogen bonds form with a weak donor (e.g. C-H···O), a weak acceptor (e.g. O-H···π) or both a weak donor and acceptor (e.g. C-H···π). One of the most common weak hydrogen

bonds is the C-H···O hydrogen bond, which when first introduced was fairly controversial, although is now accepted as a hydrogen bond.[15] Weak hydrogen bonds are not normally involved in directing primary hydrogen bonded motifs in crystal structures, however they play a subtle role in directing other elements of the crystal packing. One such example is the formation of homodimers in the 1:1 complex of 3,5-dinitrobenzoic acid and 4-dimethylaminobenzoic acid (normally heterodimers are preferred); in this case, homodimers are formed as the sterics of the component molecules are not favourable for C-H···O hydrogen bond formation if heterodimers were to form and these secondary interactions are important in defining the overall crystal packing.[16]

1.2.4 Bifurcated Hydrogen Bonds

Bifurcated hydrogen bonds (**Figure 1.3**) are a special category of hydrogen bonds which involve more than one donor or acceptor group within a single interaction. Where there are two acceptors (labelled as *DHAA*), these are often called three-centred hydrogen bonds due to the hydrogen atom being bonded to three atoms. Hydrogen bonds which involve multiple donor groups and one acceptor may also be referred to as bifurcated hydrogen bonds, specifically bifurcated donor hydrogen bonds (labelled as *DDHHA*).[17] Bifurcated hydrogen bonds arise due to the flexibility of hydrogen bonds and their long range nature which allows the interaction of multiple groups. They are often found where there is a mismatch between the number of hydrogen bond donors and acceptors in a system; formation of bifurcated hydrogen bonds means that all hydrogen bond donor and acceptor groups may be satisfied.

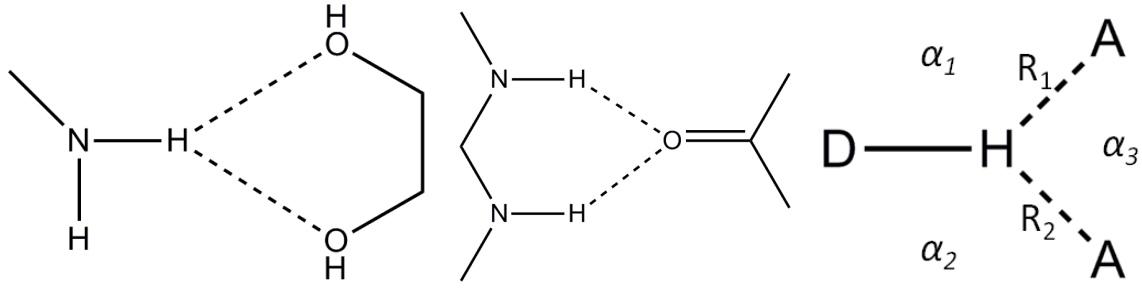

Figure 1.3 *An example of a DHAA bifurcated hydrogen bond (left), a DDHHA bifurcated hydrogen bond (centre) and a generalised schematic showing a three-centred hydrogen bond (right) with labelled bond distances (R_i) and angles (α_i).*[2]

Bifurcated hydrogen bonds may be symmetric ($R_1 = R_2$) or asymmetric ($R_1 \neq R_2$), with the latter being more common. *DHAA* bifurcated hydrogen bonds have certain geometric constraints, as they are formed from three attractive interactions to the hydrogen atom which results in the hydrogen lying approximately in the plane formed by the donor and

acceptor atoms. This results in the sum of the angles α_1, α_2 and α_3 being ~360° for a planar *DHAA* bifurcated hydrogen bond (**Figure 1.3**, right). Asymmetric bifurcated hydrogen bonds will consist of a major (stronger) and a minor (weaker) component. Normally the major component will be a moderate hydrogen bond while the minor component is a weak hydrogen bond. Symmetric bifurcated hydrogen bonds are made up of two fairly equal (often moderate) hydrogen bonds with similar D···A distances and angles. As with other types of hydrogen bonds, bifurcated hydrogen bonds may be used as a design element in crystal engineering studies.[18]

1.3 Other Intermolecular Interactions

1.3.1 Halogen Bonding

Halogen bonding[19] is a highly directional attractive interaction which involves donor and acceptor groups, in a similar manner to hydrogen bonding, where a halogen atom acts as an electron density acceptor group. A halogen bond will take the form A-B···X-Y, with B being an electron donor and X a halogen atom whilst A and Y are either carbon, nitrogen or another halogen atom. These non-covalent interactions can also play a role in determining crystal packing motifs and can be used in crystal engineering studies to develop desirable architectures,[20] sometimes competing with hydrogen bonds.[21] Generally they are viewed as not being as important as hydrogen bonds in crystal engineering as they are less common. The main difference between halogen and hydrogen bonding is in which groups can act as donors and acceptors. In hydrogen bonds, the hydrogen atom acts as an electron density acceptor whilst in a halogen bond this is replaced with a halogen atom. Halogen bonds can be classed as either type I or type II with the definitions based on bond angles. A type I halogen bond has the B···X-Y angle, θ_1, and the A-B···X angle, θ_2, equal ($\theta_1 = \theta_2$), whilst a type II halogen bond has θ_1 and θ_2 such that the donor and acceptor groups are approximately at right angles with values of $\theta_1 \approx 180°$ and $\theta_2 \approx 90°$.[22]

1.3.2 π Interactions

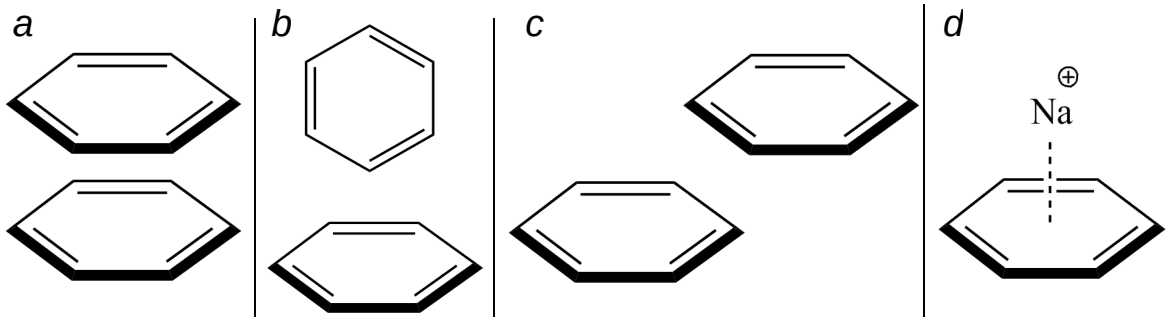

Figure 1.4 *Examples of the three conformations of π···π stacking: sandwich conformation (a), T-shaped conformation (b) and parallel-displaced conformation (c); and a cation···π interaction (d).*

There are various, generally weak, attractive interactions involving π electrons which includes the X-H···π hydrogen bonds mentioned in **Section 1.2.3**. However, the most common interaction for π electrons to be involved in are the π···π interactions (stacking)[23] of aromatic rings. There are three ways in which π ···π stacking may occur; in a sandwich conformation, a T-shaped conformation or a parallel-displaced stacked conformation (**Figure 1.4**). Cations may also form an attractive interaction to the face of an electron rich π system[24] (**Figure 1.4**) whilst the opposite interaction, anion···π interactions, are also possible where the π system is electron deficient. π interactions are of importance in many biological systems; for example they play a role in determining how proteins fold.[25]

1.4 Crystal Engineering

Crystal engineering[26-28] is the design of molecular solid-state architectures with a view to controlling the physical and chemical properties of a material. Crystal engineering studies involve the use of non-covalent interactions to design architectures, with the two most common approaches using either hydrogen bonds or coordination bonds to metal centres.[28] This normally involves attempting to grow crystals which contain more than one molecular component, known as co-crystallisation. There are many reasons for incorporating multiple components into the same crystal matrix. In the pharmaceutical industry this is often done to alter the physical properties, such as the solubility or melting point, of an active pharmaceutical ingredient (API) with a view to producing more effective drugs. Within crystal engineering studies, co-crystallisation can be used to design specific structural motifs which may have desirable properties. Co-crystallisation has been used to produce the majority of the materials studied in this work.

There has been debate as to the correct nomenclature for materials produced from co-crystallisation experiments; this has mainly centred on the use of the term co-crystal.[29-32]

This will be touched upon in **Section 1.6**; however, for simplicity, crystals which contain more than one molecular component will be described as "molecular complexes" throughout this work.

The design of molecular solid-state architectures is achieved through the use of building blocks which interact with one another in a predictable manner; the building blocks are commonly called supramolecular synthons.[33] Likely interactions can be predicted by following certain intuitive rules as to how molecules may interact in the solid-state, observing common structural motifs from the literature (by utilising structural databases such as the Cambridge Structural Database (CSD)),[34] and through the use of theory. The last of these can involve either *ab initio* structure prediction (a very difficult task) or the use of quantum chemical calculations to gauge the strength, nature and likelihood of possible interactions between different elements of the materials under study. Crystal engineering is applied in a wide variety of fields, as the need to produce solid-state materials with desirable properties is relevant in many areas of research. Recent studies have also utilised weaker interactions to attempt to direct crystal packing; these can include halogen bonds[19] and weaker hydrogen bonds (e.g. C-H···O[35] and C-H···π[36]). The effect of these weaker interactions on subtle aspects of the crystal structure is often not well-defined and this is an area which will be investigated in this work.

The use of hydrogen bonds in crystal engineering studies was made simpler after a set of rules were formalised by Etter in 1990.[37] The three general rules are:

- All good proton donors and acceptors are used in hydrogen bonding;
- Six membered ring intramolecular hydrogen bonds form in preference to intermolecular hydrogen bonds;
- The best proton donors and acceptors remaining after intramolecular hydrogen bond formation form intermolecular hydrogen bonds to one another.

Several rules for specific classes of functional groups are also given which include nitroanilines, diarylureas, nucleotide base complexes and finally carboxylic acid complexes with 2-aminopyrimidine.[37] These rules, which have been shown to have a degree of generality across many structures since their formation, aid in the prediction of how certain functional groups may interact in the solid-state and has led to certain functional groups and / or combinations of functional groups being favoured in crystal engineering studies, such as carboxylic acids, hydroxyl groups, amide groups and pyridine nitrogens. The rule stating that the best donors will hydrogen bond to the best

acceptors explains why heteromeric interactions are favourable to homomeric interactions in molecular complexes, as found by a recent survey of the CSD.[38]

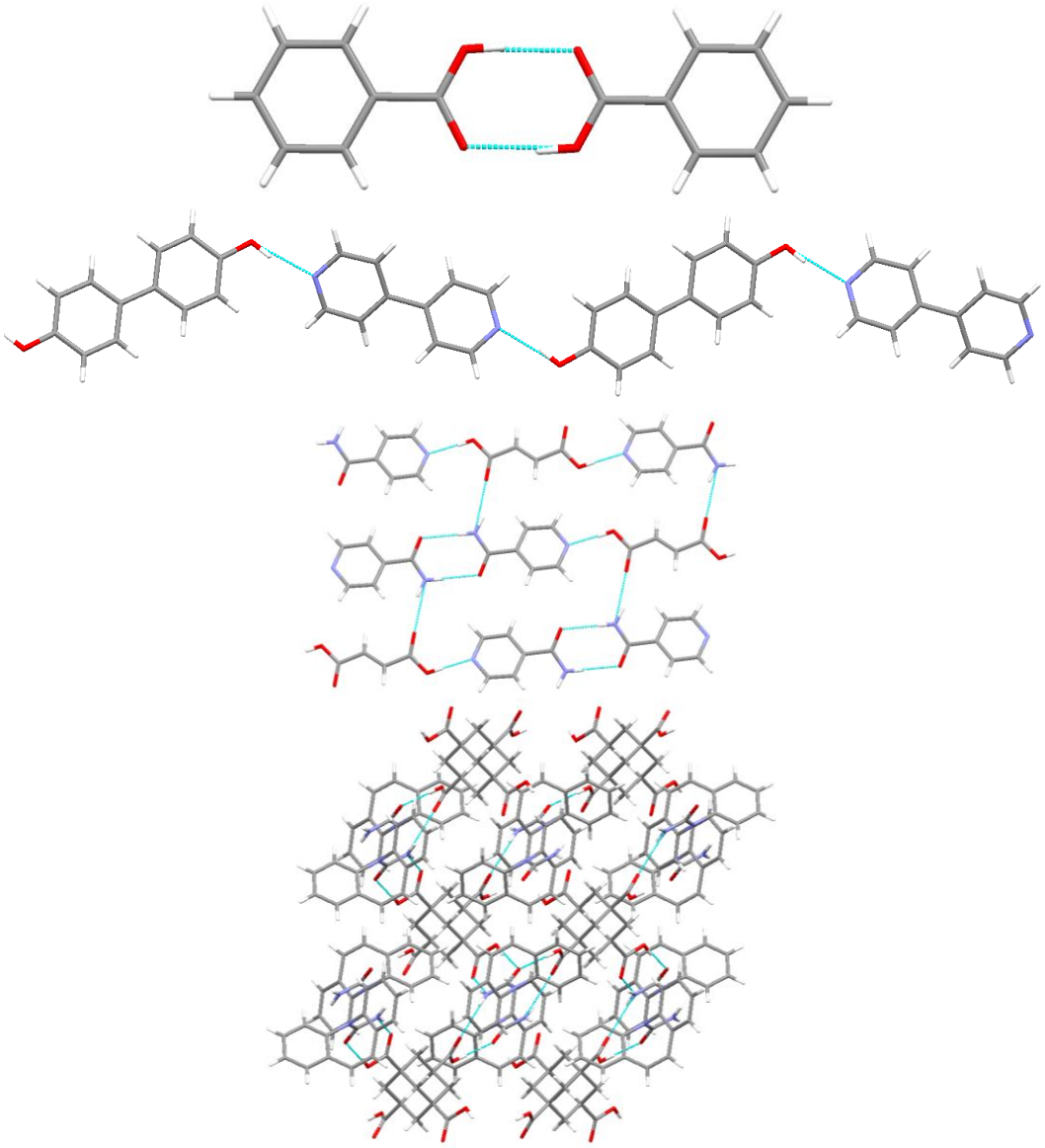

Figure 1.5 *Examples of hydrogen bonded architectures, from top to bottom: a 0-D dimer motif in benzoic acid,*[39] *a 1-D chain motif in a 1:1 complex of 4,4'-biphenol and 4,4'-bipyridine,*[40] *a 2-D sheet motif in the 2:1 complex of isonicotinamide and fumaric acid*[41] *and a 3-D motif in a 1:1 complex of carbamazepine and adamantane-1,3,5,7-tetracarboxylic acid.*[42]

There are two conventions when describing hydrogen bonded architectures in the solid-state. The first relates to the dimensionality of the hydrogen bonded network, this can be zero-dimensional (0-D), one-dimensional (1-D), two-dimensional (2-D) or three-dimensional (3-D). While there are no discrete aggregates in the solid-state due to the weak interactions which will inevitably form, structures can contain hydrogen bonded units

which do not associate strongly with other units within the structure; these structures have 0-D hydrogen bonded networks. An example of hydrogen bonded units which fall into this category would be carboxylic acid dimers, e.g. dimers of benzoic acid (**Figure 1.5**).[39] 1-D assemblies contain hydrogen bonded motifs that extend in one direction such as chains or ribbons; for example the molecular chain formed in the 1:1 complex of 4,4'-biphenol and 4,4'-bipyridine (**Figure 1.5**).[40] 2-D assemblies have hydrogen bonded networks which extend in two directions, these include many layered structures; an example is the 2-D hydrogen bonded sheets formed in the 2:1 complex of isonicotinamide and fumaric acid.[41] The final class, 3-D assemblies, have hydrogen bond networks which extend in every direction; an example would be the 3-D hydrogen bonded network in the 1:1 complex of carbamazepine and adamantane-1,3,5,7-tetracarboxylic acid.[42]

The other convention when describing hydrogen bond motifs is based on the use of graph-set notation and was developed by Etter in 1990.[37] Four kinds of motifs can be described, these are: chains (denoted by the letter C), rings (R), dimers and other finite sets (D) and intramolecular hydrogen bonds (S). The number of hydrogen bond donors and acceptors are assigned as subscripts and superscripts, respectively, while the number of atoms involved in the motif is placed in brackets. Using this notation, the carboxylic acid dimer in benzoic acid (**Figure 1.5**, top) would be designated as an $R_2^2(8)$ hydrogen bonded ring. Certain molecules and functional groups will form specific hydrogen bonded motifs preferentially when possible and these motifs can thus be ranked in terms of their likelihood. The use of graph-set notation can therefore aid in the design of hydrogen bonded architectures by applying this *a priori* knowledge of preferred motifs.

Crystal engineering studies can also utilise coordination bonds to metal centres. This approach is most commonly used to produce metal organic frameworks (MOFs), which consist of metal centres joined to organic linkers which create a framework structure. These structures often contain large pores[43] and potential applications include hydrogen storage,[44] carbon dioxide storage,[45] gas separation[46] and catalysis.[47]

Crystal engineering aims to design useful materials through knowledge of the likely interactions which will take place between structural elements. Whilst there are many examples of crystal engineering principles being applied successfully, there are still many challenges; these include polymorphism (see **Section 1.5**), solvate formation, the formation of unwanted reaction products and determining the solid form the target material will take (i.e. single crystal, powder or amorphous solid). Many of these challenges can be overcome by careful selection of the crystallisation conditions; however this usually involves a trial and error approach and often a certain amount of serendipity.

1.5 Polymorphism

Polymorphism[48] is when there is more than one crystalline form of a material differing only in the relative arrangement of the molecules. There have been many studies into polymorphism and how it may be controlled, but it is still not well understood and is difficult to control.[49] Different polymorphs may have different chemical and physical properties due to their different packing arrangements. This is of particular importance in the pharmaceutical industry where polymorphism can affect the bioactivity and bioavailability of APIs.[50,51] Polymorph control may be achieved through careful selection of the crystallisation conditions (e.g. solvent, temperature, etc.) or through seeding with crystals of the desired polymorph.[52,53] However, successful growth of a particular polymorph *via* a certain set of crystallisation conditions does not mean it will be produced every time under those same conditions and there are several examples of so called "disappearing polymorphs" where a polymorph which could once be routinely produced is no longer found.[54]

1.6 Proton Transfer

Proton transfer is the movement of a proton from one chemical species to another. This form of charge transfer is the basis of acid-base chemistry where hydrogen ions are transferred from an acidic species to a basic species. Hydrogen bonds can facilitate proton transfer and such processes are of importance in many areas including enzyme action.[55] Proton transfer normally results in charged donor and acceptor species which can lead to charge-assisted hydrogen bonds; this knowledge can be incorporated into crystal engineering studies to design materials containing charge-assisted, SSHBs in a predictable manner.[9]

In co-crystallisation experiments, the protonation state of the component materials in the resulting crystal structure is not only important in terms of the properties of the material but also in terms of the nomenclature with regards to the product. Whilst in this work the products of co-crystallisation experiments are referred to as molecular complexes, in general, when a proton is transferred from one component to another the product is referred to as a salt while if no proton transfer occurs the product is referred to as a co-crystal. As the aim of crystal engineering studies is to be able to bring elements of design and predictability to solid-state architectures, being able to predict any possible proton transfer would aid in these goals. One method that can be used in this respect is pK_a matching;[56] this method uses ΔpK_a (ΔpK_a = pK_a(base) - pK_a(acid)) values to predict whether proton transfer is likely to occur in a particular molecular complex system. It is

generally accepted that a ΔpK_a of greater than ~2 - 3 will result in proton transfer and the formation of salt whilst a ΔpK_a value of less than 0 will result in neutral co-crystal formation.[56-58] In the 0 - 3 range of ΔpK_a values, results tend to be inconclusive as to whether a salt or co-crystal will form.[56] The use of pK_a matching has other weaknesses when it comes to predicting proton transfer in the solid-state, the first of which is that pK_a values are measured in solution and may not transfer directly into the solid-state. Other difficulties arise due to the $\Delta pK_a^{50\%}$ point (where the concentrations of conjugate acid and conjugate base are equal in solution) being temperature dependent, and for complexes that do not have a 1:1 stoichiometry.[59] Further to these points is the class of compounds which show a hydrogen atom centred within a hydrogen bond and are therefore an intermediate state between salt and co-crystal; these complexes often have ΔpK_a values within the 0 - 3 range or close to these boundary values.[60] Despite these difficulties pK_a matching of molecules in the solid-state can still provide a useful guide as to whether proton transfer may be expected to occur.

When proton transfer occurs in a molecular complex it can be described as being either a static or dynamic effect. Static proton transfer is when a proton is transferred from one component to another and remains there despite varying external conditions such as temperature and / or pressure. Dynamic proton transfer is when the degree of proton transfer can be tuned by varying the temperature or pressure during the experiment. Static proton transfer is the most common form whilst dynamic effects are less common and less studied as a consequence. Examples of dynamic proton transfer effects include temperature / pressure dependent proton migration or disorder (see **Section 1.7** and **Section 1.8**). Dynamic proton transfer is a potentially useful property; for example in the 1:1 complex of squaric acid and 4,4'-bipyridine temperature and pressure dependent proton transfer was observed which was accompanied by a colour change;[61] such materials have potential uses as temperature and / or pressure sensors.

1.7 Proton Migration

Proton migration is a dynamic proton transfer effect in the solid-state, in which a proton migrates along a hydrogen bond as the temperature or pressure is varied. The effect is normally observed in SSHBs where the shape of the hydrogen bond PES (a flat bottomed single well, **Figure 1.1**, left) means that the hydrogen atom can move along the hydrogen bond with relatively little cost in energy. Proton migration is a desirable physical property for a material to possess as it is potentially "tunable" (by varying temperature or pressure) and therefore enables control of the degree of charge transfer. Proton migration is still not

a well understood phenomenon, in part due to the relatively few examples which have been found to date but also due to the fact that it can be difficult to observe. Variable temperature neutron diffraction data is usually required to observe definitively any migration of the hydrogen atom as the effect is very subtle and requires extremely accurate location of the hydrogen atom.[60,62-65] As most crystallographic studies are conducted using X-rays, migration may be missed (though X-ray studies can give some indications as to whether migration is present).[66] Computational studies can also play an important role when studying materials that display proton migration as they allow access to information which can confirm the presence of migration and lead to a greater understanding of the underlying causes.[67-69]

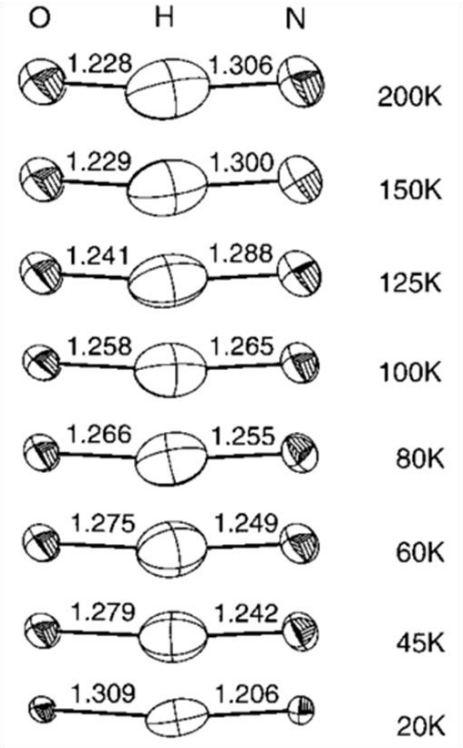

Figure 1.6 *The O-H···N hydrogen bond in the complex of pentachlorophenol and 4-methylpyridine showing the hydrogen atom migrating across the hydrogen bond as the temperature is varied.*[60]

One of the first studies to explicitly mention tunable proton migration was by Steiner *et al* in 2001.[60] In the paper, the authors presented neutron data which confirmed the presence of variable temperature proton migration in an intermolecular O-H···N hydrogen bond in the complex of pentachlorophenol and 4-methylpyridine (**Figure 1.6**). Previous X-ray studies had shown the presence of an O-H···N SSHB within the structure (O···N distance of 2.515(4) Å at 80 K),[60] though it was not possible to locate the hydrogen atom within the bond. Variable temperature structural determinations were carried out using single crystal

neutron diffraction at eight temperatures over the 20 - 200 K temperature range. The results showed that as the temperature was increased, the hydrogen atom moved from being closer to the acceptor atom to be closer to the donor atom; over the temperature range studied the D···A distance also increased slightly. The authors stated that the migration was either the result of increased thermal population of an unchanging asymmetric hydrogen bond PES or due to the shape of the PES itself being temperature dependent. The diffraction data from the complex were insufficient to make an informed decision between the two possibilities.

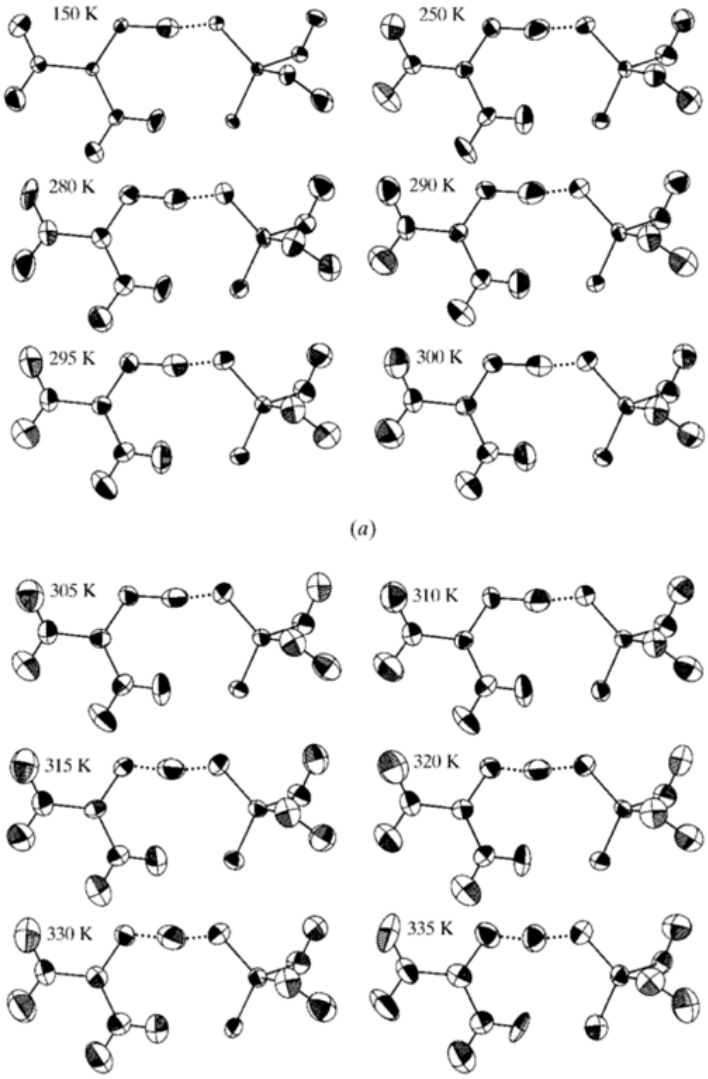

Figure 1.7 *The evolution of the short, strong hydrogen bond with temperature in the complex of urea and phosphoric acid.*[62]

Perhaps the best known system to date which displays proton migration is the 1:1 complex of urea and phosphoric acid (**Figure 1.7**). This complex has been the subject of several studies examining proton migration in the intermolecular O-H···O hydrogen bond

formed between the two materials.[62,63,66-69] As with the previous example of the complex of pentachlorophenol and 4-methylpyridine, variable temperature neutron diffraction data is essential to locate accurately the hydrogen atom of interest. The first neutron study of the urea phosphoric acid complex was conducted in 1972 by Kostansek and Busing.[70] They found that the hydrogen atom of the O-H···O SSHB (O···O distance of 2.421(3) Å at room temperature (RT)), which was not located in previous X-ray studies,[71,72] was approximately centred within the hydrogen bond and displayed a thermal ellipsoid which was elongated in the direction of the hydrogen bond at RT. Such behaviour is often indicative of a proton disordered over two sites. A second neutron structural determination by Harkema in 1993[73] at 100 K found that the SSHB was more asymmetric at lower temperature than in the previous RT study and the thermal ellipsoid was no longer elongated as it was in the structure determined at RT. This led to Wilson and co-workers conducting a series of variable temperature neutron measurements investigating whether the hydrogen atom migrated across the bond as the temperature was varied.[62,63] Over a temperature range of 150 - 350 K, the results showed that at low temperatures the hydrogen bond is asymmetric with the hydrogen atom residing closer to the acceptor atom on the urea molecule, while as the temperature is increased the proton migrates toward the donor atom and is approximately centred in the hydrogen bond at 350 K. Unlike in the complex of pentachlorophenol and 4-methylpyridine, the O···O distance of the SSHB remains invariant over the full temperature range. It was suggested that the migration in this complex is a result of a change in the shape of the hydrogen bond PES as the temperature is varied.

Wilson and Morrison followed up the confirmation of migration from the neutron data with a theoretical study in 2002.[67] Initial isolated molecule calculations did not reproduce the experimentally observed SSHB and instead produced a more conventional hydrogen bond with the hydrogen atom clearly bound to the donor molecule and an O···O distance of 2.61 Å. On the other hand, plane-wave density functional theory (DFT) calculations which produced a geometry optimised 0 K structure in a periodic (crystalline) environment, did reproduce the SSHB and showed a good agreement with the low temperature neutron data. Importantly, this showed the potential for computationally modelling proton migration systems.

The next study of urea phosphoric acid, a joint X-ray and neutron crystallographic study, was carried out by Parkin *et al.* in 2004.[66] While this study did not attempt to find the underlying features of the material which caused the proton within the short strong hydrogen bond to migrate, it did show that the migration may be observed from high

quality X-ray data, albeit with less accurate hydrogen atom positions. The authors also showed that the migration could be visualised using Fourier difference maps of the hydrogen bond with the hydrogen atom removed from the structural model. This is especially useful when trying to observe whether migration is present in a material during initial X-ray characterisations.

In 2005 Morrison *et al.* published a more in depth computational study of urea phosphoric acid.[68] Plane-wave DFT was used to carry out molecular dynamics (MD) simulations at four temperatures over a total simulation time frame of 0.6 ps; the first 0.2 ps of data was discarded and the remaining 0.4 ps was used to generate time-averaged theoretical structures. These structures agreed with those obtained from experiment and showed a similar level of migration to that seen in the variable temperature neutron diffraction experiments, though to a slightly lesser degree and with a more asymmetric hydrogen bond. The results also confirmed that the shape of the short strong hydrogen bond PES is temperature dependent, as was hypothesised by Wilson and co-workers.[62,63] The MD simulations also allowed access to the solid-state vibrational spectra at each temperature; these were in good agreement with a variable temperature IR/Raman study[74] and also allowed access to low energy vibrations which can be difficult to distinguish in experimental data. From these results the authors tentatively suggested that the migration is a consequence of coupling between the $-NH_2$ and -OH stretching modes.

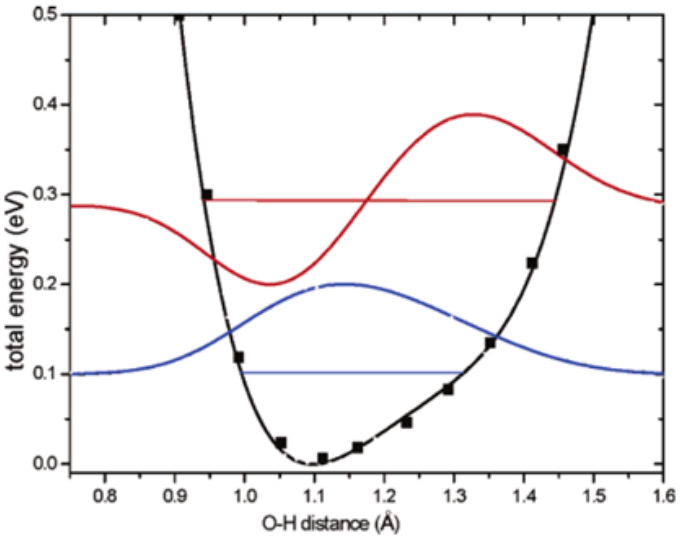

Figure 1.8 *The PES of the short, strong hydrogen bond in urea phosphoric acid (black curve). The lower blue curve shows the ground state wavefunction of the hydrogen atom (n = 0) while the upper red curve shows the first excited state (n = 1).*[69]

Fontaine-Vive *et al.*[69] then published another study on urea phosphoric acid, presenting inelastic neutron scattering (INS) data alongside complementary MD simulations and phonon calculations (**Figure 1.8**). The vibrational spectra generated from the MD and phonon calculations showed good agreement with the experimental INS data and the results again confirmed that the migration is not due to lattice expansion or the thermal population of higher vibrational energy levels in the PES. The authors stated that low energy lattice vibrations (phonons) modulate the short strong hydrogen bond PES and induce the temperature dependent migration through subtle changes in the local environment. They suggested that a large number of vibrational modes, mostly involving molecular rotation, are responsible and not simply the two that were suggested by Morrison *et al*.;[68] these differences were attributed to the simulations by Morrison *et al*. covering too short a simulation time frame to have adequate resolution with regards to the low energy modes.

Proton migration has also been observed in other materials; notably in the complex of benzene-1,2,4,5-tetracarboxylic acid and 4,4'-bipyridine[64] and also in the structure of pyridine-3,5-dicarboxylic acid.[65] In both of these materials the hydrogen atoms in the SSHBs migrate from a position closer to the acceptor atom at low temperature towards the donor at higher temperature. Both materials have also been studied using INS and theoretical calculations; the results showed a similar mechanism for the migration to urea phosphoric acid involving low energy vibrational modes modulating the PESs of the short strong hydrogens bonds. A combined neutron and DFT study of deuterated pyridine-3,5-dicarboxylic acid also showed migration in the short strong hydrogen (deuterium) bond.[75]

The work published on proton migration materials to date shows that, whilst progress has been made in understanding the underlying causes of migration, the small number of examples means that it is difficult to find an all encompassing theory to explain this subtle dynamic feature of short strong hydrogen bonds. This work aims to find further examples of materials which show temperature dependent proton migration and aid in the understanding of the processes behind migration and also how such materials may be designed in the future.

1.8 Proton Disorder

Proton disorder is another example of a dynamic proton transfer effect which may occur under specific circumstances in moderate strength hydrogen bonds. The PESs of these hydrogen bonds show an approximately symmetric double-well potential with a very small energy difference between the two sites. In such systems, it is typical for the hydrogen

atom to occupy one site at low temperature, with the hydrogen bond evolving in such a manner that a second site becomes increasingly occupied as the temperature is increased. As with proton migration, this subtle dynamic proton effect is best characterised using neutron diffraction data where accurate hydrogen atom occupancies can be refined. Because most crystallographic studies are conducted using X-ray diffraction where disorder is less obvious, and many researchers are not looking for proton disorder, there may be cases where disorder is present but is missed. Recently it has been shown that occupancies can also be refined from high resolution X-ray data which give good agreement with the neutron data.[76] Evidence for proton disorder from X-ray data may be deduced from larger than expected hydrogen thermal parameters, trends in bond lengths involving non-hydrogen atoms, for example approximately equal C-O and C=O bond lengths in the carboxylic acid group, and visualisation of two electron density peaks in Fourier difference maps.

Proton disorder is once again a tunable solid-state charge transfer process where the degree of charge transfer can be controlled by varying the temperature and / or pressure. Combined X-ray and neutron studies, complemented with theoretical calculations, provide the best route towards explaining the underlying causes of the disorder and can play a role in the future design of materials which exhibit this potentially useful property.

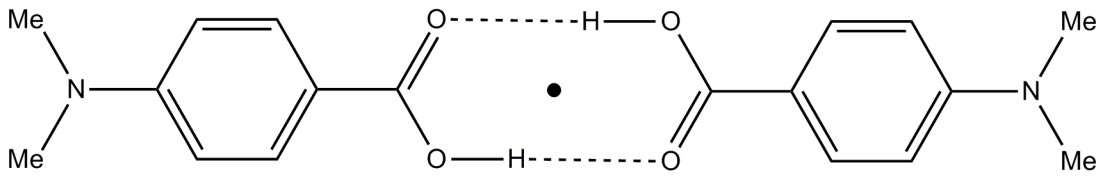

Figure 1.9 *The 4-dimethylaminobenzoic acid dimer, a system known to show proton disorder, showing the inversion centre in the dimer (black dot).*

Benzoic acid dimers, containing the carboxylic acid group, are known to be systems in which temperature dependent proton disorder can be found. This is especially true of dimers which lie on an inversion centre containing molecules which are symmetrically substituted (**Figure 1.9**), though disorder is by no means present in all such systems. This class of benzoic acid dimers contains moderate strength hydrogen bonds with a symmetric double-well PES in an isolated dimer with the possible hydrogen atom sites equal in energy. In the solid-state, however, the crystal packing and local environment affects the PESs of the hydrogen bonds linking the molecules in the dimers, removing the symmetry, so the two positions are no longer identical in energy. However, proton

disorder is still more likely in these types of benzoic acid dimers due to the two possible sites being close in energy.

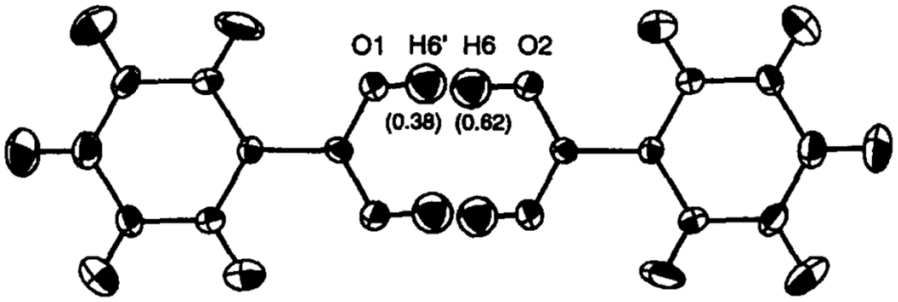

Figure 1.10 *A disordered dimer of benzoic acid at 175 K.*[77]

The best known, and most studied, material which exhibits proton disorder is benzoic acid itself (**Figure 1.10**).[39,77-81] The first X-ray study (RT), carried out by Sim *et al.* in 1955,[78] showed that the molecules formed planar dimers and had some evidence of disorder in the C-O and C=O bond lengths, though the hydrogen atoms could not be located. The next RT X-ray study by Bruno and co-workers in 1980[79] described the hydrogen atoms as being disordered over two positions within the hydrogen bond with relative occupancies of 50:50. A combined X-ray and neutron study was conducted in 1981 by Feld *et al*.[39] where disorder was assigned from the X-ray data; due to difficulties with the data, only a 5 K neutron structure was determined and did not display disorder, hinting at the temperature dependence of the effect. The definitive neutron studies were conducted by Wilson and co-workers in 1996[77,80] and data were collected at 5 temperatures from 20 to 175 K. The relative occupancies of the two hydrogen atom positions were found to evolve from 87:13 at 20 K to 62:38 at 175 K. This clearly showed the dynamic nature of the effect and how the degree of charge transfer could be controlled by temperature. A recent study has found that the proton disorder is also pressure dependent.[81] Benzoic acid has also been studied by a number of spectroscopic techniques[82-87] and using computational methods.[88-91] These studies found that tunnelling and solid-state vibrations also facilitate the proton disorder along with the thermal population of higher energy states.

Proton disorder has also been found in other materials,[76,92-97] however in this work the focus is on one class of benzoic acids which have previously shown proton disorder (**Chapter 6**). Some recent studies have investigated how the local crystalline environment affects the energetics of hydrogen bonds which may exhibit proton disorder.[76,98] A study by Adam *et al.* in 2009[98] used X-ray and neutron diffraction data together with theoretical calculations to look at the structures of two isomeric compounds, 2,4-dihydroxybenzoic acid and 2,5-dihydroxybenzoic acid. In these studies, no disorder was found in these

benzoic acid dimers from the neutron diffraction data, and this was confirmed by the theoretical calculations of the relative energies of the various possible configurations. The calculations also showed how the local environment affects the energetics of hydrogen bonds linking the dimers, opening the possibility of tuning such hydrogen bonds in similar systems through the use of crystal engineering principles. Another study by Parkin *et al.* in 2007[76] looked at how small geometric changes, affected by the local environment, in 4-dimethylaminobenzoic acid dimers impacted on potential proton disorder within the hydrogen bonds linking the dimer; this is discussed further in **Chapter 6**. Similar effects are investigated in this work with the aim of further understanding proton disorder and how systems showing this behaviour may be designed and controlled.

1.9 Urea and its Derivatives

Urea (also known as carbamide) (**Figure 1.11**) is an organic molecule first discovered in 1773 and was the first organic molecule to be artificially synthesised in 1828. Due to its molecular simplicity, it was one of the first organic crystal structures solved by X-ray diffraction[99] and has been extensively studied, with 17 entries in the CSD[34] at the time of writing.

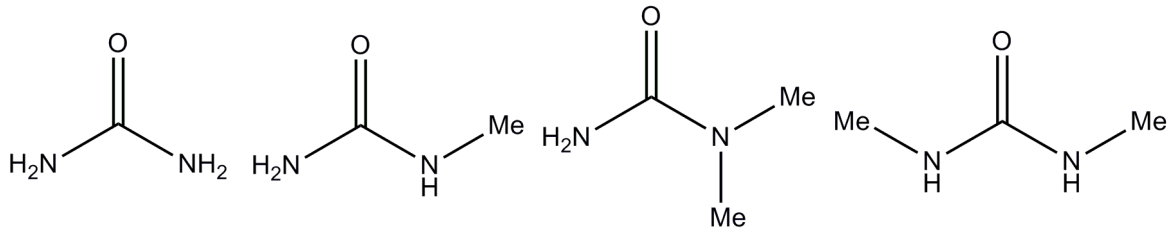

Figure 1.11 *From left to right: urea, N-methylurea, N,N-dimethylurea and N,N'-dimethylurea.*

Urea has been used extensively as a component in crystal engineering studies due its hydrogen bond forming potential, possessing two accessible hydrogen bond acceptor sites (from the two lone pairs of electrons on the carbonyl oxygen) and four hydrogen bond donor sites (from the two $-NH_2$ groups). This gives a total of six hydrogen bond donors and acceptors, all of which are used in the structure of pure urea (**Figure 1.12**). Another reason for interest in urea is the possibility that it may form predictable hydrogen bonded motifs.[100-105] As a basic material, urea is often complexed with one or more acidic components and it is well known that urea complexes can exhibit varying degrees of transfer of a hydrogen atom across a hydrogen bond from the acid molecule to urea. For example, in the 1:1 complex of urea-nitric acid, a proton is essentially fully transferred from the nitric acid to the urea carbonyl group to form a salt,[106,107] while in the 2:1 complex

of urea-oxalic acid the proton remains on the acid molecule. The latter of these, urea-oxalic acid, remains the only example of a complex of urea with an organic acid studied using neutron diffraction in both the 1:1 and 2:1 stoichiometries,[108,109] with both complexes showing a differing degree of proton transfer. This shows the importance of crystal environment (*via* stoichiometry) in determining the degree of transfer. Urea phosphoric acid (discussed in **Section 1.7**) provides an intermediate situation where the hydrogen atom is found close to the centre of the SSHB linking the two components.[62,63] The fact that urea complexes show this variation makes them an attractive target system when attempting to construct architectures containing SSHBs.

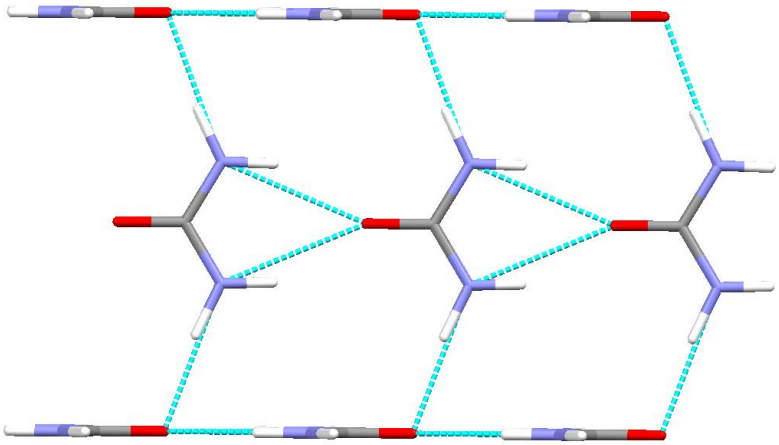

Figure 1.12 *The structure of urea showing the tape motif which involves bifurcated hydrogen bonds.*[110]

A recent study by Alhalaweh *et al.*[105] investigated common structural motifs found in urea-dicarboxylic acid complexes and found that the stoichiometry of the complex determines whether the solid-state structure formed is based on one of three distinct supramolecular motifs: U-A (urea-acid)(1:1), U-A-U (2:1), or A-U-A (1:2). This element of predictability in the structures of urea complexes opens the possibility for the design of materials with predictable hydrogen bond motifs, solid-state arrangements, and (potentially) degree of proton transfer, with a view to introducing potentially useful physical properties.

Complexes of substituted ureas are much less common than those of the parent material. While they may still allow the formation of the SSHBs which are of interest in this work, the effect of substitution on the hydrogen bonded network and the overall crystal structure provides an added level of interest to the study of these materials. There are only two examples of *N*-methylurea complexed with organic acids (nitric acid[111] and oxalic acid),[112] whilst neither *N,N*-dimethylurea or *N,N'*-dimethylurea have previously been reported in such complexes with organic acids.

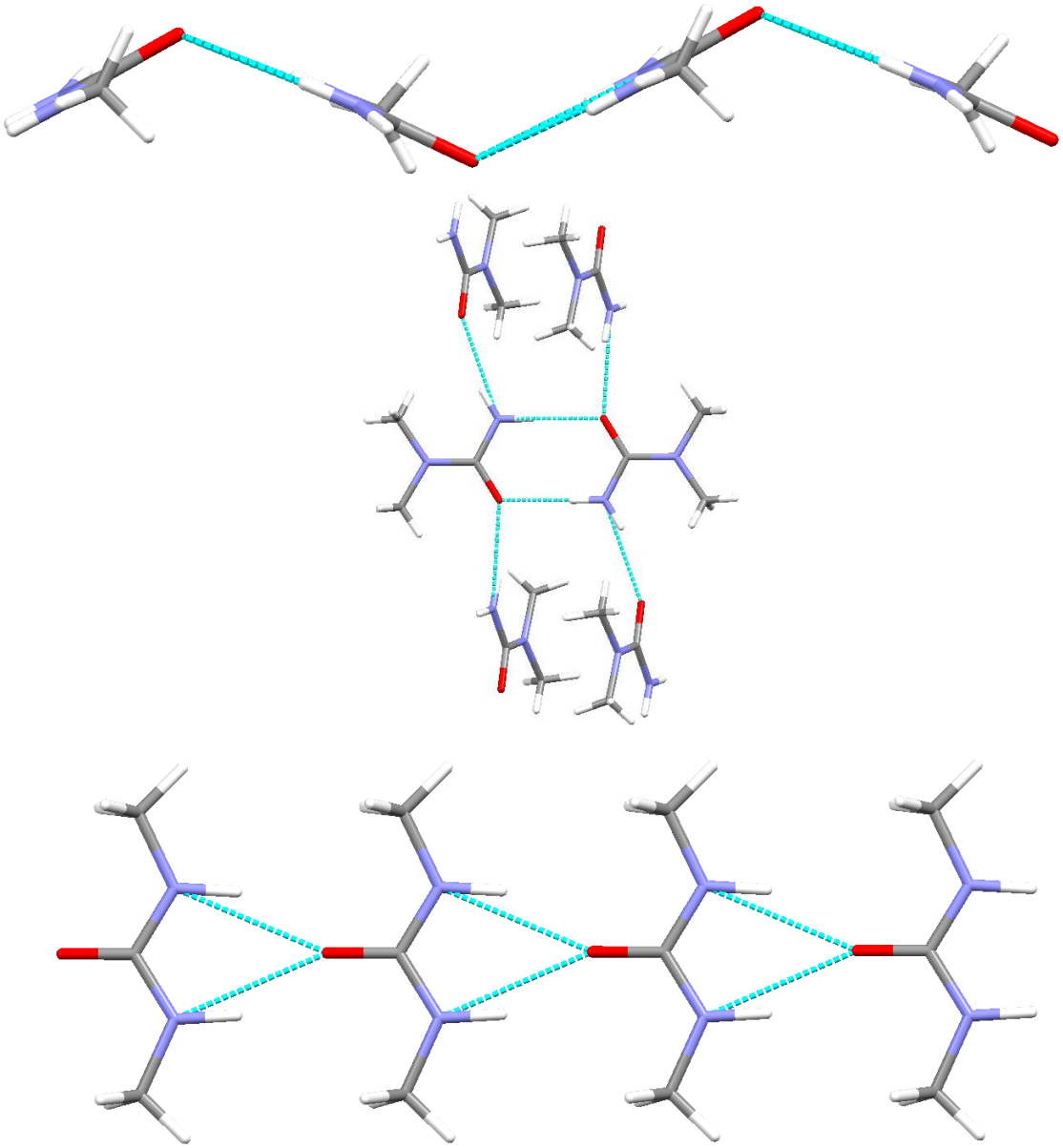

Figure 1.13 *The structures of N-methylurea (top),*[113] *N,N-dimethylurea (centre)*[114] *and the Cc polymorph of N,N'-dimethylurea (bottom).*[115]

The addition of methyl groups to urea affects the crystal packing of the pure materials. Whilst planar tapes form in the structure of urea, in the structure of *N*-methylurea tapes with a herring bone arrangement form and the hydrogen bonds between tapes are altered due to the presence of the methyl group (**Figure 1.13**, top).[113] In the structure of *N,N*-dimethylurea (**Figure 1.13**, centre), dimers form through amide···amide interactions with only one hydrogen bond donor and acceptor left on each molecule to interact with other dimers.[114,116] The structure of *N,N'*-dimethylurea (**Figure 1.13**, bottom), for which there are two polymorphs with similar structures, shows planar tapes formed, similar to those in

urea. However, the only interactions between other tapes are weak C-H···N interactions.[115,117]

The simple substitution of urea, a component known to form complexes exhibiting proton migration effects (e.g. in urea phosphoric acid), allows the effect of subtle changes on the electronics of a predictable hydrogen bonded unit to be probed and the effect of other weaker interactions influencing the proton migration unit to be investigated. The use of methylureas (**Figure 1.11**) instead of urea would not be expected to alter the primary hydrogen bonding motifs but could encourage the formation of shorter, stronger hydrogen bonds due to an increased basicity of the urea moiety. This key crystal engineering design principle could thus enhance the potential for synthesising complexes likely to exhibit interesting properties such as proton migration. This effect has already been observed in the complex of *N*-methylurea and oxalic acid,[112] in which a hydrogen bond was formed which was shorter than those seen in the related urea oxalic acid complexes.[108,109]

Urea has also been used in the solid-state to create urea inclusion compounds (also known as clathrates, host-guest compounds and adducts).[118] In these materials urea molecules form a hexagonal porous network where the pore dimensions are of the order of molecular dimensions and may therefore host guest molecules.

1.10 DMAN

1,8-Bis(dimethylamino)naphthalene (DMAN)[119] is a highly basic molecule which may form stable ionic complexes with a variety of acids. When complexed with an acid the DMAN molecule will often accept a proton (becoming $DMANH^+$) and form a strong intramolecular $[N\cdots H\cdots N]^+$ hydrogen bond (**Figure 1.14**). For this reason, DMAN may be classed as a proton sponge.[120] The addition of substituents to the naphthalene rings makes it possible to tune the N···N distance,[121] with there now being a large number of naphthalene-based proton sponges in existence.[122]

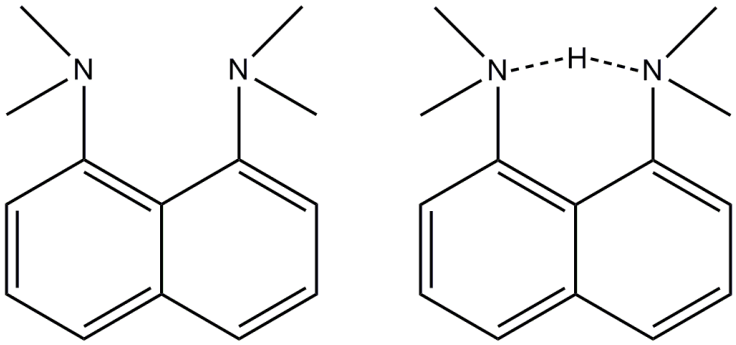

Figure 1.14 *Unprotonated (left) and protonated (right) DMAN molecules.*

The proton within the intramolecular N-H···N hydrogen bond in complexes of DMAN does not always take up the same position within the hydrogen bond. An X-ray charge density study of four DMAN-acid complexes found that the electron density in the N-H···N hydrogen bond was asymmetric and dependent on the local environment.[123] In other work, a variable temperature X-ray study of the complex of DMAN with 4,5-dichlorophthalic acid found that the behaviour of the hydrogen atom electron density within the N-H···N intramolecular hydrogen bond was temperature dependent.[124] At lower temperatures the hydrogen atom electron density appeared disordered over two sites while at higher temperatures the density was smeared out across the bond, suggesting behaviour similar to that observed in proton migration materials. This change in the behaviour of the hydrogen atom was attributed to changes in the local environment of the molecule arising from the expansion of the lattice with temperature.

A recent study by Kállay[125] studied a range of DMAN-acid complexes and found that the behaviour of the hydrogen atom within the N-H···N hydrogen bond may depend on the acid component of the complex, though the hydrogen atom positions were ambiguous from the X-ray diffraction data. In this work, neutron data has been collected on a number of the complexes studied by Kállay to understand better how hydrogen atoms behave and how this may be related to the local environment of the molecules. In several of the complexes studied by Kállay the acid component of the complex is a substituted benzoic acid, which forms a single strong charge-assisted O-H···O hydrogen bond linking pairs of acid molecules in a dimer. These types of bond are also relevant for study using neutron diffraction as they may also show anomalous hydrogen atom behaviour which could only be accurately described using this technique.

Chapter 2

2. Theory

2.1 Crystallography

Crystallography is the study of the structure of crystalline materials by diffraction of electromagnetic radiation or particles. A crystalline solid is a material made up of a large number of identical units (consisting of atoms or molecules) arranged in a regular and ordered manner. A basic unit is defined (the unit cell) which is repeated by translation infinitely in each direction, making up the crystal. The most common diffraction experiments for studying crystalline materials use X-rays, while neutrons, which have been used extensively in this work, and electrons can also be used. Neutron diffraction experiments are less common due to the large scale facilities (reactors or accelerator-based sources) needed to generate an adequate flux of neutrons, while electron diffraction experiments primarily probe the surface of a sample and not the bulk. Each technique has its own advantages and disadvantages and each provides different types of information about the structure of materials due to the different ways in which the radiation or particles are scattered from the sample.

2.1.1 The Lattice and Unit Cell

Table 2.1 *Unit cell types with possible lengths and angles and the possible Bravais lattices.*

Triclinic	$a \neq b \neq c$	$\alpha \neq \beta \neq \gamma \neq 90°$	P
Monoclinic	$a \neq b \neq c$	$\alpha = \gamma = 90° \beta \neq 90°$	P, C
Orthorhombic	$a \neq b \neq c$	$\alpha = \beta = \gamma = 90°$	P, C, F, I
Tetragonal	$a = b \neq c$	$\alpha = \beta = \gamma = 90°$	P, I
Rhombohedral **Or**	$a = b \neq c$ $a = b = c$	$\alpha = \beta = 90° \gamma = 120°$ $\alpha = \beta = \gamma < 120°$	R
Hexagonal	$a = b \neq c$	$\alpha = \beta = 90° \gamma = 120°$	
Cubic	$a = b = c$	$\alpha = \beta = \gamma = 90°$	P, I, F

P = primitive, C = centred, F = face-centred, I = body-centred, R = rhombohedral

A crystalline material can be thought of as a lattice made up of a regular array of identical points. These points are related by translation and on each point the basic repeating unit, or unit cell, can be placed. The three-dimensional unit cell is described by the lengths of

the three cell edges (*a*, *b*, *c*) and the three angles between them (*α*, *β*, *γ*). There are seven types of crystal systems depending on the unit cell parameters and the relationships between these (**Table 2.1**).

There are many possibilities when choosing a unit cell and any set of lattice points can be described using a primitive cell containing one lattice point. If using a primitive cell, the choice of cell is often arbitrary; however if there is symmetry present it is conventional to describe the cell so that it best displays the symmetry elements of the structure. This often means choosing a unit cell that contains more than one lattice point, leading to centred and rhombohedral cells, which are termed non-primitive cell settings. Centred cells can be centred on two faces, centred on all faces (face-centred) or be body-centred; the different combinations of these with the seven crystal systems give the 14 Bravais lattices (**Table 2.1**). In addition, several types of internal symmetry are allowed within the unit cells, including mirror planes, rotation axes and inversion. The different combinations of these symmetry elements give rise to 32 point groups. The point groups can be combined with translational symmetry elements within the unit cell (glide planes and screw axes) to give a total of 230 possible space groups to which all crystals belong. In terms of describing the contents of the unit cell, a sub-unit of the cell is defined, the asymmetric unit, which when the internal symmetry of the cell is applied followed by translation in all directions, builds up the entire crystal.

2.2 Diffraction

2.2.1 History

The theory of diffraction was known long before it was used as a technique to study crystalline materials leading to the field of crystallography. The first steps were taken towards the study of atomic structures using diffraction with the discovery of X-rays by Röntgen in 1895[126] and then when Max von Laue first demonstrated that they could be diffracted by crystals in 1912.[127] This led to the first atomic scale structural determination from an X-ray diffraction pattern in 1913, the structure of table salt.[128] Several other simple inorganic structures were determined shortly after, with the first organic structure being determined in 1923.[129] These early discoveries spawned the growth of the field of crystallography which is now relevant in many areas of chemistry, physics and biology. Thanks to modern technology and techniques, determining the structure of a material can be a quick and straight forward process and gives information on the atomic positions, atomic motions about these positions (thermal parameters) and any inter- or intramolecular bonding involved in the material under study.

2.2.2 Diffraction of X-rays, Neutrons and Electrons

As stated in **Section 2.1**, diffraction experiments mostly use one of X-rays, neutrons or electrons. The main difference between X-ray, neutron and electron diffraction is the way in which the different forms of radiation interact with matter. X-rays are a form of electromagnetic radiation which interact with the electron clouds of atoms and can be used to probe the electronic structure of the sample. Neutrons are neutral particles which interact with the nuclei of atoms through the nuclear strong force and this yields information of the nuclear positions in a crystal structure. While neutrons have no charge they do have a spin meaning that they can also interact with unpaired electron spins, giving information about the magnetic structure of a material. Due to the small size of the nucleus of an atom relative to the electron cloud surrounding it, neutrons penetrate very deeply into samples, probing the bulk, and meaning that larger samples are often required. Both X-rays and neutrons typically have wavelengths of the order of Ångstroms so are ideally suited to studying molecular structures due to the similarity in magnitude to chemical bond lengths. Electrons are charged particles which interact with the electron cloud of an atom through the Coulomb force. As this is a strong interaction electrons do not penetrate significantly into a sample and hence electron diffraction is mainly a surface technique.

Diffraction from each unit cell in the sample contributes to the diffraction pattern which contains many diffraction peaks or reflections. The observed positions and intensities of these peaks can be treated mathematically to give information about the location of the atoms within the sample and reveal the crystal structure.

X-ray single crystal diffraction is the principal technique used for crystal structure determination, routinely being used as a rapid and accurate method for studying molecular crystal structures. X-ray powder diffraction is used mainly to characterise samples though modern techniques now allow for structure determination from powder diffraction data alone. Neutrons can be used for both single crystal and powder diffraction though these techniques are less common due to the large facilities needed to generate neutrons. These are typically large scale national or international facilities and experiments are often costly and time consuming when compared with routine laboratory X-ray experiments. For the study of small or weakly diffracting samples and / or samples with very large unit cells (e.g. proteins) powerful X-ray beams generated at synchrotron facilities can be used. Again these experiments are not routine due to the large scale facilities required.

2.2.3 The Laue Equations

When a crystal is placed in an incident beam of radiation of appropriate wavelength diffraction can occur. The diffraction pattern that is recorded during an experiment is created due to the constructive and destructive interference of diffracted beams. Each scattered beam will travel a different distance and for constructive interference to occur the scattered beams must be in phase with one another; in other words the difference in path length must be equal to an integer number of wavelengths. This can be visualised for a one-dimensional array of atoms (**Figure 2.1**):

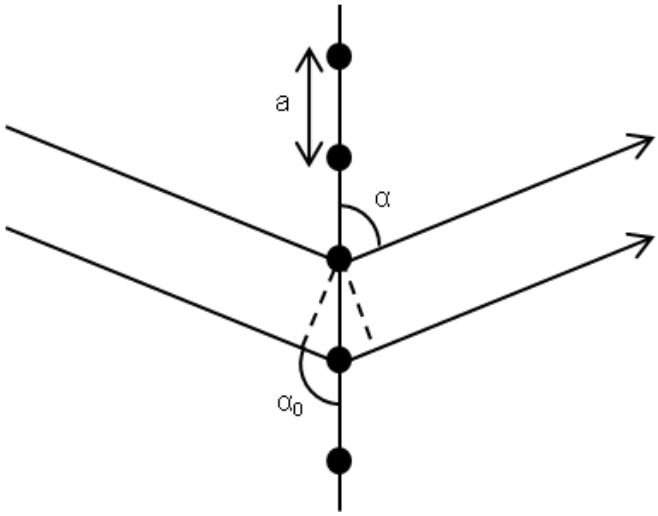

Figure 2.1 *Diffraction from a one-dimensional array of atoms.*

From **Figure 2.1**, the difference in path length for diffracted beams from atoms separated by distance *a* can thus be expressed as:

Equation 2.1 $\text{Path difference} = a \cdot \cos\alpha - a \cdot \cos\alpha_0 = h\lambda$

where α and α_0 are the angles of the diffracted and incident beams, respectively. When considering three dimensions there are three equations which must be satisfied; these are the Laue equations:

Equation 2.2 $a(\cos\alpha - \cos\alpha_0) = h\lambda$

Equation 2.3 $b(\cos\beta - \cos\beta_0) = k\lambda$

Equation 2.4 $c(\cos\gamma - \cos\gamma_0) = l\lambda$

These equations contain the interatomic spacings *a, b* and *c*, the angle of the incident and diffracted beams, integers *h, k* and *l* and the wavelength, λ. The Laue equations provide a

useful way for visualising how diffraction occurs and when these equations are satisfied constructive interference occurs and a diffraction spot is observed.

2.2.4 Bragg's Law

A more common way to visualise the diffraction process is through Bragg's law. A diffraction spot is formed when constructive interference takes place between diffracted beams from parallel planes; this only happens when these beams are in phase with one another. As for the Laue equations, for beams to be in phase, the difference in the path length of the beam through the sample must be equal to an integer number of wavelengths of the radiation used (**Figure 2.2**).

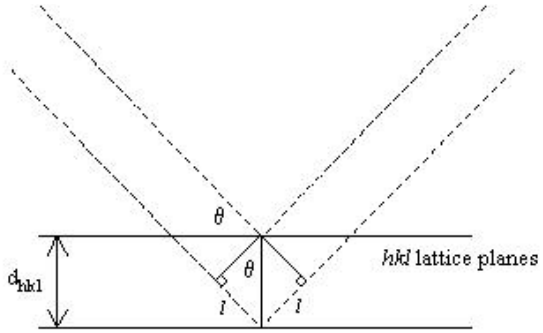

Figure 2.2 *Diagram of Bragg's law and the difference in path length between two diffracted beams.*

The path difference (*2l*) can be calculated from the angle of incidence of the radiation relative to the plane (θ) and the distance between the parallel planes d_{hkl} (**Figure 2.2**). Bragg's law can therefore be summarised by **Equation 2.5** below:

Equation 2.5 $\quad$ *Path difference* $(l + l) = n\lambda = 2d_{hkl}\sin\theta_{hkl}$

where *n* is an integer and λ is the wavelength of the incident beam of radiation.

Each spot recorded in the diffraction pattern is assigned a set of Miller indices (*hkl*). These Miller indices represent the plane within the crystal which the X-rays were diffracted from. The planes cut through the unit cell axes at *a*/*h*, *b*/*k* and *c*/*l*; where *a*, *b* and *c* are the unit cell axes. Certain spots may appear in the diffraction pattern more than once depending on the symmetry of the system being studied and data collection strategy being implemented.

2.2.5 Reciprocal Space and the Ewald Sphere

Reciprocal space is another important concept in diffraction experiments. The interference of X-ray beams leads to a three-dimensional pattern of spots, which is then

measured in two dimensions on the detector of a diffractometer. These spots can also be related to the so-called reciprocal lattice, in which each set of parallel lattice planes is represented by a point in reciprocal space whose position is determined by the inverse of the lattice spacing ($1/d_{hkl}$) and the direction of the perpendicular to the lattice plane. The lattice can be described in reciprocal space with dimensions $\underline{a}^*$, $\underline{b}^*$ and $\underline{c}^*$ from **Equation 2.6**:

Equation 2.6 $\underline{a}^* = (\underline{b} \times \underline{c})/V \quad \underline{b}^* = (\underline{a} \times \underline{c})/V \quad \underline{c}^* = (\underline{a} \times \underline{b})/V$

where $\underline{a}$, $\underline{b}$ and $\underline{c}$ are vectors representing the unit cell dimensions in real space and V is the volume of the unit cell.

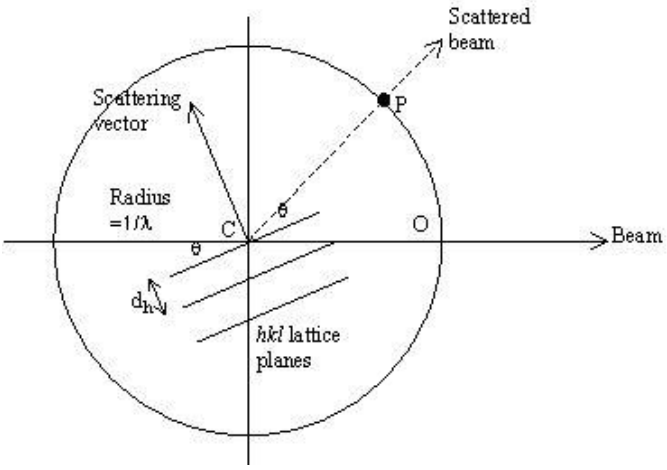

Figure 2.3 *Ewald sphere showing diffraction from parallel planes.*

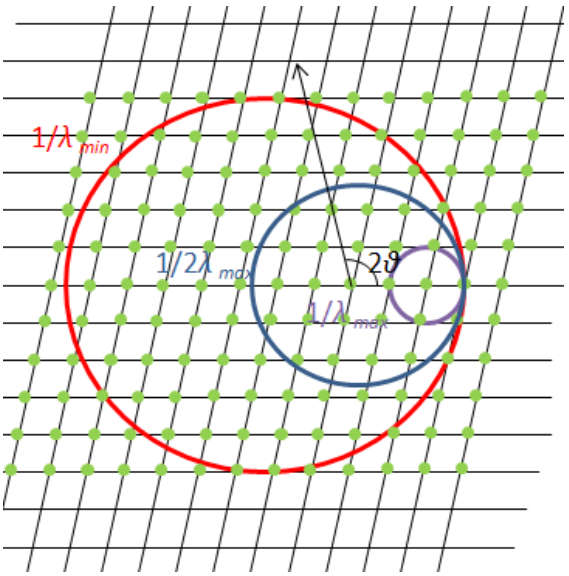

Figure 2.4 *Ewald sphere for Laue diffraction: all reciprocal lattice points located between the λ_{min} and λ_{max} spheres will be collected in one image.*

Another important visualisation tool is the Ewald sphere (**Figure 2.3**) which allows the determination of the location of Bragg spots. To construct the sphere, the crystal is placed at the centre with a sphere of radius *1/λ* drawn around it (where *λ* is the wavelength of the incident radiation). The origin of reciprocal space is then placed on the edge of the sphere. For a diffracted beam to be measured, the scattering vector must be equal in length and in the same direction as a vector going from the origin O, to the reciprocal lattice point P. For Bragg's law to be satisfied, the reciprocal lattice point must be on the edge of the sphere; other lattice points can be observed by changing the orientation of the crystal so that they lie on the edge of the sphere.

Using a different wavelength changes the size of the sphere (**Figure 2.4**) and a larger λ will produce a small sphere. In experiments where a range of wavelengths is used (e.g. Laue diffraction) large sections of reciprocal space can be studied in one crystal orientation as all lattice points located between the λ_{min} and λ_{max} spheres can be measured on one image. This is important in the context of this work due to the Laue method which has been used to collect the neutron diffraction data.

2.2.6 Fourier Synthesis

Once data have been collected, it is then necessary to interpret the diffraction patterns obtained. As peak intensities are measured in reciprocal space the first step is to transfer from reciprocal space back into real space where the crystal structure resides. This can be done mathematically using a Fourier transform, transforming the diffraction pattern into an electron density map from which a model of the crystal structure can be produced. The intensities of the diffraction spots in a pattern are related to the atoms present in the unit cell, though these are also affected by other properties of the crystal such as size, quality, absorbance and mosaicity. Before a Fourier transform takes place a series of corrections are applied to the measured intensities to account for absorption, extinction, etc. The quantity that is related to the scattering density in a diffraction experiment is the structure factor, F_{hkl}, which is proportional to the square root of the intensity, I_{hkl}:

Equation 2.7

$$|F_{hkl}| \propto \sqrt{I_{hkl}}$$

The structure factor can be expressed in terms of the atoms in the unit cell, providing a link between the observed diffraction and the molecular structure:

Equation 2.8

$$F(hkl) = \sum_{j=1}^{N} f_j \exp[2\pi i(hx_j+ky_j+lz_j)]$$

summing over N atoms in the unit cell, with the atom *j* having an atomic scattering factor f_j and position x_j, y_j, z_j in the unit cell.

Equation 2.9 $$B_i = 8\pi^2 U_i^2$$

Structure factors are affected by the atom type and also the Debye-Waller temperature factors. As X-rays are scattered by electrons, heavier atoms have a larger atomic scattering factor (f_j) as this increases with Z^2. The Debye-Waller factor, *B*, takes into account the effect of temperature on peak intensities and can be calculated from **Equation 2.9**, where B_i is the Debye-Waller factor for atom *i* and U_i^2 is the mean square displacement the atom. At higher temperatures a smearing out of the electron cloud occurs from thermal motion; this is most prominent for reflections at larger Bragg angle and affects X-ray determined structure factors more significantly than neutrons due to the small size of the nucleus. For neutron experiments the structure factor is replaced by the neutron scattering length.

The electron density in the cell is then represented by:

Equation 2.10 $$\rho(x,y,z) = 1/V \sum_{hkl} F(hkl)\, exp[-2\pi i(hx+ky+lz)]$$

where *V* is the volume of the unit cell and (*x*, *y*, *z)* the fractional coordinates within the unit cell. In order that this expression can be evaluated to allow the link between observed diffraction pattern and the molecular structure, not only the observed magnitude but also the phase of the structure factor F_{hkl} must be known. The process by which these phases are determined is called structure solution and is discussed below.

2.2.7 Structure Solution

Crystal structures are not normally solved from neutron data and all the structures presented in this work were first solved from X-ray data. In this section only structure solution from X-ray data will be discussed.

2.2.7.1 The Phase Problem

To be able to calculate the electron density and therefore solve the crystal structure all of the structure factors are needed (**Equations 2.8** and **2.10**); these should contain a magnitude and a phase. A reverse Fourier transform can then be applied to find the electron density and the structure can be solved. Unfortunately only the intensities are measured in an experiment and all the phase information is lost; this is known as the crystallographic phase problem. Several methods have been developed to resolve this

problem and with the chemical knowledge of the user the correct structure solution can be found.

2.2.7.2 Patterson Method

The Patterson method can be used in cases where there are heavy atoms present within the sample. It solves the phase problem by using the square of the structure factors to set all phases to 0 and generates a Patterson map:

Equation 2.11 $$P(x,y,z) = 1/V \sum_{hkl} |F(hkl)|^2 \exp[-2\pi i(hx+ky+lz)]$$

This is a map of interatomic vectors which has the largest peak located at (0,0,0) from the self-vectors of all atoms in the cell. The next largest peak will be the vector between a heavy atom and the equivalent heavy atom in the next molecule. Knowledge of the vectors between these atoms allows initial atomic coordinates to be found for the heavy atoms. From these an approximate set of phases can be generated and a starting structural model can be made. Fourier difference methods can then be used to find the rest of the atoms in the structure.

2.2.7.3 Direct Methods

By far the most common method for overcoming the phase problem is by using direct methods, a trial and error method. Arbitrary phases are assigned to the strongest reflections and the relationships between reflections are then used to generate phases for other reflections. Several assumptions are made, two of the most important are firstly, that the electron density is always positive and secondly, that atoms are discrete and have the same size, i.e. they are concentrated at well-defined maxima. These assumptions place limits on the possible structure factors which should only affect the possible phases (as the intensities have been measured directly during the experiment). Direct methods uses complicated mathematical relationships and so requires powerful computers. When the method was first introduced this posed a problem; however, the development of modern computing means that direct methods is now the most popular method of structure solution, particularly within the field of small molecule crystallography.

Placing the constraint that atoms are discrete and are the same size has two effects. The first is that the electron density map will contain peaks corresponding to the atoms making it easier to locate them. The second is that the atomic size no longer affects the structure factor as now all atoms have the same size; this means that structure factors can be converted into *E* values, or normalised structure factors. These values are normalised over a range of scattering angles to account for the fall off in intensity at higher angles.

Sayre defined a relationship stating that the *E* value of any reflection *hkl* can be calculated as the sum of the product of all pairs of reflections that sum to it:

Equation 2.12 $$E_{321} = E_{100} \,.\, E_{221} + E_{110} \,.\, E_{211} + E_{111} \,.\, E_{210} + \ldots$$

If one or both reflections in a pair are weak, then they do not contribute strongly to the E_{hkl} of a strong reflection and so can be ignored at first. For centrosymmetric space groups, this knowledge can be used to find the probable sign of the phase (+ or -) through the triplet, or $\sum_2$, relationship where three strong reflections are grouped together based on **Equation 2.12**:

Equation 2.13 $$E_{hkl} \approx E_{h'k'l'} \,.\, E_{h-h',\, k-k',\, l-l'}$$

This allows the probable sign of the phase of E_{hkl} to be determined from the signs of $E_{h'k'l'}$ and $E_{h-h',\, k-k',\, l-l'}$. If $E_{h'k'l'}$ and $E_{h-h',\, k-k',\, l-l'}$ have the same sign then the sign of E_{hkl} is probably positive whereas if they have a different sign it is probably negative. The probability of these phases being correct is related to the number of atoms, *N*, in the unit cell, hence direct methods works best for smaller molecular structures. This probability, *p*, can be expressed as:

Equation 2.14 $$p = \tfrac{1}{2} + \tfrac{1}{2}\tanh\left[(1/\sqrt{N})E_{hkl}E_{h'k'l'}E_{h-h',\, k-k',\, l-l'}\right]$$

Solution of the phase problem for structures with non-centrosymmetric space groups is slightly more complicated. Instead of finding the probable sign as in centrosymmetric structures, it is the probable phase angle, Φ_{hkl}, which must be found. A phase relationship similar to **Equation 2.13** can be derived:

Equation 2.15 $$\Phi_{hkl} \approx \Phi_{h'k'l'} \,.\, \Phi_{h-h',\, k-k',\, l-l'}$$

The phase, Φ_{hkl}, is normally derived from a large number of triplet relationships and, to this purpose, the tangent formula was developed:

Equation 2.16 $$\tan\Phi_{hkl} = \left(\sum_{h'k'l'} \chi \,.\, \sin(\Phi_{h'k'l'} + \Phi_{h-h',\, k-k',\, l-l'}\right) / \left(\sum_{h'k'l'} \chi \,.\, \cos(\Phi_{h'k'l'} + \Phi_{h-h',\, k-k',\, l-l'}\right)$$

where $\chi = N^{-1/2} \left|E_{hkl}E_{h'k'l'}E_{h-h',\, k-k',\, l-l'}\right|$ and is related to the probability of each relationship being correct in a similar way to **Equation 2.14**.

To begin structure solution, a starting set of reflections with “known” phases are used. A number of reflections with large *E* values where there is a high probability that the phase can be estimated correctly are then added to this list and these reflections make up the starting set of phases. From here an iterative process is used to assign more and more *E*

values until enough have been determined that a Fourier synthesis will reveal the positions of most or all of the atoms. If not all of the atoms are revealed, Fourier difference methods can be used to complete the structure. Depending on the software being used, atoms are assigned to electron density peaks either automatically or manually by the user.

2.2.7.4 Charge Flipping[130,131]

Charge flipping is the most recently developed method of solving the phase problem and is a dual-space iterative method (it uses constraints on both the diffraction data in reciprocal space and electron density in real space). No information on the chemical composition or symmetry of the material under study is needed; the only requirement is a single crystal of suitable quality for a diffraction experiment. All structures are solved in *P*1 (the lowest symmetry space group) and symmetry is added later using information from both the diffraction pattern and the electron density map. The two most significant constraints which are applied in charge flipping are that the electron density must be positive and the unit cell consists of individual atoms (i.e. there are a limited number of separated point-like electron density peaks in the cell), similar to the assumptions made when using direct methods. The charge flipping algorithm starts with the experimentally observed intensities and a set of randomly generated phases from which an electron density grid of the unit cell is generated. A small, positive threshold value (δ) for the electron density is set and any values below this threshold are multiplied by -1 (the charge is flipped); any values left below zero are removed. A new set of phases is then generated and the cycle is continued until certain convergence criteria are met. Charge flipping works especially well when heavy atoms are present, although it also gives reliable solutions of structures containing only light elements with up to 1000 atoms in the unit cell.

2.2.8 Structure Refinement

Once initial atomic positions have been found using one of the structure solution methods, the structural model is refined so it is in better agreement with the observed diffraction data. A least squares method is used to alter the positional (*x, y* and *z* coordinates) and thermal parameters of each atom to improve the model. The thermal parameters for each atom can be refined either isotropically (as a sphere with one parameter) or anisotropically (as an ellipsoid with six parameters). In X-ray structures all non-hydrogen atoms should be refined anisotropically and hydrogen atoms isotropically while in neutron structures all

atoms can be refined anisotropically. The level of agreement of the model with the observed data can be gauged using the crystallographic R-factor:

Equation 2.17 $$R = (\sum ||F_o| - |F_c||) / (\sum |F_o|)$$

Equation 2.18 $$wR2 = \sqrt{((\sum w(F_o^2 - F_c^2)^2) / (\sum w(F_o^2)^2))}$$

As the model is improved with each refinement cycle, the R-factor (**Equation 2.17**) should drop. Typical values for good data are usually around 0.02-0.07. If the observed data and structural model were in perfect agreement then the R-factor would be equal to zero; this is not possible as there are always errors inherent in the data while there may also be some complexities in the structure (e.g. disorder) which cannot be accurately modelled. The weighted R-factor (**Equation 2.18**) is based on weights for each reflection based on the uncertainty associated with that reflection and uses the structure factor squared. This should also decrease as the model is improved though its value will be larger than R.

Another way to evaluate the quality of the structural model is through the goodness of fit (S):

Equation 2.19 $$S = \sqrt{((\sum [w(F^o_{hkl}{}^2 - F^c_{hkl}{}^2)]) / (n-p))}$$

where n is the number of reflections and p is the number of parameters used in the refinement. This value should be close to one for a good data set with a good structural model. Generally the more data collected, the better the data set and more parameters which can be refined reliably. A good data to parameter ratio is normally in excess of 10 reflections for each parameter.

2.2.9 Fourier Difference Maps

In many cases it is not possible to find all of the atoms in the asymmetric unit directly from the electron density map generated from the structure solution; this is particularly true of hydrogen atoms. Once a refinement cycle has been carried out, a Fourier difference map can be generated which shows electron density peaks not accounted for in the current structural model (**Equation 2.20**). Atoms can be assigned to these peaks giving a better structural model and the refinement cycle repeated until all atoms have been accounted for. Hydrogen atoms are the last to be added to the model, ideally after all the other heavier atoms have been refined with anisotropic thermal parameters; this is because peaks corresponding to hydrogen atoms will be significantly smaller than those of heavier atoms due to X-ray scattering power increasing with Z. Fourier difference maps also show when an atom type has been wrongly assigned by either the presence of residual

electron density (if the type assigned has too few electrons) or a trough in the map (if the assigned atom has too many electrons).

Equation 2.20 $$\Delta\rho\,(x,y,z) = \sum_{hkl}(|F^{o}_{hkl}|-|F^{c}_{hkl}|)\exp(-2\pi i(hx+ky+lz)+\alpha^{c}_{hkl})$$

Background noise is always present in Fourier difference maps and there are a variety of sources. The most common sources are thermal motion of the atoms and electron density not accounted in the structural model (e.g. lone pairs, bonding density, etc.). Thermal motion causes all atoms in the structure to vibrate around the equilibrium position and causes electron density to be smeared out; this is particularly prominent when collecting data at higher temperatures where the maps will have significantly higher background noise. Anisotropically refined atoms are usually refined using an ellipsoid which cannot take anharmonic thermal motion into account and this will add to the background. In high-resolution data sets, peaks often appear between bonded atoms representing the bonding density; analysis of these difference maps can give insight into the nature of the bonds between atoms.

2.3 Neutron Diffraction

While advancements in diffractometers and data processing software now means that it is fairly routine to refine (isotropically) hydrogen atom parameters from high-resolution X-ray data, the technique still has certain limitations. In cases where there is unusual hydrogen atom behaviour or heavy atoms are present within the structure, it is often not possible to describe the hydrogen atom behaviour accurately using only X-ray data; this is due to the process by which X-rays are scattered by atoms. As stated in **2.2**, X-rays are scattered by electrons via the Coulomb force and the scattering intensity is proportional to Z^2, meaning that a carbon atom will scatter 36 times more strongly relative to a hydrogen atom. This causes all non-hydrogen atoms to dominate the diffraction pattern and in cases where hydrogen atoms are disordered with only partial occupancy, the problem of describing the hydrogen behaviour is exacerbated further.

Neutrons, on the other hand, are scattered from the nuclei of atoms via the nuclear strong force. The neutron scattering lengths do not vary in the same way with Z as those for X-rays and the values for each element have more of a random distribution (**Figure 2.5**). They still have some dependence on Z though, and the scattering factors vary depending on the number of protons and neutrons present in the nuclei. This is important as it means that neutrons can be used to distinguish between elements close to each other in the periodic table and also different isotopes of the same element, as the scattering

lengths will be different. Neutron scattering lengths tend to be of the same order of magnitude as each other and values do not differ as greatly as those for X-rays, though some elements have a negative scattering factor. Hydrogen is one of the elements with a negative scattering length so appears as a trough when viewed in a Fourier difference map. These combined factors mean that neutron diffraction is the ideal technique for unambiguous refinement of the positional and anisotropic thermal parameters of hydrogen atoms.

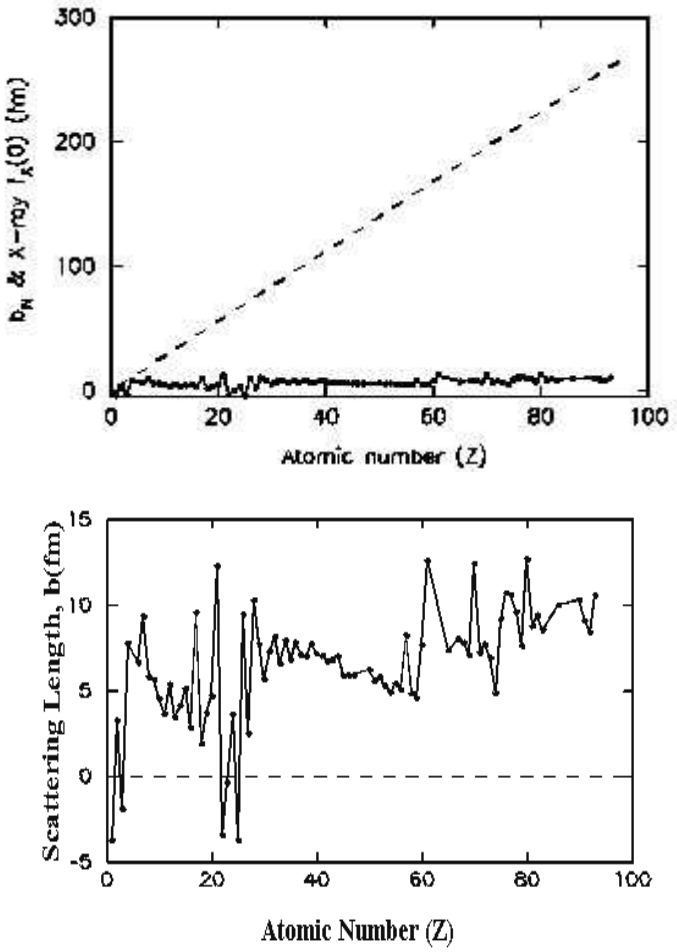

Figure 2.5 *X-ray scattering factors (dotted line) compared with those for neutrons (top) and an expanded view of neutron scattering factors (bottom).*

One other reason why neutron diffraction would be preferable to X-ray diffraction is that it is relatively easier to obtain high-resolution data. This is due to the fall off in scattering factor with increasing scattering angle for X-rays. This occurs because of the large size of the electron cloud and makes it difficult to obtain good intensities at high angles, corresponding to small d-spacings and therefore higher resolution data. Neutron diffraction does not suffer from this problem as the atomic nuclei by which neutrons are

scattered are much smaller and closer in nature to a point-like object. It should be remembered that there will still, however, be a fall off in intensity at higher temperatures as thermal motion still affects the intensities.

2.4 Computational Chemistry

Computational chemistry has grown rapidly as a field in recent years driven by the increasing power and availability of modern computers so that there are now very few areas which could not benefit from theoretical modelling. Different types of calculations can be performed ranging from *ab initio* quantum mechanical studies to those based on classical mechanics. The type of calculation carried out depends on what information the user wishes to obtain and the type of system to be studied. While these calculations can never completely replace experimental studies, they can be used to complement experimental work by giving further information about the material under study. In the areas where theory and experiment overlap, agreement between the two can be used to strengthen observed experimental results. Calculations can also provide access to information which is not directly attainable by experiment, such as the energetics of specific bonds within a crystal structure or the behaviour of a material under extreme conditions.

2.4.1 Molecular Mechanics

Molecular mechanics, or force field methods, is the name given to calculations which use classical mechanics as their basis. In these types of calculations atoms are treated as being large enough to obey the laws of classical mechanics and are connected through bonds which behave like harmonic springs. Electrons are not treated as being large enough to obey these laws and so are ignored. The properties of functional groups are transferable so that, for example, all C-H bonds have the same properties regardless of the surrounding environment. Collecting this information from all of the functional groups and atoms in a system allows a force field to be generated which can give the energy penalty for any bond stretch, rotation, etc away from the lowest energy equilibrium structure. More sophisticated force fields can include terms which improve on the simple harmonic approximation and these can be tailored to model particular systems, e.g. proteins. The main advantage of these types of calculations is that they are relatively quick and computationally cheap so can be applied to large systems. There are however some major disadvantages. As electrons are ignored, any property which relates to the electronic structure is unavailable so the amount of information which can be extracted from the calculations is limited. Force fields are derived from experimental data, so the

types of systems for which a suitable force field exists is also restricted, meaning that there are many systems for which the use of quantum mechanical calculations is the only sensible approach.

2.4.2 Quantum Mechanical Calculations

Quantum mechanical calculations enable non-classical particles, such as electrons, to be considered in calculations and therefore provide much more information than is obtainable when using molecular mechanics. Quantum mechanics governs the behaviour of electrons, which are responsible for the interactions between atoms and molecules, and allows intra- and inter- molecular bonding to be investigated. The Schrödinger equation is the fundamental basis of quantum mechanics:

Equation 2.21 $$\hat{H}\Psi = (-\hbar/2m_e)\nabla^2\Psi + V\Psi = E\Psi$$

where $-(\hbar/2m_e)\nabla^2\Psi$ is the kinetic energy term, $V\Psi$ the potential energy term. $\hat{H}$, the Hamiltonian operator, therefore incorporates both the kinetic and potential energy terms. E is the total energy of the system. Ψ is the wavefunction, a mathematical description of an atomic orbital, the square of which is equal to the probability of finding an electron in a particular region of space. Quantum mechanical calculations aim to solve the Schrödinger equation for the system under study, however an exact solution can only be found in a few very specific cases such as the particle in a box, the harmonic oscillator and the hydrogen atom. This means that the Schrödinger equation is insoluble analytically for any of the systems studied in this work as these all contain more than one electron. The potential energy term in the Schrödinger equation accounts for the n^+ - n^+ repulsion, the e^- - e^- repulsion (which cannot be solved exactly for a multi-electron system) and the n^+ - e^- attraction. The kinetic energy term accounts for the kinetic energy of both the nuclei and the electrons. Therefore, to solve the Schrödinger equation in a multi-electron system, certain approximations must be made and different types of quantum mechanical calculations will use different approximations.

2.4.1.1 The Born-Oppenheimer Approximation

Atoms can be considered to be made up of the nuclei and the surrounding electrons. As electrons are much lighter than the nuclei and move at greater than 1000 times their speed, the nuclei can be considered as stationary with respect to the electrons and their kinetic energy set to zero. This means that the n^+ - n^+ repulsion term becomes a constant which can be calculated using Coulomb's law. This reduces the five terms involved in the Hamiltonian operator to three (kinetic energy of e^-, potential energy of e^- - e^- repulsion and

potential energy of n^+ - e^- attraction) and helps in finding an approximate solution to the Schrödinger equation.

2.4.1.2 Hartree-Fock Theory

Ideally, in an *N* electron system, it would be possible to solve the Schrödinger equation one electron at a time to give *N* atomic orbitals. This is not possible, as no account has been taken of the electron correlation and the electron exchange. Electron correlation is the fact that the movement of one electron will affect all others around it while electron exchange is the pairing up of electrons of opposite spins in molecular orbitals (obeying the Pauli exclusion principle).

The most drastic solution to the problem of electron correlation is to ignore it; this is done by presuming that each electron moves in a uniform field generated by the other electrons and is known as Hartree theory. By ignoring the electron correlation it is still possible to account for up to 99% of energy in a system, which for many calculations can be sufficient. The electron exchange can be taken into account using Fock theory. This uses an anti-symmetric wavefunction so that the Pauli exclusion principle is always satisfied. Combining the two gives Hartree-Fock theory which ignores electron correlation while calculating the electron exchange exactly. This is the most basic level of *ab initio* molecular orbital theory.

Molecular orbitals can then be expressed as a linear combination of atomic orbitals (LCAO):

Equation 2.22 $$\Psi = \sum_i c_i \Phi_i$$

A molecular orbital Ψ can be expressed as a sum of *i* Gaussian functions, Φ, representing atomic orbitals with a weighting coefficient *c*. This collection of Gaussian functions is known as a basis set.

Various methods have been developed to try and take account of the missing correlation energy while using Hartree-Fock theory as their basis. These different levels of theory include the Møller-Plesset series (MP), the couple cluster series (CC) and the configuration interaction (CI).

2.4.1.3 Polarisation and Diffuse Functions

Methods using basis sets based on atomic orbitals, such as Hartree-Fock theory, do not work as well when atoms come together to form molecules. When molecules are formed the atomic orbitals are likely to undergo significant change to their size, shape or charge.

The basis sets can be modified to include corrections for polarisation and diffuseness and so improve the model.

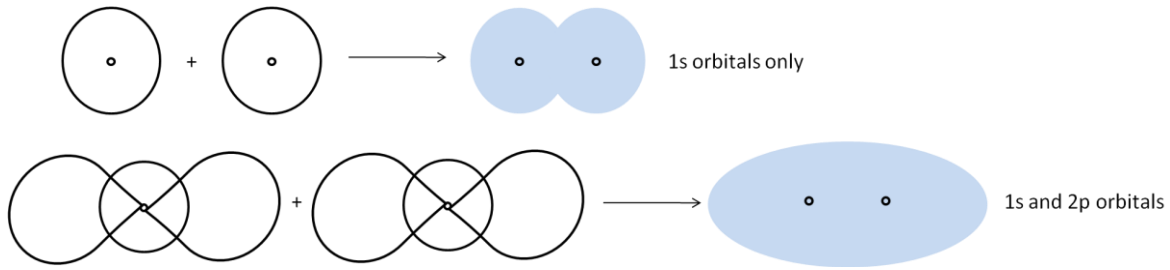

Figure 2.6 *The improved hydrogen molecular orbital model when the higher angular momentum 2p orbital is included.*

Polarisation functions allow the shape of the orbital to be changed by adding orbitals with higher angular momentum. For example, addition of a *p* orbital when molecular hydrogen is formed (**Figure 2.6**). These functions are so important that they included in almost all basis sets.

Diffuse functions allow the orbitals to occupy more space than they normally would. These are important for molecules which carry a negative charge, molecules in excited states or highly electronegative elements.

2.4.2 Density Functional Theory

Density functional theory (DFT) provides an alternative way of modelling matter by calculating the electron density, which is experimentally observable, as opposed to the wavefunction; in practice, however, single-electron wavefunctions are still used. The energy functional used in DFT can be defined as:

Equation 2.23 $$E[\rho(\mathbf{r})] = \int V_{ext}(\mathbf{r})\rho d\mathbf{r} + F[\rho(\mathbf{r})]$$

The energy is therefore the sum of two terms; the $V_{ext}(\mathbf{r})$ term accounts for the interactions of the nuclei and electrons via Coulomb's law while the $F[\rho(\mathbf{r})]$ term deals with the e^- - e^- interactions including the kinetic energy of the electrons. The Born-Oppenheimer approximation is still used to simplify the e^- - nuclei interactions. The $F[\rho(\mathbf{r})]$ term can be expressed as a sum of its three constituent parts:

Equation 2.24 $$F[\rho(\mathbf{r})] = E_{KC}[\rho(\mathbf{r})] + E_H[\rho(\mathbf{r})] + E_{XC}[\rho(\mathbf{r})]$$

$E_{KC}[\rho(\mathbf{r})]$ is the kinetic energy of non-interacting electrons, $E_H[\rho(\mathbf{r})]$ is the energy arising from the Coulomb interaction between electrons and $E_{XC}[\rho(\mathbf{r})]$ is the exchange-correlation

energy associated with both the electron exchange and the electron correlation. Difficulties again arise when calculating the exchange-correlation energy and so approximations must be made. Different approximations give rise to different types of functionals, the three most common methods are the localised density approximation (LDA), the generalised gradient approximation (GGA) and hybrid DFT.

Functionals using the LDA approach are based on a uniform electron gas where ρ is constant over all space. In reality the electron density is of course not uniform and varies from point to point in a system. Therefore in this approximation, the electron density is fixed over a certain small volume but can vary when moving from one volume element to another. LDA is a good model to use in metallic systems where the electron density does not change much from one point to another, but it is not well suited to molecular systems, in which the electron density can vary rapidly.

GGA functionals contain information on the gradient of the electron density and how it varies at each point along with its value. These types of functionals are more suited to the rapidly varying electron density observed in molecular systems.

Hybrid DFT uses elements of Hartree-Fock theory combined with DFT. Hartree-Fock theory calculates the electron exchange exactly while ignoring the electron correlation while DFT approximates both the exchange and correlation. Thus by combining the two methods it is possible to calculate the exact electron exchange while still being able to approximate the electron correlation. A well known example of a hybrid functional is B3LYP which combines all of the LDA, GGA and Hartree-Fock approaches to create a versatile functional suitable for use in many different systems.

2.4.2.1 Plane-waves and Pseudopotentials

The methods discussed so far have only dealt with isolated molecules in the gas phase; to carry out calculations in the solid-state further considerations must be made. The calculations must now take into account the periodic nature of the crystalline solid-state so periodic boundary conditions must be applied. The electrons are now essentially modelled as delocalised so the periodic boundary conditions are needed so that electrons do not fall off the end of the model and instead appear at the other side. The wavefunction is now represented as a series of plane-waves and can be expanded in terms of the reciprocal lattice vector, *G*, to give:

Equation 2.25 $$\Psi(r) = \sum c_G exp(\mathbf{i}G.\mathbf{r})$$

where $\Psi(r)$ is the molecular wavefunction at position $\boldsymbol{r}$, c_G is a weighting coefficient and $exp(iG.r)$ is the representation of a plane-wave.

The quality of the plane-wave basis set is defined by the energy cut-off value. This value is found when the addition of further plane-waves only lowers the total energy of the system by a negligible amount. This means that plane-wave basis sets are much more flexible than Gaussian basis sets and can be tuned to the specific system under study.

Modelling the electrons as delocalised and allowing them to move anywhere within the periodic boundary can create problems when the valence electrons interact with the core electrons. The valence electrons must maintain orthogonality with the core electrons and so areas with large amounts of kinetic energy develop around the nuclei; this is particularly true of systems containing heavy atoms as there are a larger number of core electrons. To model this accurately would require a basis set containing a huge number of plane-waves and the calculation would quickly become unmanageable.

The core electrons do not generally contribute to the chemical and physical properties of atoms and molecules and so can instead be replaced by pseudopotentials to simplify the calculations. The pseudopotential combines the core electrons and nuclei providing a screen for the valence electrons should they come too close to the core electrons. Using pseudopotentials in place of the core electrons means that fewer plane-waves are required in the basis set and the calculation becomes less computationally demanding.

2.4.3 Computational Simulations

All of the calculations performed in this work used a mixture of traditional DFT and plane-wave DFT. The periodic boundary conditions were fixed to the unit cell parameters as observed from the experimental data. The cell parameters and initial atomic coordinates were extracted from the lowest temperature single crystal X-ray or neutron data available. There are different stages to the calculations which will be outlined below; at each stage it is possible to extract different pieces of information.

2.4.3.1 Geometry Optimisation

The first step when running simulations is geometry optimisation. To do this the atoms must be allowed to move in order to find the minimum on the potential energy surface (PES) of the structure so the Born-Oppenheimer approximation must be lifted. The objective of this step is to find the 0 K, vibration-free, structure.

Starting with the initial atomic coordinates from experiment, the energy of the structure is calculated. From here the forces on the atoms are calculated and the force constants estimated. The Born-Oppenheimer approximation is lifted, the atoms moved, and the process repeated. This goes on until certain convergence criteria are met; usually that the force on the atoms and the atomic displacement between cycles are close to zero. Once these criteria have been met, the optimised 0 K vibration free structure should have been found.

2.4.3.2 Molecular Dynamics

Molecular dynamics simulations can introduce time and temperature into simulations providing a time-averaged structure and vibrational frequencies of the system at a specific temperature. The output is essentially a molecular movie with each frame differing by the time-step δt. A molecular dynamics simulation will use the geometry optimised atomic positions as its start point. From here the forces on the atoms are calculated and, instead of moving the atoms to reduce the forces to close to zero as in the geometry optimisation, they are converted into velocities and accelerations through Newtonian mechanics and move according to the chosen time step. At the start of a simulation, the system is given a certain amount of energy and atoms are assigned random velocities according to the specific temperature chosen. The position of an atom, $\boldsymbol{r}$, at a specific time, t, is calculated based on its previous position and can be expressed as a truncated Taylor series:

Equation 2.26 $$r(t + \delta t) = r(t) + \delta t v(t) + \tfrac{1}{2}\delta t^2 a(t)$$

Only the first and second derivatives (velocity and acceleration respectively) are available and higher derivatives such as the change in force with time cannot be calculated. If a small enough time step is chosen, the higher derivatives should not have a great impact on the atomic position so **Equation 2.26** is accurate. It is therefore possible to calculate the atomic position at any time in the future, $t + \delta t$, from its original position. The time step is chosen so that the bond with highest energy vibrational frequency (usually O-H or N-H in molecular systems) is adequately sampled. A typical time-step would be 0.5-1.0fs and dynamics simulations will usually be run for at least ~10 ps so that low energy lattice vibrations can be sampled.

Before commencing a molecular dynamics simulation, a statistical ensemble must be chosen which fixes a certain set of parameters. The parameters which may be fixed are the number of atoms (N), the volume of the unit cell (V), the pressure (P) and the temperature (T). There are three commonly used ensembles; these are *NVT*, *NVE* and *NPT*. In the *NVT* ensemble the temperature is coupled to a thermal bath which acts as a

thermostat so the temperature will only fluctuate slightly around a chosen value. *NVE* simulations have no thermostat and temperature will often split between kinetic and potential meaning that a much higher starting temperature (often twice as high) is required which can be damaging to the model. The final ensemble, *NPT*, is the closest to real experimental conditions where only the volume of the cell is allowed to change.

2.5 Solid-state Vibrations

As stated in **Section 2.4.3.2**, molecular dynamics simulations give access to the vibrational spectra of the system under study. In the solid-state, vibrational spectra are known as phonon spectra. Phonon spectra contain a high frequency area consisting of bond stretches, bends etc. and a lower frequency area made up of the external vibrations of the system where molecules are moving relative to one another. The long wavelength, low frequency vibrations are called lattice modes and they can either be acoustic or optical. Acoustic modes occur when all the molecules in the unit cell move in phase. Optical modes are induced by electromagnetic radiation (in the IR region) and are defined as when the molecules are moving out of phase with respect to one another. For a unit cell containing *N* molecules there will be 3 acoustic modes and 3*N*-3 optical modes. Interpreting phonon spectra is a complicated process due to the number of atoms/molecules involved and also the fact that molecular symmetry can be lost in a crystal lattice and therefore what would otherwise be degenerate bands can be split in the spectrum. Phonons are responsible for a variety of physical properties associated with a solid-state system, such as heat capacity, and have also been suggested to be responsible for proton migration and disorder, which is of particular relevance to the work reported here.[67,69,88]

Chapter 3

3. Techniques and Instrumentation

A complementary range of techniques have been utilised in this work to characterise fully the materials under study. These range from routine in-house laboratory techniques to experiments at large central facilities. The main methods used in this project are single crystal X-ray and neutron diffraction, complemented with quantum mechanical computational chemistry calculations. This chapter will cover all of the techniques used in detail, giving a step by step guide to each process.

3.1 Sample Preparation

Sample preparation in this work has been focused in two main areas: molecular complex synthesis, and growth of large single crystals for neutron diffraction. All of the samples studied have been obtained by solvent evaporation crystallisation.

Each analytical technique employed for sample characterisation puts different demands on the sample size and quality. The ability to solve a crystal structure from single crystal X-ray data is heavily reliant on the quality of the sample and a good single crystal should be used. Single crystals can be initially identified under an optical microscope; the regularity of the shape is not necessarily important but good crystals for diffraction should not have a concave vertex and should uniformly extinguish polarised light. Ideally, a crystal selected for X-ray diffraction should have length ~0.2 - 0.4 mm in each dimension, though it is possible to use crystals larger or smaller than this. The neutron Laue technique is more demanding on the sample, requiring crystals of even higher quality which would ideally be ≥1mm^3 in volume. The large wavelength band utilised in the method, coupled with a large incoherent scattering cross section for hydrogen, adds to the background and crystals must be of a higher quality for good structural refinement to be obtained. In both cases, single crystals would preferably have a low mosaicity, have no smaller crystallites or powder on any of the faces and be free from defects and twinning.

3.1.1 Crystallisation

In organic chemistry, crystallisation is often used for purification of the products of a synthesis, generally resulting in very small crystals of the product (often too small for study by single crystal X-ray diffraction). In crystallography and solid-state chemistry, crystallisation is used with the aim of growing larger samples suitable for study by diffraction and can also be used to synthesise multicomponent molecular complexes of materials. While there are many crystallisation routes, the most common is solvent

evaporation. This is a very simple technique which still allows a large region of the crystallisation phase space to be explored through changing a range of variables.

The crystallisation vessels used in this work were mostly 7 mm^3 sample vials. Lids / parafilm were placed over the vials containing the sample solution, with holes punched in them to allow the solvent to evaporate; the number and size of holes can be used to control the rate of evaporation. The general experimental procedure involved the dissolution of stoichiometric molar quantities of the target chemicals in the chosen solvent. Common crystallisation ratios employed when aiming to grow crystals of molecular complexes were 1:1 and 2:1 with respect to the two components, dissolved in an excess of solvent; however this did not necessarily lead to the complex forming with the same stoichiometric ratio as that used in the preparation. Typical quantities of up to ~0.1g of starting materials were dissolved in each vial in ~2-5ml of solvent. In some cases heating of the solution with stirring and / or a sonicator were used to help dissolve the starting materials. Once these were dissolved, the vials were left in place (i.e. free from agitation) at the set crystallisation temperature until the solvent had evaporated or suitable crystals were formed. Vials were examined visually and where single crystals or powders had formed, the solid sample was extracted for study by diffraction methods. In general, many crystallisations were set up in parallel for a particular target complex, at a variety of temperatures and using a variety of solvents. If the initial crystallisations were unsuccessful the crystallisation conditions were varied until the desired crystalline products were formed.

The choice of solvent can play an important role in the outcome of the crystallisation. Often a single solvent is used though solvent mixtures are also possible. Typical solvents used in this work were methanol, ethanol, isopropanol, acetonitrile, acetone, water, dimethylformamide and diethyl ether. The solvent may be chosen based on the physical properties of the materials (in particular the solubility of the components) and can also be used to control the evaporation rate which can be important for finding the kinetically / thermodynamically most stable form of a material and also for determining the size of the resulting crystals (slow evaporation tending to favour larger crystals). The solvent may become incorporated into the crystal structure, e.g. as a hydrate, or can in some cases even form a reaction product with the target material.

Figure 3.1 *Photographs of the temperature controlled hotplates (left) and the ReactArray Microvate (right) used in sample preparation.*

The temperature of the sample solution can be varied to control the rate of evaporation and therefore the rate of crystal growth. In this work the solution temperature was set at a fixed value throughout the crystallisation process. This can be done at higher temperature using specially adapted hotplates (**Figure 3.1**, left) and for crystallisation at lower temperatures, by placing samples in a fridge or cold room to allow the solvent to evaporate at ~4°C. Crystallisation at higher temperatures increases the evaporation rate and may favour kinetic products and smaller crystals, while the use of lower temperatures may favour the thermodynamic product and larger crystals, though this is not always the case. While holding the sample solution at a fixed temperature is the most common method employed for crystallisation, other temperature regimes can be used. A more sophisticated method of temperature control was achieved in this work using the ReactArray Microvate crystalliser (**Figure 3.1**, right). This is a programmable temperature control device which offers the possibility of twelve different temperatures (from -20°C to 160°C) or temperature ramping regimes with up to four samples held in the array at each setting. This instrument allows the temperature to be raised or cooled at a set ramp rate to encourage larger crystal formation or the production of different crystal forms. Samples are removed from the hotplates / Microvate as soon as the solvent has evaporated, to minimise the risk of leaving single crystal samples at elevated temperatures which may cause them to shatter on removal from the sample vial. This is not a problem for powder samples where the powder should be completely dry before analysis.

3.1.2 Sample Characterisation and Screening

In this work, the aim during the crystallisation process was always to produce single crystals of the target material. However, this did not always occur, particularly in cases where the target material was a molecular complex of two (or more) materials. In these cases it was not uncommon for there to be multiple crystalline phases, powders and / or liquid oils present as products within the same sample vial. These different phases could contain complexes with different stoichiometric ratios of components, starting materials and possibly reaction products. It is therefore important that the full contents of the sample vial are examined to determine whether any new complexes had been formed. This can initially be done by eye followed by examination under a microscope. If there are multiple crystalline phases present it is often possible to distinguish between them through the presence of different crystal shapes, sizes and colours. The position within the vial where the crystal has grown can also be used to identify different product materials as, for example, one crystal form may grow preferentially on the side of the vial as opposed to the bottom.

Most of the target molecular complexes readily formed single crystals of sufficient quality for a diffraction experiment, meaning that powder diffraction studies were often unnecessary. Where only powders formed, samples were analysed to determine which powders contained a potential target molecular complex and the crystallisation conditions were varied around those which had produced the desired product until suitable single crystals were obtained. Unit cell screening was used to determine whether new products had been formed. This involves comparing the unit cell of the crystal under study to those of the starting materials and other known compounds reported in the Cambridge Structural Database (CSD).[34] If the unit cell does not match either the starting materials or any other known complexes or compounds (e.g. hydrates) then it is likely a new complex has been formed and data collection can begin.

3.2 Single Crystal X-ray Diffraction

All of the structures presented in this work were determined from single crystal X-ray diffraction data. X-ray diffraction is usually carried out using laboratory sources making it a relatively cheap and straightforward technique. Laboratory X-ray sources accelerate electrons through a potential towards a metal target and on collision with the target produce electromagnetic radiation in the form of X-rays. The wavelength of the radiation produced depends on the metal target used; Cu and Mo are the most common targets with K_α wavelengths of 1.542 Å and 0.7107 Å, respectively.

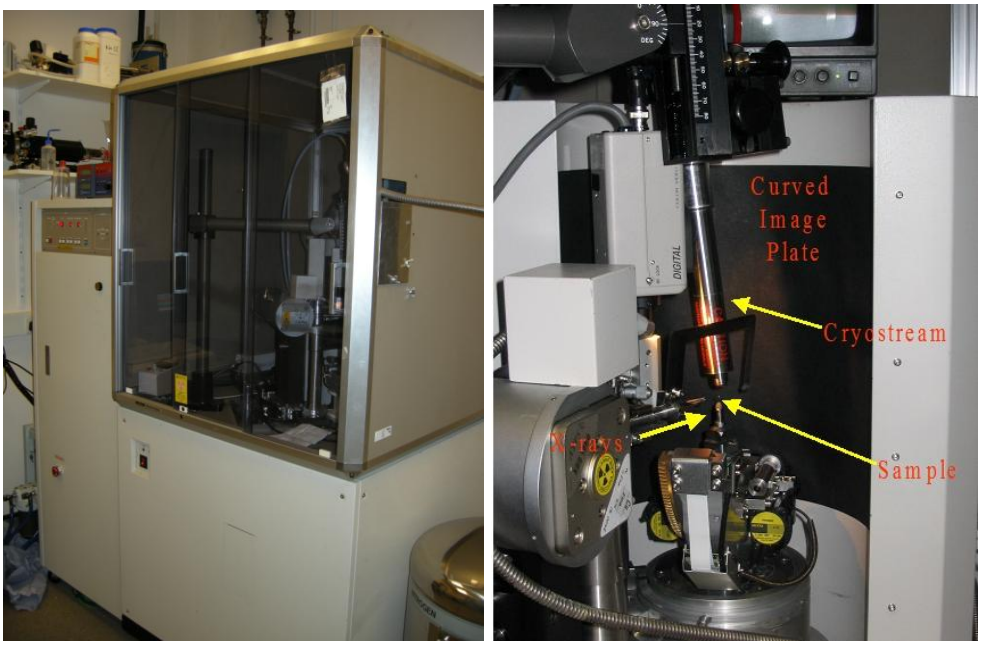

Figure 3.2 *Photographs of the Rigaku R-AXIS / RAPID diffractometer.*

Two different in-house diffractometers were used: a Bruker Nonius Kappa diffractometer with a CCD area detector[132] and a Rigaku R-AXIS / RAPID diffractometer with an image plate detector (**Figure 3.2**).[133] Both diffractometers use Mo K_α radiation and are fitted with an Oxford Cryosystems Cryostream low temperature device allowing data collection at temperatures down to ~77 K. Data collection on the Kappa used the Collect[134] software and data processing was carried out using DENZO / SCALEPACK[135] and an absorption correction applied using SADABS.[136] Data collection on the RAPID used the d*trek software while processing was done using FSPROCESS, both within the CRYSTALCLEAR suite of programs,[133] while an absorption correction was applied using ABSCOR.[137] While the software used in these processes are different, the steps in the experimental procedures are the same for both diffractometers.

3.2.1 Unit Cell Determination by Indexing of Peaks

Once a suitable single crystal has been selected, it is mounted on a glass fibre attached to a goniometer and placed on the diffractometer to allow the unit cell to be determined. The crystal is centred in the X-ray beam and initial diffraction patterns (typically 4 - 10) are collected with the crystal in different orientations. Reflections are auto-indexed and the primitive cell and orientation are calculated based on the observed reflections and then refined. The crystal system, Bravais lattice and unit cell are then determined from the position of spots in the diffraction patterns. If there is any doubt as to the symmetry of the sample a lower symmetry system is chosen before beginning data collection to ensure a complete data set. For higher symmetry systems fewer data are required and, since all

diffraction patterns have an inversion centre, even for the lowest symmetry systems it is necessary to collect only a hemisphere of data to observe all unique reflections.

3.2.2 Data Collection

The data collection strategy is determined based on the symmetry of the sample. For X-ray diffractometers, the computer software will be able to determine the possible unit cell and space group from the initial diffraction patterns collected and the user can choose the most sensible solution. Once these have been selected the software will suggest a suitable data collection strategy and diffraction patterns can be collected. A typical data collection will have a completeness of nearly 100% at 0.8 Å resolution and a redundancy (the average number of times each unique reflection is observed) of around five. The amount of time needed for the data collection depends on a number of factors including the size and symmetry of the sample, how well it diffracts and the intensity of the incident X-rays, though a typical data collection would take in the order of a few hours to one day.

Once a data collection has finished the space group is determined from the symmetry of the diffraction pattern through systematic absences which may be present in the diffraction intensities. The data are then integrated, reducing the peak intensities to structure factors. Several corrections are applied at this stage including a multiplicity correction and corrections for absorption and extinction, and an *hkl* file is produced. The *hkl* file contains one line per reflection with values for h, k, l, F_o^2 and $\sigma(F_o^2)$ for each observed reflection.

3.2.3 Structure Solution and Refinement

Structures were solved by direct methods using the SHELXS-97[138] program while structure refinement was carried out using SHELXL-97.[138] PLATON[139] was used to check the space group assigned. All of these programs were used embedded within the WinGX software suite.[140] For complexes where neutron data were collected, the initial atomic coordinates were always taken from the X-ray structure. Non-hydrogen atoms are freely refined first with isotropic and then anisotropic thermal parameters, while hydrogen atoms are only refined with isotropic thermal parameters for the X-ray data. When neutron data are available, hydrogen atoms can be refined anisotropically. On completion of the structure refinement the results can be viewed in a structural visualisation program such as Mercury.[141] All schematics of structures presented in this work have the thermal ellipsoids set at the 50% probability level for clarity. Where the scattering density is imaged explicitly, two-dimensional Fourier difference maps in the region of the hydrogen

bonds were generated with the hydrogen atom of interest removed from the structural model, using the MAPVIEW option within WinGX.[140]

3.2.4 Variable Temperature Measurements

Proton disorder and migration are temperature dependent effects and therefore require data to be collected at multiple temperatures in order that the evolution of the hydrogen atom parameters can be observed over a set temperature range. The trends found in repeated collections also give added strength to observed results which can be particularly important when analysing subtle structural details. In the cases of proton migration and disorder, differences would be expected to be observed, in the hydrogen atom position and the relative occupancies of two atom sites, respectively. A typical multiple temperature data collection would involve data sets being collected at 100, 200 and 300 K, with the possibility of collecting data at further temperatures if interesting or anomalous behaviour is observed. Variable temperature methods were applied to almost all crystal structures in this work, primarily to observe the hydrogen bond evolution though also to observe and characterise any other temperature dependent structural properties.

3.3 X-ray Powder Diffraction

If single crystals of sufficient size and quality are not produced from the sample preparation other analytical techniques such as powder diffraction may be used. The demands on a powder sample are very different from those of a single crystal. Powders can either form naturally in a sample vial after solvent evaporation or can be produced by grinding single crystals. Grinding can sometimes cause other reactions to occur and can even be used to produce molecular complexes in some cases, either with or without the addition of small amounts of solvent.[53] These types of reactions are not always desirable so care should be taken whenever preparing a sample in this way. Samples for powder diffraction should be dry, well-mixed powders with small randomly oriented crystallites, both making it easier to load the sample in a capillary and giving better quality data. In this work powder diffraction has only been used for sample screening and observing phase transitions – no structures were determined or refined from powder diffraction data.

The most common uses of powder diffraction are for monitoring phase transitions, phase identification (fingerprinting), assessing the purity of samples and sample screening. It is extremely useful for following phase transitions where single crystals would be destroyed and transitions can be observed *in situ* by following specific diffraction peaks while varying the temperature or pressure to induce the transition. As each crystal structure will have a unique powder diffraction pattern, or fingerprint, powder patterns from batches can be

compared with the known powder patterns of the target materials to show what is present and in what quantity. This procedure is often used in the pharmaceutical industry to confirm that the desired products have been produced and is also used to identify the presence of any impurities.

Screening of samples, whether they are new complexes or new polymorphs, can be a very time consuming process when using only single crystals, due to the time required to find a good quality sample, mount it and determine the unit cell multiple times. Another problem posed by this method is that one single crystal extracted from a sample vial is not necessarily representative of the bulk of the sample preparation, where there could be multiple crystalline phases mixed together. Powder diffraction is a faster method of sample screening which can be used to study the complete contents of a sample vial in one data collection. This method can be used to identify the presence of any new complexes or polymorphs formed without the need to grow or find good quality single crystals. If a new material of interest is found, a concerted effort can then be made to grow single crystals for study by single crystal X-ray (and possibly neutron) diffraction so that the crystal structure can be solved and analysed in detail.

Powder diffraction reduces the three-dimensional reciprocal space into a one-dimensional pattern of intensity varying with the diffraction angle, 2θ. A powder diffraction sample should contain many small crystallites oriented randomly with respect to each other; the resulting diffraction pattern will have all of the diffraction patterns for each crystallite overlaid forming rings at given d-spacing values as opposed to the individual Bragg peaks which are observed by single crystal diffraction. A lot of information is lost in compressing the data into a one-dimensional pattern, and while it should be possible to find the unit cell of any new phase it is still very difficult to solve a crystal structure from powder diffraction data despite recent advances in instrumentation and data processing software.

The powder diffractometer used in this work was a Bruker D8 diffractometer[142] equipped with a Cu Kα X-ray source (λ = 1.5406 Å) and a Oxford Cryosystems Cryostream low temperature device (**Figure 3.3**, left). Powders were extracted directly from sample vials or single crystals were ground to produce a powder which was mounted on the diffractometer in a glass capillary. Data were typically collected over a 2θ range of 5 – 50° at a scan rate of 1 degree / minute with a typical data collection taking 45 minutes. The resulting data were then plotted as 2θ angle vs. intensity (**Figure 3.3**, right).

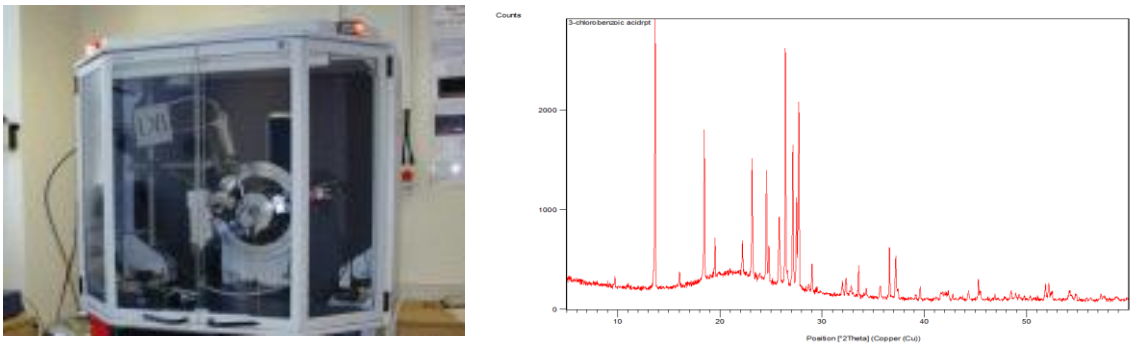

Figure 3.3 *A photograph of the D8 powder diffractometer (left) and a typical powder diffraction pattern (right).*

3.4 Single Crystal Neutron Diffraction

Single crystal neutron diffraction has been used extensively in this work, as it is the best available method to determine hydrogen positional and anisotropic thermal parameters accurately and unambiguously. This is particularly important when studying systems which exhibit subtle hydrogen atom behaviour such as proton disorder or migration. Ideally, neutron diffraction would be used in any case where ambiguous hydrogen atom behaviour presents itself. However, there are several difficulties that must be overcome in order to obtain good neutron diffraction data. The nature of neutron production means that access to large central facilities is required, meaning that proposals must be submitted, often well in advance of any allocated beam time, and there is much competition at each proposal round. The inherently low flux of neutrons and the way in which they interact with matter leads to a requirement for large single crystal samples (>1mm^3); growth of samples of this size can pose significant problems and in some cases is not possible. In addition, processing of neutron data is often much more complicated than for X-ray data collected on laboratory diffractometers. The relatively small number of neutron facilities globally means that software can be unique to each instrument and specific expertise is required to obtain results.

While these problems may pose some difficulties, recent advances in instrumentation are aiming to address some of these issues and make neutron diffraction a more accessible technique. Historically, neutron diffraction studies require data to be collected for several hours at each sample/detector orientation because of the low neutron flux available, resulting in several days being required to collect a complete data set. The use of a white neutron beam contributes to resolving this problem by increasing the neutron flux by up to an order of magnitude compared with a monochromatic instrument. This enables much faster data collection (a typical complete data set could be collected in a matter of hours)

and also opens up the possibility to use sub-mm^3 samples. This technique, the Laue method, is used on several modern neutron diffractometers such as SXD[143] at ISIS[144] in the UK, Koala[145] at the Australian Nuclear Science and Technology Organisation (ANSTO)[146] in Australia and VIVALDI[147] at the Institut Laue-Langevin (ILL)[148] in Grenoble, France, the instrument used in the majority of this work.

Advancements in neutron detection have also helped to speed up experiments and provide high quality diffraction data. Large area detectors are now common place, for example arrays of ^{3}He gas detectors and multiple scintillator position-sensitive detectors (PSDs), such as those used on SXD, can also be used to obtain much more data than would be possible with a single PSD or point detector in one exposure. VIVALDI and Koala each use a cylindrical image plate detector which allows large areas of reciprocal space to be studied in each Laue diffraction pattern meaning fewer patterns are required for a complete data set. The global shortage and the consequent rise in price of ^{3}He have led to a new wave of research into neutron detection with new technologies currently being introduced at neutron sources around the world. These new detectors will hopefully continue to improve the speed and quality of neutron experiments worldwide.

Four different diffractometers were used to collect neutron data at three different neutron sources over the course of this work. Almost all of the data presented were collected on VIVALDI at the ILL reactor source in Grenoble, France and this will be discussed at length in section **3.4.3** and **3.5**. Other diffractometers used were: the monochromatic instrument D19,[149] also at the ILL; the time-of-flight (TOF) Laue diffractometer, SXD, at the ISIS spallation source in the UK; and Koala located at the OPAL reactor, ANSTO, Australia. Koala is a clone of VIVALDI and operates on the same principles with a few minor differences detailed in **3.4.3.1**.

3.4.1 Neutron Sources

There are two main sources of neutrons for scattering experiments: spallation sources and reactor sources.

3.4.1.1 Spallation Sources

Spallation sources generate neutrons by colliding high energy proton beams with a heavy metal target. These collisions eject fragments from the metal target which mostly consist of neutrons. Examples of this type of neutron source include SNS[150] at the Oak Ridge National Laboratory in the USA, and ISIS, where some of the data presented in this work were collected, at the Rutherford Appleton Laboratory in the UK (**Figure 3.4**).

The neutron production process begins with a source of negative hydrogen ions, H^-. The ions are first accelerated in a linear accelerator (linac) before passing through an aluminium oxide foil which strips them of their electrons producing a proton beam. The protons are then fed into a synchrotron where they separated into bunches and accelerated further by powerful electromagnets. Once the protons have gained sufficient energy they are released towards the heavy metal target. The type of metal used as the target varies; at SNS a liquid mercury target is used, while ISIS uses a solid tungsten target. When the pulsed proton beams hit the target, neutrons are ejected. Moderators are placed around the target which slow the neutrons to speeds (and hence wavelengths, *via* the de Broglie relationship) useful for condensed matter research. The neutrons are then directed towards the instrument suites by neutron guides. The pulsed nature of spallation sources make them particularly powerful when carrying out TOF experiments.

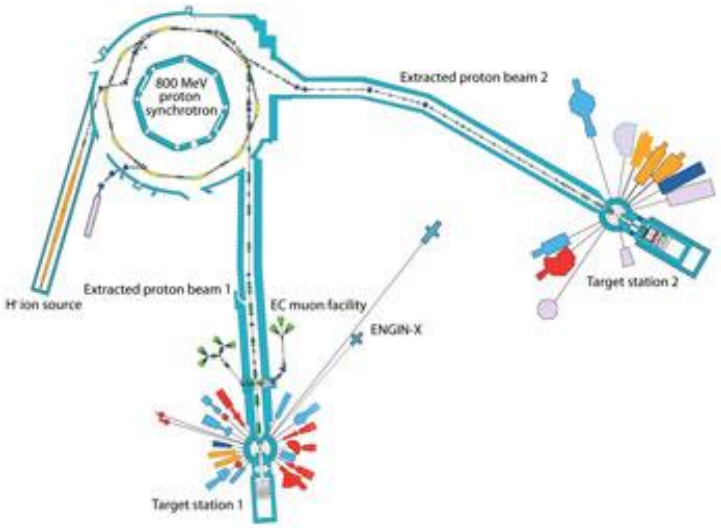

Figure 3.4 *Schematic layout of ISIS. SXD is located at target station 1.*[144]

3.4.1.2 Reactor Sources

The other method by which neutrons can be produced is using a nuclear reactor. These research reactors are of far lower power, with a smaller core, compared with nuclear reactors used for power generation (the ILL reactor has a thermal power of 58.3 MW whereas a typical nuclear power plant will have a thermal power of 500 – 2000 MW) but are specially designed to maximise the number of neutrons produced in the fission process that can be extracted from the reactor and directed towards the instrument suites. Two reactor sources were used in this work – the Open Pool Australian Lightwater (OPAL) reactor at the Bragg Institute, ANSTO, Australia and the ILL reactor source at the European Photon and Neutron (EPN) campus[151] in Grenoble, France. As the majority of

the results presented in this work were obtained at the ILL, the neutron production process of the ILL reactor will be discussed in detail. Other reactor sources work on the same principle with only slight differences in the production process.

3.4.1.3 The ILL Reactor Source

The high flux ILL reactor (**Figure 3.5**) is the most intense continuous neutron source in the world with a neutron flux of 1.5 x 10^{15} neutrons per second per cm^2. The reactor operates up to 250 days a year over a number of fifty day cycles allowing for a change of fuel element between cycles. Neutrons are produced through the fission of ^{235}U nuclei. To begin the fission process, control rods (neutron absorbers) within the fuel element are slowly removed allowing random fission events to start a chain reaction. On average each fission event will produce 2.5 neutrons, 1.5 of these neutrons are required to maintain the chain reaction leaving one useable neutron per fission event. Throughout the fifty day cycle, the control rods are slowly and progressively lifted out to keep the neutron flux constant as the fuel is used up. At the end of the cycle the control rods are dropped back into place to stop the chain reaction so that the fuel element can be removed and replaced.

Figure 3.5 *Diagram of the ILL reactor core showing: 1. Safety rod; 2. Neutron guide pool; 3. Reflector tank; 4. Double neutron guide; 5. Vertical cold source; 6. Reactor core; 7. Horizontal cold source; 8. Control rod.*[148]

As with spallation sources, neutrons produced in the core of the ILL reactor will have energies too high for use in most experiments. Typically these energies will be in the order of MeV and they have to be reduced to meV to be useful for the types of structural

studies conducted within this work. The energy of the neutrons is reduced through moderation. The ILL uses three different kinds of moderators; liquid D_2 at 20 K gives cold neutrons (energies of 0.1 – 10 meV), liquid D_2O at 300 K gives thermal neutrons (energies of 10 – 100 meV) and a hot graphite moderator heated by γ radiation from the reactor to 2000K provides hot neutrons (energies of 100 – 500 meV). As each energy of neutron has a different wavelength, they can be used to study different properties of matter; only thermal neutrons have been used in this work.

The moderation process works through the inelastic scattering of neutrons with the moderator material, slowing these down to reach a thermal equilibrium. Most nuclear fission reactors will use either H_2O or D_2O as moderators, in which the neutrons are scattered predominantly by the hydrogen and deuterium atoms, respectively. H_2O is a better moderator in terms of the number of collisions with neutrons and the distance required for moderation (i.e. how much moderator the neutrons need to pass through) but problems arise from the large absorption cross section of hydrogen for neutrons. It is for this reason that the ILL uses a D_2O moderator to produce thermal neutrons, as the absorption cross section of deuterium for neutrons is smaller. This allows the ILL reactor to produce the highest thermal neutron flux in the world.

3.4.2 SXD at ISIS

The single crystal diffractometer (SXD) at ISIS uses a Laue TOF method to collect data on samples which can vary in size from 1 mm^3 up to 100 mm^3. Temperature control is achieved through the use of a helium cryostat or a furnace, allowing data to be collected between ~1.5 and 1200 K. It is also possible to fit a high pressure cell on the instrument enabling the study of materials under extreme pressures. The sample is normally placed under vacuum and diffraction patterns collected while the sample is rotated in ω (vertical axis) and tilted in χ. The instrument uses 11, optically encoded, ZnS scintillator PSDs covering a large area of reciprocal space, reducing the number of sample orientations required for a complete data set. Six of the detectors are in the equatorial plane of the sample with four others tilted at 45° and one directly below the sample (**Figure 3.6**).

One issue that arises through the use of a white neutron beam is difficulty in the data integration due to peak overlap and background accumulation. The TOF method minimises these difficulties and is possible on SXD due to the pulsed nature of the incident neutron beam. The production process at a pulsed source means that all neutrons are produced at the time of impact of the proton beam on the target. Neutrons of different wavelengths will take a different amount of time to travel from the source to the

detector, and the neutrons arriving at the same pixel on the detector will therefore do so at different times and can be separated by their wavelength. This makes the peak integration process much simpler.

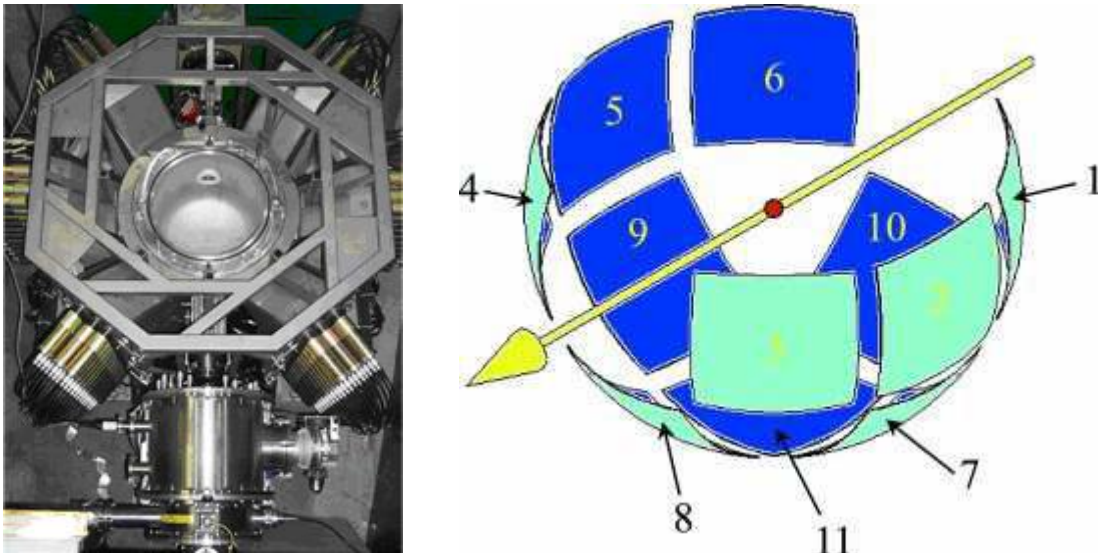

Figure 3.6 *SXD viewed from above (left) and diagram of the detector layout with the direction of the neutron beam shown (right).*[143]

3.4.3 VIVALDI at ILL

The instrument used to collect the majority of the neutron data presented in this work is the Very Intense Vertical Axis Laue Diffractometer (VIVALDI) at the ILL (**Figure 3.7** and **Figure 3.8**). Like SXD at ISIS, VIVALDI uses a white neutron beam providing a greatly increased neutron flux. It is equipped with a cylindrical image plate detector enabling large areas of reciprocal space to be analysed in one diffraction pattern. The high flux from the unmonochromated beam and the large image plate detector mean that experiments on VIVALDI can be conducted one to two orders of magnitude faster than those on a monochromatic diffractometer. Alternatively, the increased flux available at VIVALDI means that it is possible to use much smaller samples than is usually possible during a neutron experiment. Crystals down to ~0.01 mm^3 in volume for a strongly diffracting material can be used, while most of the crystals used in this work were ~1 – 5 mm^3 in volume. VIVALDI can be fitted with a helium cryostat allowing data collection at temperatures down to ~1.5 K while furnaces and high pressure cells can also be used to give a greater variety of available sample environments.

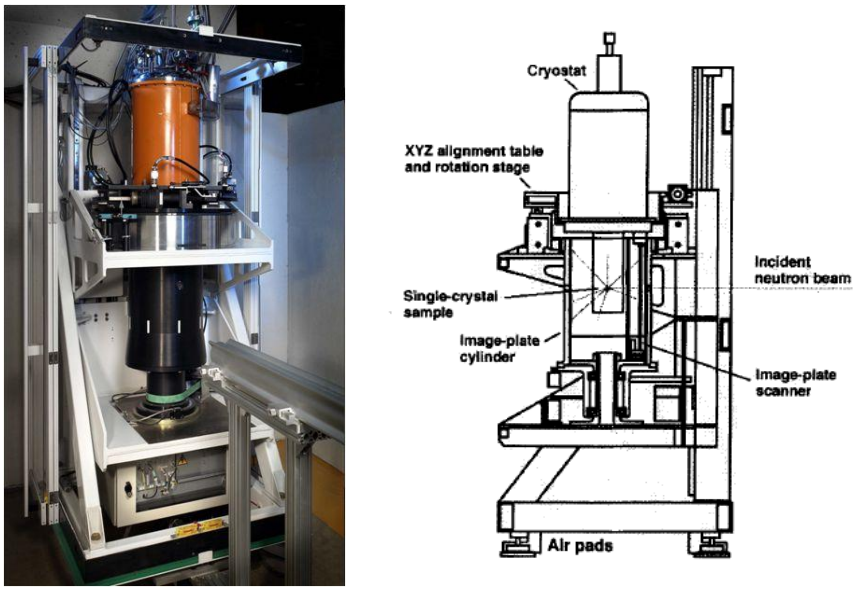

Figure 3.7 *VIVALDI with orange cryostat mounted (left) and schematic diagram of the instrument (right).*[147]

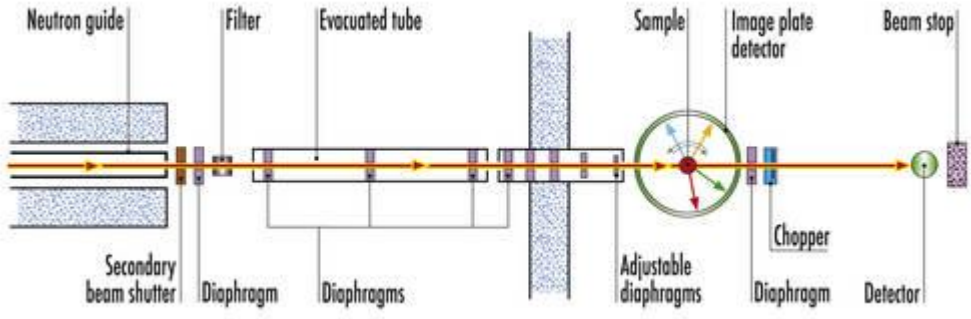

Figure 3.8 *Plan view of VIVALDI from neutron guide to beam stop showing the cylindrical detector.*[148]

There are two monochromatic instruments (a powder diffractometer, D1B, and a strain scanner, SALSA) upstream of VIVALDI on the same neutron guide. These instruments take out segments of the wavelength band resulting in VIVALDI not receiving a truly white beam. Not only does the presence of these instruments reduce the flux received at VIVALDI by a factor of ~2 but it also causes numerous sharp dips in the wavelength distribution. This makes the wavelength normalisation process (see **3.5.4**) more difficult and is one of the main challenges in processing data obtained from VIVALDI.

The cylindrical image plate detector used on VIVALDI is similar to those used in X-ray image plate detectors; a storage phosphor of BaFBr doped with Eu^{2+} is combined with Gd_2O_3, with the Gd^{3+} ions acting as a neutron converter due to their high neutron capture cross section. Following exposure to measure the neutron diffraction pattern, the image

plate is read by a laser scanning line by line from the bottom to the top with a readout time of ~3.5 minutes and an erasure time of one minute. The use of image plates offers high resolution, a large dynamical range and no pixel dead time. Another advantage of using image plates is that they are relatively cheap when compared with other types of neutron detectors. Placing the detector drum vertically simplifies the mounting of different sample environments such as cryostats and pressure cells.

As mentioned in **3.4.2**, another possible complication which arises when using a white neutron beam is the superposition of harmonic reflections. The large wavelength band means that it is possible for two reflections, for example *hkl* and *2h2k2l*, to diffract at the same 2θ angle and therefore appear at the same point on the detector. On SXD this problem is overcome by using the TOF method made available from the pulsed nature of the neutron beam. At a continuous neutron source such as the ILL, this would only be possible by using a beam chopper which would greatly reduce the neutron flux and therefore negate one of main advantages of using the Laue method. Historically, the problem of peak overlap meant that it was thought that it would not be possible to use the Laue method to study complex structures. It has however been shown that this does not affect most reflections and at least ~82% of observed spots are single[152] so the Laue method can be used for complex structural studies. This fraction is further increased due to the finite width of the waveband on a neutron guide; VIVALDI has a λ_{min} ~ 0.8 Å and a λ_{max} ~ 5.2 Å.

A typical experiment on VIVALDI begins with the sample being wrapped in aluminium foil to avoid contact with glue and strains on the crystal as it is cooled, and mounted on a vanadium sample pin before being placed on the instrument. An initial Laue diffraction pattern is collected from a short exposure and indexed and the unit cell determined to ensure that the correct sample has been mounted on the diffractometer and is of sufficiently high quality to lead to well-defined diffraction peaks. Normally four to ten diffraction patterns separated by a rotation of 20° or 30° around the vertical detector axis are collected. The number of patterns required is usually determined by the symmetry of the sample. When collecting data on triclinic samples it is routine to collect several patterns then remove and remount the crystal in a different orientation before collecting the remaining patterns to ensure adequate coverage of the unique volume of reciprocal space. The exposure time depends on the size of the sample and how strongly it diffracts. In this work, the time needed to collect one pattern ranged from 10 minutes to a few hours.

3.4.3.1 Koala at the Bragg Institute

Koala is essentially a clone of VIVALDI with a few minor differences. Similar types of sample environments are available, though the system in place on Koala allows more rapid change of sample and more rapid (flash) cooling. The one major difference between Koala and VIVALDI is the wavelength spectrum received at the instrument. Koala has one other instrument upstream on the same guide (a strain scanner, Kowari); however the beam to Koala does not pass through the monochromator, meaning that the wavelength spectrum which the instrument receives is much cleaner than that of VIVALDI with less dips making the wavelength normalisation process more straight forward. Even though the OPAL reactor is less powerful than the ILL reactor (20 MW compared to 58.3 MW), it is a more modern reactor with state of the art neutron guides, and Koala receives a neutron flux comparable to that of VIVALDI.

Figure 3.9 *Koala at the Bragg Institute.*[145]

3.5 Data Reduction and Processing on VIVALDI

Processing neutron diffraction data is often not a straightforward process. The relatively low number of neutron sources and instruments worldwide means that there are less specialist neutron crystallographers available to write and update software, compared with the commercial programs which are available for X-ray data and provided as standard with modern X-ray diffractometers. Neutron diffraction instruments are often unique and therefore separate software must often be written for each individual diffractometer, taking into account the different instrument designs (VIVALDI, Koala and LADI-3 (also at the ILL)

as very similar instruments are exceptions to this, with a degree of commonality in data collection and reduction procedures). The software available for neutron data reduction is not as automated and user-friendly as X-ray data reduction, with more user input and knowledge required.

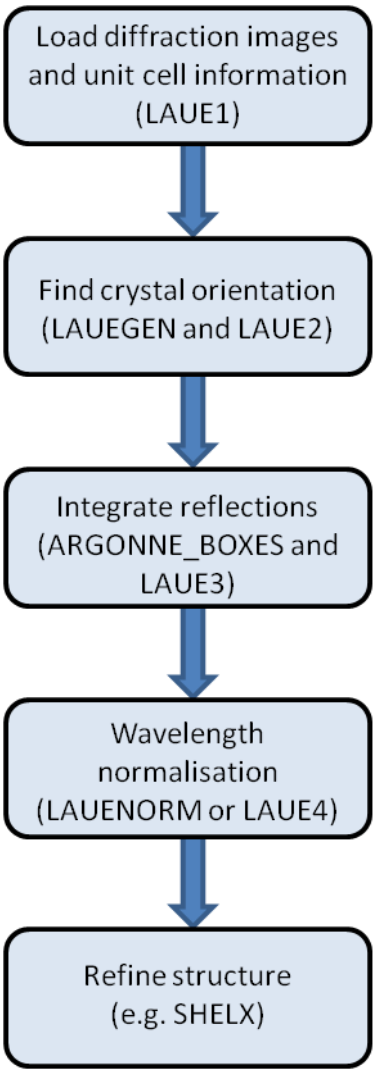

Figure 3.10 *Flow diagram of the data processing and reduction steps for VIVALDI.*

The suite of programs used for processing data from VIVALDI is adapted from the programs used on another Laue diffractometer at ILL, LADI-3,[153] used to analyse data from macromolecular crystals. The three main steps in the data reduction process are: (i) finding and refining the crystal orientation, (ii) reflection intensity integration, and (iii) wavelength normalisation. The programs / codes used for these three steps are LAUEGEN,[154] ARGONNE_BOXES[155] and LAUENORM,[156,152] respectively. A new piece of software was developed at ANSTO towards the end of this work, the LAUE1234 program

suite (**Figure 3.10**).[157] This uses adapted versions of LAUEGEN and ARGONNE_BOXES with a new program for wavelength normalisation, LAUE4.

3.5.1 Sample Orientation and Indexing – LAUEGEN

Diffraction patterns collected on VIVALDI are saved as *tif* files. As patterns are read out from bottom to top by the laser, the first step in processing the data collected is to reformat the image files to the internal convention assumed by LAUEGEN which are then saved as *reo* files. The LAUEGEN interface (**Figure 3.11**) can either be accessed directly by opening the program or through LAUE1. In LAUEGEN, the first pattern is loaded and information on the crystal system, lattice type, symmetry and unit cell parameters input. If LAUEGEN is accessed through LAUE1 this information is entered earlier so once LAUEGEN opens all of the parameters are already available. In this work, all of the unit cell information is known beforehand from X-ray structures. The Laue method at a continuous neutron source, such as VIVALDI at ILL, only allows relative linear cell dimensions to be determined, so for this reason X-ray determined unit cell parameters were always used in the final refinements.

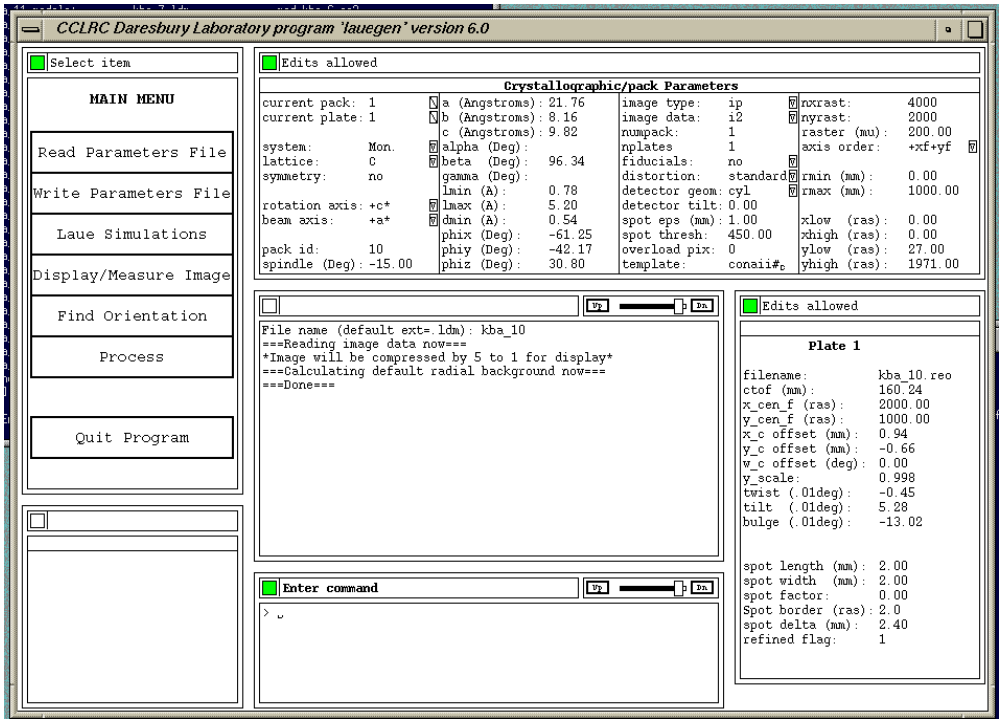

Figure 3.11 *The LAUEGEN interface.*

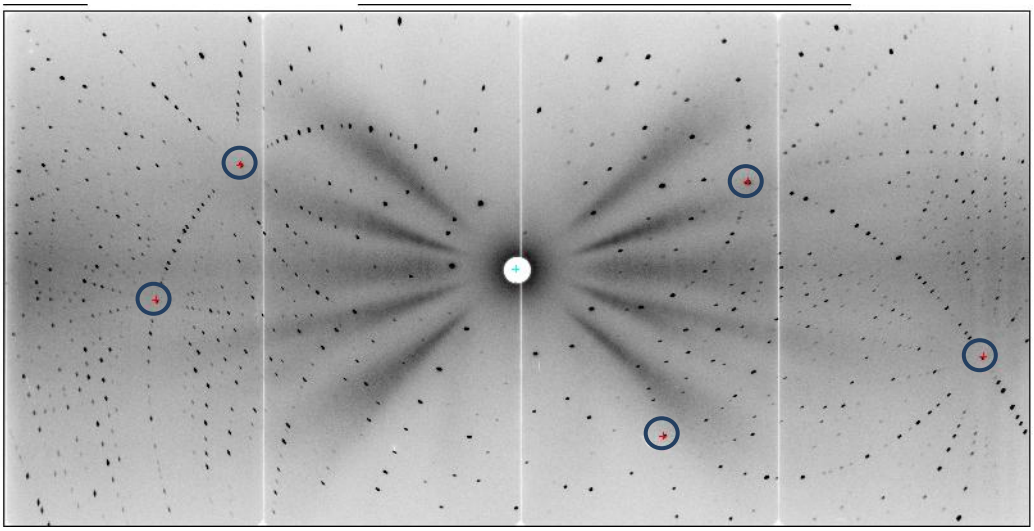

Figure 3.12 *Typical diffraction pattern collected on VIVALDI showing the spots used to determine the orientation matrix circled and in red. The transmitted beam exits the detector through the hole in the middle.*

Once the necessary information has been input, the next step is to find the crystal orientation. This is done by selecting 5 – 8 spots on the diffraction pattern which have low *hkl* values. These spots can usually be identified where different arcs of spots intersect on the diffraction pattern (**Figure 3.12**); if there are not enough of these spots visible, a few spots with the greatest intensity are added. From the initial spots, the program will generate several solutions representing different orientation matrices; the predicted diffraction patterns of these solutions can be overlayed on the measured diffraction pattern to find the best match. If no good solutions are produced it may be necessary to select different spots and generate new solutions until a match is found.

Once a solution has been chosen, the orientation matrix is refined to give a better agreement to the observed data. This is done using a least squares method, refining the sample position, unit cell axes and adding corrections for distortion. Refinement cycles are repeated until the root mean square (RMS) difference between the spots in the predicted and observed diffraction patterns is ~0.2 mm (the usual pixel size). The final step is to refine the "soft limits"; these are λ_{min} and d_{min}. λ_{min} is the lowest limit of the wavelength of the incident neutrons and is ~0.8 Å on VIVALDI and should not normally need to be changed. d_{min} is the minimum d-spacing measured and is a measure of the scattering power of the crystal and the quality of the data. Reducing the values of λ_{min} and d_{min} will increase the number of spots in the predicted diffraction pattern. Values should be chosen so that all observed reflections are accounted for in the predicted pattern. It is sensible to choose a d_{min} value slightly lower than that of the actual data to be sure all

spots are accounted for as the location of spots in the predicted pattern determines where the integration code acts. A typical d_{min} value for a high quality data set would be ~0.56 Å.

Once all the necessary refinements have been carried out an *ldm* file is written which contains information on each reflection, including the *hkl* values and position on the detector, along with the unit cell parameters. The *ldm* file for the first pattern can be used to generate files for the other patterns in the data set by knowledge of the sample rotation angle between patterns. The orientation matrices for the subsequent patterns should then be refined; this can be done as a batch process using either the command file newlauegen.com or LAUE2. It is not uncommon for the batch refinement process to fail for some, or even all, other patterns, in which case a manual refinement must be carried out for those patterns.

3.5.2 Integration – ARGONNE_BOXES

The next step in the data reduction process is peak integration; this is done using ARGONNE_BOXES, either as a standalone code or as the version integrated into LAUE3. Before running the integration code, areas of the image plate which should not be integrated must be identified. These areas are the beam stop and other non-active areas including plate joins and borders (the white bars in **Figures 3.12**). The x and y coordinates of these areas are input into a file linked to ARGONNE_BOXES before the code is run.

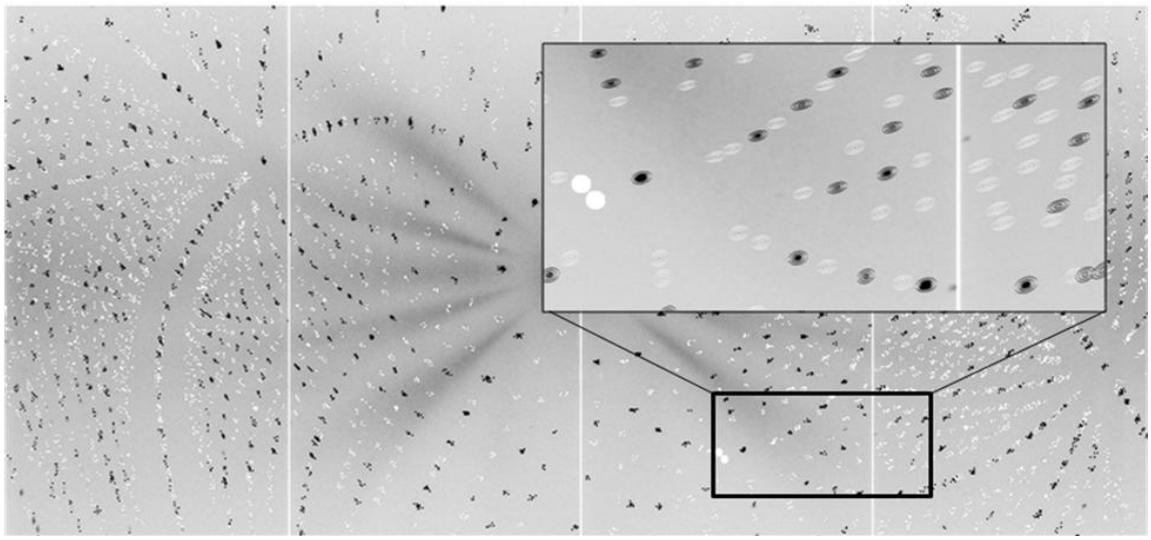

Figure 3.13 *VIVALDI diffraction pattern showing the areas over which reflections are integrated in the form of three ellipses; dark ellipses correspond to strong reflections and white ellipses to weaker ones. The two white circles mask off a scratch on the image plate.*

ARGONNE_BOXES uses *a priori* information about strong peaks to optimise the integration of the weaker peaks using the minimum $\sigma(I)/I$ approach.[155,158] Strong peaks are selected from the diffraction patterns based on their relative height compared to the background. The two-dimensional profiles of these strong peaks are used as models for the integration of the weaker peaks. Based on the model peaks, each peak is integrated within three ellipses: a core ellipse, an intermediate ellipse, and an outer ellipse; the core ellipse should account for ~80% of the peak. The way in which strong peaks are used in the integration process means it is important not to saturate areas of the image plate giving peaks with flat tops; it is therefore important that sensible counting times are chosen during the data collection. The outputs from the integration are *ge1* files, used in the normalisation, and *img* files which display the areas of integrated intensity (**Figure 3.13**) and can be examined to ensure that all peaks have been integrated.

3.5.3 Absorption Correction

If the sample contains elements which absorb neutrons or scatter incoherently, then an absorption correction may need to be applied. This is especially true if the sample shape differs greatly from a sphere and a precise absorption correction can be made using the LADIABS code.[159] Information about the shape and location of the crystal faces along with information about all of the elements present in the sample and their absorption cross sections are entered into the input file. LADIABS estimates the attenuation factor and mean path length for each reflection by summation of the individual attenuation factors and path lengths point by point over a three-dimensional grid within the crystal boundaries.[160] The main contributor to absorption in the compounds in this work is hydrogen, which has a large incoherent contribution.[161] However, due to the small size of the crystals used in this work, absorption corrections did not improve the quality of data and were not used.

3.5.4 Wavelength Normalisation – LAUENORM / LAUE4

Wavelength normalisation is a key step in the reduction process for Laue data. The integrated intensities must be normalised with respect to the wavelength of the neutrons arriving at the instrument. There are two different codes which can be used to do this; LAUENORM and LAUE4.

LAUENORM works by comparing repeated measurements and equivalent reflections measured at different wavelengths over the full series of patterns to determine an empirical normalisation curve. To begin with all wavelengths have a scaling factor of 1.0 and the true calibration curve is found by iteration. The curve is often defined in terms of

a 7th order polynomial and reflections are assigned to a number of bins (usually 20) to ensure the curve is smooth. Each pattern is also assigned a scale factor to account for any movement of the crystal in the beam between patterns. An output file is produced showing whether the normalisation has been successful along with an *hkl* file to be used in the structural refinement.

LAUE4 was used in the processing of all neutron data presented in this work. LAUE4 performs a similar normalisation to LAUENORM but with a number of additional corrections or options that yield data of significantly better quality than those obtained from LAUENORM. An early version of the LAUE4 code tailored specifically for the Koala wavelength spectrum was used, however this still gave good quality results when used to treat data collected on VIVALDI. One of the shortcomings of LAUENORM is that the wavelength curve is created from evenly spaced steps corresponding to the bin size (wavelength range) and does not work if there are too few reflections in a bin. LAUE4 creates the curve using a quadratic piece-wise spline fit where the curve can vary more accurately even when there are no reflections observed corresponding to certain wavelengths. LAUENORM also assumes constant detector efficiency across the whole image plate, while LAUE4 accounts for that fact the neutron path length through the image plate can vary across the plate and intensities can appear reduced. LAUE4 can also correct for secondary extinction and for absorption. As for LAUENORM, after normalisation an *hkl* file is output to be used in the refinement.

3.5.5 Refinement

The final structure refinement step is similar to that for X-ray diffraction data and the output reflection file can be formatted for use in several refinement packages including FULLPROF[162] and SHELXL-97.[138] The only change which must be made is that neutron atomic scattering factors must be used in the refinement input files in place of the standard X-ray values. During the structural refinement it may be necessary to apply other corrections to the data, such as extinction,[163] although this is better made during the normalisation process.

3.6 Computational Methods

Quantum chemical calculations have been used in parallel with diffraction techniques to study a range of complexes containing short strong hydrogen bonds. In this work periodic solid-state calculations have been used to probe hydrogen bond potential energy surfaces (PES), molecular dynamics (MD) and time-averaged atomic positions.

The majority of the computational work was carried out using HECToR (High End Computing Terascale Resources), the UK's national supercomputer.[164] Other local computer clusters within the Department of Chemistry at the University of Bath and at the School of Chemistry at the University of Edinburgh were used for the preparation of files submitted to HECToR and the analysis of results.

3.6.1 CP2K and QUICKSTEP[165]

Calculations were performed using QUICKSTEP within the CP2K program suite.[165,166] CP2K can be used to perform atomistic and molecular simulations on solid-state, liquid and biological systems using a variety of computational methods.

QUICKSTEP is an element of CP2K which uses a mixed Gaussian plane-wave (GPW) approach to carry out MD simulations in the gas or condensed phase. In traditional DFT calculations the computational cost of a simulation does not increase linearly with the size of the system, instead increasing much more rapidly. This makes the computational cost of calculations on systems involving a large number of atoms restrictive. The GPW approach provides a method whereby large systems can be handled at a reduced computational cost. The method uses an atom based Gaussian basis set to describe the wavefunctions and an auxiliary plane-wave basis set to describe the density. This means that the computational cost does increase linearly with system size and is therefore ideally suited to calculations in the liquid and solid-state.

3.6.2 Methodology

All unit cell vectors were fixed at the values determined from the X-ray diffraction data and from these approximately cubic supercells were constructed. This was necessary as a precursor to analysing the phonon spectra of the systems; however this was not possible in this work due to time restrictions.

In traditional DFT calculations the basis set is defined as the number and type of Gaussian functions used to construct the molecular orbitals. As the number of Gaussian functions increases, a more accurate description of the molecular orbitals can be generated; however, the computational cost will also increase. In plane-wave DFT calculations the basis set is defined by an energy cut-off, increasing the number of plane waves in the basis set will again give a more accurate description of the structure but, again, at a higher computational cost. In both cases a compromise must be found whereby the calculations remain computationally feasible while still providing accurate results. In this work, a dual basis set comprising localised (DZVP-GTH-PBE) functions

and plane-waves (300 Ry, which converged the total energy of the system to within 1 meV / atom) coupled to pseudopotential (GTH-PBE) functions was employed, together with the DFT functional PBE.

Following geometry optimisation, a series of MD calculations were performed within the NVT ensemble at a number of temperatures for each system. The MD calculations were advanced in time increments of 0.65 fs until trajectories amounting to ~10 ps were collected for each temperature. The atomic coordinates from each frame were then binned to the relevant space group producing a *cif* file containing the time-averaged atomic positions. This was done using in-house codes created within the School of Chemistry at the University of Edinburgh.

One-dimensional PESs were generated by moving the hydrogen atom of the short strong hydrogen bond in the systems along the hydrogen bond. Steps of 0.05 - 0.10 Å were used and a single point energy calculations was carried out at each step with the energies used to generate the PES.

Chapter 4

4. Proton migration

To further the understanding of molecular systems which display temperature dependent proton migration (**Section 1.7**), it is necessary to identify new systems which exhibit this behaviour. With such a limited number of examples currently known, only limited insight can be gained into the underlying causes and, importantly, this reduces the potential for designing proton migration systems to make use of these dynamic charge transfer effects. The approach that has been undertaken in this work is to use the best known system which displays proton migration, urea-phosphoric acid,[62,63] as a basis for the design of other systems that contain short strong hydrogen bonds (SSHBs) within which the proton undergoes temperature dependent migration.

Urea has been utilised as a building block in this work based on its potential to form SSHBs when synthesised in molecular complexes with co-components and its proven capability to form a proton migration complex when crystallised with phosphoric acid.[62,63] Methyl substituted ureas have also been introduced into the crystal matrices with the aim of producing shorter, stronger hydrogen bonds to the acid component (A) than those observed in urea complexes due to the increased basicity (this has already been observed in the structures of urea-oxalic acid and *N*-methylurea-oxalic acid).[108,109,112] In this chapter, two complexes of dimethylureas (DMU) with oxalic acid are presented to investigate the possible presence of SSHBs and the potential proton migration which may occur within these hydrogen bonds.[167]

Haloanilic acids are strong acids which are known to provide strong proton donation properties. In this work, they have been complexed with ureas to investigate their potential to form SSHBs which may exhibit proton migration effects. The two haloanilic acids used in this work, chloranilic acid (CLA) and bromanilic acid (BRA), have not been studied extensively as components of solid-state molecular complexes though some studies have been carried out showing the potential for varying degrees of charge transfer across hydrogen bonds[168] and also ferroelectricity[169] in complexes of CLA. There are also limited examples of CLA complexes which contain fairly short, strong hydrogen bonds. For example, the complex of CLA with 3-picoline contains an O-H···O hydrogen bond between two CLA moieties with an O···O distance of 2.544(1) Å,[18] while the complex with 1,4-diazine contains an O-H···N hydrogen bond with an N···O distance of 2.558(2) Å.[170] The presence of these SSHBs makes complexes of haloanilic acids a suitable target for proton migration studies. Complexes of BRA are even less well studied than those of

CLA, and the substitution of a chlorine atom for a bromine atom allows any potential differences in the behaviour of the acid moieties to be investigated whilst not significantly changing the strength of the acid component (BRA and CLA have pK_a values of 1.34 and 1.38, respectively). The molecules discussed in this chapter are presented in **Figure 4.1**.

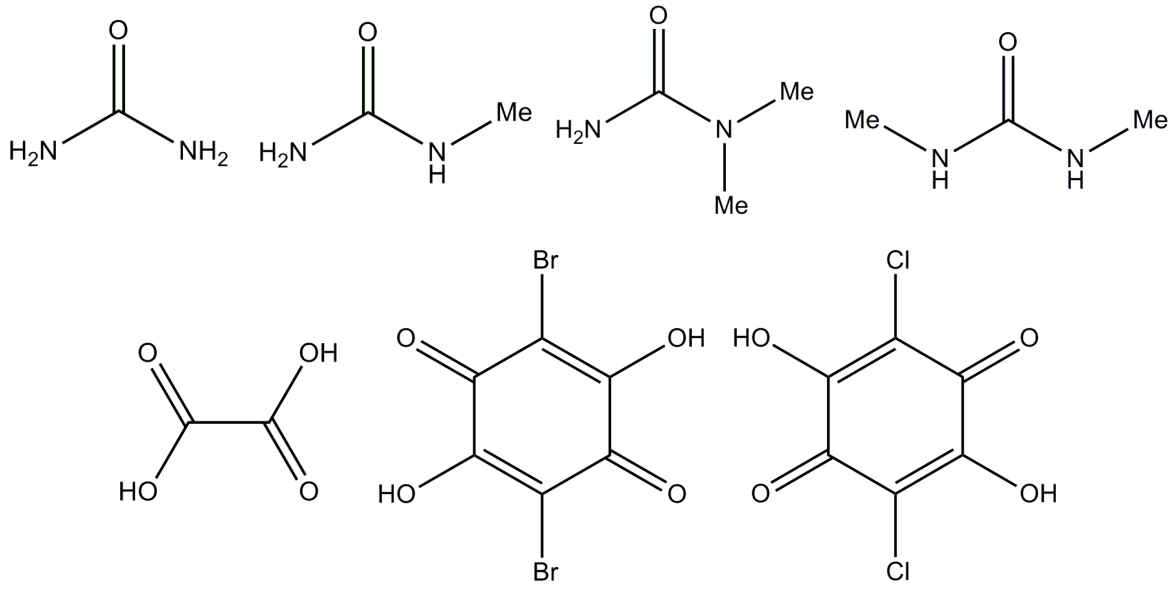

Figure 4.1 *Clockwise from top left: molecular structures of urea, N-methylurea, N,N-dimethylurea, N,N'-dimethylurea, chloranilic acid, bromanilic acid and oxalic acid.*

The crystallographic studies presented here are complemented with quantum chemical calculations. Variable temperature theoretical structures have been generated to investigate the origins of proton migration and to investigate the limits of current computational methods and agreement with experimental results. In some cases potential energy surfaces (PESs) of the SSHBs have been generated to analyse any possible temperature dependent behaviour of the PES which contributes to the presence of proton migration.

4.1 Experimental

4.1.1 Crystallography

2:1 Complex of *N,N*-dimethylurea and oxalic acid

Large, colourless crystals of the 2:1 complex of *N,N*-dimethylurea and oxalic acid were grown by slow evaporation from isopropanol at RT. Single crystal X-ray diffraction data were collected on a Rigaku R-AXIS / RAPID diffractometer at 100, 200 and 300 K. The structure was solved using SHELXS-97[138] and refined with SHELXL-97[138] within the WinGX package.[140] Neutron data were collected on VIVALDI at the ILL at 150, 175, 200,

225, 250, 275 and 300 K. The neutron structures were refined using SHELXL-97[138] taking the X-ray atomic coordinates as a starting model. Crystallographic data are given in **Table 4.1**.

2:1 Complex of *N,N'*-dimethylurea and oxalic acid

Large, colourless crystals of the 2:1 complex of *N,N'*-dimethylurea and oxalic acid were grown by slow evaporation from ethanol at RT. Single crystal X-ray diffraction data were collected on a Rigaku R-AXIS / RAPID diffractometer at 100, 200 and 300 K. The structure was solved using SHELXS-97[138] and refined with SHELXL-97[138] within the WinGX package.[140] Neutron data were collected on VIVALDI at the ILL at 4, 200, 240 and 280 K. The neutron structures were refined using SHELXL-97[138] taking the X-ray atomic coordinates as a starting model. Crystallographic data are given in **Table 4.2**.

2:1 Complex of *N*-methylurea and chloranilic acid

Large, deep red crystals of the 2:1 complex of *N*-methylurea and chloranilic acid were grown by slow evaporation from methanol at RT. Single crystal X-ray diffraction data were collected on a Rigaku R-AXIS / RAPID diffractometer at 100, 200 and 300 K. The structure was solved using SHELXS-97[138] and refined with SHELXL-97[138] within the WinGX package.[140] Neutron data were collected on VIVALDI at the ILL at 200 and 250 K. The neutron structures were refined using SHELXL-97[138] taking the X-ray atomic coordinates as a starting model. Crystallographic data are given in **Table 4.3**.

2:1 Complex of *N*-methylurea and bromanilic acid

Deep red crystals of the 2:1 complex of *N*-methylurea and bromanilic acid were grown by slow evaporation from methanol at RT. Single crystal X-ray diffraction data were collected on a Rigaku R-AXIS / RAPID diffractometer at 100, 200 and 300 K. The structure was solved using SHELXS-97[138] and refined with SHELXL-97[138] within the WinGX package.[140] Crystallographic data are given in **Table 4.4**.

2:1 Complex of urea and bromanilic acid

Deep red crystals of the 2:1 complex of urea and bromanilic acid were grown by slow evaporation from ethanol at room temperature (RT). Single crystal X-ray diffraction data were collected on a Bruker Nonius Kappa CCD diffractometer at 110, 200 and 300 K. The structure was solved using SHELXS-97[138] and refined with SHELXL-97[138] within the WinGX package.[140] Crystallographic data are given in **Table 4.5**.

4.1.2 Computational

Variable temperature molecular dynamics (MD) simulations have been carried out on the complexes of *N*-methylurea and chloranilic acid, *N,N*-dimethylurea and oxalic acid and *N,N'*-dimethylurea and oxalic acid using the QUICKSTEP program within the CP2K suite of programs.[165] The MD simulations were run on geometry optimised structures within the NVT ensemble (the number of atoms, unit cell volume and temperature are fixed in the simulations), advancing in time increments of 0.65 fs until ~10 ps of data had been collected. Unit cell parameters were fixed in all simulations to the X-ray unit cell parameters of the lowest temperature data set available. Theoretical *cif* files were generated by binning the atomic coordinates from each frame to the appropriate space group to generate a time averaged structure. PESs were generated by varying the atomic position of the hydrogen atom within the SSHB and carrying out a single-point energy calculation at each coordinate position to construct the PES.

No zero point energy (ZPE) corrections have been made to theoretical bond distances. The models used are a simplistic model for the systems under study, aimed at analysing the general behavioural trends of the materials.

Table 4.1 *X-ray and neutron data collection and refinement information for the 2:1 complex of N,N-dimethylurea and oxalic acid.*[a]

Compound	**2:1 *N,N*-Dimethylurea : Oxalic acid**									
Diffractometer	Rigaku R-AXIS RAPID	VIVALDI	VIVALDI	Rigaku R-AXIS RAPID	VIVALDI	VIVALDI	VIVALDI	VIVALDI	Rigaku R-AXIS RAPID	VIVALDI
Radiation	X-ray	Neutron	Neutron	X-ray	Neutron	Neutron	Neutron	Neutron	X-ray	Neutron
Formula	$C_8H_{18}N_4O_6$	$C_8H_{18}N_4O_6$	$C_8H_{18}N_4O_6$	$C_8H_{18}N_4O_6$	$C_8H_{18}N_4O_6$	$C_8H_{18}N_4O_6$	$C_8H_{18}N_4O_6$	$C_8H_{18}N_4O_6$	$C_8H_{18}N_4O_6$	$C_8H_{18}N_4O_6$
Molecular weight (g mol^{-1})	266.26	266.26	266.26	266.26	266.26	266.26	266.26	266.26	266.26	266.26
T (K)	100	150	175	200	200	225	250	275	300	300
Space group	*P2$_1$/n*	*P2$_1$/n*	*P2$_1$/n*	*P2$_1$/n*	*P2$_1$/n*	*P2$_1$/n*	*P2$_1$/n*	*P2$_1$/n*	*P2$_1$/n*	*P2$_1$/n*
***a* (Å)**	16.988(2)	7.74	7.76	7.7875(6)	7.79	7.81	7.84	7.86	7.879(3)	7.88
***b* (Å)**	6.4333(7)	6.43	6.44	6.4451(4)	6.45	6.45	6.46	6.46	6.4650(17)	6.47
***c* (Å)**	14.992(2)	12.99	13.00	13.0165(11)	13.02	13.03	13.05	13.07	13.082(4)	13.08
***β* (°)**	130.103(8)	102.89	102.66	102.417(3)	102.42	102.17	101.96	101.71	101.461(12)	101.46
Volume (Å^3)	1253.3(3)	630.2	633.9	638.03(8)	638.9	641.6	646.6	649.8	653.1(4)	653.6
Z	4	2	2	2	2	2	2	2	2	2
Reflections collected	14721	7056	6421	8007	6073	5604	4845	4227	8126	4004
Independent	2754	1449	1435	1460	1341	1240	964	915	1485	803
Observed > 2σ(I)	2098	925	919	1183	832	755	663	581	1022	539
R_{int}	0.021	0.195	0.164	0.017	0.163	0.163	0.140	0.147	0.017	0.136
Parameters	235	164	164	107	164	164	164	164	108	164
GooF	1.08	1.53	1.68	1.12	1.67	1.70	1.72	1.57	1.09	1.59
R_1 (observed)	0.0451	0.0706	0.0684	0.0490	0.0672	0.0649	0.0584	0.0578	0.0583	0.0567
R_1 (all)	0.0575	0.1310	0.1244	0.0562	0.1303	0.1302	0.1024	0.1109	0.0744	0.0962
wR_2 (all)	0.1349	0.1224	0.1231	0.1543	0.1234	0.1248	0.1127	0.1071	0.2064	0.1045
Δρ (max, min) / e$^-$ /Å^3 or fm/Å^3	0.34, -0.21	0.08, -0.11	0.08, -0.10	0.29, -0.25	0.07, -0.09	0.07, -0.08	0.05, -0.06	0.04, -0.05	0.26, -0.19	0.04, -0.05

[a] *It is not possible to accurately determine unit cell parameters from a Laue experiment at a continuous neutron source so no errors are listed. X-ray determined values are used where available.*

Table 4.2 *X-ray and neutron data collection and refinement information for the 2:1 complex of N,N'-dimethylurea and oxalic acid.*[a]

Compound	**2:1 *N,N'*-Dimethylurea : Oxalic acid**						
Diffractometer	VIVALDI	Rigaku R-AXIS RAPID	Rigaku R-AXIS RAPID	VIVALDI	VIVALDI	VIVALDI	Rigaku R-AXIS RAPID
Radiation	Neutron	X-ray	X-ray	Neutron	Neutron	Neutron	X-ray
Formula	$C_8H_{18}N_4O_6$	$C_8H_{18}N_4O_6$	$C_8H_{18}N_4O_6$	$C_8H_{18}N_4O_6$	$C_8H_{18}N_4O_6$	$C_8H_{18}N_4O_6$	$C_8H_{18}N_4O_6$
Molecular weight (g mol^{-1})	266.26	266.26	266.26	266.26	266.26	266.26	266.26
T (K)	4	100	200	200	240	280	300
Space group	*P2$_1$/n*	*P2$_1$/n*	*P2$_1$/n*	*P2$_1$/n*	*P2$_1$/n*	*P2$_1$/n*	*P2$_1$/n*
***a* (Å)**	3.73	3.8247(3)	3.8973(3)	3.90	3.93	3.96	3.9806(3)
***b* (Å)**	13.26	13.228(1)	13.188(1)	13.19	13.17	13.16	13.150(1)
***c* (Å)**	12.36	12.4122(7)	12.4699(7)	12.47	12.49	12.51	12.524(1)
***β* (°)**	95.00	94.883(2)	94.635(3)	94.64	94.45	94.30	94.263(3)
Volume (Å^3)	609.0	625.70(8)	638.80(8)	639.4	644.5	650.1	653.73(8)
Z	2	2	2	2	2	2	2
Reflections collected	6416	7649	6976	6271	5405	10447	8124
Independent	1756	1411	1443	1626	1330	1202	1485
Observed > 2σ(I)	1161	1290	1309	1127	901	869	1144
R_{int}	0.240	0.017	0.015	0.131	0.151	0.153	0.019
Parameters	164	118	118	164	164	164	118
GooF	1.18	1.06	1.07	1.16	1.26	1.56	1.08
R_1 (observed)	0.0645	0.0294	0.0331	0.0415	0.0483	0.0513	0.0368
R_1 (all)	0.1179	0.0322	0.0359	0.0801	0.0867	0.0859	0.0475
wR_2 (all)	0.1273	0.0763	0.0933	0.0857	0.0950	0.0951	0.1151
Δρ (max, min) / fm/Å^3	0.15, -0.13	0.36, -0.19	0.33, -0.17	0.05,-0.05	0.05, -0.05	0.05,-0.05	0.18 -0.18

[a] *It is not possible to accurately determine unit cell parameters from a Laue experiment at a continuous neutron source so no errors are listed. X-ray determined values are used where available.*

Table 4.3 *X-ray and neutron data collection and refinement information for the 2:1 complex of N-methylurea and chloranilic acid.*[a]

Compound	**2:1 *N*-Methylurea : CLA**				
Diffractometer	Rigaku R-AXIS RAPID	Rigaku R-AXIS RAPID	VIVALDI	VIVALDI	Rigaku R-AXIS RAPID
Radiation	X-ray	X-ray	Neutron	Neutron	X-ray
Formula	$C_{10}H_{14}Cl_2N_4O_6$	$C_{10}H_{14}Cl_2N_4O_6$	$C_{10}H_{14}Cl_2N_4O_6$	$C_{10}H_{14}Cl_2N_4O_6$	$C_{10}H_{14}Cl_2N_4O_6$
Molecular weight (g mol^{-1})	357.15	357.15	357.15	357.15	357.15
T (K)	100	200	200	250	300
Space group	*P2$_1$/n*	*P2$_1$/n*	*P2$_1$/n*	*P2$_1$/n*	*P2$_1$/n*
***a* (Å)**	4.6147(7)	4.6337(4)	4.63	4.64	4.6504(6)
***b* (Å)**	10.7709(11)	10.7828(7)	10.78	10.79	10.7969(12)
***c* (Å)**	14.250(2)	14.367(1)	14.37	14.44	14.511(2)
***β* (°)**	91.287(5)	90.687(4)	90.69	90.34	90.011(6)
Volume (Å^3)	708.1(2)	717.78(9)	717.17	722.93	728.6(2)
Z	2	2	2	2	2
Reflections collected	8765	8929	6037	5685	10237
Independent	1607	1630	1150	1079	1665
Observed > 2σ(I)	1180	958	834	738	907
R_{int}	0.044	0.051	-	-	0.050
Parameters	128	128	163	163	128
GooF	1.08	1.18	1.35	1.30	1.05
R_1 (observed)	0.0367	0.0381	0.0525	0.0515	0.0425
R_1 (all)	0.0554	0.0800	0.0878	0.0963	0.0897
wR_2 (all)	0.0942	0.1144	0.1007	0.1003	0.1103
Δρ (max, min) / e$^-$ /Å^3 or fm/Å^3	0.32, -0.39	0.32, -0.38	0.06, -0.06	0.05, -0.05	0.24, -0.27

[a] *It is not possible to accurately determine unit cell parameters from a Laue experiment at a continuous neutron source so no errors are listed. X-ray determined values are used where available.*

Table 4.4 *X-ray data collection and refinement information for the 2:1 complex of N-methylurea and bromanilic acid.*

Compound	**2:1 *N*-Methylurea : BRA**		
Diffractometer	Rigaku R-AXIS RAPID	Rigaku R-AXIS RAPID	Rigaku R-AXIS RAPID
Formula	$C_{10}H_{14}Br_2N_4O_6$	$C_{10}H_{14}Br_2N_4O_6$	$C_{10}H_{14}Br_2N_4O_6$
Molecular weight (g mol^{-1})	446.07	446.07	446.07
T (K)	100	200	300
Space group	*P*2$_1$/*n*	*P*2$_1$/*n*	*P*2$_1$/*n*
***a* (Å)**	4.5639(4)	4.6050(4)	4.6486(5)
***b* (Å)**	10.6442(9)	10.7340(12)	10.7857(11)
***c* (Å)**	14.997(2)	15.031(2)	15.092(3)
***β* (°)**	90.754(5)	90.366(5)	89.861(6)[b]
Volume (Å^3)	728.47(13)	742.99(14)	756.7(2)
Z	2	2	2
Reflections collected	8794	9901	8851
Independent	1620	1684	1684
Observed > 2σ(I)	1382	1235	1051
R_{int}	0.043	0.054	0.056
Parameters	128	128	128
GooF	1.09	1.08	1.02
R_1 (observed)	0.0290	0.0386	0.0406
R_1 (all)	0.0397	0.0607	0.0788
wR_2 (all)	0.0661	0.1007	0.1005
Δρ (max, min) / e$^-$/Å^3	0.62, -0.37	0.83, -0.79	0.54, -0.38

[b] *The β angle of the unit cell decreases with increasing temperature. The non-conventional value for the β angle is used for the 300 K data so that all the structures may be refined using the same atomic coordinates and directly compared.*

Table 4.5 *X-ray data collection and refinement information for the 2:1 complex of urea and bromanilic acid.*

Compound	**2:1 Urea : BRA**		
Diffractometer	Bruker Nonius Kappa CCD	Bruker Nonius Kappa CCD	Bruker Nonius Kappa CCD
Formula	$C_{16}H_{20}Br_4N_8O_{12}$	$C_{16}H_{20}Br_4N_8O_{12}$	$C_{16}H_{20}Br_4N_8O_{12}$
Molecular weight (g mol^{-1})	836.04	836.04	836.04
T (K)	110	200	300
Space group	*P-1*	*P-1*	*P-1*
***a* (Å)**	8.6949(1)	8.7890(1)	8.9090(1)
***b* (Å)**	10.5941(2)	10.6073(2)	10.6307(1)
***c* (Å)**	15.4491(2)	15.4426(2)	15.4335(1)
***α* (°)**	75.926(1)	75.905(1)	75.810(1)
***β* (°)**	83.702(1)	83.852(1)	84.05(1)
***γ* (°)**	73.837(1)	73.927(1)	74.29(1)
Volume (Å^3)	1324.46(3)	1340.53(3)	1363.10(2)
Z	2	2	2
Reflections collected	45122	45815	43227
Independent	6038	6131	6193
Observed > 2σ(I)	5567	5420	5308
R_{int}	0.026	0.028	0.028
Parameters	441	441	441
GooF	1.03	1.02	1.02
R_1 (observed)	0.0199	0.0200	0.0244
R_1 (all)	0.0207	0.0257	0.0322
wR_2 (all)	0.0411	0.0468	0.0576
Δρ (max, min) / e$^-$/Å^3	0.43, -0.39	0.62, -0.60	0.75, -0.83

4.2 *N,N*-Dimethylurea Oxalic Acid (2:1)[167]

4.2.1 Crystallographic Data

The 2:1 complex of *N,N*-dimethylurea and oxalic acid crystallises in the space group $P2_1/c$ with one *N,N*-dimethylurea molecule and half an oxalic acid molecule in the asymmetric unit above 120 K (**Figure 4.2**). This complex undergoes a phase transition on cooling below ~120 K, resulting in a doubling of the unit cell and hence asymmetric unit, which below 120 K comprises two *N,N*-dimethylurea molecules and one oxalic acid molecule.

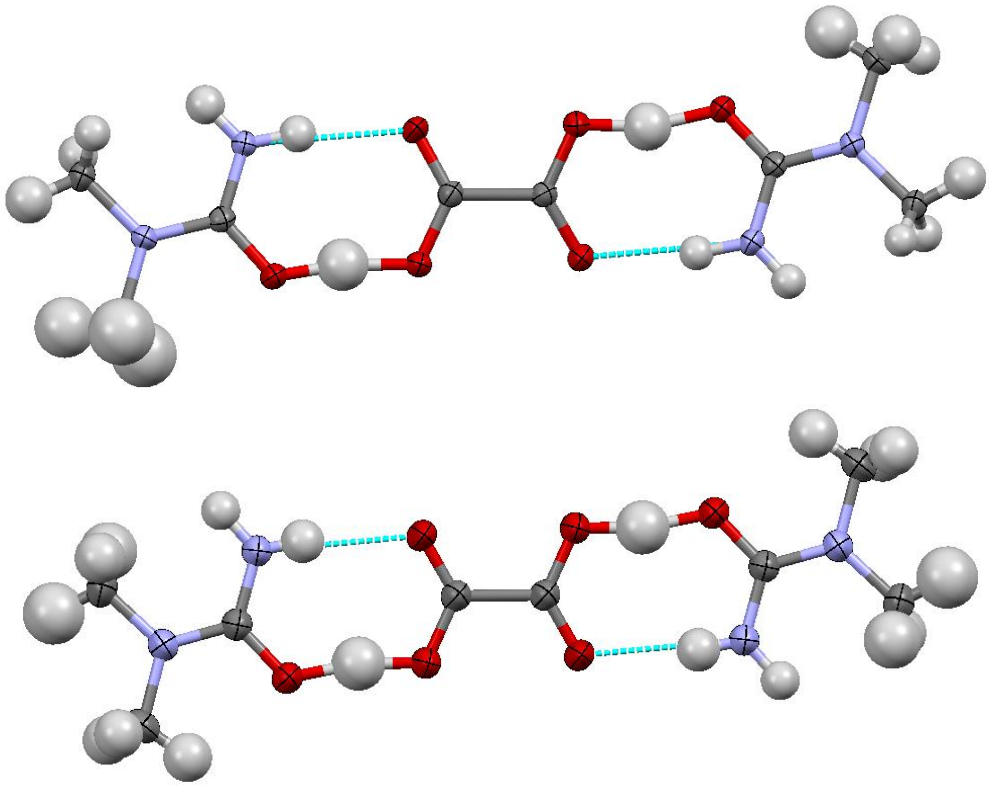

Figure 4.2 *Hydrogen bonded three molecule "DMU-A-DMU" units in the low- (top at 100 K) and high- (bottom at 200 K) temperature phases of the 2:1 complex of N,N-dimethylurea and oxalic acid, as refined from the X-ray data.*

An oxalic acid molecule is linked by hydrogen bonds to two *N,N*-dimethylurea molecules to form a three molecule "DMU-A-DMU" hydrogen bonded unit. These are linked by two O-H···O SSHBs (with O···O distances of 2.4398(15) and 2.4423(15) Å at 100 K) with almost centred hydrogen atoms (**Table 4.6**), and assisted by medium strength N-H···O hydrogen bonds (with N···O distances of 2.914(2) and 2.860(2) Å at 100 K). These hydrogen bonds are formed between the carboxyl groups of the acid and the carbonyl and amide groups of the

N,N-dimethylureas, forming an $R_2^2(8)$ hydrogen bonded ring (**Figure 4.3**, top). These units form layers in the plane of the *ac* diagonal (**Figure 4.3**, bottom). Each unit is linked to the next unit in the layer through lateral hydrogen bonds between the *N,N*-dimethylurea amide group and the oxygens of the acid (with N···O distances of 2.927(2) and 3.046(2) Å), forming chains (**Figure 4.3**, top) of the three-molecule units along the *b*-axis. The chains on either side have a different orientation, rotating ~76° in the plane with this pattern then repeating. Between the layers there are weak interactions involving the methyl groups of one layer and both the hydroxyl and carbonyl oxygen atoms of the acid in the neighbouring layers, with C···O distances of 3.470(2) and 3.559(2) Å, respectively.

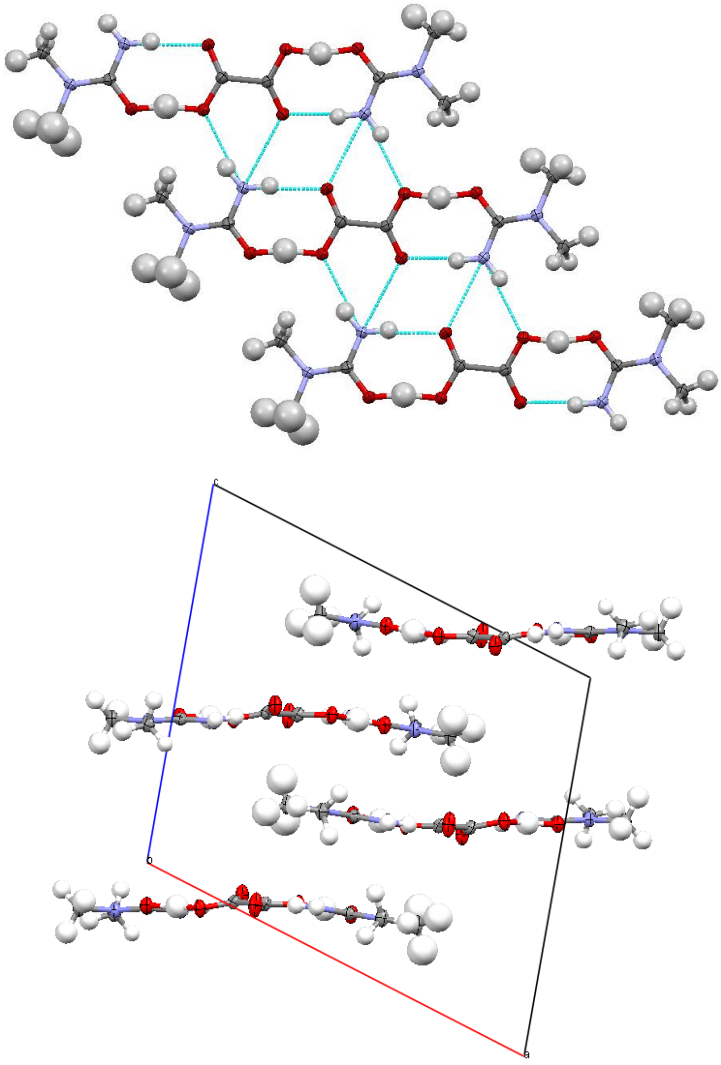

Figure 4.3 *Three molecule "DMU-A-DMU" hydrogen bonded units assembled into a hydrogen bonded chain in the low temperature phase of the N,N-dimethylurea oxalic acid molecular complex (top) and layers of these units viewed along the b-axis (bottom), both from the 100 K X-ray data.*

Table 4.6 *Lengths of the short, strong O-H···O hydrogen bond in the three molecule "DMU-A-DMU" units of the complex of N,N-dimethylurea with oxalic acid.*

T/K	r(O-H)/Å		r(H···O)/Å		r(O-H···O)/Å	
	X-ray	Neutron	X-ray	Neutron	X-ray	Neutron
100[a]	1.18(3)	-	1.28(3)	-	2.4398(15)	-
	1.26(3)	-	1.19(3)	-	2.4423(15)	-
150	-	1.213(5)	-	1.228(5)	-	2.430(4)
175	-	1.213(5)	-	1.227(5)	-	2.430(4)
200	1.19(3)	1.212(6)	1.26(3)	1.232(6)	2.436(2)	2.432(4)
225	-	1.206(6)	-	1.246(7)	-	2.439(5)
250	-	1.187(7)	-	1.256(7)	-	2.430(5)
275	-	1.183(7)	-	1.268(7)	-	2.439(5)
300	1.14(4)	1.168(8)	1.33(4)	1.277(8)	2.439(2)	2.430(6)

[a] *The two values at 100 K correspond to the two unique short strong hydrogen bonds present in the larger asymmetric unit of the low temperature phase.*

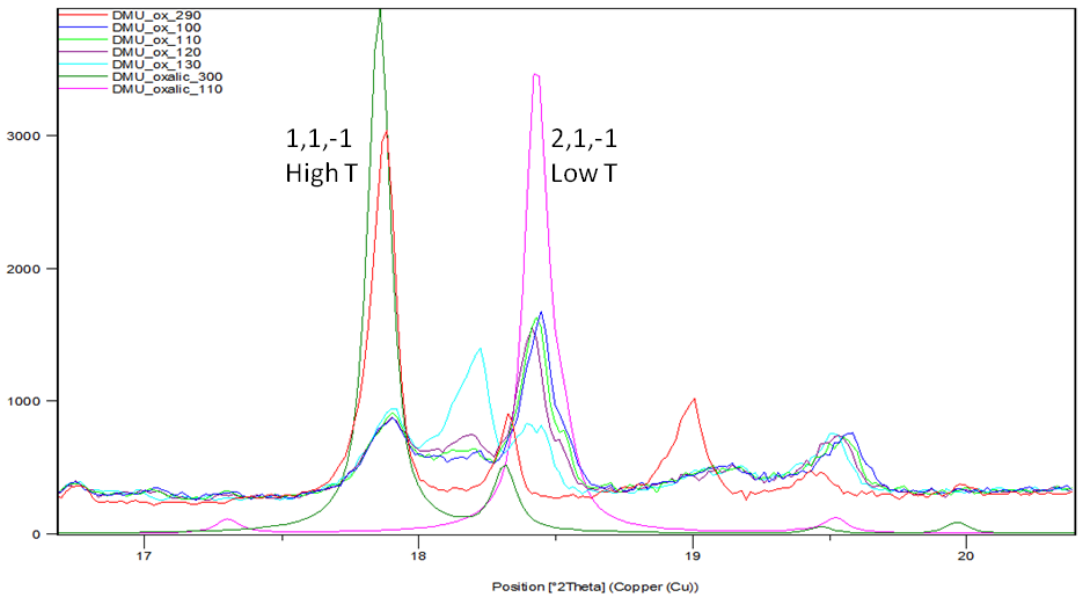

Figure 4.4 *Variable temperature X-ray powder diffraction patterns showing a significant peak shift in the (1,1,-1) refection of the high temperature phase from its position at low temperature (indexed as (2,1,-1) reflecting the doubling of the a-axis) through the phase transition. To allow the shift to be seen more easily, the pink and green profiles represent the calculated patterns from single crystal diffraction data for the low and high temperature phases, respectively. The peak shift occurs between 120 and 130 K.*

The temperature at which the phase transition occurs was confirmed by X-ray powder diffraction to be between 120 and 130 K (**Figure 4.4**). In the higher temperature phase the connectivity of the hydrogen bonded network remains the same, based on the "DMU-A-DMU" hydrogen bonded unit (**Figure 4.2**), as does the general crystal structure. The O-H···O SSHB motif is present in both phases (two of these, equivalent in the high T phase, but distinct in the low T phase) with the hydrogen atom remaining approximately centred in the hydrogen bonds involved. As stated above, the transition involves a doubling of the asymmetric unit below ~120 K which is accompanied by an approximate doubling of the *a*-axis (7.7944(3) to 14.992(2) Å) between 200 and 100 K based on the X-ray data. These changes also coincide with a slight change in the β angle from 111.407(2)° at 200 K to 107.306(12)° at 100 K. Over the same temperature range the *b*- and *c*-axes only decrease slightly (6.4482(2) to 6.4333(7) Å and 13.6550(6) to 13.610(2) Å for the *b*- and *c*-axes, respectively, between 200 and 100 K), which is in line with what would normally be expected with the decrease in temperature. As a result, the unit cell volume is almost exactly doubled, from 638.95(4) to 1253.2(3) $Å^3$, between 200 and 100 K.

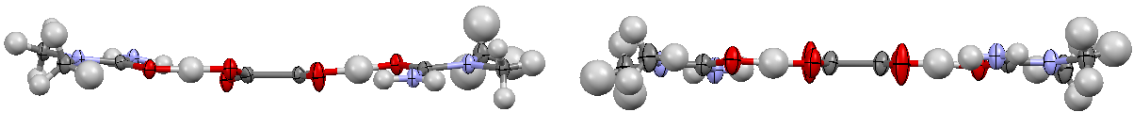

Figure 4.5 *Three molecule "DMU-A-DMU" units in the low (left, at 100K) and high (right, at 200K) temperature phases of the N,N-dimethylurea oxalic acid molecular complex from the X-ray data. In the high temperature phase the unit is flatter and more symmetric.*

The differences between the two phases become clear when the structural differences between the two phases are examined. In the low temperature phase, the oxalic acid molecule is asymmetrically twisted, causing the two *N,N*-dimethylurea molecules to deviate from co-planarity. This can be seen in the angles between the planes formed by the carboxyl groups at each end of the acid and the amide groups of the *N,N*-dimethylureas to which they are hydrogen bonded. These angles are 9.20(14)° and 17.01(16)° at 100 K indicating that one end of the unit is considerably more bent than the other. This is not the case in the high temperature phase where the two ends of the unit are symmetry equivalent and the angle between the planes of the carboxyl and amide groups is 8.13(18)° at 200 K;

the unit is now flatter (**Figure 4.5**). In the low temperature phase the bend of the units affects the orientation of the surrounding chains, this is not the case in the high temperature phase and the layers are flatter as a consequence. As the planes lie in the *ac* diagonal this slight shift in the orientation of the layers causes the slight change in the *β* angle and also accounts for why the *a*-axis at 100 K is slightly less than double the value at 200 K. Through the transition at ~120 K the length of the O-H···O SSHB is invariant while the length of the unique N-H···O hydrogen bond (N···O 2.908(2) Å) lies between the values determined for the two distinct hydrogen bonds of this type at 100 K. The same types of weak interactions are still present between the layers, though the relative positions of units in alternate layers have shifted slightly through the transition. In the X-ray structures of the high temperature phase at 200 and 300 K, it was not possible to resolve the methyl group hydrogen positions and these have been fixed to standard bond lengths and angles.

The X-ray data gives an indication of the presence of proton migration within this complex. The hydrogen atom is approximately centred within the SSHB and the hydrogen atom electron density is significantly elongated in the direction of the hydrogen bond when visualised in Fourier difference maps, with a large isotropic thermal displacement parameter (**Figure 4.6**, left). The electron density is so diffuse within the SSHB that at 100 K it appears as if there are two electron density peaks which would be indicative of proton disorder, a highly unlikely effect in this type of hydrogen bond. This has led to poorly refined hydrogen atomic positions which are not in good agreement with the peaks of electron density; this is particularly evident in the X-ray Fourier difference map at 300 K. The O···O distance of the SSHB does not change greatly with temperature, similar to the situation found in urea-phosphoric acid (see **Section 1.7**).[62,63]

In order to investigate the SSHB and the possibility of proton migration more fully, neutron diffraction data were collected at seven temperatures between 150 and 300 K for the high temperature phase. The large size of the neutron sample meant that the crystal did not survive through the phase transition due to mechanical damage and therefore no data were collected on the low temperature phase. While in the X-ray structure the methyl hydrogens had to be fixed at 200 and 300 K, the neutron data show the methyl hydrogens have large anisotropic displacement parameters indicating libration of the methyl groups (**Figure 4.7**). As the methyl groups are only involved in weaker interactions with nearby oxygen atoms, they are free to undergo

these rotations. This effect has previously been investigated in the crystal structure of aspirin.[171]

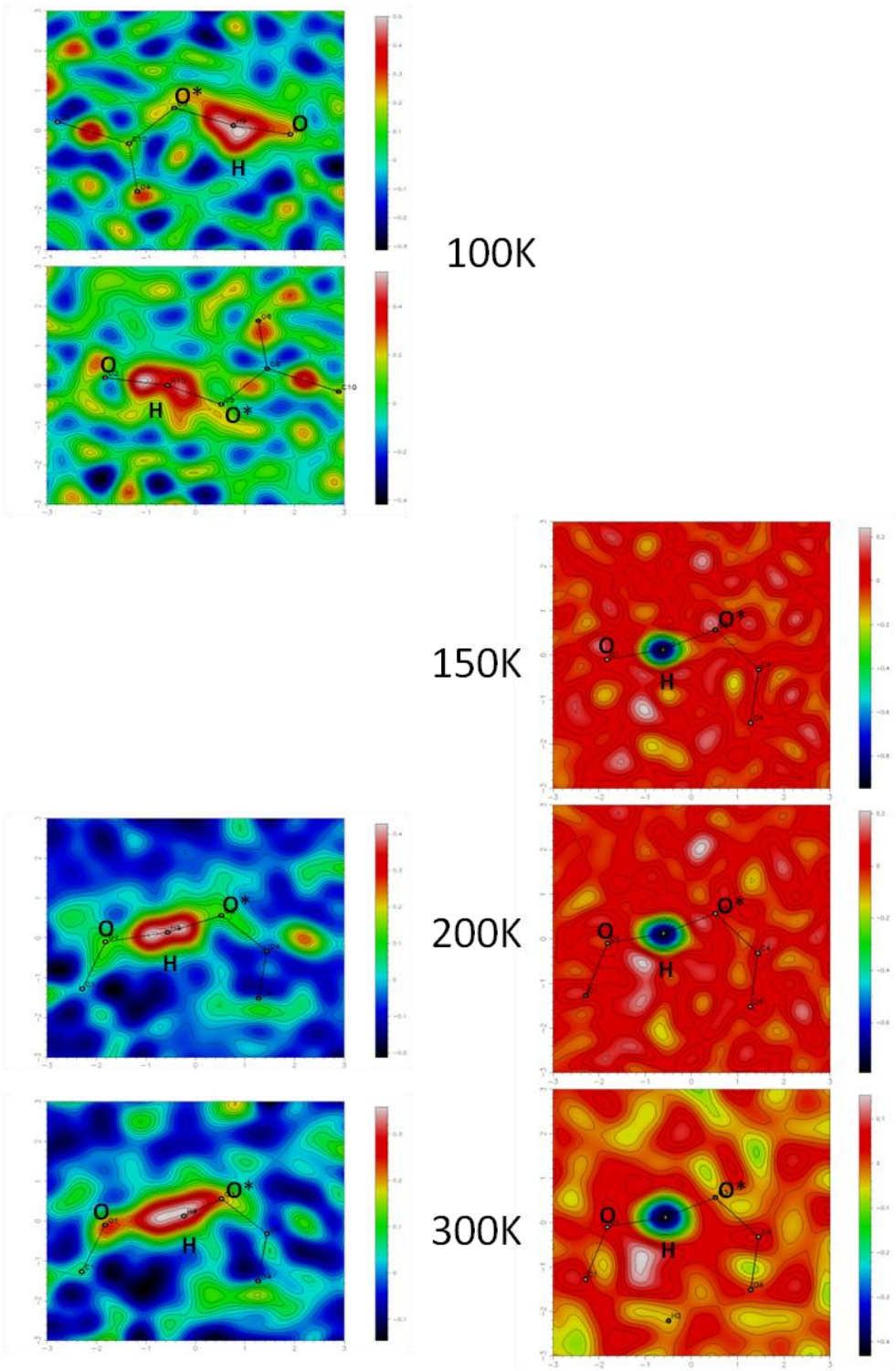

Figure 4.6 *Fourier difference maps showing the electron (left) and nuclear (right) density of the hydrogen atom in the short, strong hydrogen bond in the 2:1 complex of N,N-dimethylurea and oxalic acid. The acid oxygens are denoted with an asterisk (*).*

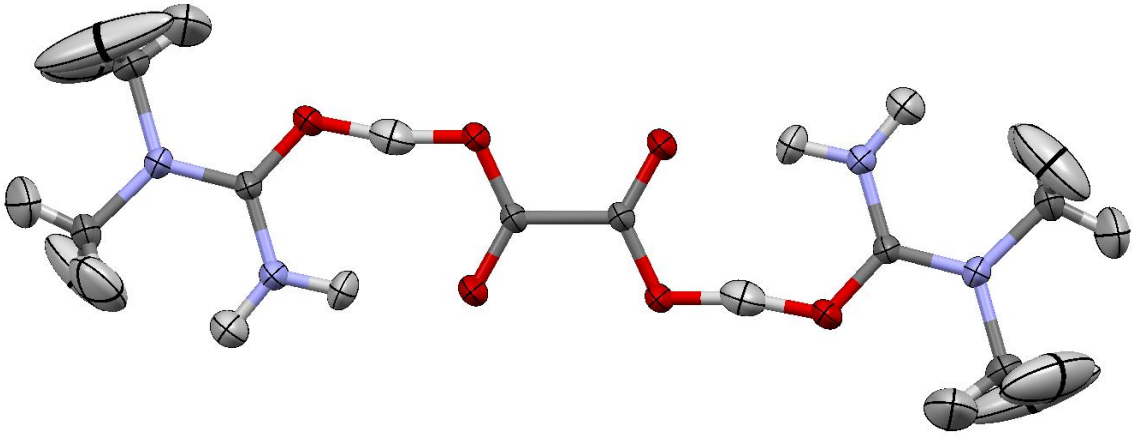

Figure 4.7 *A "DMU-A-DMU" molecular unit from the neutron structure of the 2:1 complex of N,N-dimethylurea and oxalic acid at 150 K.*

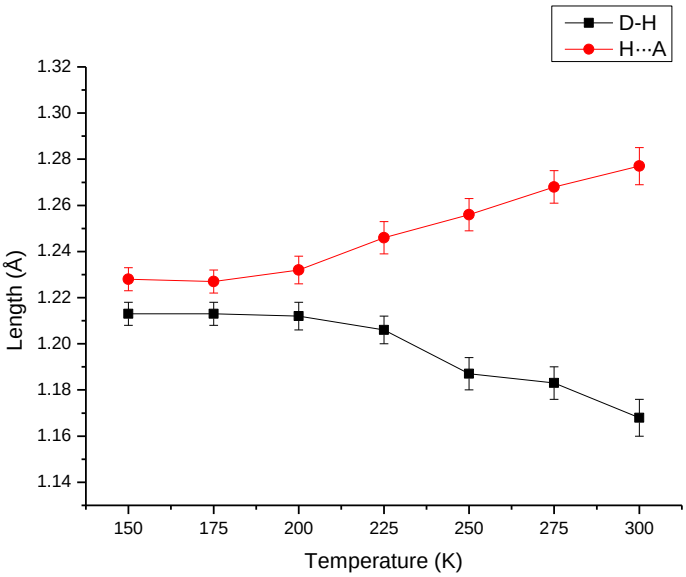

Figure 4.8 *The change in D-H and H···A distances in the short, strong hydrogen bond of the 2:1 complex of N,N-dimethylurea and oxalic acid determined by neutron diffraction as a function of temperature.*

Visualising the hydrogen atom nuclear density in the Fourier difference maps generated from the neutron diffraction data, confirms that the hydrogen atom in the SSHB is located in a single position at all temperatures, indicative of it residing in a single well potential, as would be expected in a hydrogen bond with such a short D···A distance (**Figure 4.6**, right). The neutron data confirms that the hydrogen atom shows significant migration towards the donor atom as the temperature is increased (**Table 4.6** and **Figure 4.8**). The proton migration is of magnitude 0.045(9) Å between 150 and 300 K; this is of a similar magnitude to that observed in urea-

phosphoric acid.[62,63] This result shows by increasing the basicity of the urea component through dimethyl substitution, a SSHB shorter than those in the urea-[108,109] and *N*-methylurea-oxalic acid[112] complexes has been formed in which the proton undergoes temperature dependent migration. This is in contrast to the urea- and *N*-methylurea-oxalic acid complexes which do not display temperature dependent proton migration.

4.2.2 Computational Data

Table 4.7 *Lengths of the short, strong O-H···O hydrogen bond in the three molecule "DMU-A-DMU" units in the high temperature phase of the complex of N,N-dimethylurea with oxalic acid from the neutron diffraction and theoretical data.*

T/K	r(O-H)/Å		r(H···O)/Å		r(O-H···O)/Å	
	Neutron	**Theory**	**Neutron**	**Theory**	**Neutron**	**Theory**
150	1.213(5)	1.275	1.228(5)	1.167	2.430(4)	2.431
175	1.213(5)	-	1.227(5)	-	2.430(4)	-
200	1.212(6)	1.267	1.232(6)	1.175	2.432(4)	2.429
225	1.206(6)	-	1.246(7)	-	2.439(5)	-
250	1.187(7)	1.260	1.256(7)	1.181	2.430(5)	2.428
275	1.183(7)	-	1.268(7)	-	2.439(5)	-
300	1.168(8)	1.262	1.277(8)	1.181	2.430(6)	2.430

The theoretical structures generated from the CPMD simulations at four temperatures agree with the trend of migration of the proton within the SSHB towards the donor atom as the temperature is increased. The experimental data show the hydrogen atom located more centrally within, and on the other side of, the SSHB than in the theoretical data (i.e. the hydrogen atom is transferred across the hydrogen bond according to the theoretical data), while the experimental and theoretical O···O distances are in good agreement (**Table 4.7**). The magnitude of the migration is less significant in the theoretical structures than in the experimental neutron diffraction data. In this case, a migration of 0.013 Å is observed between 150 and 300 K from the theoretical data, with a migration of 0.045(9) Å observed in the experimental data over the same temperature range. Interestingly, in the theoretical data the migration only occurs up until 250 K, with the position invariant between 250 and 300 K. This is likely to be a consequence of the difficulty in

modelling such subtle effects using computational simulations, an effect already shown in the differences in the magnitude of migration between theory and experiment. However, the observation that both theory and experiment support the trend of migration is encouraging. Theoretical PESs of the SSHB have not been generated for this structure due to time restrictions.

4.3 *N,N'*-Dimethylurea Oxalic Acid (2:1)[167]

4.3.1 Crystallographic Data

Table 4.8 *Lengths of the short, strong O-H···O hydrogen bond in the three molecule "DMU-A-DMU" units of the complex of N,N'-dimethylurea with oxalic acid.*

T/K	r(O-H)/Å		r(H···O)/Å		r(O-H···O)/Å	
	X-ray	Neutron	X-ray	Neutron	X-ray	Neutron
4	-	1.182(5)	-	1.265(5)	-	2.437(3)
100	1.13(2)	-	1.33(2)	-	2.4469(9)	-
200	1.12(2)	1.166(3)	1.35(2)	1.293(3)	2.4507(10)	2.448(2)
240	-	1.164(4)	-	1.295(4)	-	2.448(2)
280	-	1.151(5)	-	1.311(5)	-	2.452(3)
300	1.06(3)	-	1.42(3)	-	2.4548(12)	-

The 2:1 complex of *N,N'*-dimethylurea and oxalic acid crystallises in the $P2_1/n$ space group with one *N,N'*-dimethylurea molecule and half an oxalic acid molecule in the asymmetric unit. The complex also forms bent hydrogen bonded three-molecule "DMU-A-DMU" units similar to those found in the low temperature phase of the complex of *N,N*-dimethylurea and oxalic acid (**Section 4.2**), with an angle between the planes of the carboxyl and amide groups of 11.8(2)° at 100 K (**Figure 4.9**, top). The molecules in the unit are again held in place by two symmetry equivalent O-H···O SSHBs (with O···O distances of 2.4469(9) Å at 100 K) with almost centred hydrogen atoms (**Table 4.8**) and weaker N-H···O hydrogen bonds (with N···O distances of 2.8460(11) Å) between the carboxyl groups of the acid and the carbonyl and amide groups of the N,N'-dimethylureas, forming $R_2^2(8)$ hydrogen bonded rings. However, this unit is where the similarities in the *N,N*-dimethylurea and *N,N'*-dimethylurea structures end, as this complex does not form a layered structure due to the methyl groups blocking interactions between the acid oxygens and the amide nitrogens. Instead each molecular unit is surrounded by other units

in a different orientation aligned at ~70° to the original unit (**Figure 4.9**, middle). This motif is repeated along the *c*-axis with the adjacent units held in place through *DHAA* bifurcated N-H···O hydrogen bonds (N···O lengths 3.1996(11) and 3.0069(11) Å) between the amide groups of *N,N'*-dimethylurea and two oxygen atoms bridging the two carboxylic acid groups of oxalic acid molecules, along with weaker C-H···O interactions involving methyl groups with oxalic acid carboxylic acid groups (C···O distances of 3.163(1) and 3.552(1) Å) and with urea oxygens (C···O distances of 3.128(1) Å) (**Figure 4.9**, bottom).

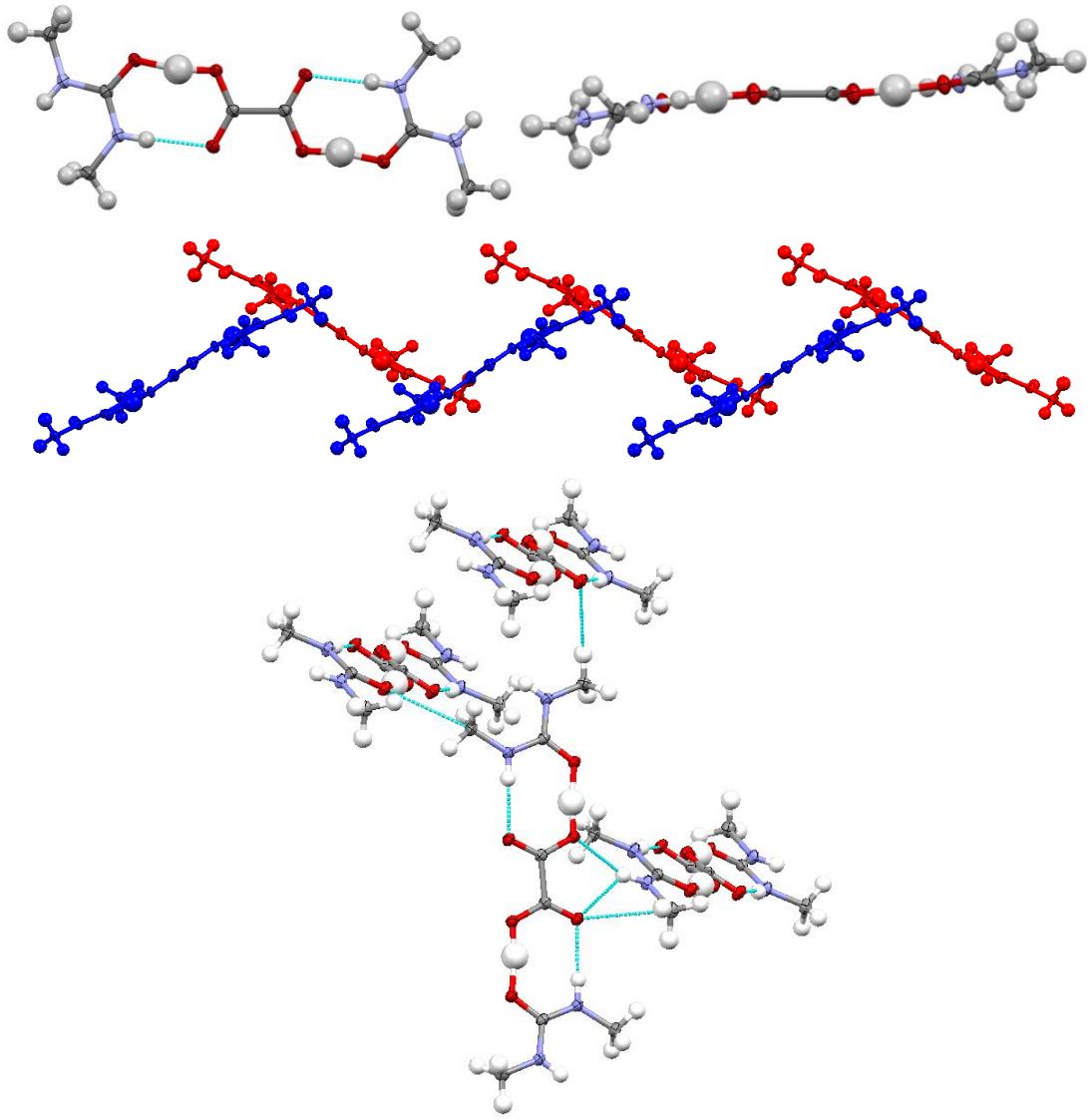

Figure 4.9 *One "DMU-A-DMU" molecular unit of the molecular complex of N,N'-dimethylurea with oxalic acid, (top), the relative orientations of adjacent units (red and blue) looking along the c-axis (middle) and the DHAA bifurcated hydrogen bond and weaker interactions betwen molecular units (bottom), from the 100 K X-ray data.*

The X-ray data show that, whilst the hydrogen atom is not centred within the SSHB, the D-H distance is elongated compared to what would be expected for a normal O-H covalent bond, consistent with the electron density being pulled towards the centre of the SSHB. Fourier difference maps generated from the X-ray data show elongation of the density within the SSHB and also show poorly refined hydrogen atomic positions with respect to the electron density peaks (**Figure 4.10**, left). Similar to the previous *N,N*-dimethylurea complex with oxalic acid, the O···O distance does not increase greatly with temperature, with distances of 2.4469(9) and 2.4548(12) Å at 100 and 300 K, respectively.

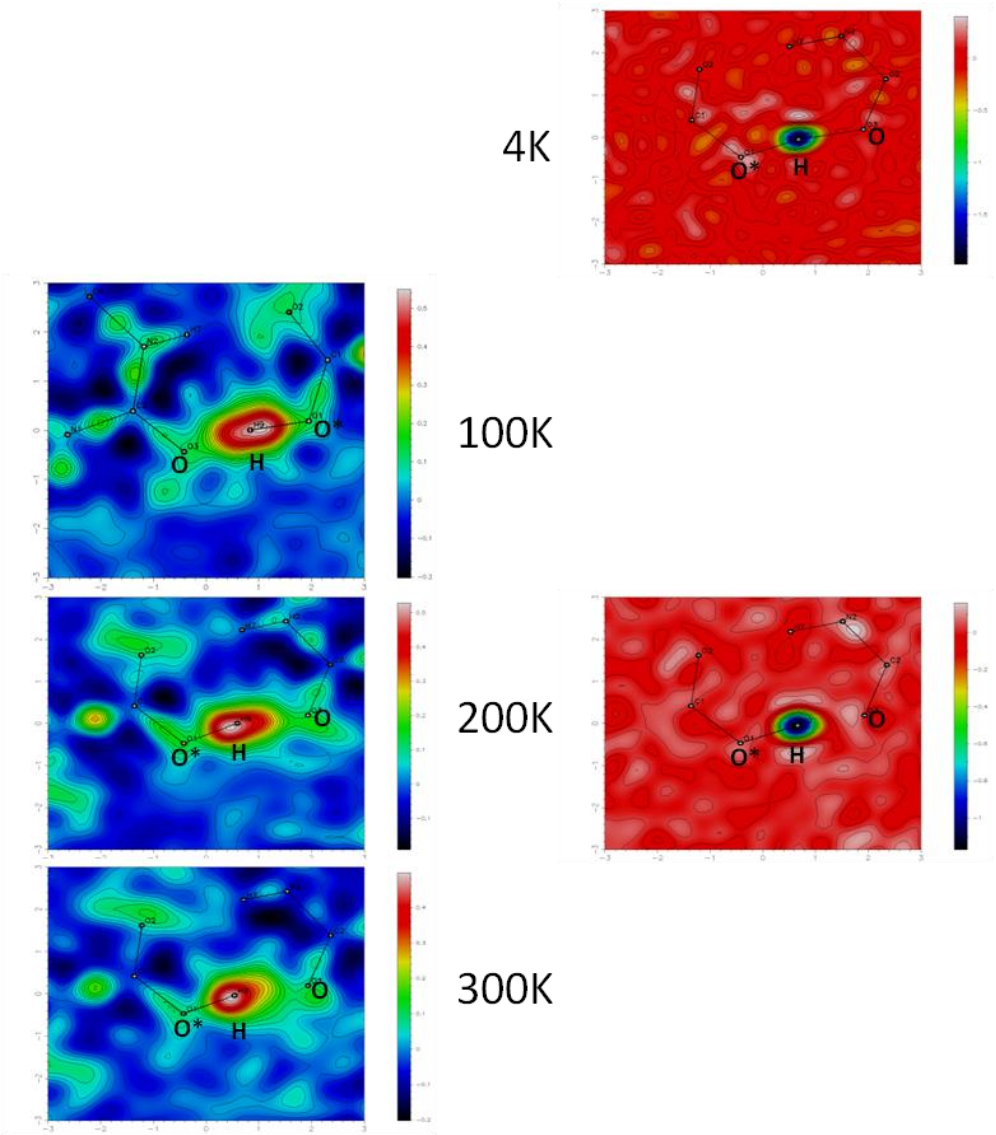

Figure 4.10 *Fourier difference maps showing the electron (left) and nuclear (right) density of the hydrogen atom in the short, strong hydrogen bond in the 2:1 complex of N,N'-dimethylurea and oxalic acid, at selected temperatures. The acid oxygen is denoted with an asterisk (*).*

Neutron diffraction data were collected at four temperatures between 4 and 280 K (**Figure 4.11**). Fourier difference maps of the SSHB generated from the neutron diffraction data show a single, localised position for the hydrogen atom in contrast to the elongated electron density from the X-ray data (**Figure 4.10**, right). The neutron data confirms a migration of 0.031(7) Å towards the donor atom between 4 and 280 K (**Table 4.8** and **Figure 4.12**). This result again confirms the potential for rational design of SSHBs which contain a migrating proton through the use of dimethyl substituted ureas (see **Section 4.2**).

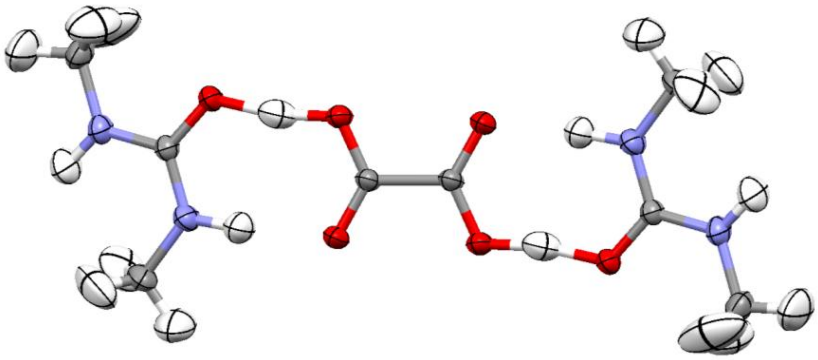

Figure 4.11 *A "DMU-A-DMU" molecular unit from the neutron structure of the 2:1 complex of N,N'-dimethylurea and oxalic acid at 200 K.*

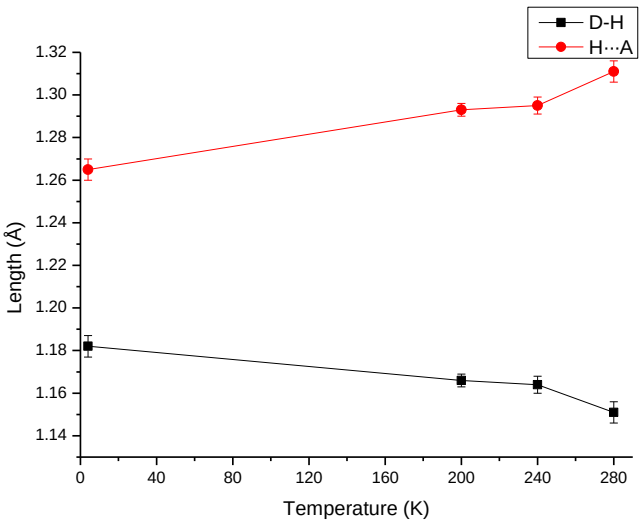

Figure 4.12 *The change in D-H and H...A distances in the short, strong hydrogen bond of the 2:1 complex of N,N'-dimethylurea and oxalic acid determined by neutron diffraction as a function of temperature.*

4.3.2 Temperature Dependent Structural Effects

While this complex does not show a phase transition on cooling (as in the case of the *N,N*-dimethylurea complex), it does show some other interesting structural changes with temperature. As the temperature is increased, the *b*-axis contracts from 13.2281(11) Å at 100 K to 13.1500(9) Å at 300 K based on the X-ray data (the unit cell parameters obtained from X-ray data are more accurate than those in the neutron data). Over the same temperature range, the *a*- and *c*-axes both expand in a manner which would be expected with an increase in temperature, the *a*-axis slightly more rapidly, while the *β* angle remains relatively constant.

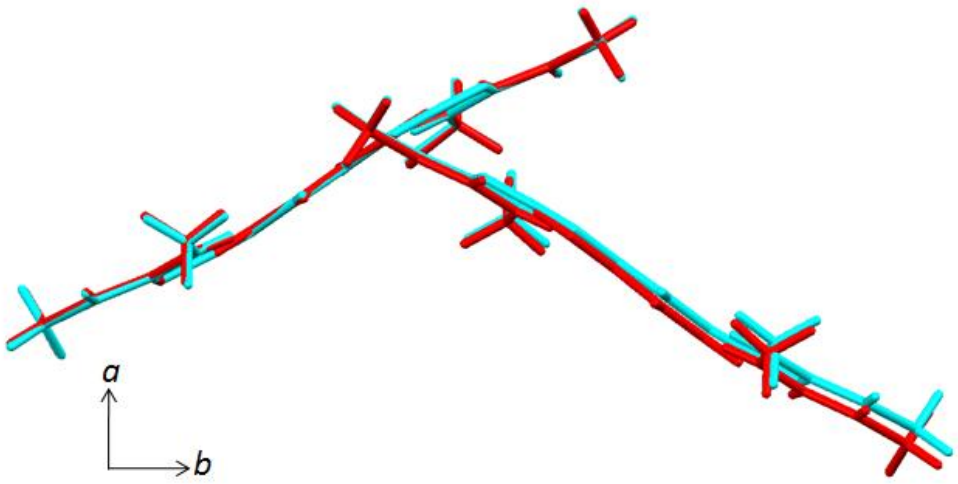

Figure 4.13 *Structural overlay of two adjacent three-molecule "DMU-A-DMU" units viewed along the c-axis in the molecular complex of N,N'-dimethylurea with oxalic acid, at 100 K (cyan) and 300 K (red). The structural overlay is optimised for the unit on the left and separation of the units occurs as a function of temperature, which can be seen in the unit to the right.*

The contraction of the *b*-axis arises from a slight shift in the positions of the molecular units relative to each other as the temperature is increased (**Figure 4.13**). If one molecular unit is overlayed in the 100 and 300 K structures, the layers of units remain along the *c* axis so the movement only occurs in the *a*- and *b*-axes, with the *b*-axis contracting and the *a*-axis increasing more rapidly (when compared with the behaviour of the *c*-axis).

4.3.3 Computational Data

The theoretical structures generated from the CPMD simulations at three temperatures agree with the observation of proton migration within the SSHB of this complex. The theoretical data show the hydrogen atom position within the SSHB to be more centred and on the other side of the SSHB than in the experimental data where it is located closer to the donor atom, similar to the observation in the *N,N*-dimethylurea-oxalic acid complex (see **Section 4.2.2**). The theoretical O···O distance is invariant with temperature and slightly shorter than the experimentally determined values, perhaps an artefact of the unit cell parameters being fixed to the same values at all temperatures in the calculations. The theoretical data show a migration of 0.026 Å between 100 and 300 K, close to the values of 0.031(7) Å obtained from experiment between 4 and 280 K (**Table 4.9**), and in the same direction – i.e. towards the original donor oxygen atom. When compared over a similar temperature range, the theoretical data show a migration of 0.009 Å between 200 and 300 K, while the neutron diffraction data shows a migration of 0.015(6) Å between 200 and 280 K. These values for the magnitude of migration suggest a better agreement between experiment and theory than was achieved in the other dimethylurea complex studied using computational methods in this chapter.

Table 4.9 *Lengths of the short, strong O-H···O hydrogen bond in the three molecule "DMU-A-DMU" units in the high temperature phase of the complex of N,N'-dimethylurea with oxalic acid from the neutron diffraction and theoretical data.*

T/K	r(O-H)/Å		r(H···O)/Å		r(O-H···O)/Å	
	Neutron	**Theory**	**Neutron**	**Theory**	**Neutron**	**Theory**
4	1.182(5)	-	1.265(5)	-	2.437(3)	-
100	-	1.266	-	1.180	-	2.434
200	1.166(3)	1.249	1.293(3)	1.200	2.448(2)	2.434
240	1.164(4)	-	1.295(4)	-	2.448(2)	-
280	1.151(5)	-	1.311(5)	-	2.452(3)	-
300	-	1.240	-	1.208	-	2.437

Analysing the PESs of the SSHB generated from the theoretical data shows a single, broad well (**Figure 4.14**). At 100 K this is asymmetric, becoming significantly flatter and more symmetric at 300 K. This confirms the temperature dependent

nature of the PES, which facilitates the observed proton migration, and the change in shape of the PES is pronounced.

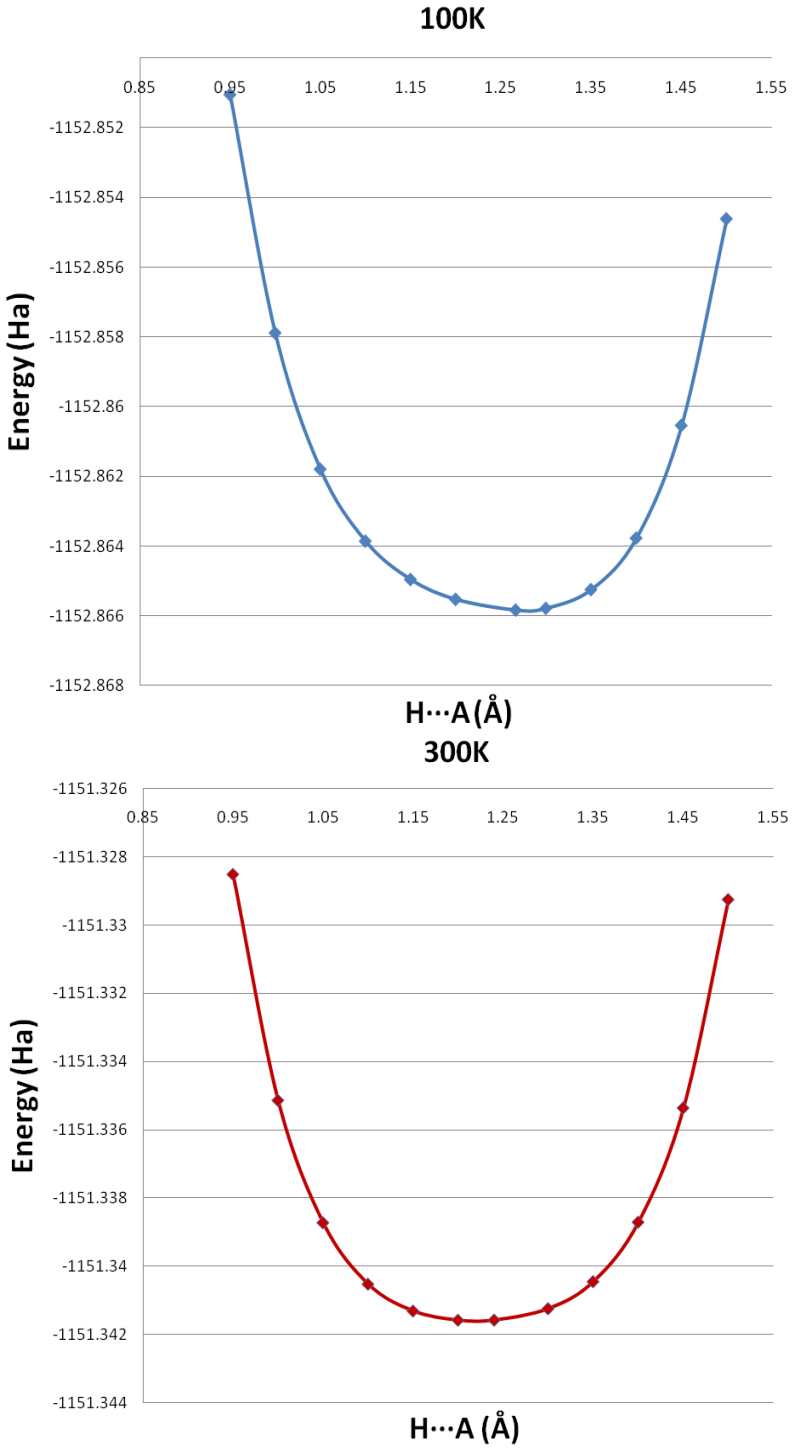

Figure 4.14 *The potential energy surfaces of the short, strong hydrogen bond in the 2:1 complex of N,N'-methylurea and oxalic acid at 100 K (top) and 300 K (bottom), generated from the theoretical data.*

4.4 *N*-Methylurea Chloranilic Acid (2:1)

4.4.1 Crystallographic Data

The 2:1 molecular complex of *N*-methylurea and CLA crystallises in the $P2_1/n$ space group and contains one *N*-methylurea molecule and half a CLA molecule in the asymmetric unit; the methyl group of the *N*-methylurea is in the *syn* position relative to the carbonyl oxygen.

The planar three molecule "MU-A-MU" units contain two symmetry equivalent O-H···O SSHBs (O···O distance of 2.459(2) Å at 100 K) (**Table 4.10**) and two symmetry equivalent N-H···O hydrogen bonds (N···O distance of 2.903(2) Å) between the *N*-methylurea and CLA moieties (**Figure 4.15**, box in top image). Within the molecular units, the *N*-methylurea molecules are tilted slightly with respect to the CLA ring, at an angle of 6.1(3)°. Molecular units within the same layer interact with one another through bifurcated hydrogen bonds and halogen interactions. The two amide hydrogens which point away from the CLA molecule of the same unit are both involved in *DDHHA* bifurcated interactions to neighbouring units. One hydrogen has interactions with the CLA oxygen not involved in the SSHB and with the *N*-methylurea oxygen, with N···O distances of 3.076(2) and 3.161(2) Å, respectively. The other amide hydrogen also interacts with the CLA oxygen not involved in the SSHB and with the Cl atom of the same CLA molecule, with N···O and N···Cl distances of 2.933(2) and 3.461(2) Å, respectively. There is also a C-H···Cl weak hydrogen bond between adjacent molecular units with a C···Cl distance of 3.427(2) Å. The CLA aromatic rings are involved in parallel-displaced π interactions at a distance of ~3.2 Å (**Figure 4.15**, bottom).

Table 4.10 *Lengths of the short, strong O-H···O hydrogen bond in the three molecule "MU-A-MU" units of the complex of N-methylurea with chloranilic acid.*

T/K	r(O-H)/Å		r(H···O)/Å		r(O-H···O)/Å	
	X-ray	Neutron	X-ray	Neutron	X-ray	Neutron
100	1.12(3)	-	1.35(3)	-	2.459(2)	-
200	1.13(4)	1.230(6)	1.36(4)	1.256(5)	2.471(3)	2.459(4)
250	-	1.206(6)	-	1.294(7)	-	2.467(4)
300	1.10(4)	-	1.42(4)	-	2.484(3)	-

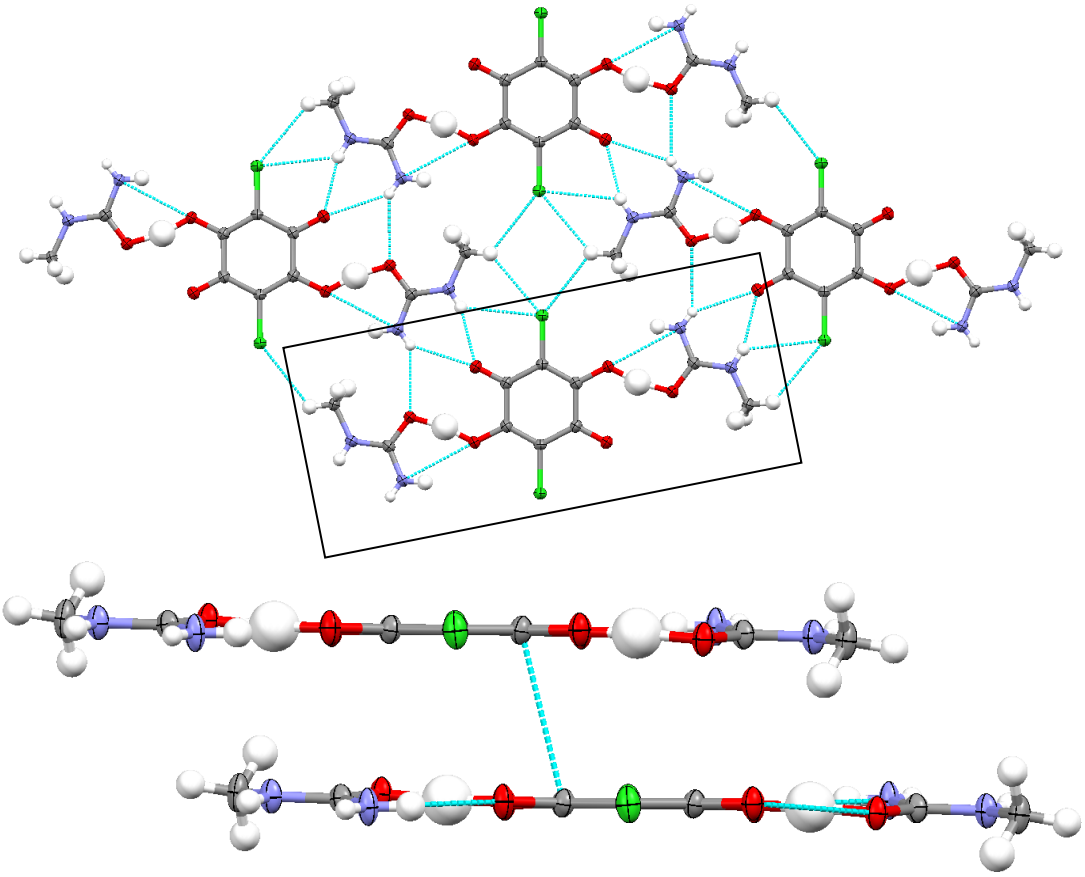

Figure 4.15 *Interactions between "MU-A-MU" units (unit highlighted in box in top image) in the same layer (top) and in different layers (bottom) in the 2:1 complex of N-methylurea and chloranilic acid at 100 K (X-ray).*

From the X-ray data, there are again several indicators of the possible presence of proton migration within this complex. The hydrogen bond is very short (O···O distance of 2.459(2) Å at 100 K) and the hydrogen atom located within the SSHB has a larger thermal displacement parameter than the other hydrogen atoms in the structure. The O···O distance of the SSHB increases significantly with temperature, from 2.459(2) Å at 100 K to 2.484(3) Å at 300 K, in contrast to the two previous complexes (**Section 4.2** and **Section 4.3**). However, such an increase in the donor-acceptor distance in a proton migration complex was previously observed in the N-H···O SSHB of the complex of pentachlorophenol and 4-methylpyridine where the proton displayed temperature dependent migration (see **Section 1.7**).[60] Visualisation of the electron density through Fourier difference maps shows that the electron density is elongated in the direction of the hydrogen bond, particularly at 100 K when the hydrogen bond is shortest, and the hydrogen atomic positions are

poorly refined (**Figure 4.16**, left); both of these effects are common in systems which display proton migration.

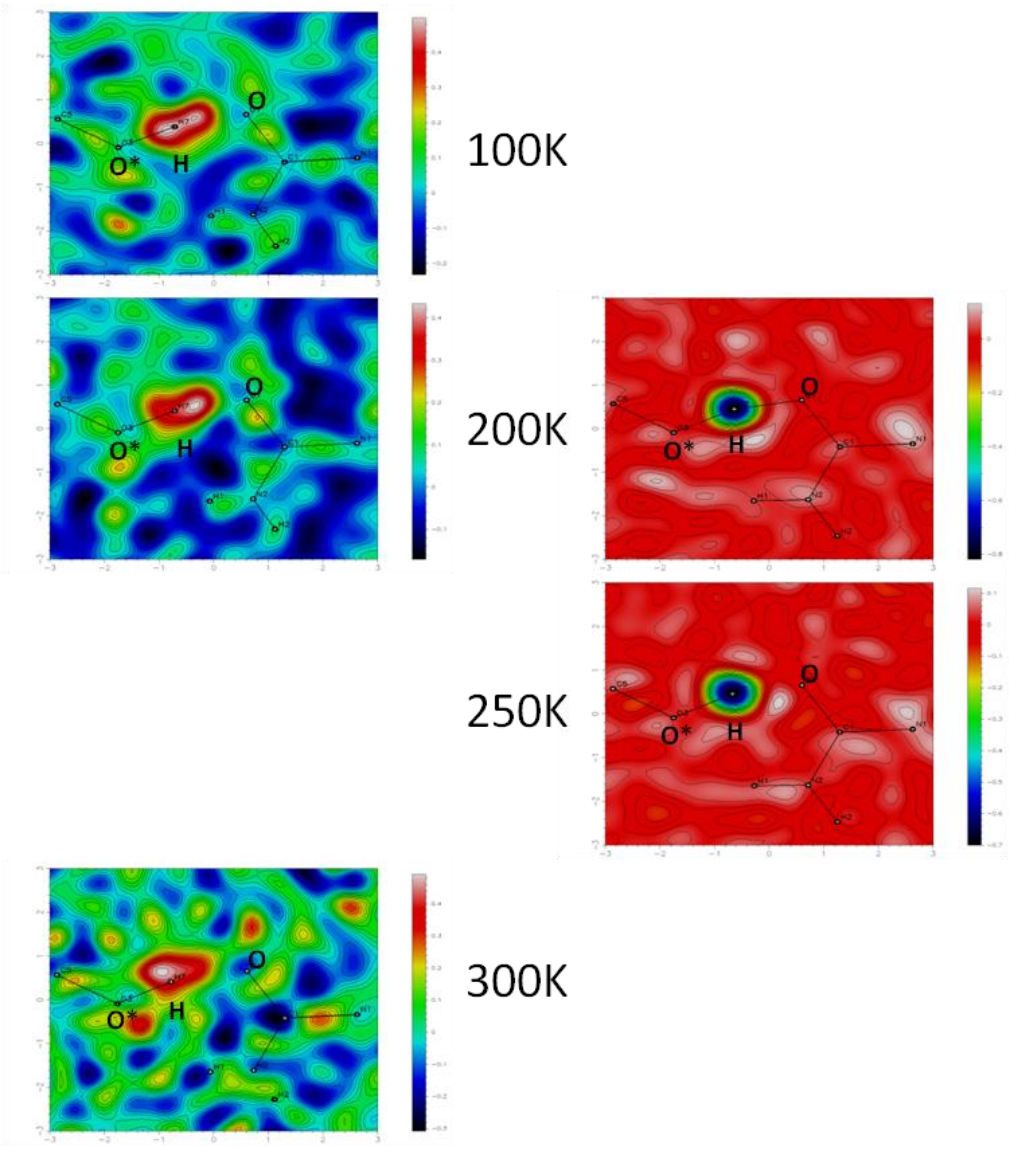

Figure 4.16 *Fourier difference maps showing the electron (left) and nuclear (right) density of the hydrogen atom in the short, strong hydrogen bond in the 2:1 complex of N-methylurea and chloranilic acid. Acid oxygens are marked with an asterisk (*).*

Instability of the sample at low temperatures led to neutron data only being collected at 200 and 250 K for this complex. However, these data provide strong evidence of temperature dependent proton migration. The refined neutron structures (**Figure 4.17**) are in good agreement with the X-ray structures and Fourier difference maps of the hydrogen atom nuclear density show a well localised, single position at both 200 and 250 K (**Figure 4.16**, right). A migration of 0.024(8) Å is observed towards the donor atom between 200 and 250 K, whilst over the same temperature range

the O···O distance only increases slightly (from 2.459(4) Å at 200 K to 2.467(4) Å at 250 K) (**Table 4.10**). This magnitude of migration over a small 50 K temperature range is surprisingly large when compared with other systems which display proton migration. As only two neutron data sets have been collected, it is not possible to establish a migratory trend over a larger temperature range. To investigate further the migration behaviour in this complex, further data from quantum chemical calculations are presented below (**Section 4.4.2**).

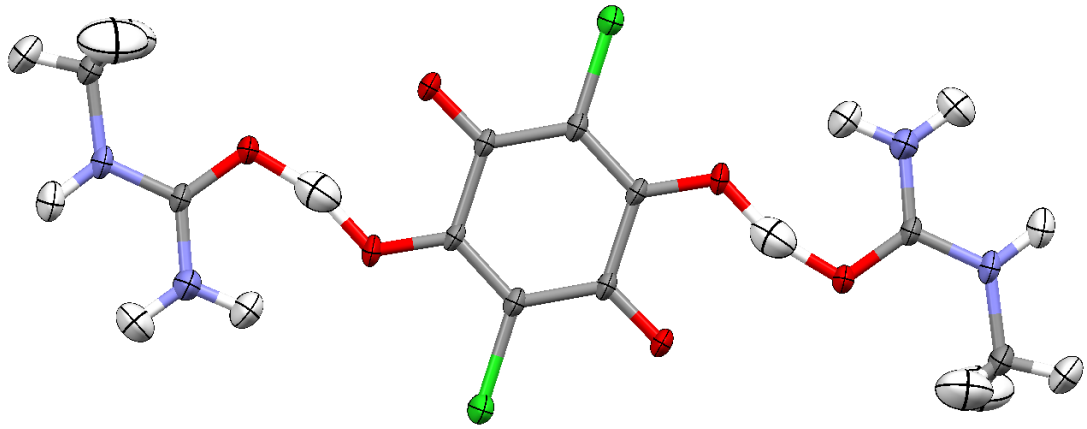

Figure 4.17 *An "MU-A-MU" molecular unit from the neutron structure of the 2:1 complex of N-methylurea and chloranilic acid at 200 K.*

4.4.2 Computational Data

The theoretical structures generated from CPMD simulations agree with the presence of proton migration observed in the experimental data, also predicting a migration towards the donor atom as the temperature is increased. The neutron diffraction data again show the hydrogen atom to be more centred within the SSHB than is found in the theoretical data, with the hydrogen atom once again transferred across the SSHB and closer to the acceptor group from theory (**Table 4.11**). The O···O distance in the theoretical data is invariant between 100 and 300 K, in contrast to the experimental data (**Table 4.10**); this is likely due to the unit cell parameters being fixed in the theoretical data. The magnitude of the migration from theory is smaller than that observed in experiment, with a migration of 0.024(8) Å observed in the experimental data between 200 and 250 K compared with a migration of 0.011 Å over the same temperature range in the theoretical data. Over the full temperature range studied (100 to 300 K), the theoretical data shows a migration of 0.028 Å towards the donor atom. Whilst there is not a good agreement in the magnitude of migration between experiment and theory, the fact that both

display a trend of migration of the proton towards the donor atom strengthens the case for proton migration being present in this complex.

Table 4.11 *Lengths of the short, strong O-H···O hydrogen bond in the three molecule "MU-A-MU" units of the complex of N-methylurea with chloranilic acid from the neutron diffraction and theoretical data.*

T/K	r(O-H)/Å		r(H···O)/Å		r(O-H···O)/Å	
	Neutron	Theory	Neutron	Theory	Neutron	Theory
100	-	1.374	-	1.099	-	2.451
200	1.230(6)	1.363	1.256(5)	1.110	2.459(4)	2.451
250	1.206(6)	1.352	1.294(7)	1.119	2.467(4)	2.449
300	-	1.346	-	1.128	-	2.450

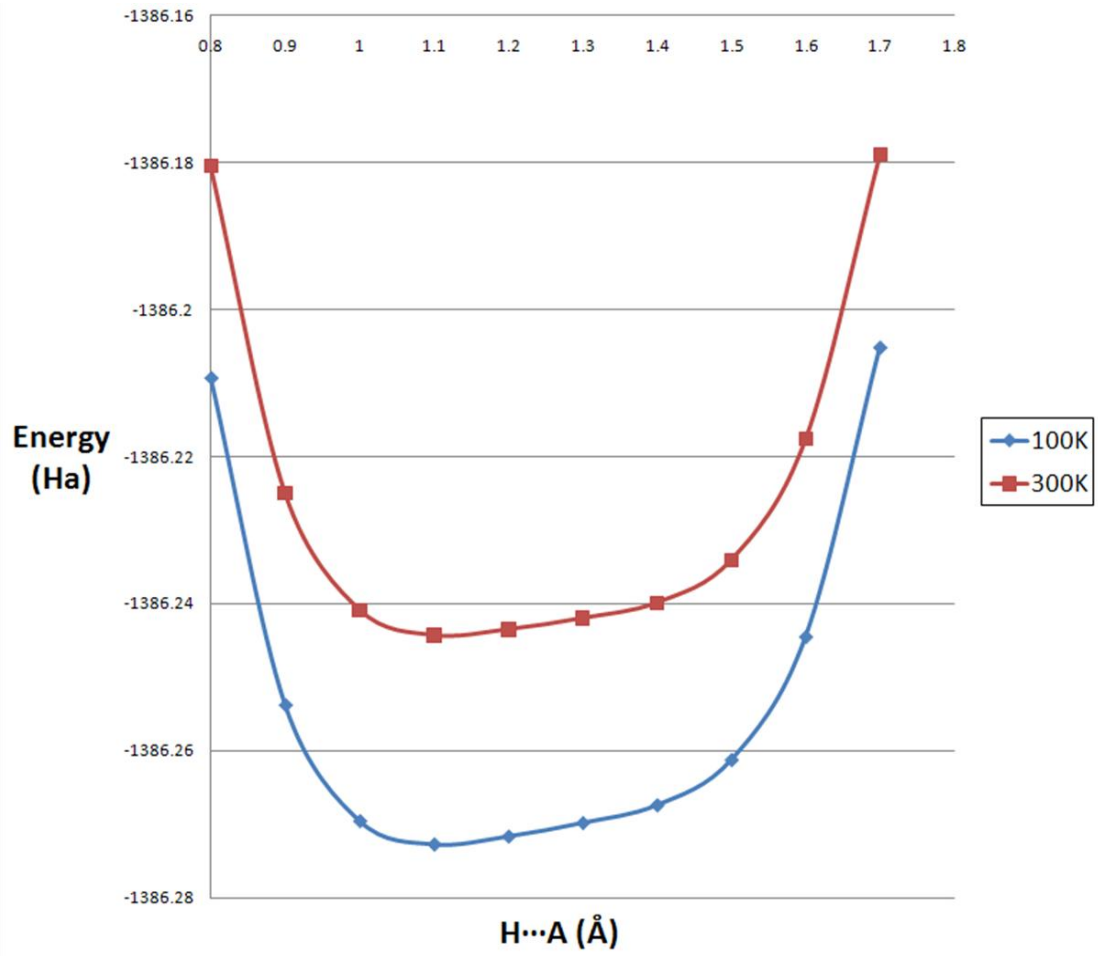

Figure 4.18 *The potential energy surfaces of the short, strong hydrogen bond in the 2:1 complex of N-methylurea and chloranilic acid at 100 and 300 K, generated from the theoretical data.*

In previous computational studies of urea-phosphoric acid, it was shown that the shape of the SSHB PES was temperature dependent and this facilitated the observed proton migration.[68] This was found to be caused by low energy phonons affecting the local environment of the SSHB and altering the shape of the PES as the temperature changes. Analysis of the theoretical PESs of the SSHB in the complex of *N*-methylurea and CLA shows a broad, asymmetric, single well which evolves with temperature, becoming flatter at high temperatures (**Figure 4.18**). This flattening of the PES is subtle and consistent with the observed migration of the proton towards the donor atom as the temperature is increased in both the experimental and theoretical data. The temperature dependence of the PES coupled with the experimental data further supports the presence of temperature dependent migration within this complex, and offers an insight into its cause.

4.5 *N*-Methylurea Bromanilic Acid (2:1)

The 2:1 molecular complex of *N*-methylurea and BRA crystallises in the $P2_1/n$ space group and contains one *N*-methylurea molecule and half a BRA molecule in the asymmetric unit; the methyl group of the *N*-methylurea is in the *syn* position relative to the carbonyl oxygen. This structure is isostructural with that of *N*-methylurea-CLA described in **Section 4.4** above.

Layers of planar three molecule "MU-A-MU" units are formed which contain two symmetry equivalent O-H···O SSHBs (O···O distance of 2.455(3) Å at 100 K) (**Table 4.12**) and two symmetry equivalent N-H···O hydrogen bonds (N···O distance of 2.931(3) Å) between the *N*-methylurea and BRA moieties (**Figure 4.19**, box in top image). Within the molecular units, the *N*-methylurea molecules are tilted slightly with respect to the BRA ring at an angle of 11.8(5)°. Molecular units in the same layer interact with one another through a *DDHHA* bifurcated N-H···O hydrogen bond (N···O distances of 2.976(3) and 3.198(3) Å) between an *N*-methylurea molecule and the oxygen of BRA which is not involved in the SSHB, an N-H···O hydrogen bond (N···O distance of 3.181(3) Å) between two *N*-methylurea molecules and finally through a C-H···Br weak hydrogen bond with a C···Br distance of 3.586(3) Å. There is also a weak C-H···O hydrogen bond (C···O distance of 3.591(4) Å) from the *N*-methylurea methyl group to a BRA oxygen in a neighbouring plane, whilst BRA rings are involved in parallel-displaced π interactions with a ring separation of ~3.2 Å (**Figure 4.19**, bottom).

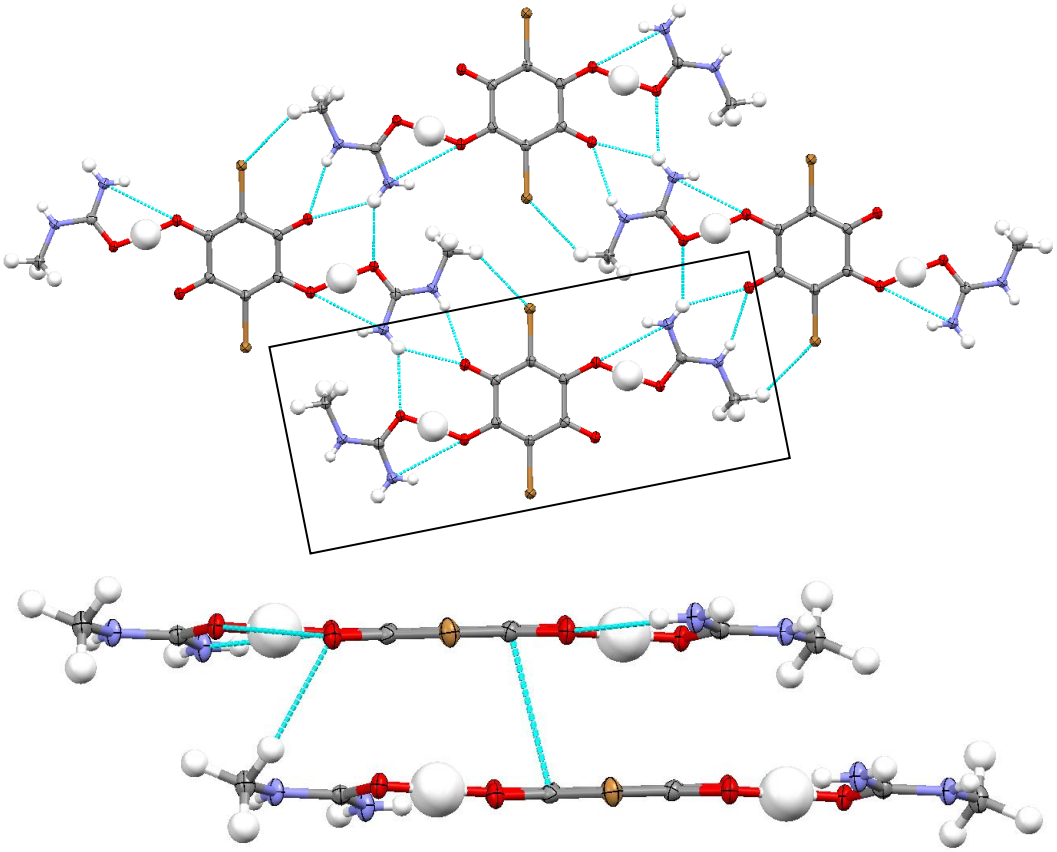

Figure 4.19 *Interactions between "MU-A-MU" units (unit highlighted in box in top image) in the same layer (top) and in different layers (bottom) in the 2:1 complex of N-methylurea and bromanilic acid at 100 K (X-ray).*

Table 4.12 *Lengths of the short, strong O-H···O hydrogen bond in the three molecule "MU-A-MU" units of the complex of N-methylurea with bromanilic acid, from the X-ray data.*

T / K	r(O-H) / Å	r(H···O) / Å	r(O-H···O) / Å
100	1.23(6)	1.23(6)	2.455(3)
200	1.07(9)	1.45(9)	2.475(4)
300	1.12(7)	1.41(7)	2.494(4)

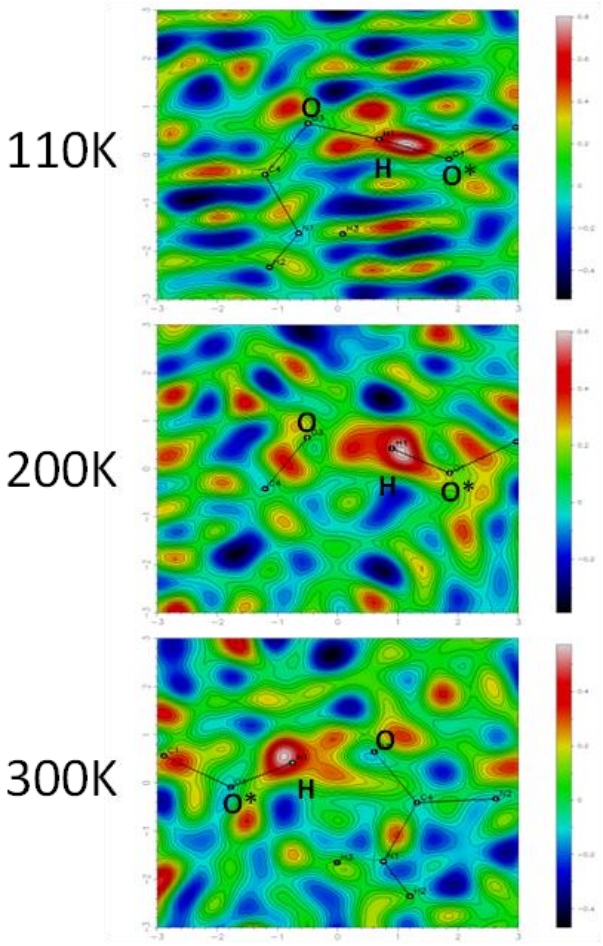

Figure 4.20 *Fourier difference maps showing the electron density of the hydrogen atom in the short, strong hydrogen bond in the 2:1 complex of N-methylurea and bromanilic acid. The acid oxygen is marked with an asterisk (*).*

It was not possible to grow crystals of this complex suitable for study by neutron diffraction methods. The X-ray diffraction data presented here again gives some clues as to the possible presence of temperature dependent proton migration. The O-H···O hydrogen bond is very short at 100 K with the hydrogen atom approximately centred within the SSHB. The O···O distance again increases significantly with temperature, from 2.455(3) Å at 100 K to 2.494(4) Å at 300 K, and the hydrogen atom within the SSHB has a large isotropic thermal displacement parameter when compared with other hydrogen atoms in the structure. Examination of the hydrogen atom electron density through Fourier difference maps again shows hydrogen atomic positions which do not correspond well to the electron density peaks, together with an elongation of the electron density along the hydrogen bond (**Figure 4.20**). It should be noted that there is increased background noise in the Fourier difference maps for this complex due to the presence of the bromine atom in the

structure; this makes accurate location of the hydrogen atom in the SSHB more difficult. The absence of neutron diffraction data means proton migration cannot be confirmed within this complex. However, the presence of proton migration may be inferred from the evidence presented in the isostructural complex containing CLA. This is discussed further in **Section 4.7**.

4.6 Urea Bromanilic Acid (2:1)

The 2:1 molecular complex of urea and BRA crystallises in the $P\bar{1}$ space group and contains four urea molecules and two BRA molecules in the asymmetric unit. A complex structure consisting of non-planar layers of molecules is formed, which contains one O-H···O SSHB amongst many other moderate and weak hydrogen bonds. A proton has also transferred to one of the urea molecules from a BRA molecule. Despite many attempts at crystallising these materials together, only complex structures were formed, in contrast with the majority of the complexes presented in work (see also the urea-BRA monohydrate presented in **Chapter 8**).

The structure can be treated as two subunits, each containing one BRA molecule and two urea molecules. The first subunit (blue BRA with orange and pink urea molecules in **Figure 4.21**) shows proton transfer from the BRA molecule (blue) to a urea molecule (pink). This has caused the C-O bonds on the deprotonated side of the molecules to take almost equal lengths of 1.221(2) and 1.234(3) Å at 100 K. The transfer is not simply across a hydrogen bond, and the protonated urea (pink) interacts with an oxygen on the other side of the BRA molecule (blue), in an O^+-H···O charge-assisted hydrogen bond (O···O distance of 2.579(2) Å). The two urea molecules are tilted slightly with respect to the BRA molecule, at angles of 23.6(2)° (orange) and 8.1(2)° (pink) to the BRA ring. There is another O-H···O hydrogen bond (O···O distance of 2.607(2) Å) between the other urea moiety in the subunit (orange) and the hydroxyl group of the BRA (blue). Within the subunit there are several N-H···O hydrogen bonds, one is between the carbonyl oxygen of one urea (orange) and an amide hydrogen of the other (pink), with an N···O distance of 2.921(2) Å. The oxygen atoms on the deprotonated side of the BRA molecule (blue) are each involved in a *DDHHA* bifurcated hydrogen bond. One is an asymmetric bifurcated hydrogen bond to one urea moiety (pink) with N···O distances of 2.828(2) and 3.043(2) Å; the other is to both the urea moieties and is approximately symmetric, with N···O distances of 2.928(2) Å (to the orange urea) and 2.959(2) Å (to the pink urea). One urea moiety (orange) of the subunit is also

involved in N-H···O hydrogen bonds to the BRA (green) (N···O distance 2.958(2) Å) and a urea (purple) (N···O distance 3.051(2) Å) in the other subunit.

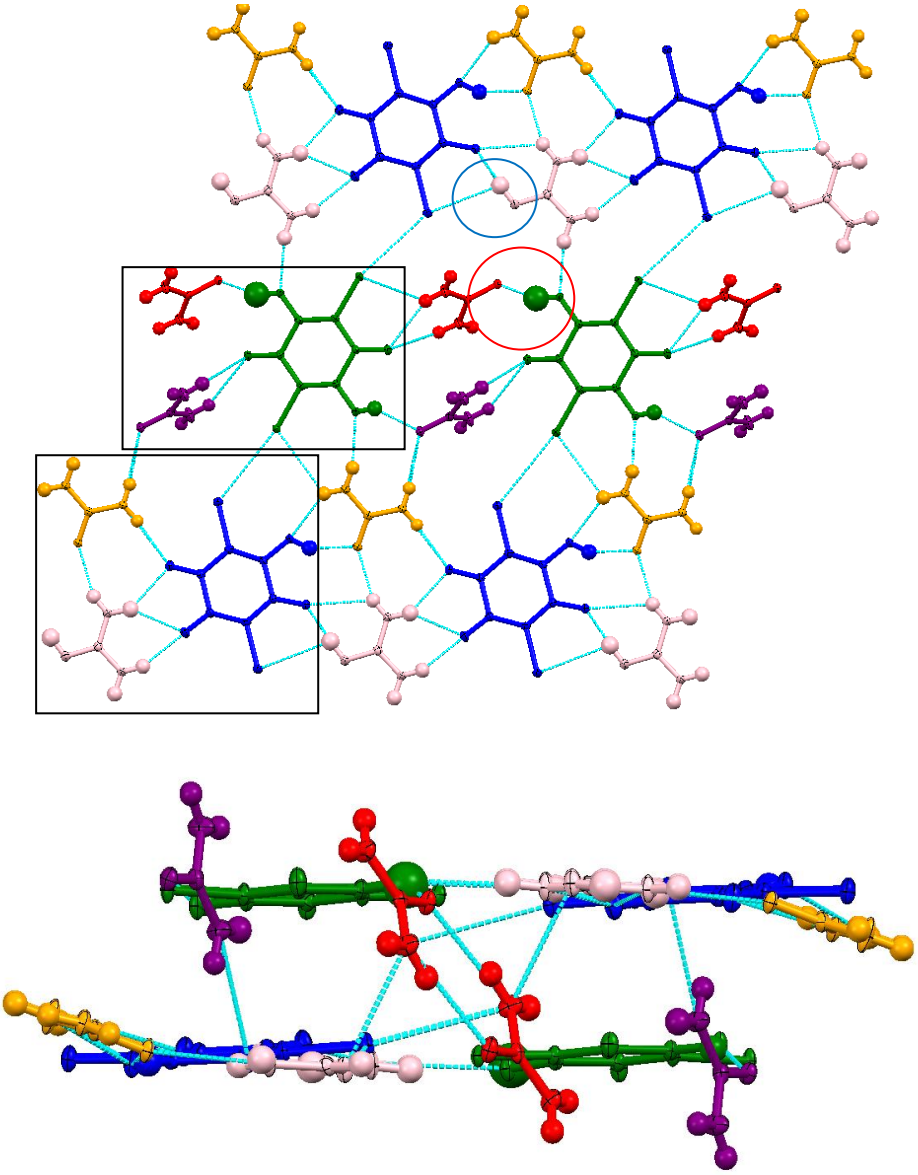

Figure 4.21 *Interactions within a layer (top) and between layers (bottom) showing the different urea (orange, pink, red and purple) and bromanilic acid (blue and green) environments in the 2:1 complex of urea and bromanilic acid at 110 K (X-ray). In the top image the two subunits are highlighted in boxes while the short, strong hydrogen bond and transferred proton are circled in red and blue, respectively.*

The second subunit (green BRA with red and purple urea molecules in **Figure 4.21**) contains entirely neutral species and has the two urea molecules at a greater tilt to the BRA ring than in the first subunit, at angles of 67.79(11)° (red) and 83.47(11)°

(purple). The O-H···O SSHB is between the BRA (green) and one of the urea moieties (red) of this subunit and has an O···O distance of 2.425(2) Å (**Table 4.13**), similar in length to the SSHB in urea-phosphoric acid.[62,63] It is surprising, and worthy of note, that this hydrogen bond is shorter than the charge-assisted hydrogen bond in the other subunit. There is a second O-H···O hydrogen bond within the subunit between the BRA (green) and the other urea moiety (purple) with an O···O distance of 2.585(2) Å. There are two sets of N-H···O *DDHHA* bifurcated hydrogen bonds between the ureas and the BRA carbonyl oxygens with N···O distances of 3.137(2) and 3.196(2) Å for one (red), and values of 3.132(3) and 3.263(2) Å for the other (purple). There is also a Br···Br contact with a length of 3.5244(3) Å between the two BRA moieties within the structure, which is shorter than the sum of van der Waals radii of 3.70 Å.

The two urea moieties with the largest tilts to the layer (red and purple) form hydrogen bonded amide···amide dimers with their equivalent molecules in the next layer. Each dimer consists of two equivalent N-H···O hydrogen bonds with N···O distances of 2.979(2) Å in one dimer (red), and 2.980(2) Å in the other (purple). The other interactions between layers are parallel-displaced π interactions between the two BRA moieties in different layers, with a distance of ~3.3 – 3.5 Å between the two ring planes.

It was unfortunately not possible to grow single crystals of this complex suitable for neutron diffraction studies. However, the X-ray diffraction data provides strong evidence that temperature dependent proton migration may occur within this complex. There are several indicators which point towards the possibility of migration being present. The first is the length of the O-H···O SSHB (**Table 4.13**); at 110 K, the O···O distance is 2.425(2) Å. The O···O distance again increases with temperature, with an O···O distance of 2.448(2) Å at 300 K, which is still well within the range to be classed as an SSHB. Further evidence of migration is given from the larger than expected thermal displacement parameter associated with the hydrogen atom in the SSHB, whilst the refined hydrogen atomic position from the X-ray data also appears to migrate towards the donor atom. However, examination of the electron density in the Fourier difference maps of the hydrogen bond shows that the refined atomic positions are not located at the peaks of the elongated electron density (**Figure 4.22**). It should be noted that the elongation of the electron density in this manner is another possible indicator of the presence of proton migration. As in the case of the *N*-methylurea-BRA complex (**Section 4.5**), the Fourier difference

maps for this complex have added noise in the background due to the presence of the bromine atom and this makes accurately resolving the hydrogen atom positions more difficult. In the absence of neutron diffraction data is not possible to state definitively that proton migration is present, though it seems possible in the case of this complex.

Table 4.13 *Lengths of the short, strong O-H···O hydrogen bond in the complex of urea with bromanilic acid.*

T / K	r(O-H) / Å	r(H···O) / Å	r(O-H···O) / Å
110	0.91(4)	1.57(4)	2.425(2)
200	0.88(4)	1.60(4)	2.435(2)
300	0.77(4)	1.71(4)	2.448(2)

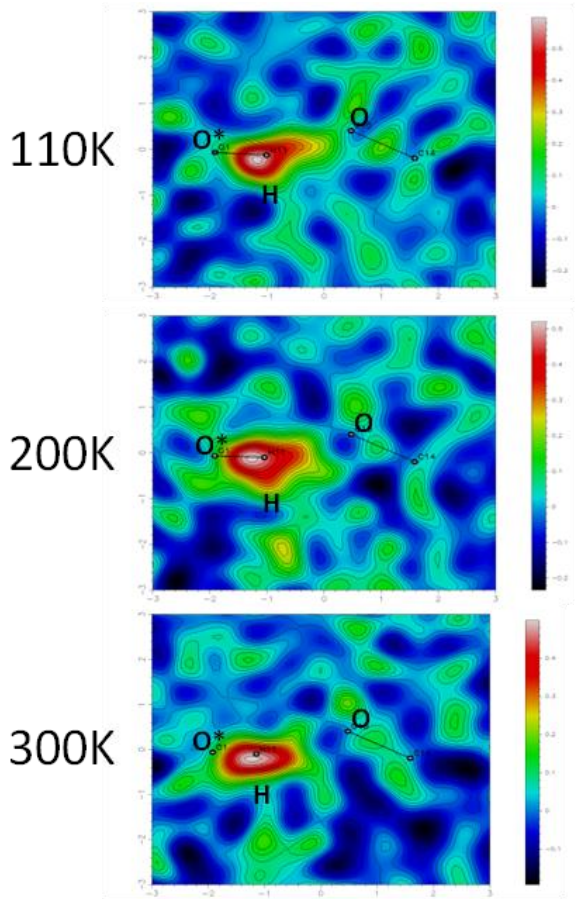

Figure 4.22 *Fourier difference maps showing the electron density of the hydrogen atom in the short, strong hydrogen bond in the 2:1 complex of urea and bromanilic acid. The acid oxygens are marked with an asterisk (*).*

4.7 Understanding and Designing Systems Which Display Proton Migration

As there are so few examples of systems which display temperature dependent proton migration, the discovery of any new systems can potentially lead to a greater understanding of this dynamic charge transfer effect. The synthesis and characterisation by neutron diffraction of three complexes which definitively display proton migration, and two where there is strong evidence for this effect from the X-ray diffraction data, is therefore an important step. Analysis of these proton migration complexes can aid in the design of complexes with similar properties for future studies.

The most important feature for a material to possess in order to display temperature dependent migration of a proton within a hydrogen bond is that a sufficiently short hydrogen bond should be present. At low temperatures, all of the O-H···O SSHBs are less than 2.46 Å in length; at higher temperatures some of the O···O distances increase, but are still less than 2.50 Å in all of the structures presented here. It is conceivable that there is a threshold for the D···A distance, below which it is possible for migration to occur. All of the examples of proton migration within O-H···O hydrogen bonds studied to date, have shown D···A distances of <2.50 Å (the O···O distance in urea-phosphoric acid is ~2.42 Å). Based on the current evidence, it therefore seems that ~2.50 Å is a sensible choice of a threshold estimate for the D···A distance below which temperature dependent proton migration may occur within an O-H···O hydrogen bond. As there are still only a small number of proton migration materials known, this only a preliminary finding and further examples are needed to test this hypothesis.

It may be possible to gain insight as to the likely degree of solid-state proton migration, when the length of the SSHB is favourable, by studying ΔpK_a values. Complexes with hydrogen atoms almost centred in intermolecular hydrogen bonds can be thought of as intermediate between salts and co-crystals and the complexes presented here are in this category. The complex of urea with BRA displays several degrees of proton transfer within one crystal structure, including one example of an SSHB, while the other complexes contain SSHBs with the hydrogen atom located close to the centre of the hydrogen bond. As the magnitude of migration differs depending on the complex it is also possible to envisage a situation where a material could cross from co-crystal to salt gradually, perhaps even over a smaller temperature range than those studied here. Of the three urea-acid complexes in which the temperature dependent migration has been studied in detail with variable

temperature neutron diffraction (*N,N*-dimethylurea-oxalic acid, *N,N'*-dimethylurea-oxalic acid and urea-phosphoric acid;[62,63] *N*-methylurea-CLA is excluded as data were only collected at two temperatures), the *N,N*-dimethylurea complex shows the most significant migration followed by urea-phosphoric acid[62,63] and then the *N,N'*-dimethylurea complex. The respective ΔpK_a values for these complexes are -1.56, -1.87 and -1.94, all indicating that neutral co-crystal formation should be expected. It is noticeable that a correlation can be drawn from these ΔpK_a values and the degree of migration observed; the most significant migration is found in the complex showing the least negative ΔpK_a value. Even considering the difficulties in transferring pK_a values to the solid-state and applying ΔpK_a values to molecular complexes which do not have a 1:1 stoichiometry[59] the analysis presented here suggests that these values may be applied to designing other proton migration systems. If this were proven to be the case, it may be possible to identify other systems with temperature tunable hydrogen migration behaviour through consideration of the relative proton affinities of the molecules along with the local crystal environments of the hydrogen bond showing proton migration.

In the complexes containing haloanilic acids, the ΔpK_a values for the urea-BRA, *N*-methylurea-BRA and *N*-methylurea-CLA complexes are -1.24, -1.53 and -1.57, respectively. These values may suggest that the urea-BRA complex could show the most significant proton migration, although the crystal structure is complex, while the *N*-methylurea complexes may be expected to have a magnitude of migration similar to the *N,N*-dimethylurea-oxalic acid complex (ΔpK_a = -1.56). The neutron data show a migration of 0.024(8) Å between 200 and 250 K in the *N*-methylurea-CLA complex, while a migration of 0.028 Å between 100 and 300 K is predicted from the theoretical data. With only two data points available, it is not known if the neutron diffraction data results, showing a very large migration over a small temperature range, are anomalous, and a trend cannot be established. From the theoretical data, the migration of 0.017 Å between 200 and 300 K is greater than that in the *N,N*-dimethylurea-oxalic acid complex over the same temperature range of 0.005 Å. This difference may arise due to the inaccuracies in the theoretical data compared with experiment, though it also underlines the fact that predictions of migration from ΔpK_a values only provide a guide and are not numerically accurate, even if there is a correlation between migration and ΔpK_a in the three examples where extensive neutron diffraction studies have been carried out. When comparing the ΔpK_a values with the length of the SSHB formed in the complexes

(**Table 4.14**), it is clear that differences in pK_a again cannot be used as anything more than a guide as to what may occur and whether a SSHB of <2.50 Å is formed. In this case, the ΔpK_a values and the SSHB lengths do not show an obvious correlation, though it should be noted that neither sets of values cover a large numerical range. This concept is discussed further in a set of complexes with wider ranging values for pK_a differences and SSHB length in **Chapter 5**.

Table 4.14 *ΔpK_a values and short, strong hydrogen bond distances from the 100 K X-ray data (110 K in the case of urea-BRA) for the proton migration complexes presented in this chapter.*

Complex	ΔpK_a	r(O-H···O) / Å
Urea-BRA	-1.24	2.425(2)
***N*-MU-BRA**	-1.53	2.455(3)
***N,N*-DMU-oxalic acid**[a]	-1.56	2.4398(15)
	-1.56	2.4423(15)
***N*-MU-CLA**	-1.57	2.459(2)
***N,N'*-DMU-oxalic acid**	-1.94	2.4469(9)

[a] *The two values for the N,N-dimethylurea-oxalic acid complex correspond to the two unique short strong hydrogen bonds present in the larger asymmetric unit of the low temperature phase.*

The change in shape of the SSHB PES with temperature is another necessary feature for migration of the proton within the hydrogen bond to occur. Computational studies on urea-phosphoric acid attributed the change in shape of the PES to subtle changes in the local environment caused by phonons.[68,69] It was not possible in this work to analyse the theoretical phonon spectra of the proton migration complexes due to time restrictions, though it should be noted that it is debatable whether these calculations would be accurate, given the disagreements in the magnitude of migration between experiment and theory. However, by studying two isostructural complexes (*N*-methylurea with BRA and CLA) and two complexes with different crystal structures and only conformational differences in the molecular components (the two dimethylurea complexes), the effect of changes in the local environment can still be probed. The theoretical data presented here confirms the temperature dependent nature of the SSHB PES in the two complexes where it has been studied, in agreement with the previous theoretical studies of urea-phosphoric acid.[68,69]

In the complexes of *N*-methylurea with BRA and CLA, similar O···O distances for the SSHB are observed at all temperatures, showing that the change in halogen atom has little effect on the global crystal structure and hydrogen bonded network. There is possibly a slight difference in the behaviour of the hydrogen atom electron density within the SSHB in the two complexes visualised from Fourier difference maps (**Figure 4.5** and **Figure 4.7**), with the electron density being slightly more diffuse in the complex with CLA. However, this is may be a consequence of the data quality and a more uneven background is observed in the Fourier difference maps of the BRA complex due to the presence of a heavier atom. Any possible difference in the behaviour is small and it appears likely that the two complexes show very similar behaviour in all aspects. In the absence of neutron diffraction data, the presence of proton migration in the BRA complex can be inferred from the neutron diffraction and theoretical data of the isostructural CLA complex where proton migration is observed.

The complexes of the dimethylureas with oxalic acid, and the different packing environments in each, provide an opportunity to analyse the effects of the local environment on the behaviour of the SSHB, as neutron diffraction and theoretical data have been collected for both complexes. The lengths of the SSHBs in both complexes are quite similar, with the O···O distance in the SSHB of the complex with *N,N'*-dimethylurea being slightly longer at higher temperatures (2.4548(12) Å at 300 K (X-ray), compared with 2.439(2) Å in the *N,N*-dimethylurea complex at the same temperature). The magnitude of migration of the proton within the SSHB is different in the two complexes, both from experiment and theory. From the neutron diffraction data, the proton in the *N,N*-dimethylurea complex migrates 0.045(9) Å between 150 and 300 K, while in the *N,N'*-dimethylurea complex there is a migration of 0.031(7) Å between 4 and 280 K. These are of a similar order of magnitude to the migration observed in urea-phosphoric acid (~0.040 Å between 150 and 350 K).[62,63] When compared over similar temperature ranges, the proton migration is of magnitude 0.030(9) Å in the *N,N*-dimethylurea complex (between 200 and 275 K) and 0.015(6) Å in the *N,N'*-dimethylurea complex (between 200 and 280 K). From the theoretical data, the proton in the *N,N*-dimethylurea complex migrates 0.005 Å between 200 and 300 K, while the proton in the *N,N'*-dimethylurea complex migrates 0.009 Å over the same temperature range, in contrast to the results from the experimental data. The differences in the magnitude of the migration of the proton in these two complexes must be related to the differences in the solid-state

structures (the *N,N*-dimethylurea complex structure is layered while the other is not) and the weaker interactions between adjacent molecular units. These results therefore show the impact subtle differences in the local crystalline environment can have on the behaviour of the SSHBs within these complexes.

One final point for discussion is the accuracy of the theoretical data. Clearly, in the three examples presented here, the theoretical data predicts a much smaller migration of the proton within the SSHB than is observed in experiment. The theoretical data also predicts a greater degree of proton transfer across the SSHB, away from the donor molecule, than is shown in the experimental data. The choice of basis sets / functionals and level of theory will obviously affect the results and modelling a subtle effect such as proton migration is difficult. Whilst there may not be an exact agreement between experiment and theory, it is encouraging that both show a trend of migration of the proton towards the donor atom. The simplistic model used to generate the SSHB PESs also shows the temperature dependent nature of the PES which would be expected in a system which displays proton migration. This work has shown that theory can certainly play a complementary role in proton migration studies, though care must be taken not to over-interpret the results and to choose the parameters of the simulations carefully.

4.8 Conclusions

The crystal structures of five complexes have been presented, all forming in a 2:1 (urea:acid) ratio and all containing a SSHB, although the urea-BRA complex shows a number of other hydrogen bonds in addition, including proton transfer to the urea moiety. Temperature dependent proton migration has been observed in three of the complexes from variable temperature neutron diffraction data, whilst strong evidence of proton migration is found in the other two complexes. Crystallographic data have been complemented with theoretical studies which predict migration in the three complexes studied by this method, while PESs of the SSHBs were generated for two complexes and were found to be temperature dependent in nature, as would be expected of a SSHB in which the proton undergoes migration.

The presence of a SSHB in these complexes is key for proton migration to occur. Based on the evidence of known proton migration complexes, a D···A distance of <2.50 Å seems an appropriate threshold to postulate, below which temperature dependent proton migration may occur within O-H···O hydrogen bonds. Some care must be taken in using this length threshold as a guide, as a D···A distance of

<2.50 Å by no means suggests proton migration will definitely occur and, due to this finding being based on a small number of examples, further studies are needed to test this hypothesis.

The differences in the magnitude of the migration within the SSHBs shows that changes in the local environment and weak interactions to the SSHB have an impact on the behaviour of the proton within the SSHB. This is particularly evident in the two structures of the isomers of dimethylurea with oxalic acid. The molecular components differ only in their conformation, whilst both complexes display different crystal packing motifs. Even though SSHBs of a similar length are formed in both complexes, the magnitude of migration is different. This difference must arise due to the change in local environment and this shows how subtle changes in the interactions can affect the dynamic charge transfer processes which are occurring in these complexes.

The results presented here show that crystal engineering principles can be used to design complexes containing SSHBs, the key requirement for proton migration to occur. This includes the use of methyl substituted ureas, with both the dimethylurea-oxalic acid complexes containing shorter hydrogen bonds than the equivalent urea and methylurea complexes, and also haloanilic acids which have shown their potential to form SSHBs. Two of the complexes show other interesting temperature dependent structural features. The complex of *N,N*-dimethylurea and oxalic acid undergoes a phase change which involves a doubling of the asymmetric unit, while the complex of *N,N'*-dimethylurea and oxalic acid shows unusual thermal expansion properties where one unit cell axis contracts as the temperature is increased.

The theoretical data presented in this chapter shows an agreement in the presence of proton migration within the three complexes studied. There was also an agreement in the direction of the migration, with both theory and experiment showing a migration towards the donor atom as the temperature is increased. The theoretical results show that the computational simulations can model the effect of proton migration up to a point, with disagreements in the hydrogen atom position and the magnitude of any migration, and the SSHB PESs were found to vary with temperature in all cases. Taking these factors into consideration, it would be of benefit to study the theoretical phonon spectra which can be generated from the MD simulations as part of the future work in this area of the project. These results

would hopefully confirm whether the changes in the shape of the SSHB PES arise due to phonons, as was described in the case of urea-phosphoric acid.[68,69]

Further work utilising haloanilic acids would involve the synthesis of other complexes with a view to control the charge transfer properties, both static and dynamic, of these materials. The complex of urea-BRA may be of particular interest due to the varying degrees of static charge transfer which have occurred in the presence of the dynamic proton migration effect. This is further underlined in a urea-BRA hydrate, discussed in **Chapter 8**.

This work shows the complementarity of X-ray, neutron and theoretical data, with greater insight available when the techniques are used together. The variable temperature neutron data presented here also show the potential of high throughput neutron experiments, made possible by the technical setup on the VIVALDI Laue diffractometer. Being able to study the structure at multiple temperatures is key in these types of studies, and the increased speed of data collection enables more samples and temperatures to be studied within the allocated neutron beam time.

Chapter 5

5. Molecular Complexes of Dicarboxylic Acids with Urea and Methyl Substituted Ureas

Urea and its derivatives have been widely used as a component in crystal engineering studies due to their potential to act as both multiple hydrogen bond donors and acceptors.[100,104,105] When urea has been crystallised with organic dicarboxylic acids, the complexes formed have been shown to contain robust, predictable hydrogen bonded motifs which correspond to the stoichiometric ratio of the component materials in the complex.[105] As discussed in **Section 1.9**, 1:1 complexes show a urea (U) - acid (A) motif while 2:1 (urea:acid) and 1:2 complexes show "U-A-U" and "A-U-A" motifs, respectively. 1:1 and 2:1 complexes are the most common, with there only being one known example of a 1:2 complex (urea-maleic acid).[100] Systematic modification of the substituents of the components in a molecular complex can potentially have a significant impact on the crystallographic motif displayed in the structure and can lead to a consequent change in the properties of a material; this is often related to the addition or removal of hydrogen bonding sites which impacts on the crystal packing.

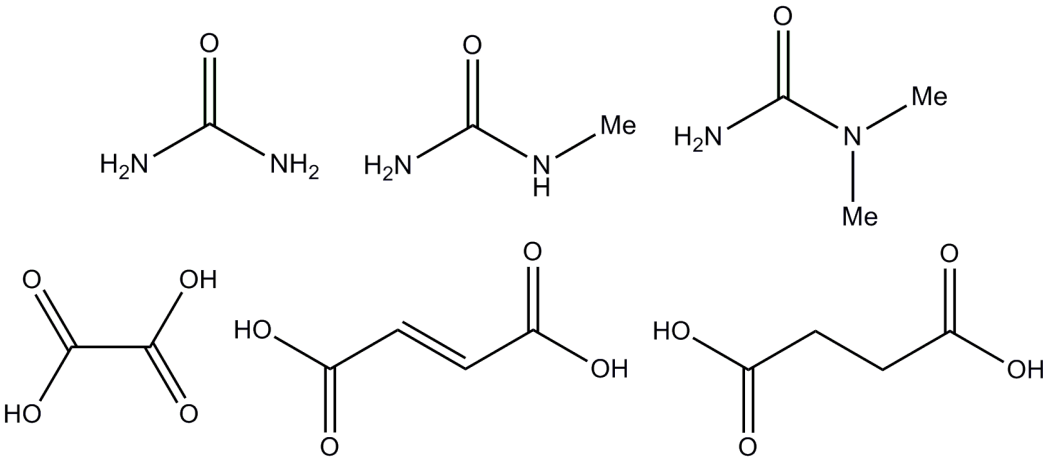

Figure 5.1 *Clockwise from top left, molecular structure diagrams of: urea, N-methylurea, N,N-dimethylurea, succinic acid, fumaric acid and oxalic acid.*

Complexes containing *N*-methyl substituted ureas are much less studied than those containing the parent urea molecule and there is only one example of a complex with an organic dicarboxylic acid; the 2:1 complex of *N*-methylurea and oxalic acid.[112] Complexes containing urea, *N*-methylurea (MU) and *N*,*N*-dimethylurea (DMU) complexed with a series of dicarboxylic acids: succinic acid, fumaric acid and oxalic acid have been studied in this work (**Figure 5.1**); three of these complexes

(urea succinic acid,[100,105,172] urea fumaric acid[102,172] and *N*-methylurea oxalic acid)[112] have been studied previously by X-ray diffraction, while the other complexes are previously unreported. Variable temperature X-ray data were collected on seven complexes, with variable temperature neutron data also collected on five of these. The objective of these investigations is to study the effect of blocking hydrogen bond donor sites on the ureas through *N*-methyl substitution has on the crystal structures. The use of succinic and fumaric acid offers the possibility of isostructurality of complexes due to the similarity of the molecules, whilst the potential flexibility of the alkyl chain in succinic acid is another facet of the crystal packing which can be investigated.

These complexes should also provide a system wherein short, strong hydrogen bond (SSHB) lengths between components can be varied. As in **Chapter 4**, there is an interest in the potential formation of these hydrogen bonds and whether proton migration may be present in any of these complexes, with a view to the future design of materials with these properties. In this respect, the need for variable temperature data is paramount to observe the evolution of the hydrogen atom behaviour and the crystal structure as a whole.

5.1 Experimental

2:1 Complex of urea and succinic acid (**US**)

Large block shaped colourless crystals of the 2:1 complex of urea and succinic acid were grown by slow evaporation from a 1:1 ethanol / dimethylformamide mixture at 50 °C. Single crystal X-ray diffraction data were collected on a Rigaku R-AXIS / RAPID diffractometer at 100, 200 and 300 K. The structure was solved using SHELXS-97[138] and refined with SHELXL-97[138] within the WinGX package.[140] Neutron data were collected on VIVALDI at the ILL at 100, 200 and 300 K. The neutron structures were refined using SHELXL-97[138] taking the X-ray atomic coordinates as a starting model. Crystallographic data are given in **Table 5.1**.

2:1 Complex of urea and fumaric acid (**UF**)

Large block shaped colourless crystals of the 2:1 complex of urea and fumaric acid were grown by slow evaporation from ethanol at room temperature (RT). Single crystal X-ray diffraction data were collected on a Rigaku R-AXIS / RAPID diffractometer at 100, 200 and 300 K. The structure was solved using SHELXS-97[138] and refined with SHELXL-97[138] within the WinGX package.[140] Neutron data

were collected on SXD at ISIS at 30, 100, 200 and 300 K. The neutron structures were refined using SHELXL-97[138] taking the X-ray atomic coordinates as a starting model. Crystallographic data are given in **Table 5.2**.

2:1 Complex of *N*-methylurea and succinic acid (**MUS**)

Large block shaped colourless crystals of the 2:1 complex of *N*-methylurea and succinic acid were grown by slow evaporation from ethanol at RT. Single crystal X-ray diffraction data were collected on a Rigaku R-AXIS / RAPID diffractometer at 100, 200 and 300 K. The structure was solved using SHELXS-97[138] and refined with SHELXL-97[138] within the WinGX package.[140] Neutron data were collected on VIVALDI at the ILL at 20, 100, 200 and 300 K. The neutron structures were refined using SHELXL-97[138] taking the X-ray atomic coordinates as a starting model. Crystallographic data are given in **Table 5.3**.

2:1 Complex of *N*-methylurea and fumaric acid (**MUF**)

Large block shaped colourless crystals of the 2:1 complex of *N*-methylurea and fumaric acid were grown by slow evaporation from isopropanol at RT. Single crystal X-ray diffraction data were collected on a Rigaku R-AXIS / RAPID diffractometer at 100, 200 and 300 K. The structure was solved using SHELXS-97[138] and refined with SHELXL-97[138] within the WinGX package.[140] Crystallographic data are given in **Table 5.4**.

2:1 Complex of *N*-methylurea and oxalic acid (**MOX**)

Block shaped colourless crystals of the 2:1 complex of *N*-methylurea and oxalic acid were grown by slow evaporation from ethanol at RT. Single crystal X-ray diffraction data were collected on a Rigaku R-AXIS / RAPID diffractometer at 200 and 300 K. The structure was solved using SHELXS-97[138] and refined with SHELXL-97[138] within the WinGX package.[140] Crystallographic data are given in **Table 5.5**.

2:1 Complex of *N,N*-dimethylurea and succinic acid (**DMUS**)

Large block shaped colourless crystals of the 2:1 complex of *N,N*-dimethylurea and succinic acid were grown by slow evaporation from ethanol at RT. Single crystal X-ray diffraction data were collected on a Rigaku R-AXIS / RAPID diffractometer at 100, 200 and 300 K. The structure was solved using SHELXS-97[138] and refined with SHELXL-97[138] within the WinGX package.[140] Neutron data were collected on VIVALDI at the ILL at 20 and 50 K. The neutron structures were refined using

SHELXL-97[138] taking the X-ray atomic coordinates as a starting model. Crystallographic data are given in **Table 5.6**.

2:1 Complex of *N,N*-dimethylurea and fumaric acid (**DMUF**)

Large block shaped colourless crystals of the 2:1 complex of *N,N*-dimethylurea and fumaric acid were grown by slow evaporation from ethanol at RT. Single crystal X-ray diffraction data were collected on a Rigaku R-AXIS / RAPID diffractometer at 100, 200 and 300 K. The structure was solved using SHELXS-97[138] and refined with SHELXL-97[138] within the WinGX package.[140] Neutron data were collected on VIVALDI at the ILL at 20, 100, 200, 250 and 300 K. The neutron structures were refined using SHELXL-97[138] taking the X-ray atomic coordinates as a starting model. Crystallographic data are given in **Table 5.7**.

Table 5.1 *X-ray and neutron data collection and refinement information for the 2:1 complex of urea and succinic acid.*[a]

Compound	**2:1 Urea : Succinic acid**					
Diffractometer	Rigaku R-AXIS RAPID	VIVALDI	Rigaku R-AXIS RAPID	VIVALDI	Rigaku R-AXIS RAPID	VIVALDI
Radiation	X-ray	Neutron	X-ray	Neutron	X-ray	Neutron
Formula	$C_6H_{14}N_4O_6$	$C_6H_{14}N_4O_6$	$C_6H_{14}N_4O_6$	$C_6H_{14}N_4O_6$	$C_6H_{14}N_4O_6$	$C_6H_{14}N_4O_6$
Molecular weight (g mol^{-1})	238.21	238.21	238.21	238.21	238.21	238.21
T (K)	100	100	200	200	300	300
Space group	*P2$_1$/c*	*P2$_1$/c*	*P2$_1$/c*	*P2$_1$/c*	*P2$_1$/c*	*P2$_1$/c*
***a* (Å)**	5.7109(7)	5.71	5.6706(5)	5.67	5.6366(6)	5.64
***b* (Å)**	7.9698(11)	7.97	8.1227(7)	8.12	8.2568(10)	8.26
***c* (Å)**	12.1580(15)	12.16	12.2182(10)	12.22	12.2790(13)	12.28
***β* (°)**	96.160(4)	96.16	96.375(3)	96.38	96.659(4)	96.66
Volume (Å^3)	550.17(12)	550.19	559.30(8)	559.13	567.61(11)	568.22
Z	2	2	2	2	2	2
Reflections collected	7014	7869	7340	4829	7067	8028
Independent	1255	1403	1280	826	1293	1049
Observed > 2σ(I)	1085	1087	1065	659	812	791
R_{int}	0.023	-	0.017	-	0.026	-
Parameters	101	137	101	137	101	137
GooF	1.07	1.26	1.09	1.24	1.14	1.37
R_1 (observed)	0.0299	0.0453	0.0315	0.0355	0.0351	0.0423
R_1 (all)	0.0350	0.0734	0.0382	0.0565	0.0621	0.0678
wR_2 (all)	0.0830	0.0800	0.0896	0.0691	0.1074	0.0787
Δρ (max, min) / e$^-$/Å^3 or fm/Å^3	0.30, -0.18	0.65, -0.58	0.23, -0.15	0.41, -0.41	0.14, -0.18	0.39, -0.29

[a] *It is not possible to accurately determine unit cell parameters from a Laue experiment at a continuous neutron source so no errors are listed. X-ray determined values are used where available.*

Table 5.2 *X-ray and neutron data collection and refinement information for the 2:1 complex of urea and fumaric acid.*

Compound	**2:1 Urea : Fumaric acid**						
Diffractometer	SXD	Rigaku R-AXIS RAPID	SXD	Rigaku R-AXIS RAPID	SXD	Rigaku R-AXIS RAPID	SXD
Radiation	Neutron	X-ray	Neutron	X-ray	Neutron	X-ray	Neutron
Formula	$C_6H_{12}N_4O_6$	$C_6H_{12}N_4O_6$	$C_6H_{12}N_4O_6$	$C_6H_{12}N_4O_6$	$C_6H_{12}N_4O_6$	$C_6H_{12}N_4O_6$	$C_6H_{12}N_4O_6$
Molecular weight (g mol^{-1})	236.18	236.18	236.18	236.18	236.18	236.18	236.18
T (K)	30	100	100	200	200	300	300
Space group	*P2$_1$/c*	*P2$_1$/c*	*P2$_1$/c*	*P2$_1$/c*	*P2$_1$/c*	*P2$_1$/c*	*P2$_1$/c*
***a* (Å)**	5.7976(10)	5.764(5)	5.766(2)	5.671(5)	5.676(2)	5.541(5)	5.549(2)
***b* (Å)**	7.5666(10)	7.640(5)	7.666(3)	7.888(5)	7.912(3)	8.214(5)	8.239(3)
***c* (Å)**	12.351(3)	12.283(5)	12.332(5)	12.348(5)	12.366(5)	12.427(5)	12.445(4)
***β* (°)**	97.03(3)	96.901(5)	96.81(3)	96.719(5)	96.66(3)	97.314(5)	97.24(3)
Volume (Å^3)	537.7	537.0(6)	541.2	548.6(6)	551.6	561.0(7)	564.5
Z	2	2	2	2	2	2	2
Reflections collected	5451	6806	3581	7039	3023	7119	2053
Independent	5451	1230	3581	1253	3023	1285	2053
Observed > 2σ(I)	5451	1024	3581	923	3023	1024	2053
R_{int}	-	0.040	-	0.024	-	0.031	-
Parameters	204	97	182	97	193	97	193
GooF	1.12	1.04	1.05	1.13	1.09	1.20	1.10
R_1 (observed)	0.0499	0.0350	0.0552	0.0328	0.0558	0.0577	0.0566
R_1 (all)	0.0499	0.0442	0.0552	0.0481	0.0558	0.0768	0.0566
wR_2 (all)	0.1261	0.0832	0.1144	0.0951	0.1248	0.1114	0.1301
Δρ (max, min) / e$^-$/Å^3 or fm/Å^3	1.73, -1.50	0.25 -0.22	0.91,-0.90	0.17,-0.19	0.61,-0.73	0.15 -0.12	0.42,-0.37

Table 5.3 *X-ray and neutron data collection and refinement information for the 2:1 complex of N-methylurea and succinic acid.*[a]

Compound	**2:1 *N*-Methylurea : Succinic acid**						
Diffractometer	VIVALDI	Rigaku R-AXIS RAPID	VIVALDI	Rigaku R-AXIS RAPID	VIVALDI	Rigaku R-AXIS RAPID	VIVALDI
Radiation	Neutron	X-ray	Neutron	X-ray	Neutron	X-ray	Neutron
Formula	$C_8H_{18}N_4O_6$	$C_8H_{18}N_4O_6$	$C_8H_{18}N_4O_6$	$C_8H_{18}N_4O_6$	$C_8H_{18}N_4O_6$	$C_8H_{18}N_4O_6$	$C_8H_{18}N_4O_6$
Molecular weight (g mol^{-1})	266.26	266.26	266.26	266.26	266.26	266.26	266.26
T (K)	20	100	100	200	200	300	300
Space group	*P2$_1$/n*	*P2$_1$/n*	*P2$_1$/n*	*P2$_1$/n*	*P2$_1$/n*	*P2$_1$/n*	*P2$_1$/n*
***a* (Å)**	7.89	8.0244(12)	8.02	8.2868(7)	8.29	8.5398(8)	8.54
***b* (Å)**	5.79	5.7496(7)	5.75	5.6618(3)	5.66	5.5798(4)	5.58
***c* (Å)**	13.65	13.735(2)	13.74	13.7761(11)	13.78	13.838(2)	13.84
***β* (°)**	91.22	91.426(5)	91.43	91.799(4)	91.80	92.921(4)	92.92
Volume (Å^3)	623.4	633.5(2)	633.4	646.03(8)	646.3	658.84(11)	658.7
Z	2	2	2	2	2	2	2
Reflections collected	13957	8408	11410	8559	9049	8658	5368
Independent	2522	1457	1856	1480	1400	1501	893
Observed > 2σ(I)	1945	1304	1410	1147	994	851	636
R_{int}	-	0.023	-	0.018	-	0.038	-
Parameters	163	118	163	118	163	118	163
GooF	1.34	1.09	1.44	1.12	1.47	1.16	1.38
R_1 (observed)	0.0538	0.0334	0.0497	0.0353	0.0530	0.0432	0.0441
R_1 (all)	0.0896	0.0371	0.0800	0.0455	0.0906	0.0773	0.0814
wR_2 (all)	0.0860	0.0918	0.0920	0.1077	0.0983	0.1464	0.0852
Δρ (max, min) / e$^-$/Å^3 or fm/Å^3	0.12,-0.11	0.34, -0.17	0.08,-0.13	0.19, -0.14	0.06,-0.08	0.17,-0.17	0.04,-0.04

[a] *It is not possible to accurately determine unit cell parameters from a Laue experiment at a continuous neutron source so no errors are listed. X-ray determined values are used where available.*

Table 5.4 *X-ray data collection and refinement information for the 2:1 complex of N-methylurea and fumaric acid.*

Compound	**2:1 *N*-Methylurea : Fumaric acid**		
Diffractometer	Rigaku R-AXIS RAPID	Rigaku R-AXIS RAPID	Rigaku R-AXIS RAPID
Formula	$C_8H_{16}N_4O_6$	$C_8H_{16}N_4O_6$	$C_8H_{16}N_4O_6$
Molecular weight (g mol^{-1})	264.25	264.25	264.25
T (K)	100	200	300
Space group	$P2_1/n$	$P2_1/n$	$P2_1/n$
***a* (Å)**	8.3188(10)	8.5509(16)	8.7741(14)
***b* (Å)**	5.6497(5)	5.5691(8)	5.4413(7)
***c* (Å)**	13.8382(13)	13.909(2)	13.930(2)
***β* (°)**	104.156(4)	102.959(7)	100.730(6)
Volume (Å^3)	630.63(11)	645.5(2)	653.44(16)
Z	2	2	2
Reflections collected	8243	8540	8681
Independent	1449	1475	1494
Observed > 2σ(I)	1172	1002	865
R_{int}	0.033	0.043	0.047
Parameters	114	114	115
GooF	1.07	1.07	1.03
R_1 (observed)	0.0327	0.0398	0.0487
R_1 (all)	0.0435	0.0656	0.0949
wR_2 (all)	0.0804	0.1043	0.1168
Δρ (max, min) / e$^-$/Å^3	0.19, -0.17	0.17, -0.15	0.14, -0.12

Table 5.5 *X-ray data collection and refinement information for the 2:1 complex of N-methylurea and oxalic acid.*

Compound	**2:1 *N*-Methylurea : Oxalic acid**	
Diffractometer	Rigaku R-AXIS RAPID	Rigaku R-AXIS RAPID
Formula	$C_6H_{14}N_4O_6$	$C_6H_{14}N_4O_6$
Molecular weight (g mol^{-1})	238.21	238.21
T (K)	200	300
Space group	$P2_1/c$	$P2_1/c$
***a* (Å)**	5.1081(8)	5.1464(14)
***b* (Å)**	10.5388(14)	10.555(2)
***c* (Å)**	10.2233(14)	10.313(3)
***β* (°)**	102.717(7)	101.835(13)
Volume (Å^3)	536.85(13)	548.3(2)
Z	2	2
Reflections collected	7002	13815
Independent	1233	1255
Observed > 2σ(I)	816	880
R_{int}	0.034	0.049
Parameters	102	102
GooF	1.17	1.06
R_1 (observed)	0.0432	0.0508
R_1 (all)	0.0696	0.0790
wR_2 (all)	0.1261	0.1231
Δρ (max, min) / e$^-$/Å^3	0.23, -0.24	0.21, -0.16

Table 5.6 *X-ray and neutron data collection and refinement information for the 2:1 complex of N,N-dimethylurea and succinic acid.*[a]

Compound	**2:1 *N,N*-Dimethylurea : Succinic acid**				
Diffractometer	VIVALDI	VIVALDI	Rigaku R-AXIS RAPID	Rigaku R-AXIS RAPID	Rigaku R-AXIS RAPID
Radiation	Neutron	Neutron	X-ray	X-ray	X-ray
Formula	$C_{10}H_{22}N_4O_6$	$C_{10}H_{22}N_4O_6$	$C_{10}H_{22}N_4O_6$	$C_{10}H_{22}N_4O_6$	$C_{10}H_{22}N_4O_6$
Molecular weight (g mol^{-1})	294.32	294.32	294.32	294.32	294.32
T (K)	20	50	100	200	300
Space group	*P2$_1$/c*	*P2$_1$/c*	*P2$_1$/c*	*P2$_1$/c*	*P2$_1$/c*
***a* (Å)**	8.35	8.40	8.483(3)	8.6629(12)	8.797(2)
***b* (Å)**	5.44	5.47	5.5169(14)	5.6284(6)	5.6934(13)
***c* (Å)**	15.43	15.47	15.415(5)	15.152(2)	15.059(4)
***β* (°)**	101.95	101.95	101.677(8)	100.948(4)	100.764(7)
Volume (Å^3)	685.7	695.4	706.5(4)	725.34(16)	741.0(3)
Z	2	2	2	2	2
Reflections collected	15220	9617	9079	9619	9568
Independent	3055	2549	1611	1664	1700
Observed > 2σ(I)	2334	1931	1468	1468	1410
R_{int}	-	-	0.025	0.017	0.020
Parameters	190	190	135	135	135
GooF	1.28	1.22	1.09	1.08	1.07
R_1 (observed)	0.0502	0.0473	0.0308	0.0373	0.0472
R_1 (all)	0.0871	0.0800	0.0330	0.0408	0.0534
wR_2 (all)	0.0838	0.0838	0.0900	0.1113	0.1435
Δρ (max, min) / e$^-$ /Å^3 or fm/Å^3	0.13, -0.13	0.11, -0.10	0.25, -0.19	0.18, -0.19	0.18, -0.19

[a] *It is not possible to accurately determine unit cell parameters from a Laue experiment at a continuous neutron source so no errors are listed. X-ray determined values are used where available.*

Table 5.7 *X-ray and neutron data collection and refinement information for the 2:1 complex of N,N-dimethylurea and fumaric acid.*[a]

Compound	**2:1 *N*-Dimethylurea : Fumaric acid**							
Diffractometer	VIVALDI	Rigaku R-AXIS RAPID	VIVALDI	Rigaku R-AXIS RAPID	VIVALDI	VIVALDI	Rigaku R-AXIS RAPID	VIVALDI
Radiation	Neutron	X-ray	Neutron	X-ray	Neutron	Neutron	X-ray	Neutron
Formula	$C_5H_{10}N_2O_3$	$C_5H_{10}N_2O_3$	$C_5H_{10}N_2O_3$	$C_5H_{10}N_2O_3$	$C_5H_{10}N_2O_3$	$C_5H_{10}N_2O_3$	$C_5H_{10}N_2O_3$	$C_5H_{10}N_2O_3$
Molecular weight (g mol^{-1})	146.15	146.15	146.15	146.15	146.15	146.15	146.15	146.15
T (K)	20	100	100	200	200	250	300	300
Space group	*P2$_1$/n*	*P2$_1$/n*	*P2$_1$/n*	*P2$_1$/n*	*P2$_1$/n*	*P2$_1$/n*	*P2$_1$/n*	*P2$_1$/n*
***a* (Å)**	5.75	5.8025(8)	5.80	5.8640(5)	5.86	5.89	5.924(4)	5.92
***b* (Å)**	18.10	18.158(2)	18.16	18.2369(11)	18.24	18.30	18.376(9)	18.37
***c* (Å)**	6.82	6.8184(8)	6.82	6.8458(4)	6.85	6.86	6.873(5)	6.87
***β* (°)**	100.52	101.019(4)	101.02	101.330(3)	101.33	101.30	101.293(5)	101.29
Volume (Å^3)	697.9	705.15(15)	705.1	717.83(9)	717.9	725.1	733.7(8)	732.7
Z	4	4	4	4	4	4	4	4
Reflections collected	8831	9285	7157	9445	5215	4663	9713	4635
Independent	1798	1620	1415	1645	1018	921	1674	936
Observed > 2σ(I)	1231	1286	907	1317	642	531	1029	559
R_{int}	-	0.035	-	0.021	-	-	0.025	-
Parameters	181	131	181	131	181	181	131	181
GooF	1.03	1.13	1.11	1.08	1.11	1.10	1.08	1.19
R_1 (observed)	0.0502	0.0417	0.0529	0.0397	0.0567	0.0634	0.0507	0.0533
R_1 (all)	0.1034	0.0525	0.1121	0.0485	0.1215	0.1466	0.0802	0.1232
wR_2 (all)	0.0837	0.1251	0.0894	0.1196	0.0899	0.0992	0.1693	0.0902
Δρ (max, min) / e$^-$/Å^3 or fm/Å^3	0.11, -0.08	0.23, -0.22	0.07, -0.08	0.21, -0.14	0.04, -0.04	0.05, -0.06	0.18, -0.17	0.03, -0.04

[a] *It is not possible to accurately determine unit cell parameters from a Laue experiment at a continuous neutron source so no errors are listed. X-ray determined values are used where available.*

5.2 Complexes of Urea with Succinic and Fumaric Acid

5.2.1 Urea Succinic Acid (2:1) (US)

There are two known polymorphs of the 2:1 complex of urea and succinic acid (**US**) which crystallise in the $P2_1/c$[101,172] and $C2/c$[105] space groups. The data presented in this work correspond to the $P2_1/c$ form only. The structure of **US** contains a three molecule building block with a "U-A-U" motif (**Figure 5.2**) with one urea molecule and half an acid molecule in the asymmetric unit. This structure has been previously determined using X-rays at RT[101,172] and the data presented here are in good agreement with the previously determined structure.

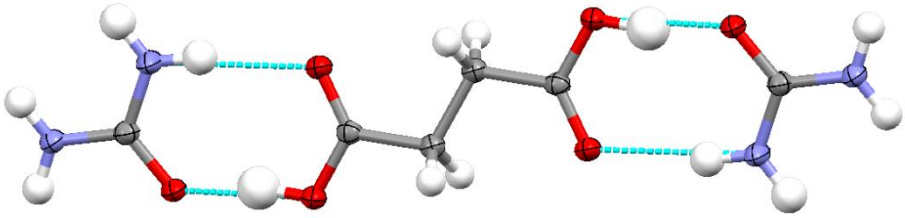

Figure 5.2 *The hydrogen bonded three molecule "U-A-U" unit in the 2:1 complex of urea and succinic acid at 100 K (X-ray).*

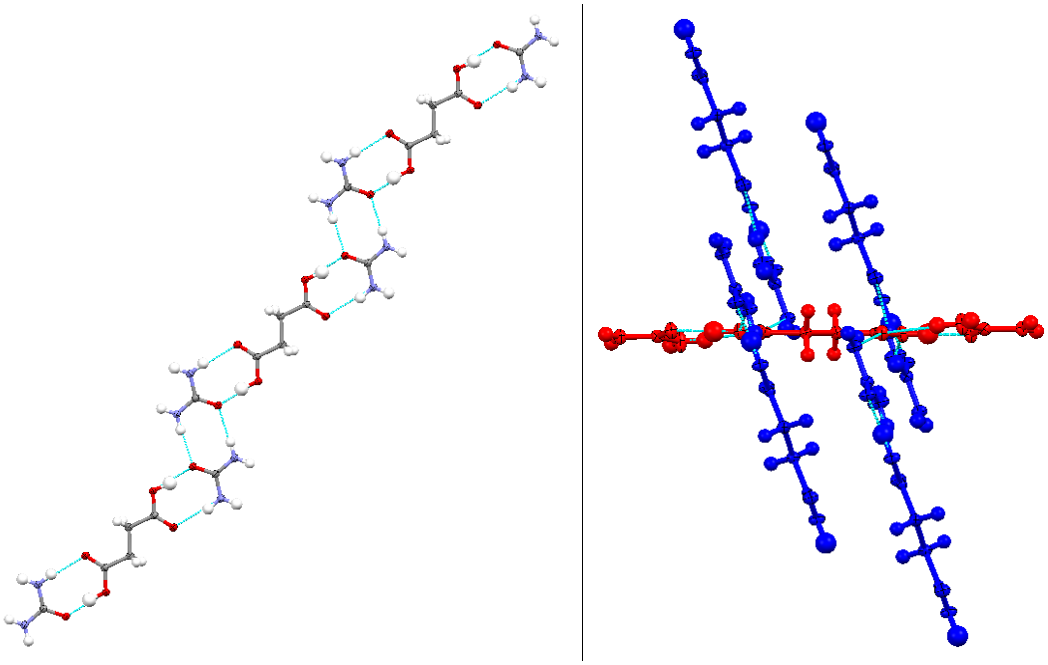

Figure 5.3 *One-dimensional zigzag molecular chain (left) and the different orientations of chains (right, red and blue) in the 2:1 complex of urea succinic acid at 100 K (X-ray).*

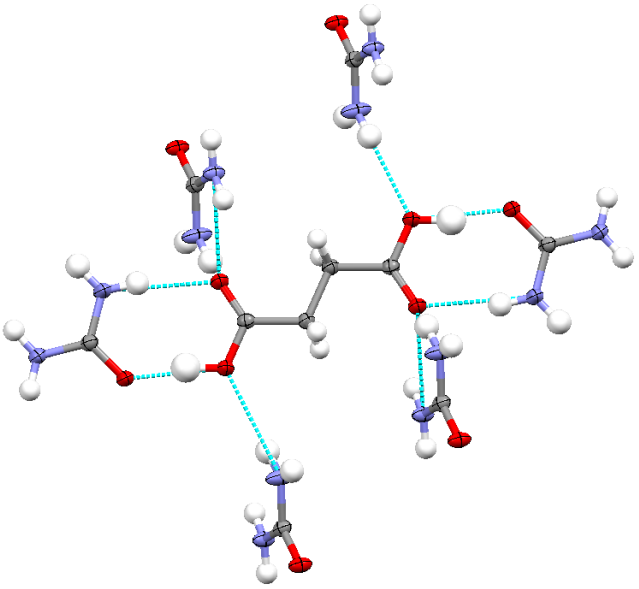

Figure 5.4 *Lateral hydrogen bonds between a molecular chain and adjacent chains in different orientations in the 2:1 complex of urea succinic acid at 100 K (X-ray).*

One-dimensional zigzag chains with a repeating "U-A-U" motif form and are held together by two $R_2^2(8)$ hydrogen bonded rings; one an amide···amide homodimer and the other an acid···amide heterodimer containing an O-H···O SSHB (**Figure 5.3**, left). The O-H···O SSHB and the N-H···O hydrogen bond of the acid···amide heterodimer in the "U-A-U" unit have lengths of 2.5149(10) and 2.9473(13) Å, respectively, at 100 K. The two equivalent N-H···O hydrogen bonds in the amide···amide homodimer, linking the "U-A-U" units, have N···O lengths of 2.9156(13) Å. The succinic acid molecules in the chains are planar with no rotation around the C-C bond in the alkyl chain. Each chain of molecules is surrounded by chains in a different orientation tilted at ~69.0° (estimated from the angle between the planes of the acid molecules in each chain) while chains in the same orientation are stacked on top of one another with a spacing of ~3.25 Å between layers (**Figure 5.3**, right). The motif of alternating chain orientations repeats along the *c*-axis and adjacent chains are held in place by lateral N-H···O hydrogen bonds (lengths of 2.9674(12) and 3.0485(12) Å) between the urea amide groups and acid oxygens in the different chains forming a complex three-dimensional hydrogen bonded network (**Figure 5.4**).

5.2.2 Urea Fumaric Acid (2:1) (UF)

The structure of the 2:1 complex of urea and fumaric acid (**UF**) contains a three molecule building block with a "U-A-U" motif (**Figure 5.5**) with one urea molecule and half an acid molecule in the asymmetric unit, crystallising in the $P2_1/c$ space group. This structure has

been previously determined using X-rays at RT[102,172] and the data presented here are in good agreement with the previous determinations. This complex is isostructural with that of **US** described in **Section 5.2.1** above.

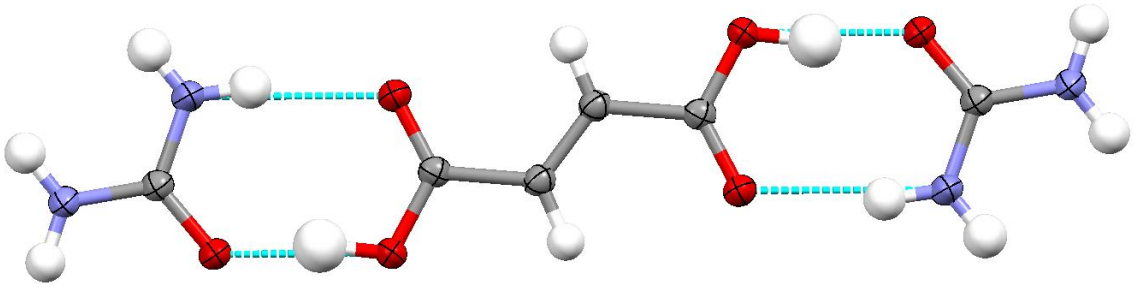

Figure 5.5 *The hydrogen bonded three molecule "U-A-U" unit in the 2:1 complex of urea and fumaric acid at 100 K (X-ray).*

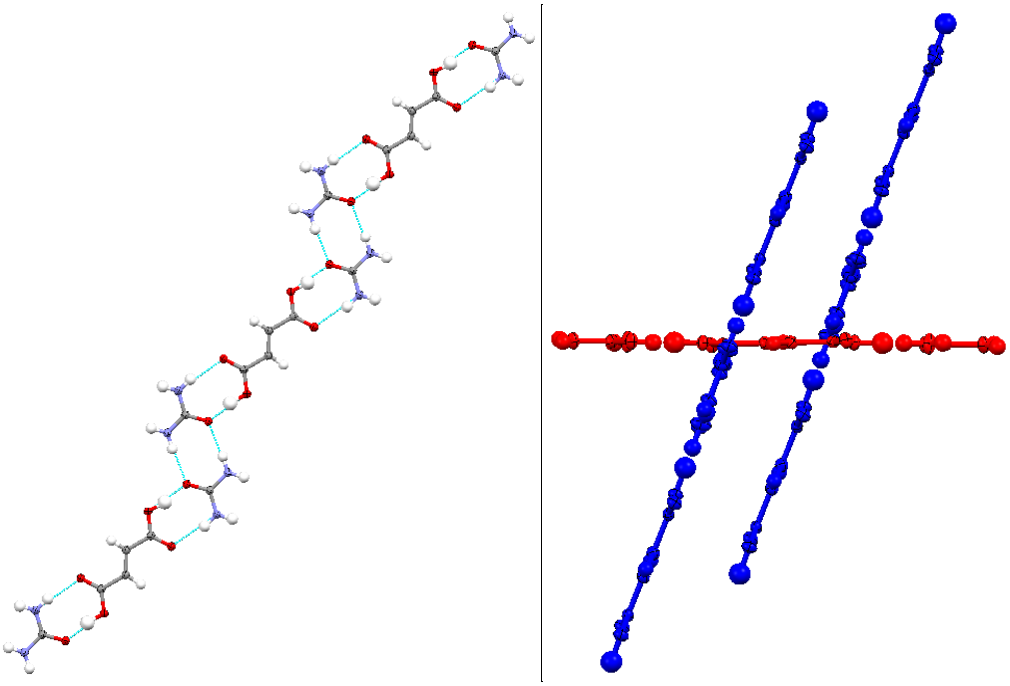

Figure 5.6 *One-dimensional zigzag molecular chain (left) and the two different orientations of chains (right, red and blue) in the 2:1 complex of urea fumaric acid at 100 K (X-ray).*

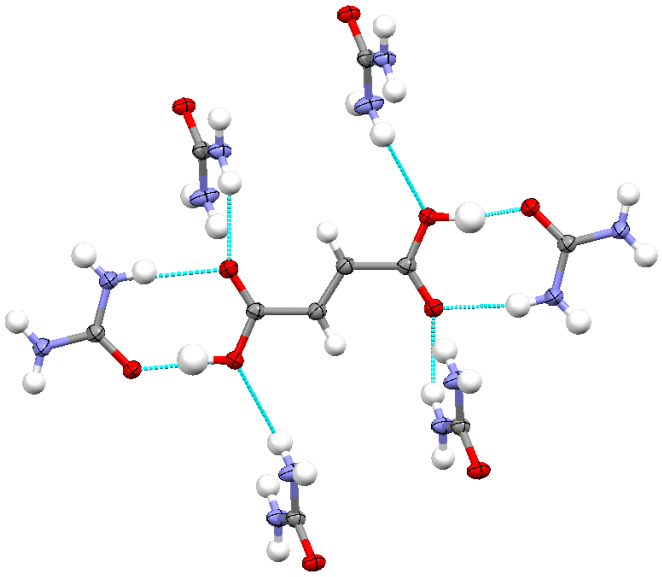

Figure 5.7 *Lateral hydrogen bonds between a molecular chain and adjacent chains in different orientations in the 2:1 complex of urea fumaric acid at 100 K (X-ray).*

One-dimensional chains made up of "U-A-U" units held together by $R_2^2(8)$ hydrogen bonded rings are formed, with the O-H···O SSHB and the N-H···O hydrogen bond of the acid···amide heterodimer in the "U-A-U" unit having lengths of 2.496(2) and 2.929(2) Å, respectively, at 100 K (**Figure 5.6**, left); both are shorter than the equivalent acid···amide hydrogen bonds in **US**. Units are linked by two equivalent N-H···O hydrogen bonds in the amide···amide homodimer with an N···O length of 2.898(3) Å. The two chain orientations are tilted at ~66.8° to each other (estimated from the angle between the planes of the acid molecules in each chain). Chains in the same orientation are stacked on top of one another with a spacing of ~2.99 Å between layers (**Figure 5.6**, right), closer than the stacked units in the complex of **US**. The lateral N-H···O hydrogen bonds have N···O lengths of 2.922(3) and 3.135(3) Å between the urea amide groups and acid oxygens in the different chains (**Figure 5.7**), more asymmetric than those in **US**.

5.3 Complexes of *N*-Methylurea with Succinic, Fumaric and Oxalic acid

5.3.1 *N*-Methylurea Succinic Acid (2:1) (MUS)

The structure of *N*-methylurea and succinic acid (**MUS**) contains a three molecule building block with a "MU-A-MU" motif (**Figure 5.8**) with one *N*-methylurea molecule and half an acid molecule in the asymmetric unit, crystallising in the $P2_1/n$ space group. The *N*-methylurea molecule adopts an *anti* conformation with the methyl group located on the opposite side of the molecule from the carbonyl group. This complex is isostructural with those of **US** and **UF** presented in **Section 5.2.1** and **Section 5.2.2**.

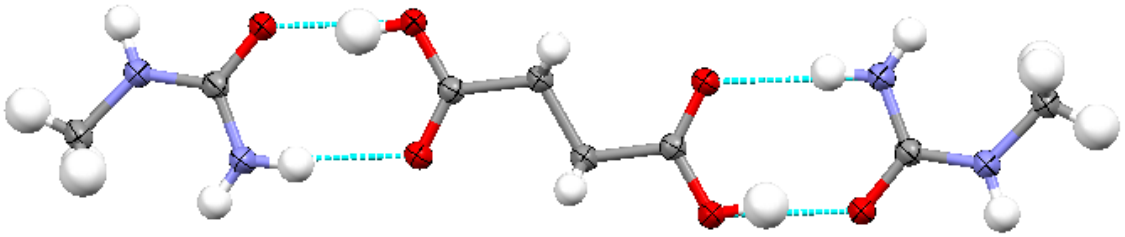

Figure 5.8 *The hydrogen bonded three molecule "MU-A-MU" unit in the 2:1 complex of N-methylurea and succinic acid at 100 K (X-ray).*

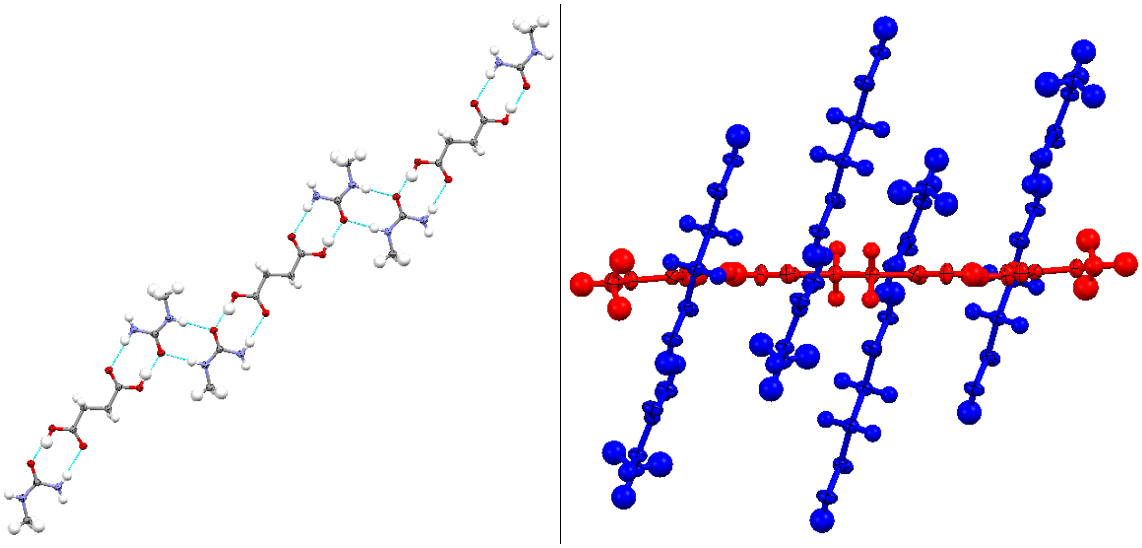

Figure 5.9 *One-dimensional zigzag molecular chain (left) and the two different orientations of chains (right, red and blue) in the 2:1 complex of N-methylurea succinic acid at 100 K (X-ray).*

One-dimensional zigzag chains with a repeating "MU-A-MU" motif are formed, held together by two $R_2^2(8)$ hydrogen bonded rings (**Figure 5.9**, left); one an amide···amide homodimer and the other an acid···amide heterodimer, similar to the urea equivalents (**US** and **UF**). The O-H···O SSHB and N-H···O hydrogen bond of the acid···amide heterodimer, which make up the "MU-A-MU" unit, have lengths of 2.5340(11) and 2.9666(13) Å, respectively, at 100 K. The two equivalent N-H···O hydrogen bonds in the amide···amide homodimer which link the "MU-A-MU" units have N···O lengths of 2.8681(13) Å. Adjacent chains in different orientations are aligned along the *c*-axis tilted at ~71.8° degrees to each other (as estimated by the planes formed by the acid molecules). Chains in the same orientation are stacked on top of each other with approximate layer spacing of 3.43 Å (**Figure 5.9**, right). Lateral N-H···O hydrogen bonds between the acid and amide groups of length 2.9895(13) Å hold adjacent chains in place, whilst there are also weaker

C-H···O interactions between the methyl groups and acid oxygens of different chains with a length of 3.247(1) Å. These come together to form a three-dimensional hydrogen bonded network (**Figure 5.10**).

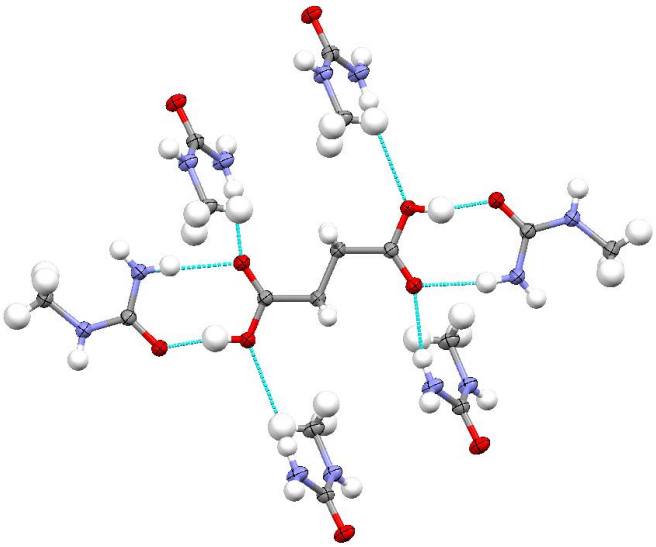

Figure 5.10 *Lateral hydrogen bonds between a molecular chain and adjacent chains in different orientations in the 2:1 complex of N-methylurea succinic acid at 100 K (X-ray).*

5.3.2 *N*-Methylurea Fumaric Acid (2:1) (MUF)

The structure of *N*-methylurea and fumaric acid (**MUF**) also contains a three molecule building block with a "MU-A-MU" motif (**Figure 5.11**) with one *N*-methylurea molecule and half an acid molecule in the asymmetric unit, crystallising in the $P2_1/n$ space group. The *N*-methylurea molecule adopts an *anti* conformation with the methyl group located on the opposite side of the molecule from the carbonyl group. This complex is again isostructural with the **US**, **UF** and **MUS** complexes described in **5.2.1**, **5.2.2** and **5.3.1**.

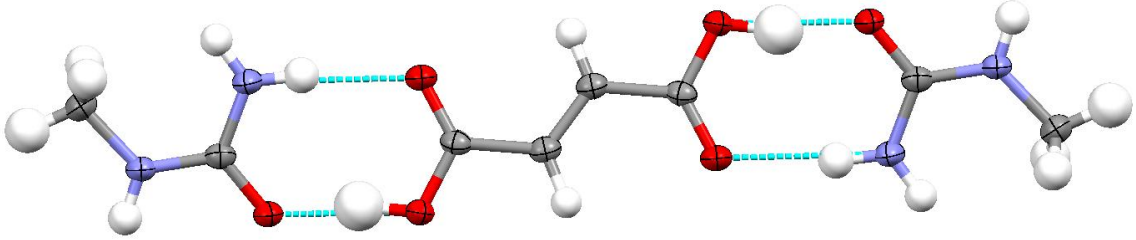

Figure 5.11 *The hydrogen bonded three molecule "MU-A-MU" unit in the 2:1 complex of N-methylurea and fumaric acid at 100 K (X-ray).*

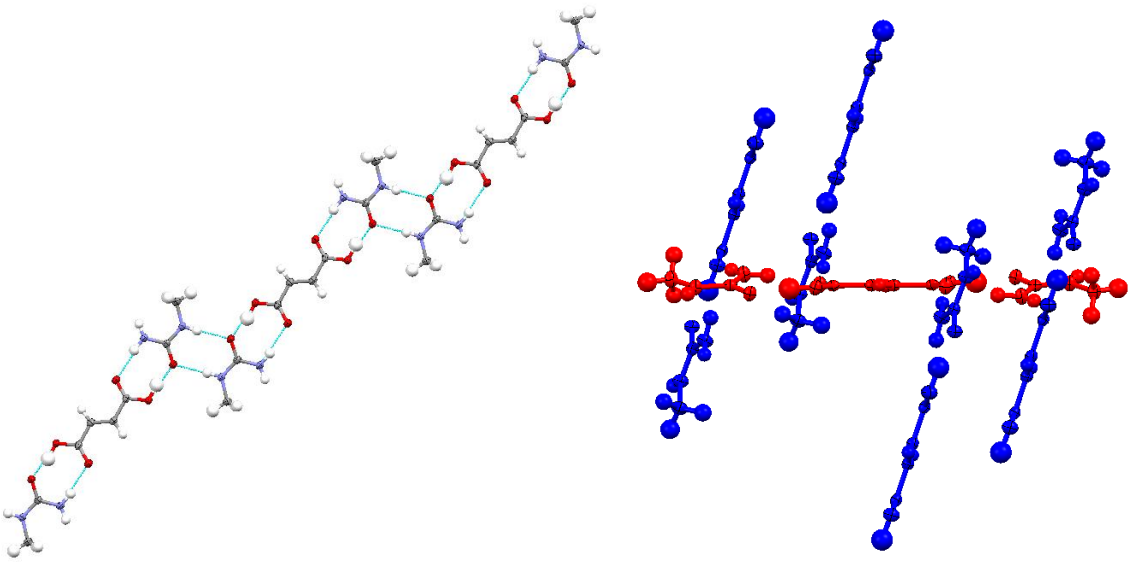

Figure 5.12 *One-dimensional zigzag molecular chain (left) and the two different orientations of chains (right, red and blue) in the 2:1 complex of N-methylurea fumaric acid at 100 K (X-ray).*

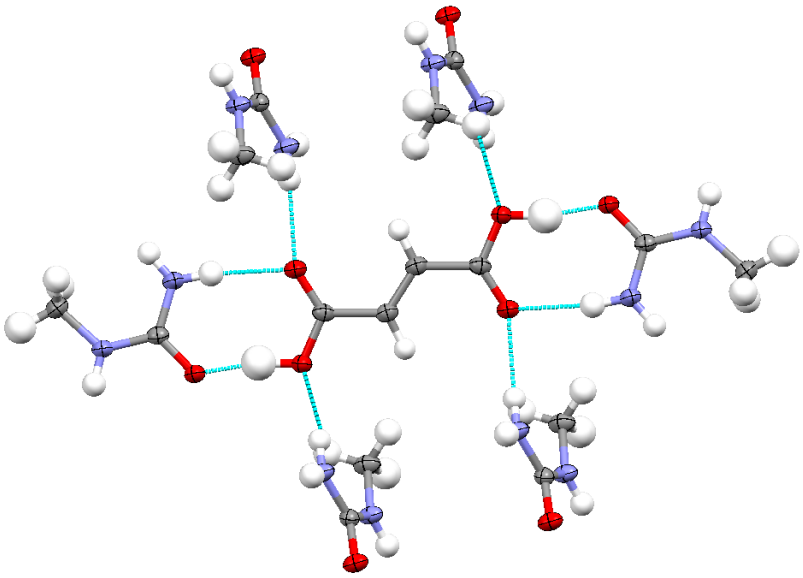

Figure 5.13 *Lateral hydrogen bonds between a molecular chain and adjacent chains in different orientations in the 2:1 complex of N-methylurea fumaric acid at 100 K (X-ray).*

One-dimensional chains containing "MU-A-MU" units are formed held together by two $R_2^2(8)$ hydrogen bonded rings; one an acid···amide heterodimer and the other an amide···amide homodimer (**Figure 5.12**, left). The "MU-A-MU" units contain an O-H···O SSHB and an N-H···O hydrogen bond with lengths of 2.5291(12) and 2.9214(15) Å, respectively, at 100 K. The hydrogen bonds within the "MU-A-MU" unit are shorter than

those in the **MUS** complex and the methylurea molecules are tilted slightly, by 16.30(8)°, to the plane of the acid molecule. "MU-A-MU" units are linked to one another through two equivalent N-H···O hydrogen bonds in the amide···amide homodimer with N···O distances of 2.8907(13) Å. The different chain orientations are tilted at ~72.6° degrees to each other (as estimated by the planes formed by the acid molecules). Chains in the same orientation have an approximate layer spacing of 3.30 Å (**Figure 5.12**, right). The lateral N-H···O hydrogen bonds have a length of 2.9548(14) Å while the weaker C-H···O interactions between the methyl groups and acid oxygens have a length of 3.217(2) Å (**Figure 5.13**), both shorter than those observed in the **MUS** complex.

5.3.3 *N*-Methylurea Oxalic Acid (2:1) (MOX)

There are two known forms of the 2:1 complex of *N*-methylurea and oxalic acid (**MOX**) which crystallise in the $P2_1/c$ and *Pnma* space groups.[112] The data presented in this work correspond to the $P2_1/c$ form only. This structure is not isostructural with any others presented so far in this chapter. The structure contains a three molecule building block with a "MU-A-MU" motif (**Figure 5.14**) with one *N*-methylurea molecule and half an acid molecule in the asymmetric unit. The *N*-methylurea molecule adopts a *syn* conformation with the methyl group located on the same side as the molecule as the carbonyl group. This structure has been previously determined using X-rays at RT[112] and the data presented here are in good agreement with the previously determined structure. The original determination was carried out 1979[112] and has been recollected here to provide more accurate hydrogen atom positions. The previous study of this complex indicated that a phase transition from monoclinic to orthorhombic symmetry should be expected to occur at ~180 K as the temperature is decreased.[112] A data collection was therefore attempted at 100 K, however, the phase transition caused a decrease in the quality of the crystal and a stable refinement could not be obtained from the 100 K data set; therefore only the 200 and 300 K X-ray structures are presented here.

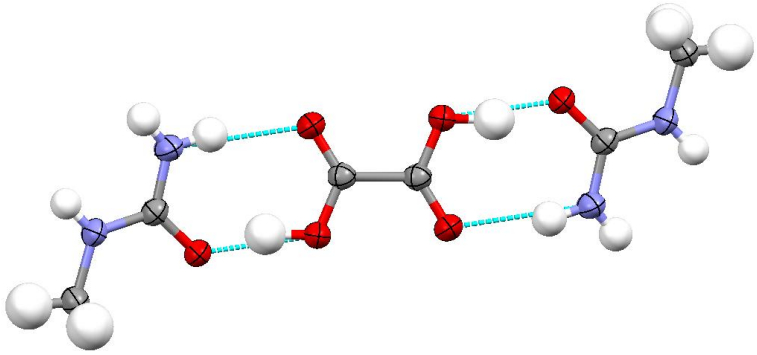

Figure 5.14 *The hydrogen bonded three molecule "MU-A-MU" unit of the 2:1 complex of N-methylurea and oxalic acid at 200 K (X-ray).*

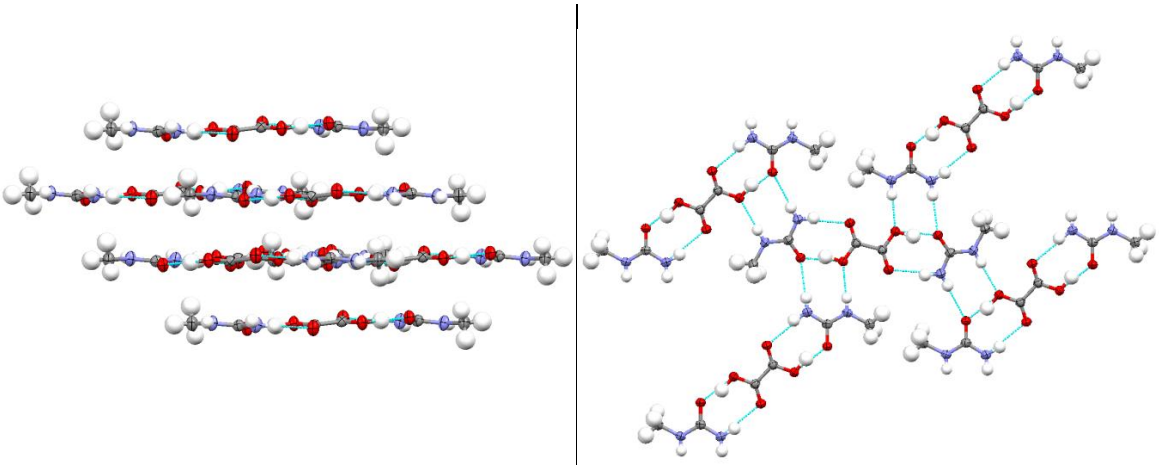

Figure 5.15 *The layered structure (left) and hydrogen bonds between three molecule units in a layer (right) of the 2:1 complex of N-methylurea and oxalic acid at 200 K (X-ray).*

The three molecule "MU-A-MU" units, containing $R_2^2(8)$ hydrogen bonded rings, are formed through acid···amide heterodimers made up of an O-H···O SSHB and an N-H···O hydrogen bond with lengths of 2.458(2) and 2.992(3) Å, respectively, at 200 K. Neighbouring units are held in place in layers by $R_3^2(8)$ hydrogen bonded rings formed between two *N*-methylurea molecules and an acid to produce a two-dimensional hydrogen bonded network (**Figure 5.15**). These hydrogen bonded rings are made up of two N-H···O hydrogen bonds of lengths 2.962(2) and 3.145(2) Å, along with the strong O-H···O hydrogen bond of the three molecule unit. The layer separation is ~2.97 Å with π···π interactions between the carbonyls of the acid and *N*-methylurea in different layers.

5.4 Complexes of *N,N*-Dimethylurea with Succinic and Fumaric Acid

5.4.1 *N,N*-Dimethylurea Succinic Acid (2:1) (DMUS)

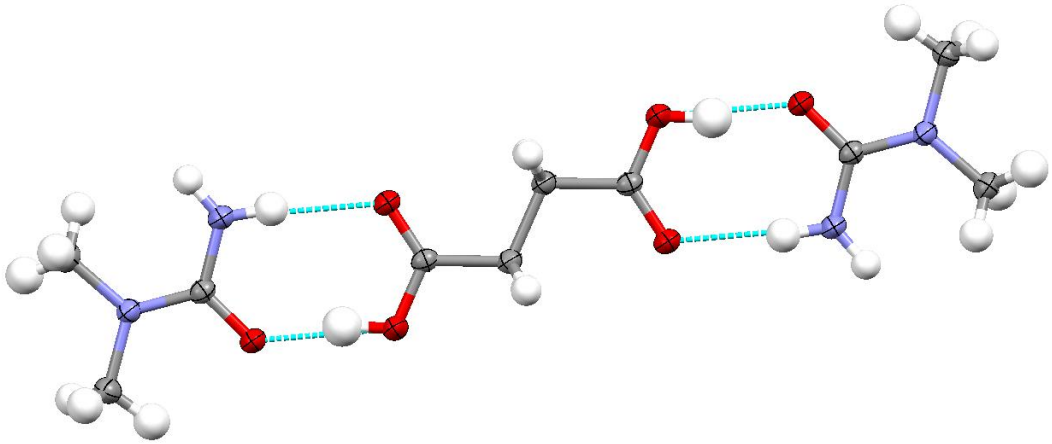

Figure 5.16 *The hydrogen bonded three molecule "DMU-A-DMU" unit of the 2:1 complex of N,N-dimethylurea and succinic acid at 100 K (X-ray).*

The structure of *N*,*N*-dimethylurea and succinic acid (**DMUS**) contains a three molecule building block with a "DMU-A-DMU" motif (**Figure 5.16**) with one *N,N*-dimethylurea molecule and half an acid molecule in the asymmetric unit, crystallising in the $P2_1/c$ space group. This structure is isostructural with those of **US**, **UF**, **MUS** and **MUF** above.

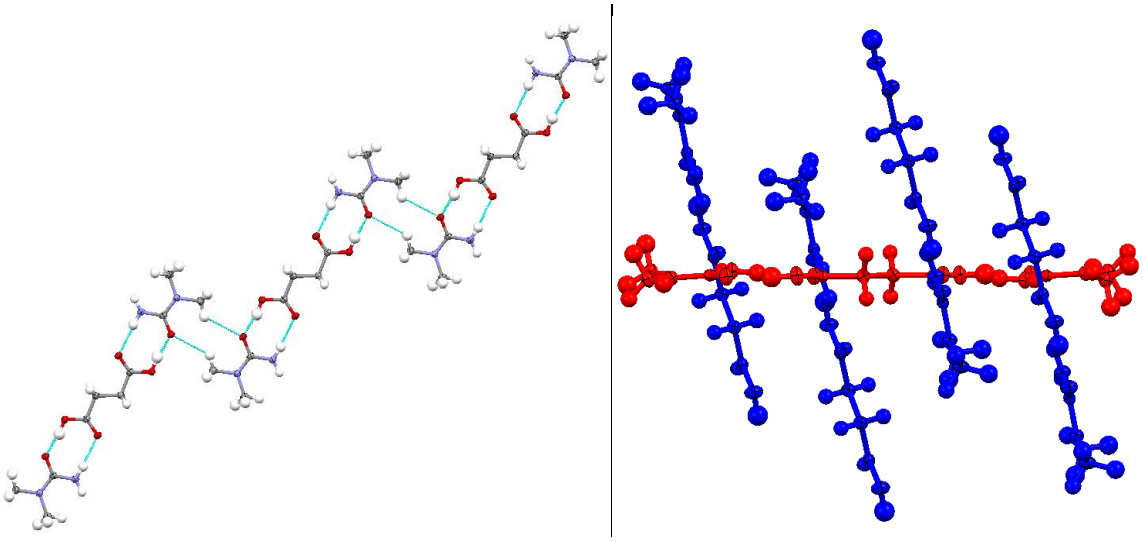

Figure 5.17 *One-dimensional zigzag molecular chain (left) and the two possible orientations of chains (right, red and blue) in the 2:1 complex of N,N-dimethylurea succinic acid at 100 K (X-ray).*

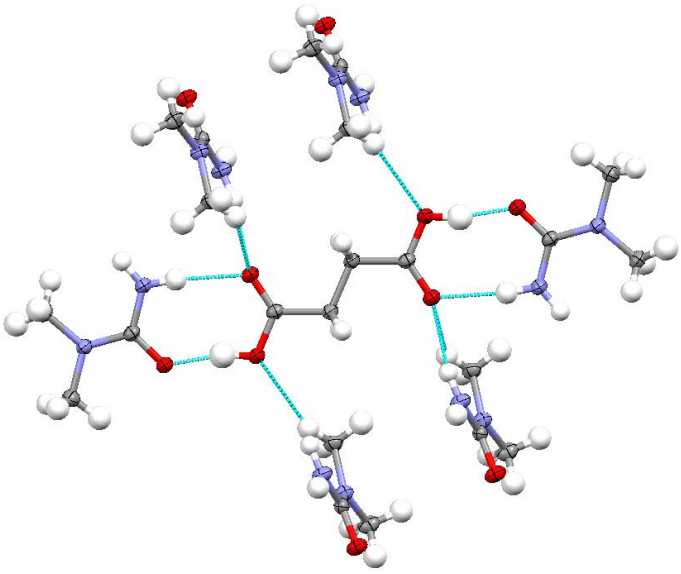

Figure 5.18 *Lateral hydrogen bonds between a molecular chain and adjacent chains in different orientations in the 2:1 complex of N,N-dimethylurea succinic acid at 100 K (X-ray).*

The three molecule "DMU-A-DMU" units, containing $R_2^2(8)$ hydrogen bonded rings, are formed through acid···amide heterodimers containing an O-H···O SSHB and an N-H···O hydrogen bond with lengths of 2.5249(11) and 2.9519(12) Å, respectively at 100 K (**Figure 5.17**, left). Three molecule units form a one-dimensional chain through two equivalent C-H···O interactions between two *N*,*N*-dimethylurea molecules with lengths of 3.396(1) Å (**Figure 5.17**, left). Adjacent chains in different orientations are aligned along the *c*-axis, tilted at ~74.3° to each other (as estimated by the angle between the planes formed by the acid molecules) and are held in place by lateral N-H···O hydrogen bonds and weaker C-H···O interactions with lengths of 2.9489(15) and 3.247(2) Å, respectively (**Figure 5.18**). Chains in the same orientation are stacked on top of one another with a layer separation of ~3.35 Å (**Figure 5.17**, right).

5.4.2 *N*,*N*-Dimethylurea Fumaric Acid (2:1) (DMUF)

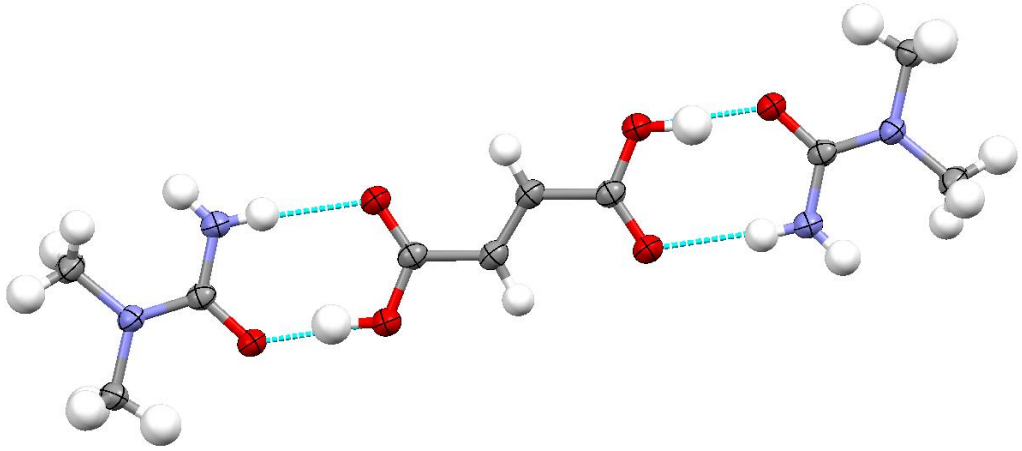

Figure 5.19 *The hydrogen bonded three molecule "DMU-A-DMU" unit of the 2:1 complex of N,N-dimethylurea and fumaric acid at 100 K (X-ray).*

The structure of *N*,*N*-dimethylurea and fumaric acid (**DMUF**) contains a three molecule building block with a "DMU-A-DMU" motif (**Figure 5.19**) with one *N,N*-dimethylurea molecule and half an acid molecule in the asymmetric unit, crystallising in the $P2_1/n$ space group. This structure is not isostructural with any others presented so far in this chapter.

"DMU-A-DMU" units, containing $R_2^2(8)$ hydrogen bonded rings, are formed through acid···amide heterodimers containing an O-H···O SSHB and an N-H···O hydrogen bond with lengths of 2.5000(15) and 2.977(2) Å, respectively, at 100 K. The units form one-dimensional chains through a $R_2^4(8)$ hydrogen bonded ring composed of two pairs of equivalent N-H···O hydrogen bonds with lengths of 2.977(2) and 3.048(2) Å between an amide group and the carbonyl oxygens of two neighbouring units (**Figure 5.20**, left).

Adjacent chains in different orientations are aligned along the *b*-axis and held in place by weak C-H···O interactions between an *N*,*N*-dimethylurea and the hydroxyl oxygen of a fumaric acid molecule and the carbonyl oxygen of another *N*,*N*-dimethylurea with lengths of 3.602(2) and 3.608(2) Å, respectively (**Figure 5.20**, right). The angle between the planes of the acid molecules in the two different chain orientations is ~86.5°. Chains in the same orientation are again layered with an approximate spacing of 3.12 Å.

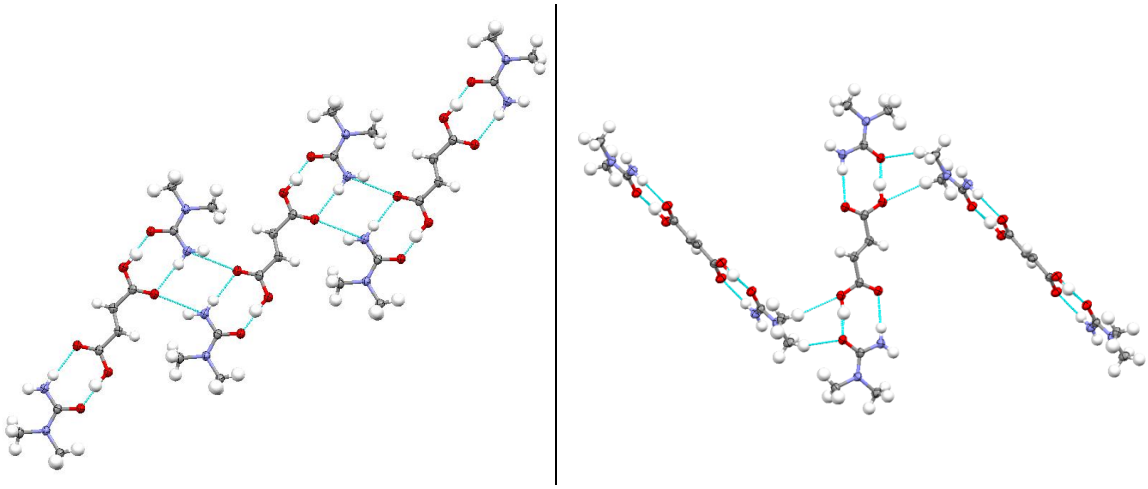

Figure 5.20 *One-dimensional chain of molecules (left) and interactions between chains in different orientations (right) in the 2:1 complex of N,N-dimethylurea and fumaric acid at 100 K (X-ray).*

5.5 Structural Similarities

The **US**, **UF**, **MUS** and **MUF** complexes are all isostructural with one another and have similar unit cell parameters (**Table 5.8**). The **DMUS** complex also packs in a similar way to the **US**, **UF**, **MUS** and **MUF** complexes, again with similar unit cell parameters. On the addition of a methyl group to the urea moiety in complexes **MUS** and **MUF**, the *c*-axis increases compared with **US** and **UF** in size due to the methyl groups pointing approximately along the *c*-axis. This occurs again on the addition of a second methyl group to the urea moiety in complex **DMUS** where the *c*-axis increases in size again. Overall, it can be said that the **US**, **UF**, **MUS**, **MUF** and **DMUS** complexes all display the same packing motif while the **MOX** and **DMUF** complexes show different packing motifs.

Table 5.8 *Unit cell parameters for the seven complexes from the 200 K X-ray data.*

Complex	US	UF	MUS	MUF	MOX	DMUS	DMUF
Space group	$P2_1/c$	$P2_1/c$	$P2_1/n$	$P2_1/n$	$P2_1/c$	$P2_1/c$	$P2_1/n$
***a* / Å**	5.6706(5)	5.671(4)	8.2868(7)	8.551(2)	5.1081(8)	8.6629(12)	5.8640(5)
***b* / Å**	8.1227(7)	7.888(5)	5.6618(3)	5.5691(8)	10.5388(14)	5.6284(6)	18.2369(11)
***c* / Å**	12.2182(10)	12.348(10)	13.7761(11)	13.909(2)	10.2233(14)	15.152(2)	6.8458(4)
β	96.375(3)	96.719(3)	91.799(4)	102.959(7)	102.717(7)	100.948(4)	101.330(3)
V	559.30(8)	548.6(15)	646.03(8)	645.5(2)	536.85(13)	725.3(2)	717.83(9)

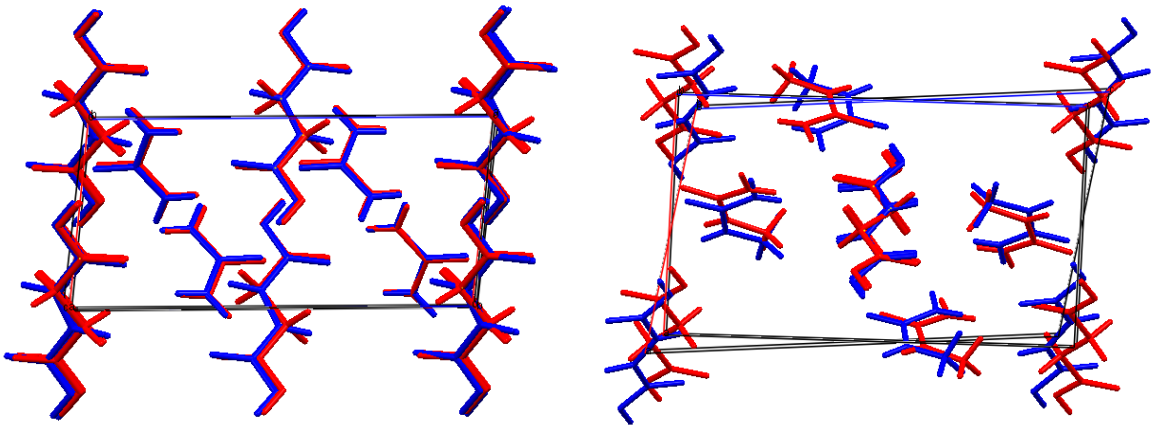

Figure 5.21 *Overlayed unit cells of the* ***US*** *(red) and* ***UF*** *(blue) complexes (left) and the* ***MUS*** *(red) and* ***MUF*** *(blue) complexes (right) looking along the b-axes from the 100 K X-ray structures.*

The fact that the **US** and **UF** complexes pack in the same way and are isostructural is not unexpected, given that the only difference between the two is the saturation of the C-C bond at the centre of the acid molecule (**Figure 5.21**, left). In the **US** complex, where the C-C bond of the acid molecule is saturated, the additional hydrogen atoms on the alkyl chain cause the distance to the chain of the same orientation in the next layer to increase at lower temperatures when compared to **UF**, while at higher temperatures the difference is much smaller (~3.25 and ~3.32 Å in **US**, ~2.99 and ~3.29 Å in **UF** from the 100 and 300 K X-ray data, respectively); this also contributes towards a larger cell volume for **US** compared with that of **UF** at all temperatures. Other contributions to the difference in volume are made from the shorter "U-A-U" unit in **UF**, arising from the C=C bond, and also from the hydrogen bonds in the homo- and heterodimers which are longer in **US** so

molecules and chains have a slightly larger separation from each other contributing to the increase in volume.

A similar observation is made in the structures of the **MUS** and **MUF** complexes (again the only difference is the saturation of the C-C bond) where the layer separation is ~3.43 and ~3.51 Å in **MUS** and ~3.30 and ~3.42 Å in **MUF** from the 100 and 300 K X-ray structures, respectively, (**Table 5.8**) and the similarity of the two structures may be expected (**Figure 5.21**, right). The majority of hydrogen bonds are longer in **MUS**, with the exception of the N-H···O hydrogen bond linking the amide···amide dimers, contributing again to an increase in volume. Again the saturated C-C bond in **MUS** leads to longer "MU-A-MU" units which also contribute to the difference in volume.

The addition of a methyl group to the urea molecule in the *anti* conformation in the **MUS** and **MUF** complexes does not perturb the one-dimensional "U-A-U" zigzag chains and the structures are very similar to those of **US** and **UF**, with the amide···amide and acid···amide homo- and heterodimers still present. The addition of a methyl group to the urea moiety has the effect of increasing the separation of chains in different orientations by replacing an N-H···O hydrogen bond with a weaker C-H···O hydrogen bond. The methyl groups point approximately along the *c*-axis which accounts for the large increase in this unit cell parameter between complexes **US**/**UF** and **MUS**/**MUF** (**Table 5.8**).

The similarity in the crystal packing of the **DMUS** complex with that of the **US**/**UF**/**MUS**/**MUF** complexes is unexpected. The addition of the two methyl groups to a nitrogen atom in the urea moiety means that it is impossible to form an amide···amide homodimer of the type found in **US**/**UF**/**MUS**/**MUF** in the presence of the acid···amide heterodimer (predicted to be one of the most stable hydrogen bonded motifs in these types of complex from computational studies).[173] Replacing the N-H···O hydrogen bond of the amide···amide dimer in the **US**/**UF**/**MUS**/**MUF** complexes with two longer, weaker and equivalent C-H···O hydrogen bonds causes a shift in the relative positions of neighbouring "U-A-U" units, though the interactions between chains in different orientations remain similar to those in **MUS** and **MUF**. The methyl groups again point approximately along the *c*-axis, accounting for the increase in this lattice parameter when compared with the **MUS** and **MUF** complexes (**Table 5.8**). The formation of chains similar to those of the **US**/**UF**/**MUS**/**MUF** complexes through different interactions indicates the remarkable stability of this packing motif even when the possibility of linking the urea moieties through an N-H···O hydrogen bond is removed.

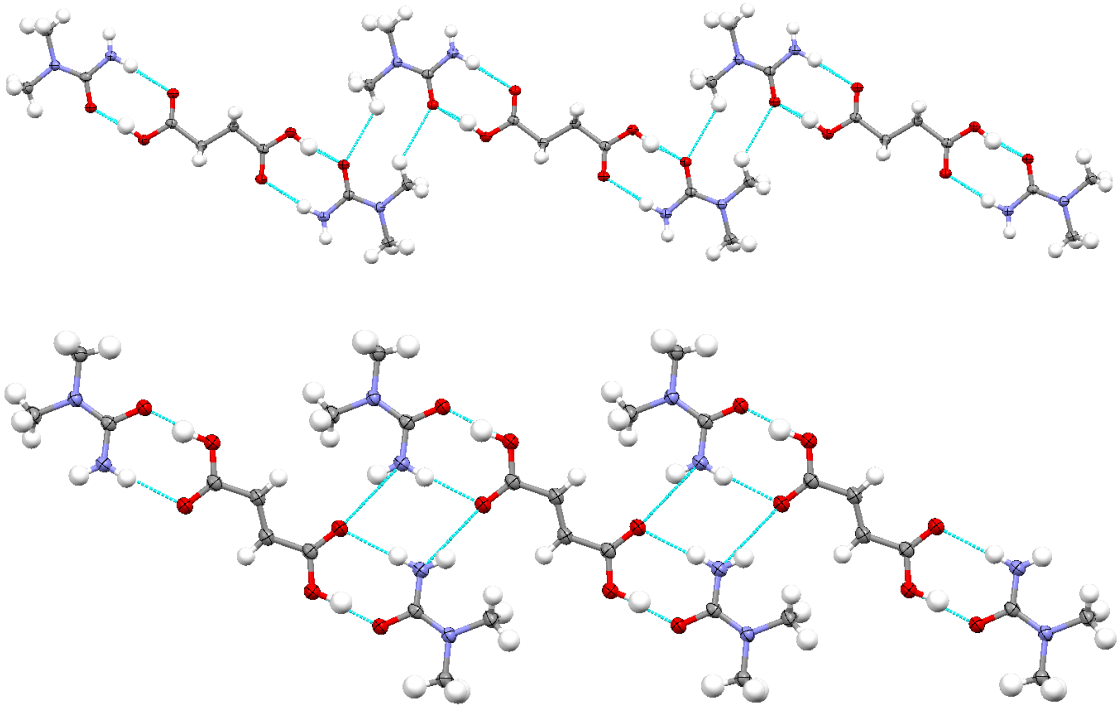

Figure 5.22 *One dimensional chains of "DMU-A-DMU" units in the N,N-dimethylurea succinic acid (top) and N,N-dimethylurea fumaric acid (bottom) at 100 K (X-ray).*

It might be expected that the **DMUS** and **DMUF** complexes would display a similar packing motif to one another, but they do not (**Figure 5.22**). In the **DMUF** complex chains are formed through an $R_2^4(8)$ hydrogen bonded ring involving the amide and acid groups of two neighbouring molecular units, in which the acid oxygen atoms are involved in *DDHHA* bifurcated hydrogen bonds to two amide hydrogens from different *N*,*N*-dimethylurea moieties. These interactions between the "DMU-A-DMU" units to form chains are stronger than those observed in **DMUS**. However, the interactions between the neighbouring chains in different orientations are weaker (consisting only of C-H···O hydrogen bonds) than in **DMUS**. The structure of **DMUF** does still have some similarities with those of **US**/**UF**/**MUS**/**MUF**/**DMUS** in that there are two possible orientations of chains tilted at similar angles to each other with chains in the same orientation stacked to form layers.

The structure of **MUOX** is altogether different from the others presented here. Oxalic acid has a shorter alkyl chain than both fumaric and succinic acid, but should still be able to pack in a similar manner to the other structures; this has already been observed in a complex of *N*,*N*'-dimethylurea and oxalic acid which contained two orientations of "DMU-A-DMU" units with those in the same orientation stacked on top of one another (see **Section 4.2**) as in **US**/**UF**/**MUS**/**MUF**/**DMUS**. However, in the case of **MUOX** a layered

structure forms. This type of packing is not unprecedented for this type of complex as layered structures of *N*,*N*-dimethylurea oxalic acid (see **Section 4.2**) and urea succinic acid[105] have previously been observed.

The one constant feature amongst all of the structures is the presence of the acid···amide heterodimer motif. The strength of this motif in directing the structure is shown by the fact that all of these complexes crystallise in a 2:1 (U:A) ratio with a repeating "U-A-U" motif present in each structure, consistent with the occurrence of one of these motifs at each end of the dicarboxylic acid molecules and which may have been predicted as a likely outcome in these complexes. The complexes studied here have confirmed this, and shown that modification of the urea moieties involved in these complexes by the addition of methyl groups removes the "competing" amide···amide homodimer preferentially over the acid···amide dimer in structures **MUOX**/**DMUS**/**DMUF**, where it is not possible to maintain both at the same time. This once again shows the preference for hetero- over homodimers in multi-component complexes where the strongest proton donor should hydrogen bond to the strongest acceptor, and reinforces these as a strong structure-directing motif.[37] Cases where only homodimers are preferentially formed are rare, although one example is the complex of 4-dimethylaminobenzoic acid and 3,5-dinitrobenzoic acid,[16,76] discussed in **Chapter 6**, where homodimers form due to steric reasons.

5.6 Short Strong Hydrogen Bonds in the Dicarboxylic Acid Complexes

All of the complexes presented contain O-H···O SSHBs between the acid hydroxyl groups and urea carbonyl oxygens, with lengths ranging from 2.45 - 2.55 Å (depending on the complex and temperature of structural determination, **Tables 5.9** - **5.11**). Proton migration (see **Chapter 4**) has been observed within SSHBs such as these and the potential presence of any migration within the set of dicarboxylic acid complexes was also investigated. Whilst none of these complexes show particular evidence of proton migration from the X-ray determinations, the only way to confirm this definitively is through analysis of variable temperature neutron diffraction data. If there is a boundary length for the SSHB below which migration may occur, a possibility discussed elsewhere in this work (**Chapter 4**), it is important to confirm that migration is not present in complexes where the hydrogen bonds are longer than the suggested boundary for migration. For this reason variable temperature neutron diffraction data were collected on VIVALDI for the **US**, **UF** (collected on SXD), **MUS**, **DMUS** and **DMUF** complexes (**Figure 5.24**). Neutron data were only collected at 20 and 50 K for **DMUS** due to technical difficulties encountered with the instrument during the data collection. The X-ray and neutron

determined bond lengths for the SSHBs are in good agreement with one another, with the expected shorter O-H distances observed in the X-ray data due to the technique visualising the bonding electron density as opposed to the atomic nuclei. The one exception to the agreement between the X-ray and neutron determinations is the case of the structure **DMUF**, where not all heavy atom positions agree with one another; this is discussed below.

Table 5.9 *Lengths of the short, strong O-H···O hydrogen bond in the three molecule "U-A-U" units of the complexes of urea with succinic and fumaric acid from the X-ray and neutron data.*

Complex	T/K	r(O-H) / Å		r(H···O) / Å		r(O-H···O) / Å	
		X-ray	Neutron	X-ray	Neutron	X-ray	Neutron
US	**100**	0.99(2)	1.041(3)	1.54(2)	1.484(3)	2.5149(10)	2.512(2)
	200	0.99(2)	1.050(4)	1.54(2)	1.481(4)	2.5211(11)	2.520(2)
	300	1.02(3)	1.039(5)	1.52(3)	1.500(4)	2.5298(15)	2.527(3)
UF	**30**	-	1.072(2)	-	1.437(2)	-	2.4983(14)
	100	1.01(2)	1.067(3)	1.49(2)	1.438(2)	2.496(2)	2.494(2)
	200	1.03(2)	1.065(3)	1.48(2)	1.443(3)	2.495(2)	2.498(2)
	300	0.99(3)	1.063(5)	1.52(3)	1.448(5)	2.498(2)	2.501(3)

Table 5.10 *Lengths of the short, strong O-H···O hydrogen bond in the three molecule "MU-A-MU" units of the complexes of N-methylurea with succinic, fumaric and oxalic acid from the X-ray and neutron data.*

Complex	T/K	r(O-H) / Å		r(H···O) / Å		r(O-H···O) / Å	
		X-ray	Neutron	X-ray	Neutron	X-ray	Neutron
MUS	**20**	-	1.034(2)	-	1.513(2)	-	2.536(2)
	100	0.92(2)	1.030(2)	1.62(2)	1.521(3)	2.5340(11)	2.540(2)
	200	0.93(3)	1.038(4)	1.64(3)	1.519(4)	2.5488(12)	2.546(3)
	300	0.98(4)	1.019(6)	1.59(4)	1.531(5)	2.553(2)	2.540(4)
MUF	**100**	1.02(2)	-	1.53(2)	-	2.5291(12)	-
	200	1.04(2)	-	1.52(2)	-	2.5333(14)	-
	300	1.07(3)	-	1.48(3)	-	2.536(2)	-
MUOX	**200**	1.06(3)	-	1.43(3)	-	2.458(2)	-
	300	1.03(3)	-	1.45(3)	-	2.461(2)	-

Table 5.11 *Lengths of the short, strong O-H···O hydrogen bond in the three molecule "DMU-A-DMU" units of the complexes of N,N-dimethylurea with succinic and fumaric acid from the X-ray and neutron data.*

Complex	T/K	r(O-H) / Å		r(H···O) / Å		r(O-H···O) / Å	
		X-ray	Neutron	X-ray	Neutron	X-ray	Neutron
DMUS	**20**	-	1.031(2)	-	1.491(2)	-	2.513(2)
	50	-	1.036(2)	-	1.494(2)	-	2.521(2)
	100	0.94(2)	-	1.60(2)	-	2.5249(11)	-
	200	0.95(2)	-	1.58(2)	-	2.5174(12)	-
	300	0.97(3)	-	1.56(3)	-	2.5234(15)	-
DMUF	**30**	-	1.057(3)	-	1.446(3)	-	2.490(2)
	100	1.01(2)	1.053(5)	1.50(2)	1.456(5)	2.5000(15)	2.496(3)
	200	1.01(2)	1.045(9)	1.50(2)	1.459(7)	2.4996(14)	2.492(5)
	250	-	1.018(14)	-	1.483(10)	-	2.489(7)
	300	1.08(4)	1.015(14)	1.45(4)	1.475(10)	2.501(2)	2.478(7)

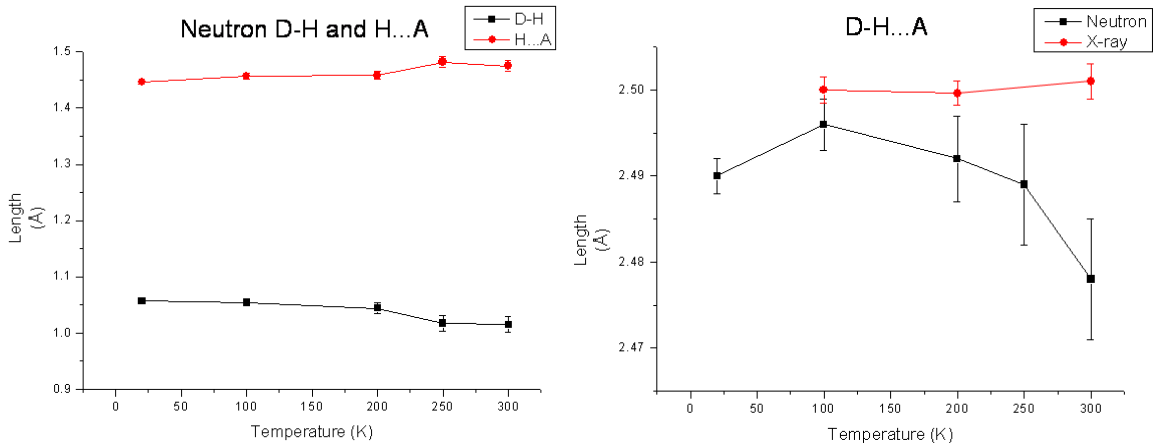

Figure 5.23 *The D-H and H···A lengths as a function of the temperature from the neutron data (left) and a comparison of the X-ray and neutron D-H···A lengths for the short, strong O-H···O hydrogen bond in the 2:1 complex of N,N-dimethylurea and fumaric acid.*

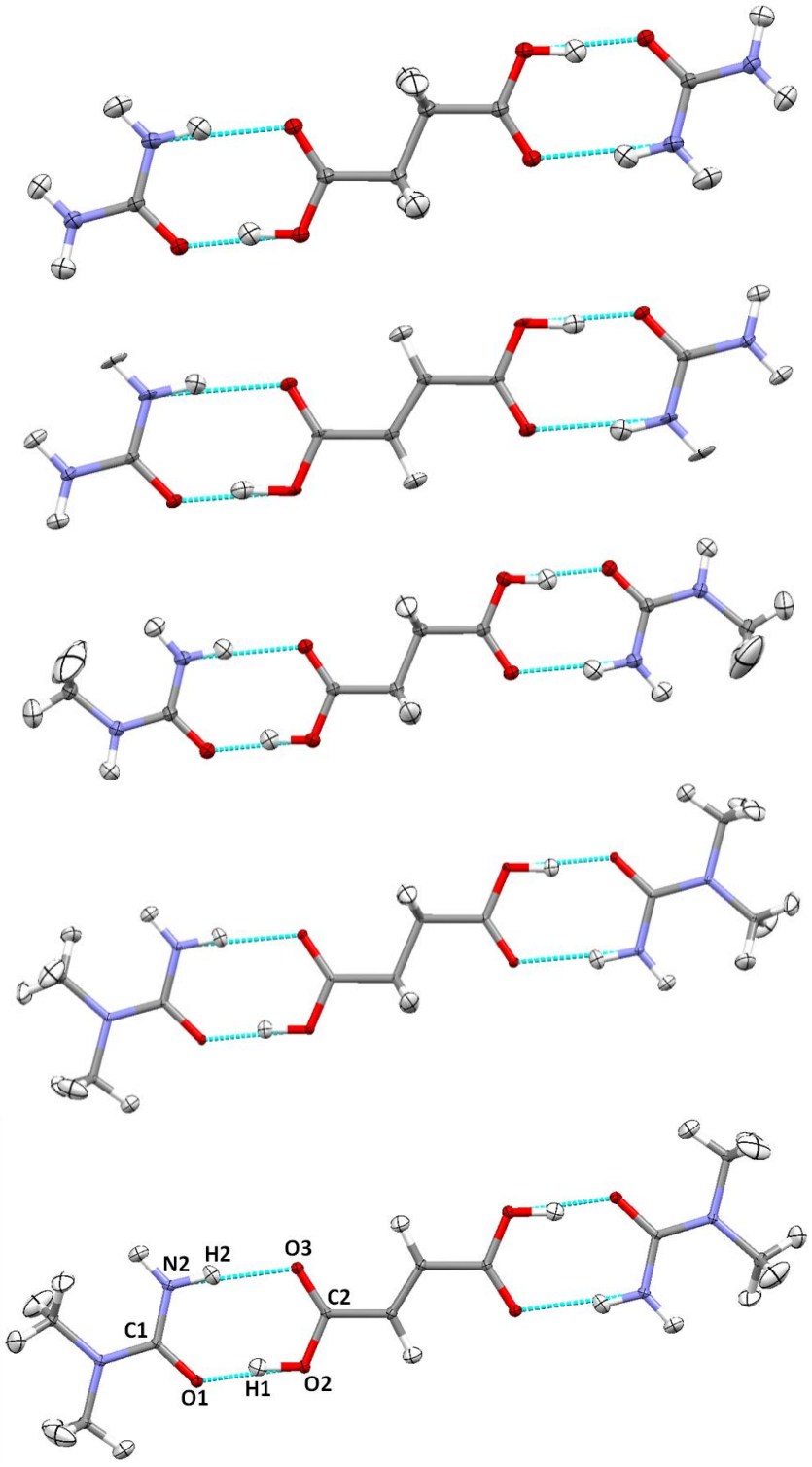

Figure 5.24 *The hydrogen bonded "U-A-U" units in the neutron structures of, from top to bottom:* ***US***, ***UF***, ***MUS***, ***DMUS*** *and* ***DMUF***. *All images are taken from the 100 K data with the exception of that for* ***DMUS*** *which is taken from the 20 K neutron structure.*

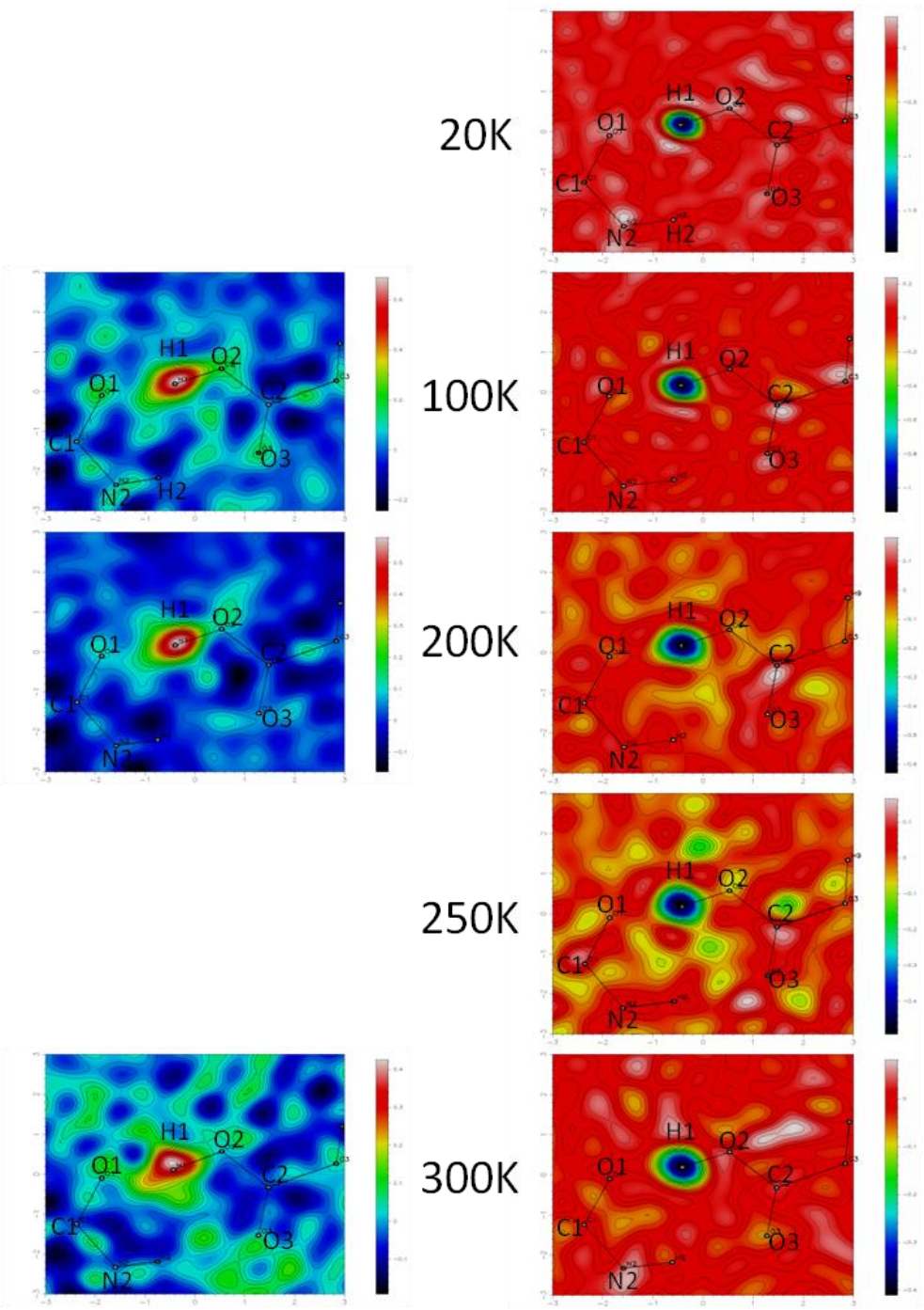

Figure 5.25 *Fourier difference maps showing the electron (left) and nuclear (right) density of the hydrogen atom in the short, strong hydrogen bond in the 2:1 complex of N,N-dimethylurea and fumaric acid. For labelling scheme see* ***Figure 5.24****.*

The only complex which appears, from the neutron data, to show significant temperature dependent migration of the proton in the SSHB is **DMUF** (**Tables 5.9** - **5.11**). Initial evidence of the possible presence of migration is given by the slight elongation of the electron density of the hydrogen atom visualised through Fourier difference maps

(**Figure 5.25**). From the neutron data, it appears that the proton migrates 0.042(14) Å towards the donor atom and 0.029(10) Å away from the acceptor atom, between 20 and 300 K, while the O···O distance decreases from 2.490(2) Å at 20 K to 2.478(7) Å at 300 K (**Table 5.11** and **Figure 5.23**, left). The migration is gradual until 200 K, while there is a significantly increased migration effect, of 0.027(13) Å towards the donor atom, between 200 and 250 K; between 250 and 300 K the proton position is essentially invariant. There is a note of caution here, however, with respect to a possible anomaly in the neutron data for this complex. The O···O distances in the X-ray and neutron data are not in agreement with each other at all temperatures (**Figure 5.23**, right). While from the X-ray data the O···O distance is invariant over the full temperature range, from the neutron data refinement this distance appears to decrease as the temperature is increased. While there is expected to be a difference in the hydrogen atom positions between X-ray and neutron data sets, the heavy atom positions should be in good agreement with each other. There is no obvious reason for this inconsistency in the data sets and this has an impact on the significance of the proton migration observed from the neutron data. While the migration between 200 and 250 K appears significant, the possibility that this is a consequence of the large disagreement between the X-ray and neutron data at 300 K cannot be ruled out. Further neutron data are required to corroborate this finding.

The other complexes, **US**/**UF**/**MUS**/**DMUS**, do not show significant migration of the proton in the SSHB when the temperature is varied. In **Chapter 4**, it was suggested that there may be a hydrogen bond distance below which migration would be expected to occur; currently migration has only been observed in O-H···O hydrogen bonds of less than 2.50 Å in length.[61-63] All but one of the SSHBs in the seven complexes presented here are ≥2.50 Å in length, with the exception being **MUOX** where the hydrogen bond distance is ~2.46 Å (**Table 5.10**). Unfortunately, it was not possible to grow crystals suitable for neutron diffraction for this complex, meaning that the definitive absence of migration could not be confirmed. However, one indicator of a migratory proton is that it is often centred within the SSHB. This is not the case from the X-ray determined structures of **MUOX** and it is probable that the proton in the SSHB in this complex also does not undergo migration as the temperature is varied. Following on from the observations in **Chapter 4**, it may be that ~2.50 Å is a plausible boundary for the hydrogen bond distance below which it may be possible to observe migration, though proton migration may is not present in all SSHBs <2.50 Å in length. Further variable temperatures studies of complexes containing short, strong O-H···O hydrogen bonds are needed to test further this postulate.

Another consideration which can potentially aid the design of systems which contain SSHBs is the difference in pK_a values of the acid and base. In **Chapter 4**, a possible correlation between ΔpK_a values and the amount of migration observed over a given temperature range was investigated, while how the ΔpK_a values affect the SSHB length was also investigated. In the limited number of examples studied, it was shown that complexes with the least negative ΔpK_a values displayed the most significant migration. Here the possibility that ΔpK_a values correlate with the SSHB length is investigated further, along with the possibility that this could be used as a tool to design complexes containing SSHBs and potentially proton migration.

Table 5.12 *ΔpK_a values and short, strong hydrogen bond distances from the 200 K X-ray data for the seven complexes presented in this chapter and the two dimethylurea oxalic acid complexes presented in* ***Chapter 4****.*

Complex	ΔpK_a	r(O-H···O) / Å
***N,N*-DMU-oxalic acid**	-1.56	2.4325(13)
MUOX	-1.57	2.458(2)
***N,N'*-DMU-oxalic acid**	-1.94	2.4507(10)
UF	-3.05	2.495(2)
DMUF	-3.33	2.4996(14)
MUF	-3.34	2.5333(14)
US	-4.14	2.5211(11)
DMUS	-4.42	2.5174(12)
MUS	-4.43	2.5488(12)

All complexes reported in **Table 5.12** have negative ΔpK_a values, indicating that neutral co-crystal formation should be expected, in agreement with the structures presented here. The least negative value occurs for the complex of *N*,*N*-dimethylurea with oxalic acid (see **Chapter 4**), which also shows the shortest O-H···O distance. As the ΔpK_a values become increasingly negative the general trend appears to be that the O-H···O distance increases. However, other factors, such as the crystal packing, can strongly influence the O-H···O distance while the difficulties in transferring pK_a values to the solid-state, and how appropriate they may be for complexes which do not display a 1:1 stoichiometry, should also be taken into consideration. These factors mean that the distance does not correlate exactly to the ΔpK_a value but that there is potential for ΔpK_a values to be used as a guide to forming complexes which may be more likely to contain a SSHB. In much the same

way, they could potentially be used to estimate the amount of migration that may be observed in a proton migration complex (see **Chapter 4**). It should be noted that the ΔpK_a value of -1.57 for **MUOX** is close to those of the proton migration complexes discussed in **Chapter 4**, though the migration complexes mostly contain a shorter hydrogen bond. This could further underline that differences in pK_a values can only be used as a guide and definitive trends cannot be predicted based solely on pK_a matching – the constituent molecules must be considered. It may also be possible that **MUOX** does in fact show migratory behaviour, however neutron data would be required to confirm this definitively.

5.7 Temperature Dependent Effects of the Crystal Packing

While none of the seven complexes appear to show any significant proton migration, they exhibit other interesting temperature dependent effects which can be related to the crystal packing. In **Section 4.3**, the complex *N,N'*-dimethylurea oxalic acid displayed unusual thermal expansion characteristics, leading to the contraction of one unit cell axis as the temperature was increased. The **US**/**UF**/**MUS**/**MUF**/**DMUS** complexes, which have nearly identical packing motifs, display the same effect on increasing temperature, which can be related to the way in which the complexes pack (**Table 5.13**); **MUOX** and **DMUF** have different packing motifs and do not display this thermal expansion property.

Table 5.13 *Unit cell parameters of selected complexes from the 100 and 300 K X-ray data with contracting unit cell axes displayed in bold.*

Complex – Temperature	***a* / Å**	***b* / Å**	***c* / Å**	***β* / °**	**V / Å^3**
US - 100 K	**5.7109(7)**	7.9698(11)	12.1580(15)	96.160(4)	550.17(3)
300 K	**5.6366(6)**	8.2568(10)	12.2790(13)	96.659(4)	567.61(3)
UF - 100 K	**5.764(2)**	7.640(2)	12.283(4)	96.901(11)	537.0(3)
300 K	**5.541(6)**	8.214(7)	12.427(12)	97.314(80	561.0(2)
MUS - 100 K	8.0244(12)	**5.7496(7)**	13.735(2)	91.246(5)	633.54(2)
300 K	8.5398(8)	**5.5798(4)**	13.8377(16)	92.291(4)	658.84(2)
MUF - 100 K	8.2188(10)	**5.6497(5)**	13.8382(13)	104.156(4)	630.63(7)
300 K	8.7741(14)	**5.4413(7)**	13.9303(19)	100.730(6)	653.44(8)
DMUS - 100 K	8.483(3)	5.5169(14)	**15.415(5)**	101.677(8)	706.49(13)
300 K	8.797(2)	5.6934(13)	**15.059(4)**	100.764(7)	740.96(11)

In general, as the temperature is increased, the unit cell volume will also increase due to the increased thermal motion of atoms and molecules within a material. In the solid-state, the expansion is often not uniform in all directions due to the alignment of molecules within the structure making expansion anisotropic – more favourable in certain directions – causing some axes or angles to increase at a different rate to others. In all of the complexes, the contraction of the unit cell axis is accompanied by an increase in the cell volume, so these complexes cannot be called negative thermal expansion materials.

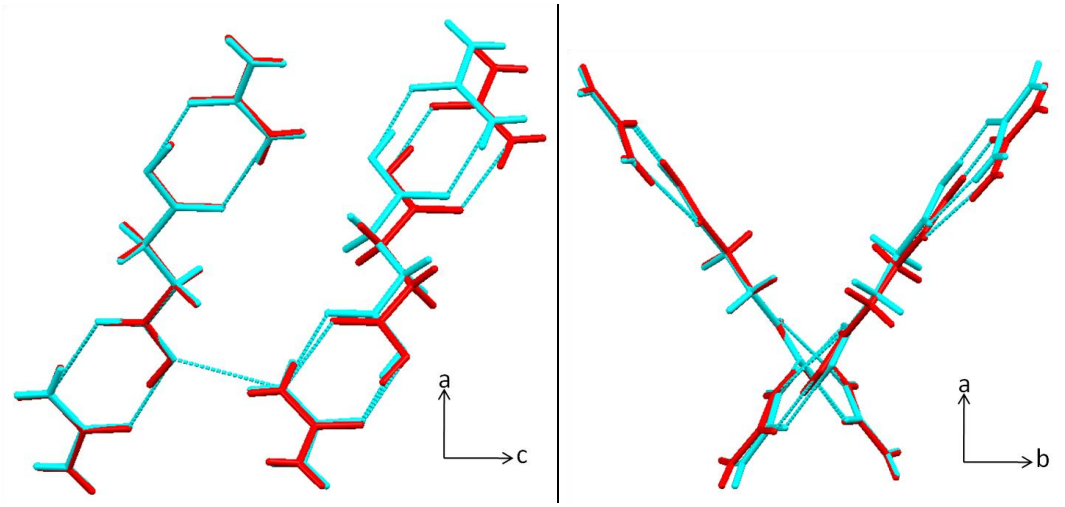

Figure 5.26 *A structural overlay showing a shift in the molecular units relative to the neighbouring units viewed along the b- (left) and c-axes (right) taken from the* ***US*** *X-ray data at 100 (cyan) and 300 K (red).*

The contraction of a single unit cell axis length can be rationalised by a shift in the hydrogen bonded molecular units as the temperature is increased (**Figure 5.26**). Several factors contribute to this and the net effect leads to the contraction of one unit cell axis. Increased thermal motion can have a pronounced effect on hydrogen bond distances as these are weaker and more flexible than covalent bonds and can increase slightly with temperature. This effect might be expected to be less pronounced for the short, strong O-H···O hydrogen bonds in these complexes and as these interactions are more covalent in nature. In the three molecule "U-A-U" unit of **US** the O-H···O distance increases from 2.515(1) to 2.530(2) Å and the N-H···O distance increases from 2.947(1) to 2.988(2) Å from the 100 and 300 K X-ray data. In **US**/**MUS**/**MUF**, both of these hydrogen bond distances in the "U-A-U" molecular unit increase, while **UF** shows only the N-H···O distance increasing, with the O-H···O distance being invariant with over the temperature range. In **DMUS**, both distances are invariant. The lateral hydrogen bonds from the

"U-A-U" three molecule unit to neighbouring chains increase in length with temperature in all of the complexes.

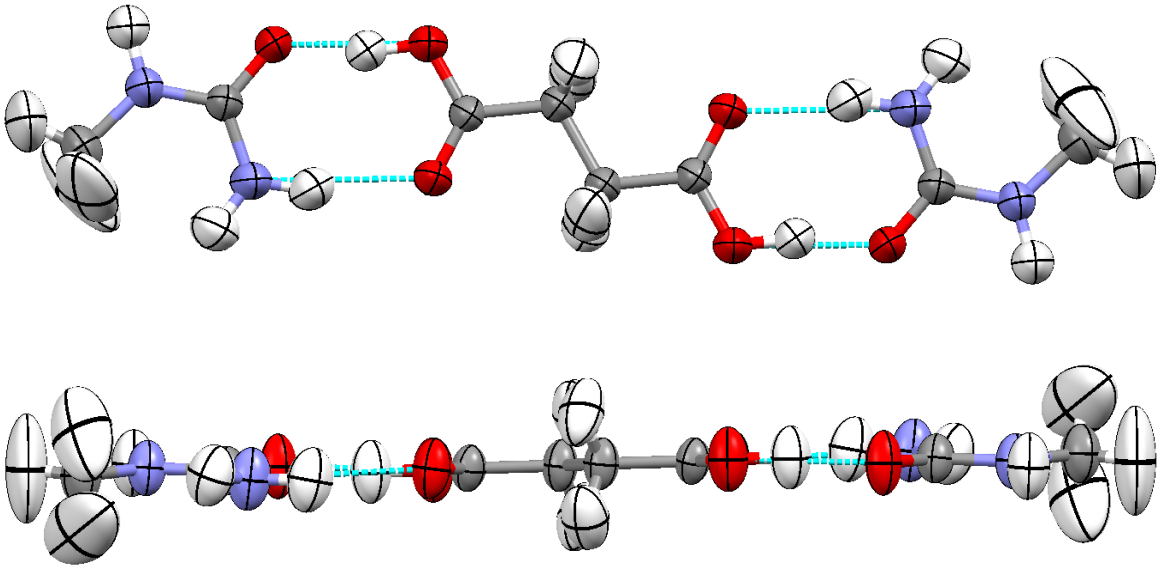

Figure 5.27 *A molecular unit viewed from above (top) and the side (bottom) showing the large anisotropic thermal parameters of the hydrogen atoms in the 300 K neutron structure of* ***MUS****.*

Increased thermal motion within the crystal structures at higher temperatures results in the atomic displacement parameters increasing in size; this is particularly the case for the hydrogen atoms (**Figure 5.27**). In **US**/**UF**/**MUS**, where neutron data is available at 300 K, the anisotropic displacement parameters of the hydrogen atoms can be refined and the direction of motion established. The hydrogen atoms with the largest displacement parameters, as might be expected, are those located on the alkyl chains of the fumaric and succinic acid molecules, which are not involved in any hydrogen bonds, and those located on methyl groups of the substituted ureas in **MUS** where there is significant libration of the methyl groups at higher temperatures.[171] Hydrogen atoms located on the amide groups of the ureas (and the nitrogen atoms themselves) also show significant motion out of the plane of the molecular unit due to a 'wagging' of the amide group. This occurs in part due to the amide group only being involved in moderate to weak hydrogen bonds and the thermal displacement parameters for these hydrogen atoms are larger than those involved in the much stronger O-H···O hydrogen bonds. The motion of these atoms out of the plane of the molecular unit can also be related to a slight increase in the distance between layers of the one-dimensional chains in all of **US**/**UF**/**MUS**/**MUF**/**DMUS**;

for example in **US** the layer separation increases from ~3.23 to ~3.30 Å in the 100 and 300 K X-ray structures. The combination of these factors has the net effect of a contraction of one unit cell axis. This effect is entirely dependent on the crystal packing and the changes that occur in the weak interactions on varying the temperature.

5.8 Conclusions

Seven complexes have been studied using variable temperature X-ray diffraction while variable temperature neutron data have also been collected on four of the seven complexes. All seven complexes have a 2:1 (urea:acid) stoichiometry and contain a common motif of a three molecule hydrogen bonded "U-A-U" unit, consistent with the observations reported in **Chapter 4** in the cases of the dimethylurea-oxalic acid complexes, and also the motifs observed in urea-dicarboxylic acid complexes reported by Alhalaweh *et al.*[105] **US**/**UF**/**MUS**/**MUF**/**DMUS** all display very similar unit cell parameters and crystal packing motifs with one-dimensional zigzag chains in two orientations where chains in the same orientation are stacked on top of one another. **DMUF** forms a different kind of hydrogen bonded chain though still has two possible chain orientations and stacking of chains in the same orientation while **MUOX** has a different packing motif and forms a layered structure.

The similarity of the packing in **US**/**UF**/**MUS**/**MUF**/**DMUS** shows the robustness of the acid···amide heterodimer which is formed preferentially over the amide···amide homodimer when methyl groups are added to the urea moiety in **MUS**/**MUF**/**DMUS**. The similarity of the packing motif in **DMUS** with those of **US**/**UF**/**MUS**/**MUF** was unexpected as the presence of two methyl groups on the urea means that an amide···amide dimer cannot form. However, a one-dimensional chain is formed through two equivalent C-H···O interactions between the methyl groups and carbonyl oxygens of the *N,N*-dimethylurea molecules.

Based on the structures presented in this chapter and in **Chapter 4**, there appear to be two packing motifs in these types of 2:1 complexes which occur more often than others. The most common is that displayed in **US**/**UF**/**MUS**/**MUF**/**DMUS**. Layered structures also form, as evidenced by **MUOX**, one of the polymorphs of urea succinic acid[105] and the *N*,*N*-dimethylurea oxalic acid complex presented in **Section 4.2**. **DMUF** appears somewhat unusual and provides a third possible packing motif which is similar to, but distinct from, that of **US**/**UF**/**MUS**/**MUF**/**DMUS**. There is no obvious reason why the packing in this complex is different to that of **DMUS** though it may be possible to find another polymorphic form that would pack in the same way by utilising different

crystallisation conditions. With the exception of **US**, all of these complexes were crystallised from solutions containing ethanol at ambient conditions. It may therefore be expected that the same packing motifs would be obtained for 2:1 complexes containing similar molecules where the acid or urea moieties are different. This element of predictability in the formation of crystal structures is important when conducting crystal engineering studies and knowledge of common hydrogen bond and packing motifs can potentially be exploited to design materials with desirable properties in future studies.

The packing motif in the **US**/**UF**/**MUS**/**MUF**/**DMUS** complexes is found to lead to unusual temperature dependent behaviour where one unit cell axis contracted on increasing the temperature. The contraction can be rationalised through a shift in the positions of adjacent molecular chains related to the increased thermal motion of the molecules and changes in the hydrogen bonds and other weaker interactions as the temperature was varied.

Neutron data were collected on four of the complexes to investigate the possible presence of proton migration in the short, strong O-H···O hydrogen bonds which are present in all of the complexes. Only **DMUF** shows any significant migration of the proton as the temperature was varied with a migration of 0.042(14) Å towards the donor atom between 20 and 300 K. However, due to an unexplained disagreement between the heavy atom positions in the X-ray and neutron data, it cannot be confirmed whether migration of the proton is really occurring or if it is an artefact of poor quality data or problems in the data reduction.

None of the other complexes show any significant movement of the proton in the SSHBs as the temperature is varied. Building on the results from **Chapter 4**, a hydrogen bond distance of ~2.50 Å was suggested below which it is possible for proton migration to occur, though further variable temperature studies of complexes containing short strong hydrogen bonds are required to test this hypothesis.

ΔpK_a values can also be examined to see if any correlation can be made with the length of the short strong hydrogen bond with a view to designing systems containing such interactions in the future. A general trend is found whereby the less negative the ΔpK_a value, the shorter the hydrogen bond formed, though this is not true in all cases. Other factors such as crystal packing have an effect on the short strong hydrogen bond distance while transferring pK_a values into the solid-state adds further complications; however the values could still potentially be used as a guide when designing crystallisation experiments.

As in **Chapter 4**, the neutron data collected on these complexes illustrate one of the potential high throughput applications of the SXD and VIVALDI Laue diffractometers. In this case, variable temperature neutron data has been used to follow the evolution of the hydrogen atom behaviour with temperature; searching for potential proton migration and also analysing the thermal behaviour of the hydrogen atoms and the effect this has on the properties of the materials.

Chapter 6

6. Proton Disorder

While proton migration can occur in short strong hydrogen bonds (see **Chapter 4**), in moderate strength hydrogen bonds temperature dependent proton disorder is a more likely effect. Proton disorder can have a significant effect on a range of properties, and there are some materials whose hydrogen bonding arrangements appear to be well disposed to allow this phenomenon to be present. In this chapter a range of such materials will be discussed, with particular reference to their proton disorder characteristics.

As has been discussed earlier in this work, when studying those properties of materials which are dependent on hydrogen atom positions, neutron diffraction studies can play a key role. In the case of temperature dependent proton disorder, neutron diffraction enables the disorder to be clearly visualised through Fourier difference maps and also allows the occupancy values to be reliably determined at each temperature in the structure refinement procedure. In addition to this, high quality X-ray diffraction data also has a significant role to play in examining these materials; such data can be used to indicate whether disorder may be present (particularly through Fourier map visualisation) and also, in favourable cases, to allow occupancy values to be obtained, though these will have a large inherent error associated with them due to the weak scattering associated with disordered hydrogen atoms. The combination of X-ray and neutron data in these studies is particularly powerful, producing the clearest picture of all, by providing information on the electronic bonding density (from X-ray) and also the locations of the hydrogen atom nuclei (from neutron) so that the disorder can be quantified accurately.

To study the nature of any proton disorder in detail, variable temperature data is essential to establish the subtle characteristics of the system, including differences in the energetics of the two possible proton sites. This means that several determinations of each structure must be made, to allow the evolution of the important parameters to be followed. The neutron studies conducted on the systems in this chapter show the potential for high throughput structural determinations; many temperatures (six or seven) have been studied in each experiment over a relatively short period of time.

Benzoic acid dimers have been identified as systems in which temperature dependent proton disorder can be found, this occurring within the double hydrogen bonded dimer system, with an $R_2^2(8)$ hydrogen bond motif.[77,80] However, disorder is by no means present in all benzoic acid homodimers. 4-Dimethylaminobenzoic acid (4-DABA;

Figure 5.1)[76,174] is an example of a molecule which has previously been identified as forming dimers exhibiting proton disorder both in its native forms[76,174] and in molecular complexes.[76,175]

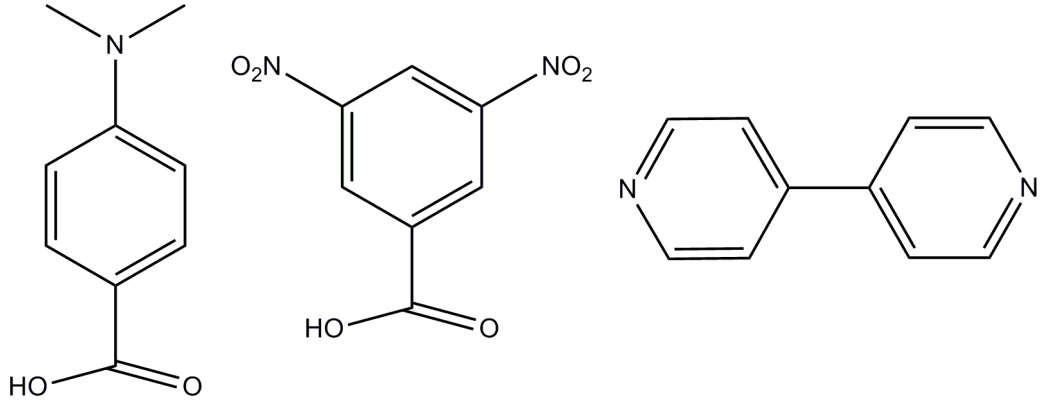

Figure 6.1 *Diagrams of 4-dimethylaminobenzoic acid (left), 3,5-dinitrobenzoic acid (centre) and 4,4'-bipyridine (right).*

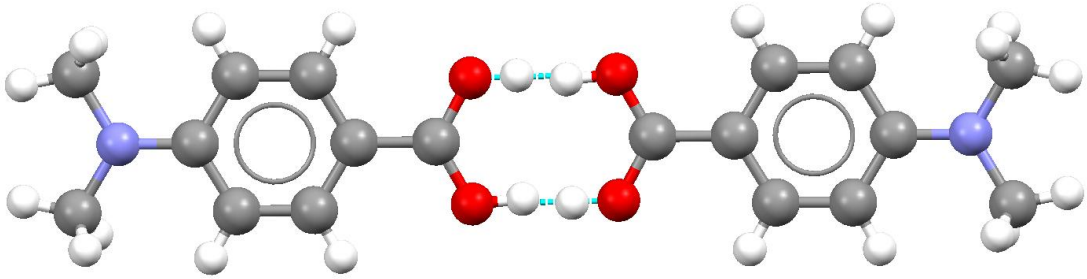

Figure 6.2 *A disordered dimer of 4-DABA in form III of the native structure.*[174]

There are three known polymorphs of 4-DABA, all contain an $R_2^2(8)$ hydrogen bonded dimer motif with an inversion centre at the centre of the ring and two of the three polymorphs (forms I and III) are reported to contain proton disorder from determinations using single crystal X-ray diffraction data. Form III has only been studied at 173 K; the asymmetric unit contains two independent 4-DABA molecules, which each form different hydrogen bonded dimers with a symmetry equivalent molecule, showing disordered hydrogen atom sites with occupancies of 57:43 and 55:45 for the two possible hydrogen atom sites within the symmetric dimer units (**Figure 6.2**).[174] As only one structural determination has been made, the temperature dependence of the disorder is not established. Form I has been studied at 100, 200 and 300 K, the data suggesting the presence of temperature dependent disorder with the occupancy factors for the two hydrogen atom sites changing from 90:10 at 100 K to 62:32 at 300 K.[76] Form II has been studied at only one temperature, 173 K, and does not show any evidence of disorder; it is

possible that disorder may manifest itself at higher temperatures though this has not been investigated.[174]

There are seven examples in which 4-DABA has been complexed with other materials. Three of these complexes do not contain $R_2^2(8)$ hydrogen bonded benzoic acid dimers and the type of double-well hydrogen bonds necessary for proton disorder are not observed. These complexes include a binary complex with 3,5-dinitrobenzamide,[176] a ternary complex with isonicotinamide and 3,5-dinitrobenzoic acid (3,5-DNBA)[177] and a binary complex with 2-amino-4-(6-methoxy-3-pyridyl)-6-methylpyrimidine.[178] The structures of these complexes were determined by X-ray diffraction at a single temperature only.

When different benzoic acids are complexed together the most common outcome is the formation of heterodimers. These dimers are stronger than homodimers due to the different proton donating and accepting abilities of the two acids, in general the strongest donor will preferentially form a hydrogen bond with the strongest acceptor.[37] There are two examples of molecular complexes of 4-DABA which display a heterodimer motif, both of which have been studied using X-ray diffraction at a single temperature. The first is a binary complex of 4-DABA with 3,5-dinitrocinnamic acid where no proton disorder is observed.[16] The second is a binary complex with 4-nitrobenzoic acid where proton disorder is observed at room temperature (RT).[179] The amount of disorder present is not stated in the literature and due to the structure only being determined at RT, the temperature dependence of any disorder is not known.

The final two complexes reported contain 4-DABA homodimers and the structures have been determined at multiple temperatures. A ternary complex containing 4-DABA, 4.4'-bipyridine (BIPY) and 3,5-DNBA in a 2:1:2 ratio[175] shows a BIPY molecule hydrogen bonded to two 3,5-DNBA molecules while the 4-DABA forms homodimers. Data were collected using single crystal X-ray diffraction at 100, 200 and 300 K and by single crystal neutron diffraction at 40, 100, 200 and 300 K. Temperature dependent proton disorder was observed from both the X-ray and neutron data and the occupancies of the two proton sites reflecting the two possible configurations refined from the neutron data. The ratio of these was found to range from 100:0 at 40 K to 60:40 at 200 K; at 300 K it was no longer possible to resolve the two proton positions due to increased thermal motion and background noise in Fourier difference maps, but the shape of the troughs in the map in the region of the proton positions and the refined position for the hydrogen atom implied approximately 50:50 disorder.

The other complex known is a binary complex of 4-DABA and 3,5-DNBA.[16,76] This is unusual in that it contains homodimers of both benzoic acids which are formed preferentially over the more common heterodimers. Sharma *et al.*[16] reported that this occurs due to steric effects blocking the formation of C-H···O interactions between the ring protons and the electronegative oxygen atoms in the structure. In this example, the weak C-H···O and π-π interactions are maximised through the formation of homodimers. X-ray data were collected at 100, 160, 175, 190, 200, 210, 225, 250 and 300 K and it was reported that proton disorder was present in the 3,5-DNBA dimers but not the 4-DABA dimers.[76] The disorder was tentatively characterised by direct imaging of the electron density through Fourier difference maps. The occupancies of the hydrogen atom sites in the 3,5-DNBA dimers varied from 66:34 at 100 K to 47:53 at 300 K showing the temperature dependent nature of the disorder. In view of this, in this work a variable temperature neutron study was conducted on this complex to quantify the disorder more accurately, with the results presented here.

To probe further the nature of temperature dependent proton disorder in 3,5-DNBA dimers, variable temperature X-ray and neutron studies were also conducted in this work on the two polymorphic forms of 3,5-DNBA. Hydrogen atom disorder has previously been identified in the $P2_1/c$ polymorph although this has only been modelled at a single temperature.[180] The structure of the $C2/c$ polymorph is known,[181,182,183] but no proton disorder was reported or modelled. However, the O-H distance for the hydrogen atom in the dimer is longer than would be expected for a conventional carboxylic acid dimer motif showing no disorder, and this lengthened covalent bond potentially indicates the presence of disorder. A variable temperature study of both polymorphs was thus undertaken; X-ray data were collected for both polymorphs and neutron data for the $C2/c$ polymorph.

6.1 Experimental

2:2 Complex of 4-DABA and 3,5-DNBA

Crystals of the 2:2 complex of 4-DABA and 3,5-DNBA were grown by slow evaporation from ethanol. Large block shaped crystals of an orange colour were obtained. Neutron data were collected on VIVALDI at the ILL at 30, 100, 150, 200, 250 and 300 K. The neutron structures were refined using SHELXL-97[138] within WinGX[140] with starting atomic coordinates taken from the X-ray structures.[76] Refined parameters are given in **Table 6.1**. X-ray data presented here were taken from structures with CSD codes GAUTAM01, GAUTAM02, GAUTAM03, GAUTAM04, GAUTAM05, GAUTAM06, GAUTAM07, GAUTAM08 and GAUTAM09.[76]

3,5-DNBA ($P2_1/c$ polymorph)

Crystals of the $P2_1/c$ polymorph of 3,5-DNBA were grown by slow evaporation from acetonitrile at 30 °C. Needle shaped crystals of a pale yellow colour were obtained. Single crystal X-ray diffraction data were collected on a Rigaku R-AXIS / RAPID diffractometer at 100, 200 and 300 K. Refined parameters are given in **Table 6.2**. The structure was solved using SHELXS-97[138] and refined with SHELXL-97[138] within the WinGX package.[140]

3,5-DNBA ($C2/c$ polymorph)

Crystals of the $C2/c$ polymorph of 3,5-DNBA were grown by slow evaporation from ethanol at RT. Large block shaped crystals of a pale yellow colour were obtained. Single crystal X-ray diffraction data were collected on a Rigaku R-AXIS / RAPID diffractometer at 100, 200 and 300 K. The structure was solved using SHELXS-97[138] and refined with SHELXL-97[138] within the WinGX package.[140] Refined parameters are given in **Table 6.3**. Neutron data were collected on VIVALDI at the ILL at 20, 50, 100, 150, 200, 250 and 300 K. The neutron structures were refined using SHELXL-97[138] taking the X-ray atomic coordinates as a starting position.

Table 6.1 *Neutron data collection and refinement information for the 2:2 complex of 4-DABA and 3,5-DNBA.*[a]

Compound	**2:2 4-DABA : 3,5-DNBA**					
Diffractometer	VIVALDI	VIVALDI	VIVALDI	VIVALDI	VIVALDI	VIVALDI
Formula	$C_{16}H_{15}N_3O_8$	$C_{16}H_{15}N_3O_8$	$C_{16}H_{15}N_3O_8$	$C_{16}H_{15}N_3O_8$	$C_{16}H_{15}N_3O_8$	$C_{16}H_{15}N_3O_8$
Molecular weight (g mol^{-1})	377.31	377.31	377.31	377.31	377.31	377.31
T (K)	30	100	150	200	250	300
Space group	$P2_1/c$	$P2_1/c$	$P2_1/c$	$P2_1/c$	$P2_1/c$	$P2_1/c$
***a* (Å)**	14.370	14.426	14.473	14.460	14.457	14.469
***b* (Å)**	6.250	6.808	6.872	6.900	6.943	6.995
***c* (Å)**	16.670	16.712	16.755	16.821	16.878	16.938
***β* (°)**	99.413	99.429	99.721	99.628	99.648	99.715
Volume (Å^3)	1477.0	1619.1	1642.5	1654.7	1670.2	1689.7
Z	4	4	4	4	4	4
Reflections collected	14797	14748	13051	12589	19936	11626
Independent	3262	3111	2721	2723	2135	1651
Observed > 2σ(I)	2235	2022	1700	1658	1410	1001
Parameters	380	378	378	378	378	379
Restraints	1	1	1	1	1	1
GooF	1.26	1.12	1.08	1.11	1.35	1.14
R_1 (observed)	0.0668	0.0545	0.0537	0.0583	0.0530	0.0547
R_1 (all)	0.1138	0.1067	0.1132	0.1204	0.1044	0.1114
wR_2 (all)	0.1416	0.1152	0.1157	0.1181	0.1037	0.0995
Δρ (max, min) / fm/Å^3	3.15, -3.36	1.00, -1.20	0.62, -0.61	0.57, -0.56	0.49, -0.50	0.36, -0.34

[a] *It is not possible to accurately determine unit cell parameters from a Laue experiment at a continuous neutron source so no errors are listed. X-ray determined values are used where available.*

Table 6.2 *X-ray data collection and refinement information for the $P2_1/c$ polymorph of 3,5-DNBA.*

Compound	**3,5-DNBA ($P2_1/c$)**		
Diffractometer	Rigaku R-AXIS RAPID	Rigaku R-AXIS RAPID	Rigaku R-AXIS RAPID
Formula	$C_7H_4N_2O_6$	$C_7H_4N_2O_6$	$C_7H_4N_2O_6$
Molecular weight (g mol^{-1})	212.12	212.12	212.12
T (K)	100	200	300
Space group	$P2_1/c$	$P2_1/c$	$P2_1/c$
***a* (Å)**	9.7845(15)	9.9026(10)	10.0486(12)
***b* (Å)**	8.9435(13)	8.9085(8)	8.8884(9)
***c* (Å)**	9.4500(12)	9.4714(7)	9.5167(8)
***β* (°)**	97.577(5)	96.533(3)	95.634(3)
Volume (Å^3)	819.7(2)	830.12(13)	845.89(15)
Z	4	4	4
Reflections collected	10134	10726	10822
Independent	1864	1886	1918
Observed > 2σ(I)	1152	1165	1246
R_{int}	0.048	0.044	0.048
Parameters	152	152	157
GooF	1.15	1.12	1.05
R_1 (observed)	0.0442	0.0423	0.0516
R_1 (all)	0.0881	0.0794	0.0893
wR_2 (all)	0.1423	0.1263	0.1282
Δρ (max, min) / e$^-$/Å^3	0.39, -0.39	0.23, -0.27	0.16, -0.19

Table 6.3 *X-ray and neutron data collection and refinement information for the C2/c polymorph of 3,5-DNBA.*[a]

Compound	**3,5-DNBA (*C2/c*)**									
Diffractometer	VIVALDI	VIVALDI	Rigaku R-AXIS RAPID	VIVALDI	VIVALDI	Rigaku R-AXIS RAPID	VIVALDI	VIVALDI	Rigaku R-AXIS RAPID	VIVALDI
Radiation	Neutron	Neutron	X-ray	Neutron	Neutron	X-ray	Neutron	Neutron	X-ray	Neutron
Formula	$C_7H_4N_2O_6$	$C_7H_4N_2O_6$	$C_7H_4N_2O_6$	$C_7H_4N_2O_6$	$C_7H_4N_2O_6$	$C_7H_4N_2O_6$	$C_7H_4N_2O_6$	$C_7H_4N_2O_6$	$C_7H_4N_2O_6$	$C_7H_4N_2O_6$
Molecular weight (g mol^{-1})	212.12	212.12	212.12	212.12	212.12	212.12	212.12	212.12	212.12	212.12
T (K)	20	50	100	100	150	200	200	250	300	300
Space group	*C2/c*	*C2/c*	*C2/c*	*C2/c*	*C2/c*	*C2/c*	*C2/c*	*C2/c*	*C2/c*	*C2/c*
***a* (Å)**	20.08	20.20	20.3727(12)	20.37	20.48	20.692(2)	20.69	20.78	21.042(3)	21.04
***b* (Å)**	8.70	8.745	8.7522(4)	8.76	8.74	8.7492(6)	8.75	8.71	8.7285(9)	8.73
***c* (Å)**	9.60	9.645	9.6991(6)	9.69	9.70	9.7407	9.73	9.70	9.7693(10)	9.76
***β* (°)**	109.75	109.80	110.093(2)	110.00	110.15	110.570(3)	110.45	110.70	111.118(4)	111.12
Volume (Å^3)	1578.4	1603.1	1624.15(16)	1624.8	1630.0	1651.0(2)	1650.5	1642.3	1673.8	1672.3
Z	8	8	8	8	8	8	8	8	8	8
Reflections collected	16009	15517	10429	14693	13642	10506	11203	9766	10811	8085
Independent	3248	3015	1867	2725	2440	1896	1901	1630	1916	1614
Observed > 2σ(I)	2631	2432	1729	2143	1878	1686	1491	1311	1543	1181
R_{int}	-	-	0.016	-	-	0.016	-	-	0.017	-
Parameters	173	173	152	173	173	157	173	173	157	173
GooF	1.03	1.01	1.04	0.87*	1.17	1.05	1.25	1.31	1.10	1.30
R_1 (observed)	0.0448	0.0424	0.0293	0.0388	0.0381	0.0314	0.0370	0.0383	0.0345	0.0431
R_1 (all)	0.0705	0.0683	0.0314	0.0633	0.0657	0.0347	0.0615	0.0585	0.0421	0.0748
wR_2 (all)	0.1387	0.1360	0.0852	0.1198	0.0696	0.0910	0.0708	0.0726	0.1059	0.0801
Δρ (max, min) / e$^-$/Å^3 or fm/Å^3	0.14, -0.14	0.11, -0.12	0.35, -0.22	0.09, -0.08	0.06, -0.06	0.28, -0.19	0.06, -0.08	0.05, -0.06	0.23, -0.15	0.07, -0.05

[a] *It is not possible to accurately determine unit cell parameters from a Laue experiment at a continuous neutron source so no errors are listed. X-ray determined values are used where available. * GooF values of <1 may arise from the neutron data due to the method of refinement.*

6.2 2:2 Complex of 3,5-Dinitrobenzoic Acid and 4-Dimethylaminobenzoic Acid

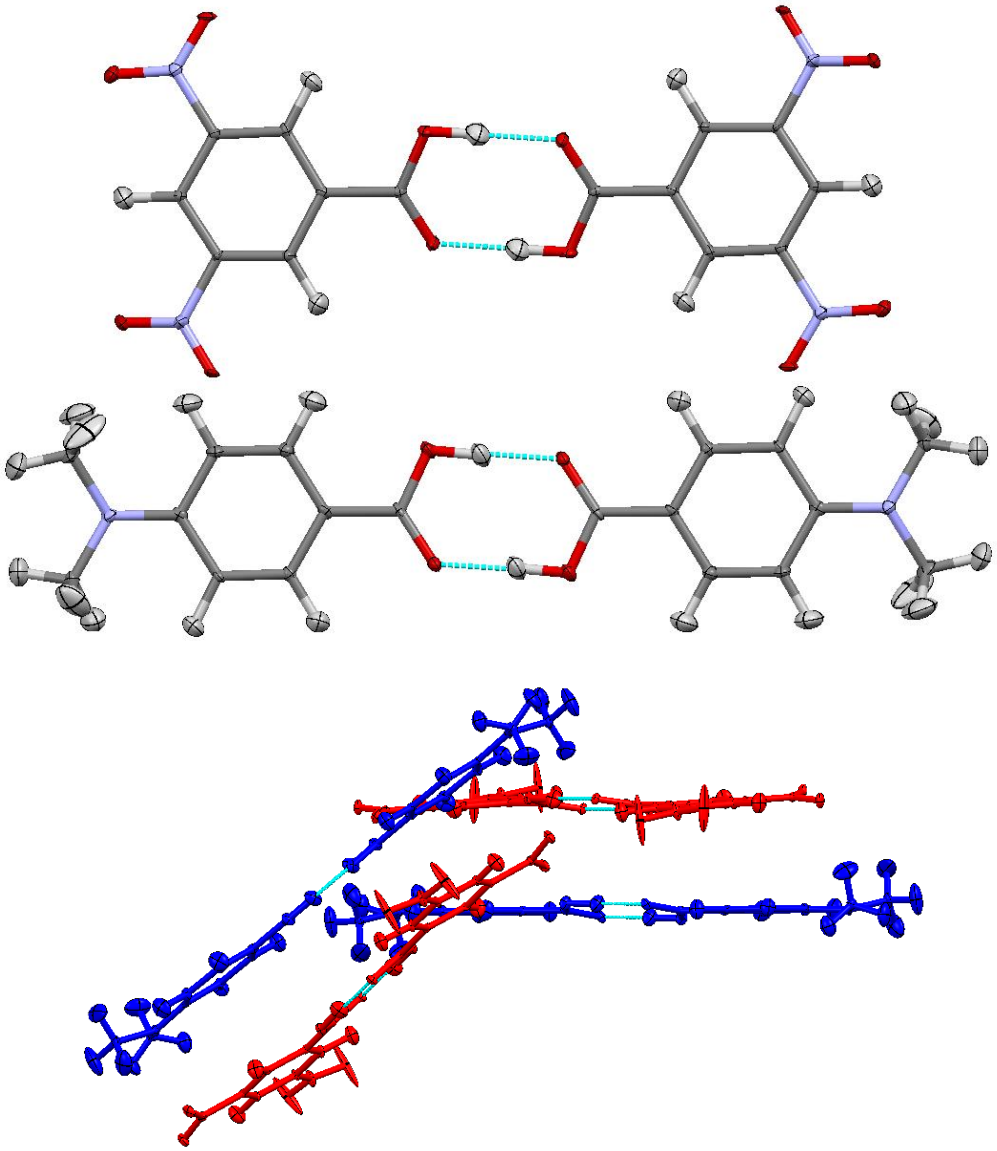

Figure 6.3 *The homodimers of 3,5-DNBA (top) and 4-DABA (middle) with the neighbouring stacks (bottom) of 3,5-DNBA (red) and 4-DABA (blue) dimers taken from the 30 K neutron data.*

4-DABA and 3,5-DNBA crystallise in a complex with a 1:1 ratio. The two components do not interact directly with each other, instead forming homodimers (**Figure 6.3**, top and centre); meaning that the structure could be better described as a 2:2 complex. The dimer arrangements are related by an inversion centre at the centre of $R_2^2(8)$ hydrogen bonded rings consisting of moderate strength hydrogen bonds (**Table 6.4**). The dimers are π-stacked in an alternating pattern of 3,5-DNBA and 4-DABA homodimers with a separation of ~3.0 Å at 30 K increasing to ~3.3 Å at 300 K. The structure is not layered

and neighbouring dimer stacks are related by a tilt of ~35° (**Figure 6.3**, bottom). The neutron structures presented here are in good agreement with the previously determined X-ray structures.[76,16]

Table 6.4 *Lengths of hydrogen bonds linking the 4-DABA and 3,5-DNBA homodimers in the complex from the neutron data. Where disorder is modelled in the 3,5-DNBA dimers, two values are given, (a) represents the major site and (b) the minor.*

T / K	4-DABA			3,5-DNBA		
	r(O-H) /Å	r(H···O) /Å	r(O-H···O) /Å	r(O-H) /Å	r(H···O) /Å	r(O-H···O) /Å
30	1.014(6)	1.585(6)	2.598(4)	0.989(6)	1.647(6)	2.635(4)
100 (a)	1.017(6)	1.597(5)	2.613(4)	0.966(9)	1.679(9)	2.643(4)
(b)	-	-	-	0.92(2)	1.73(2)	2.643(4)
150 (a)	1.009(7)	1.613(7)	2.621(5)	0.957(16)	1.696(15)	2.651(4)
(b)	-	-	-	0.92(2)	1.74(2)	2.651(4)
200 (a)	1.002(9)	1.610(8)	2.612(5)	0.963(16)	1.683(16)	2.644(4)
(b)	-	-	-	0.92 (2)	1.73(2)	2.644(4)
250 (a)	0.990(11)	1.629(9)	2.618(6)	0.96(2)	1.69(2)	2.649(5)
(b)	-	-	-	0.93(2)	1.72(2)	2.649(5)
300[a]	1.009(15)	1.614(13)	2.623(8)	1.32(2)	1.35(2)	2.667(7)

[a] *In the 3,5-DNBA dimer at 300K the two hydrogen atom sites could not be resolved, resulting in one centred, elongated thermal ellipsoid representing the two sites.*

The refined hydrogen atom position previously determined by variable temperature X-ray diffraction within the 4-DABA homodimers showed a normal O-H bond length while the isotropic displacement parameter did not change significantly over the full temperature range studied.[76] The C-O and C=O bond lengths within the dimers also showed a normal length over the temperature range studied. This is typical of a well-behaved and well-localised hydrogen atom within the hydrogen bond. Fourier difference maps directly imaging the electron density did not show indications of any anomalous behaviour of the hydrogen atom within the hydrogen bond. The refined hydrogen position determined from neutron diffraction is also invariant over the full temperature range (**Table 6.4**); the refined

anisotropic displacement parameters and hydrogen atom nuclear density imaged through Fourier difference maps also do not show any evidence of a second hydrogen atom site (**Figure 6.4**).

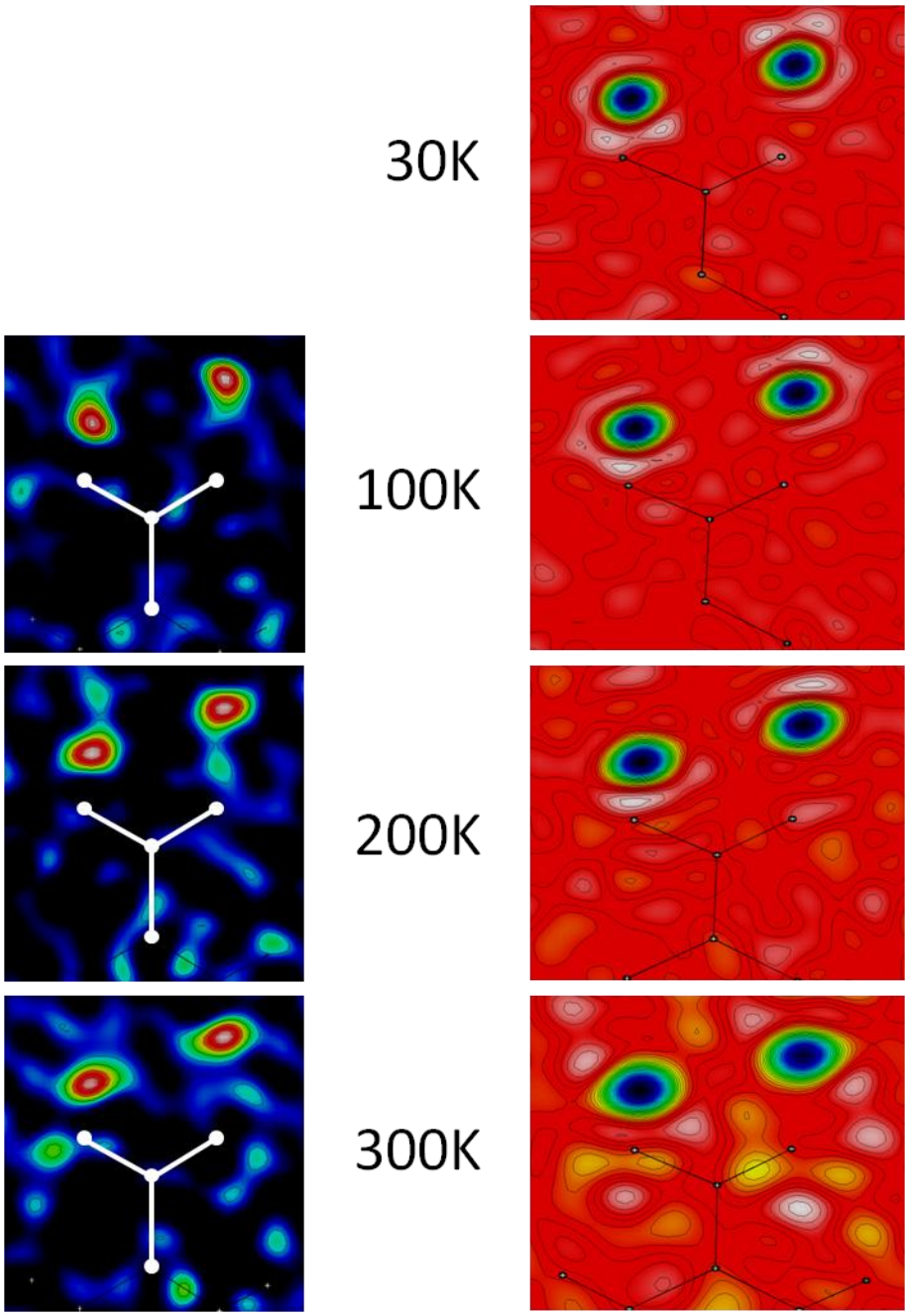

Figure 6.4 *Fourier difference maps showing the electron (left)*[76] *and nuclear density (right) in the hydrogen bond linking the 4-DABA homodimers*

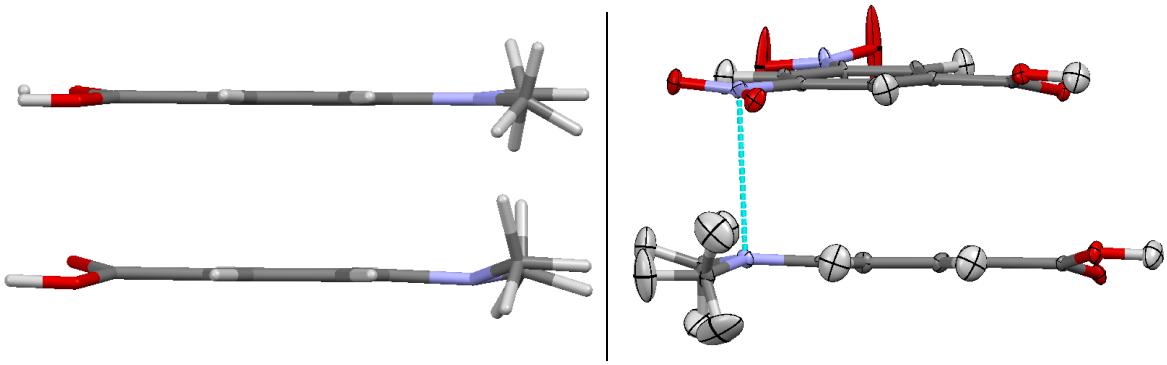

Figure 6.5 *A 4-DABA molecule in the form I native structure (top left)[76] and in the complex with 3,5-DNBA (bottom left) showing the methyl groups out of the plane of the aromatic ring and the close contact with a nitro group of 3,5-DNBA (right).*

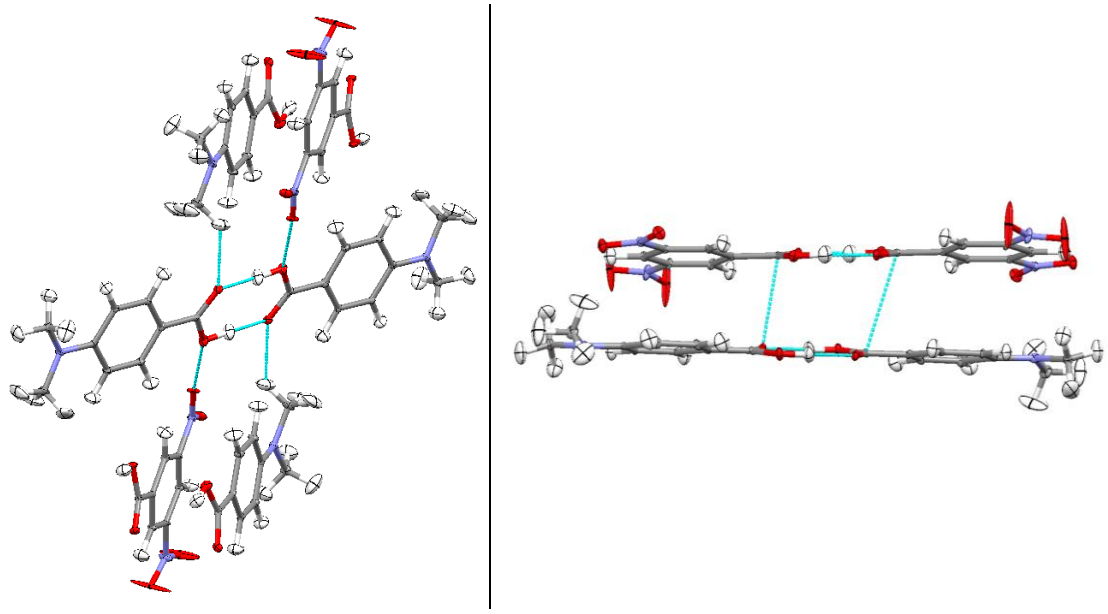

Figure 6.6 *Weak lateral interactions with the 4-DABA acid dimers (left) and interactions to a 3,5-DNBA molecule in the layer above (right).*

The fact that disorder is observed in the native structure, but not in the binary complex, may be rationalised in two ways. In the previous variable temperature X-ray study[76] the absence of disorder was ascribed to an increased pyramidalisation of the nitrogen atom in 4-DABA. The methyl groups are shifted slightly out of the plane of the aromatic ring, in contrast to the native disordered 4-DABA structure where the molecule is planar (**Figure 6.5**, left).[76] This observation is confirmed in the neutron structures. The most likely cause of the pyramidalisation is the presence of close contacts of ~3.0 Å between the 4-DABA nitrogen atom and an electropositive oxygen atom from a nitro group of 3,5-DNBA (**Figure 6.5**, right), an interaction similar to the multipolar interactions described by Paulini *et al*.,[184] and this may result from the transfer of charge from the electron rich nitro

group to the electron poor amide nitrogen. The other possible contributing factor is the presence of weak interactions of the 4-DABA acid groups involved in the dimer-linking hydrogen bonds. Each acid group is involved in lateral weak interactions to a methyl group from one oxygen (C···O distances ranging from 3.021(4) Å at 30 K to 3.246(9) Å at 300 K) and to a nitro group from the other (O···O distances of 2.950(4) and 3.05(1) Å at 30 and 300 K, respectively) (**Figure 6.6**, left) while there are weak π interactions to the acid groups of 3,5-DNBA above and below the 4-DABA dimer (lengths of ~3.0 Å at 30 K and ~3.3 Å at 300 K) (**Figure 6.6**, right). These interactions create a very asymmetric local environment with regard to the two potential hydrogen atom sites which may affect the energetics of the hydrogen bond double-well potential, resulting in one hydrogen atom position having a lower energy and being significantly favoured over the other. In the case of the 3,5-DNBA, the only weak interaction to the dimer is the π interaction to 4-DABA molecules and there are no weak interactions to the acid groups.

The hydrogen atom located within the 3,5-DNBA dimer exhibits a different behaviour to that located in the 4-DABA dimer. The 3,5-DNBA molecules are not planar with both the nitro groups and the acid group tilted out of the plane of the benzene ring. The angles between the planes of the nitro groups and the plane of the aromatic ring vary with temperature, from 5.3(2) - 2.8(4)° for one and 7.0(3) - 5.5(5)° for the other, between 30 and 300 K. Over the same temperature range the angle between the plane of the acid group and the aromatic ring decreases from 12.9(2) to 10.7(4)° (**Figure 6.5**, right).

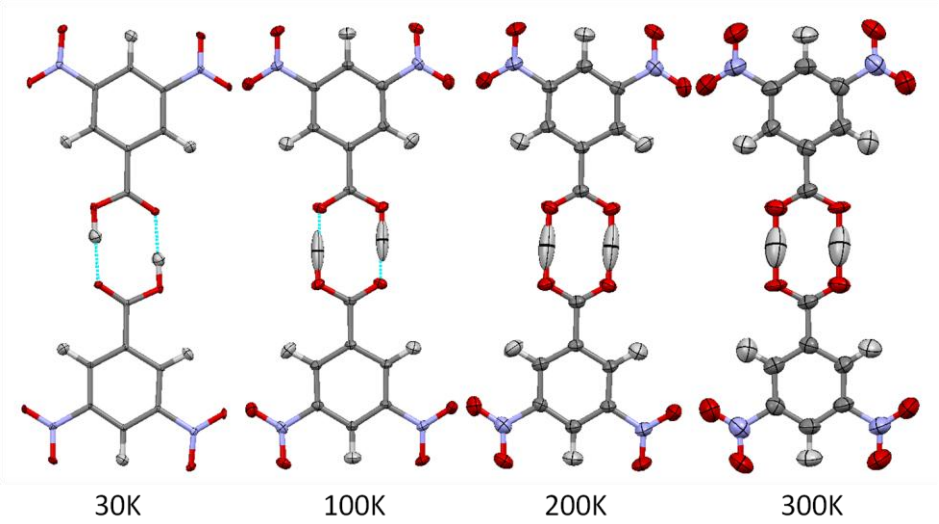

Figure 6.7 *The evolution of the anisotropic displacement parameter of the hydrogen atom in the 3,5-DNBA homodimer in the complex. A single, localised position is observed at 30 K which moves to a more elongated central position as the temperature is increased, indicative of the inadequacy of the single, non-disordered hydrogen atom model employed in these initial refinements.*

When employing a model with a single hydrogen atom site within the dimer, the anisotropic displacement parameter of the refined hydrogen atom determined from the neutron data is significantly elongated at all temperatures except 30 K when the hydrogen atom clearly adopts a single position (**Figure 6.7**). The refined hydrogen atom position indicates that the centre of the nuclear density is shifted towards the acceptor atom, becoming more centered as the temperature is increased, with O-H and H···O distances of 0.989(6) and 1.647(6) Å at 30 K and 1.32(2) and 1.35(2) Å at 300 K. The O···O distance remains invariant over the full temperature range studied (2.635(4) and 2.667(7) Å at 30 and 300 K, respectively, **Table 6.4**). The C-O bond lengths also vary with temperature, at 30 K the bond lengths are 1.203(4) and 1.310(3) Å showing a clear carbonyl and hydroxyl oxygen, respectively, while at the 300 K the values are close to equal with lengths of 1.247(6) and 1.262(6) Å. These observations strongly suggest the presence of a second hydrogen atom site.

Direct imaging of the nuclear density using Fourier difference maps, show that above 30 K, there are two minima of nuclear density for this hydrogen atom (minima as hydrogen has a negative scattering length) indicating a double-well potential where the second site is higher in energy and becomes increasingly occupied as the temperature is increased until at 300 K, the two positions in the map can no longer be resolved (**Figure 6.8**). This inability to resolve the positions of the two peaks in the neutron data occurs due to the close position of the two nuclear sites and the increased thermal motion of the atoms. The two neutron determined hydrogen atom sites are in good agreement with the model suggested from the X-ray data.[76] At 300 K, a greater resolution of the two positions can be achieved with the X-ray data which reflects the different nature of the two techniques. As X-ray diffraction images the electron density, the electron density is drawn into the covalent O-H bond resulting in a greater separation of the two electron density peaks associated with the two partially occupied hydrogen atom positions.

The behaviour of the hydrogen atom within the 3,5-DNBA dimer is best described using two isotropically refined hydrogen atoms located within the hydrogen bond, each with different occupancy values to model the disorder; this model results in a drop in the R-factors indicating that it is a better fit to the measured data (5.30% for the model with disorder and 5.39% for the model without at 250 K). The occupancy values determined from neutron data are more accurate and reliable than values from X-ray data; these values evolve with temperature and a trend can be established. A disorder model was refined at 100, 150, 200 and 250 K. The refined isotropic displacement parameters for the two positions are well separated from one another until 250 K where increased thermal

motion causes some overlap to be observed (**Figure 6.9**). Modelling the hydrogen as disordered results in the O-H distances taking more conventional values ranging from 0.966(9) and 0.919(17) Å at 100 K to 0.96(2) and 0.93(2) Å at 250 K (**Table 6.4**). The distance separating these two hydrogen positions remains invariant over the temperature range with maximum and minimum values of 0.782(16) and 0.76(2) Å at 150 and 250 K, respectively. At 300 K, the overlap of the displacement parameters is significant, meaning that it is less reliable to resolve the two positions without the use of restraints on the refinement. However, it is possible to estimate the disorder ratio at 300 K to be 50:50 from the central position of the refined nuclear density and the shape of the trough in the Fourier difference map.

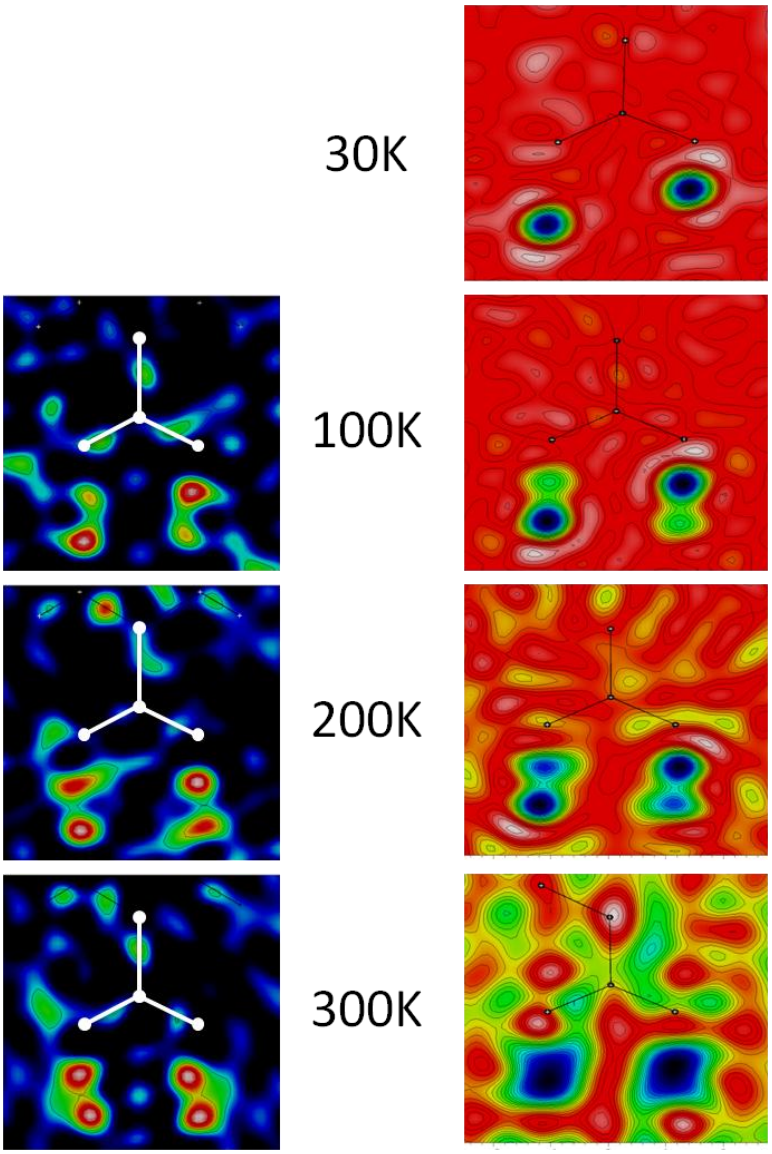

Figure 6.8 *Fourier difference maps showing the electron (left)[76] and nuclear density (right) of the disordered hydrogen bond linking the 3,5-DNBA homodimers in the complex.*

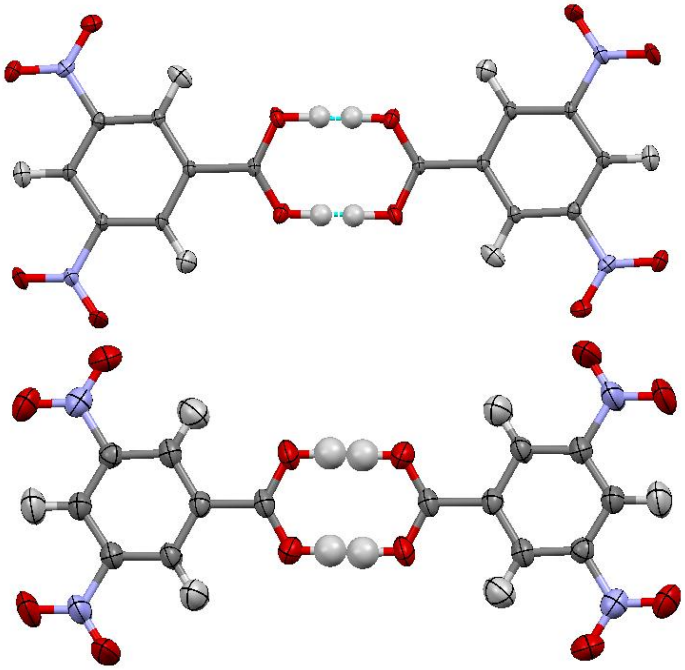

Figure 6.9 *The 3,5-DNBA homodimers in the complex at 100 K (top) and 250 K (bottom) showing the split occupancy hydrogen atom. A gap is clearly visible between the disordered hydrogen displacement parameters at 100 K while at 250 K the displacement parameters are almost overlapping.*

The disorder follows the same trend which was estimated from the X-ray data[76] where the occupancy of the second, minor site gradually increases with temperature until, in this case, the occupancy of both sites is approximately equal at 200 K (**Table 6.7**). There is a remarkable agreement between the two methods taking into account the estimated 10% error of the X-ray determined values; this demonstrates that it is possible in favourable cases to estimate hydrogen atom occupancies reliably from high quality X-ray data. The proportion of disorder in the dimers increases up to 200 K at which point there is approximately 50:50 occupancy of the two sites; increasing the temperature to 300 K does not cause these values to change further. This change in the occupancies, from 100:0 at 30 K to around 50:50 above 200 K, could imply that either:

- The shape of the potential well has changed with temperature and that the two sites now have equal energies as opposed to one low and one high energy site as observed at 30 K; or

- This may reflect an increased occupancy of the second site due to increased thermal energy.

In contrast to the 4-DABA dimers, the acid groups of 3,5-DNBA dimers are relatively isolated and are not involved in weak interactions to surrounding molecules. If weak interactions affect the energetics of the hydrogen bond and play a role in determining whether disorder is present, as may be the case in the 4-DABA dimers, then the disorder observed in the 3,5-DNBA dimers in the absence of weak interactions adds weight to this hypothesis. To probe further the effect of the weak crystal packing interactions on the presence of disorder in benzoic acid dimers, disorder in the homodimers of the two polymorphs of 3,5-DNBA was investigated.

6.3 3,5-Dinitrobenzoic Acid (*P*2$_1$/*c* Polymorph)

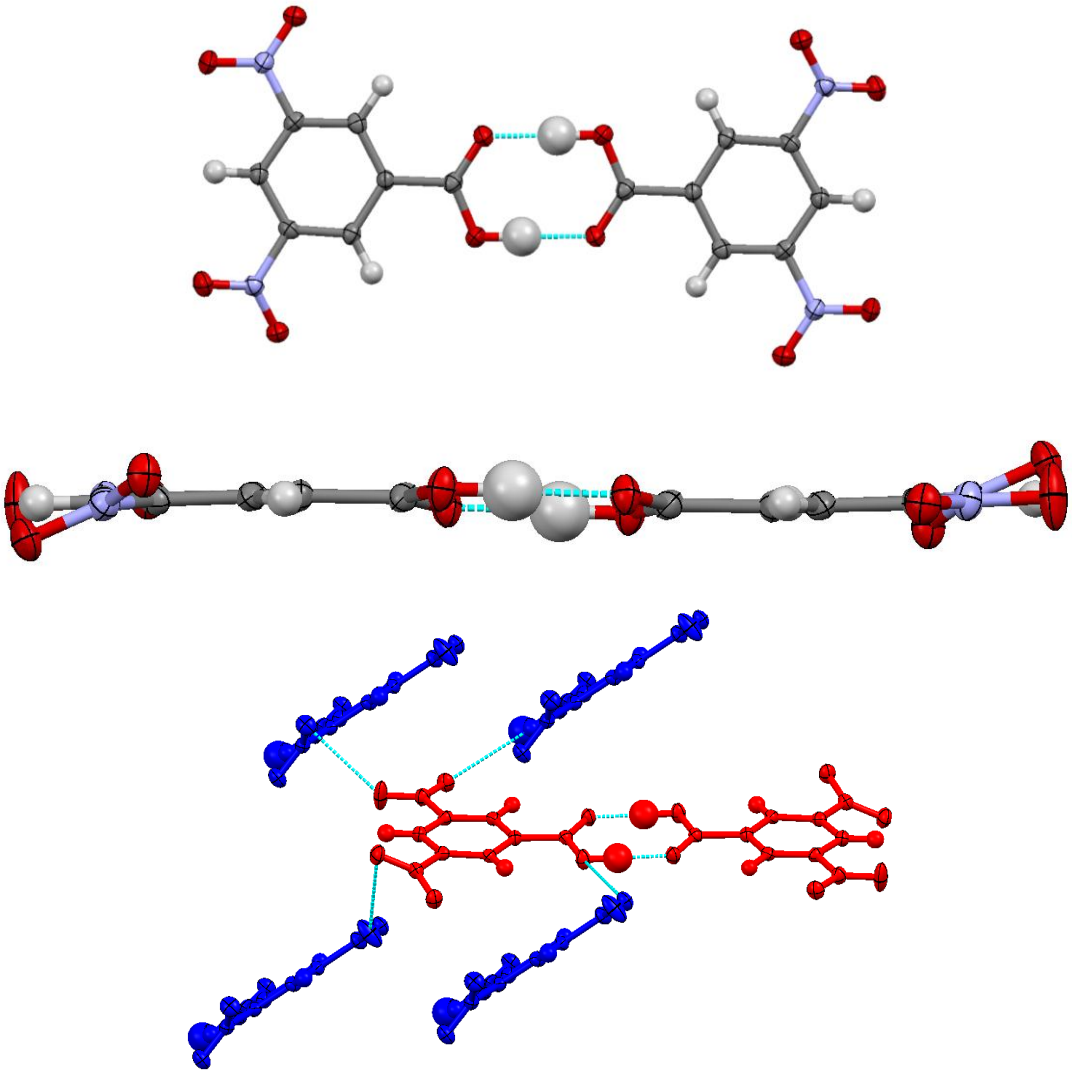

Figure 6.10 *A dimer of 3,5-DNBA (top), a side-on view of a dimer showing the nitro and acid groups slightly out of the plane of the ring (middle) and short contacts between a 3,5-DNBA dimer (red) and surrounding molecules showing layers of dimers (bottom), all taken from the X-ray structure of the P2$_1$/c polymorph at 100 K.*

The polymorph of 3,5-DNBA which belongs to the $P2_1/c$ space group has one molecule in the asymmetric unit and has previously been studied at 100 K and RT, where disorder was modelled with relative occupancies of 63:37.[180] The molecules form $R_2^2(8)$ dimers held together by moderate strength O-H···O hydrogen bonds between the acid groups (O···O distances of 2.635(3) Å at 100 K, **Table 6.5**) (**Figure 6.10**, top). The molecules in the dimers are related by an inversion centre at the centre of an $R_2^2(8)$ hydrogen bonded ring. The acid and one nitro group lie slightly out of the plane of the benzene ring with angles of 23.8(4)° and 7.6(4)°, respectively to the aromatic ring while the other nitro group is approximately coplanar with an angle of 1.3(4)° to the ring at 100 K (**Figure 6.10**, middle). Neighbouring dimers are tilted at ~41° to each other, as estimated by the angles between the planes of the aromatic rings. The two dimer orientations form a two-dimensional layered structure where the rings of stacked dimers do not stack directly on top of one another but are displaced in the surrounding layers (**Figure 6.10**, bottom). There are several short contacts between each molecule and four others in the tilted orientation (**Figure 6.10**, bottom). These consist of C-H···O interactions between ring protons and nitro oxygens with C···O distances ranging from 3.302(3) to 3.458(3) Å at 100 K. There is also an interaction between two nitro oxygens on neighbouring molecules at a distance of 3.004(3) Å at 100 K. Finally there are interactions between one of the acid oxygens and a nitro group oxygen and also with a ring C-H with distances of 3.021(3) and 3.407(3) Å, respectively, at 100 K.

Table 6.5 *Lengths of hydrogen bonds linking the 3,5-DNBA dimers in the P21/c polymorph from the X-ray data. Where disorder is modelled in the 3,5-DNBA dimers two values are given, (a) represents the major site and (b) the minor.*

T / K	r(O-H) / Å	r(H···O) / Å	r(O-H···O) / Å
100	1.01(5)	1.63(5)	2.635(3)
200	1.10(3)	1.53(3)	2.628(2)
300 (a)	0.88(5)	1.77(5)	2.643(2)
(b)	0.84(10)	1.83(10)	2.643(2)

Due to crystal morphology and size, it was only possible to obtain crystals which were suitable for X-ray diffraction measurements on this polymorph. Preliminary indications of proton disorder in the 3,5-DNBA dimer of this polymorph are given by longer than

expected O-H bond lengths extending towards the centre of the hydrogen bond, although this is less significant than that found in the molecular complex of 3,5-DNBA with 4-DABA (see section **6.2**), with O-H distances of 1.01(5) and 1.15(3) Å at 100 and 300 K, respectively. This is accompanied by a large isotropic displacement parameter for the hydrogen atom in the hydrogen bond at 300 K. The O···O distance remains invariant over the temperature range studied with values of 2.635(3) and 2.637(2) Å at 100 and 300 K, respectively. A further indication of the presence of proton disorder is given by the variation in the C-O bond lengths of the acid groups, which become more equalised as the temperature is increased, with values of 1.235(4) and 1.307(3) Å at 100K and 1.254(3) and 1.271(2) Å at 300 K.

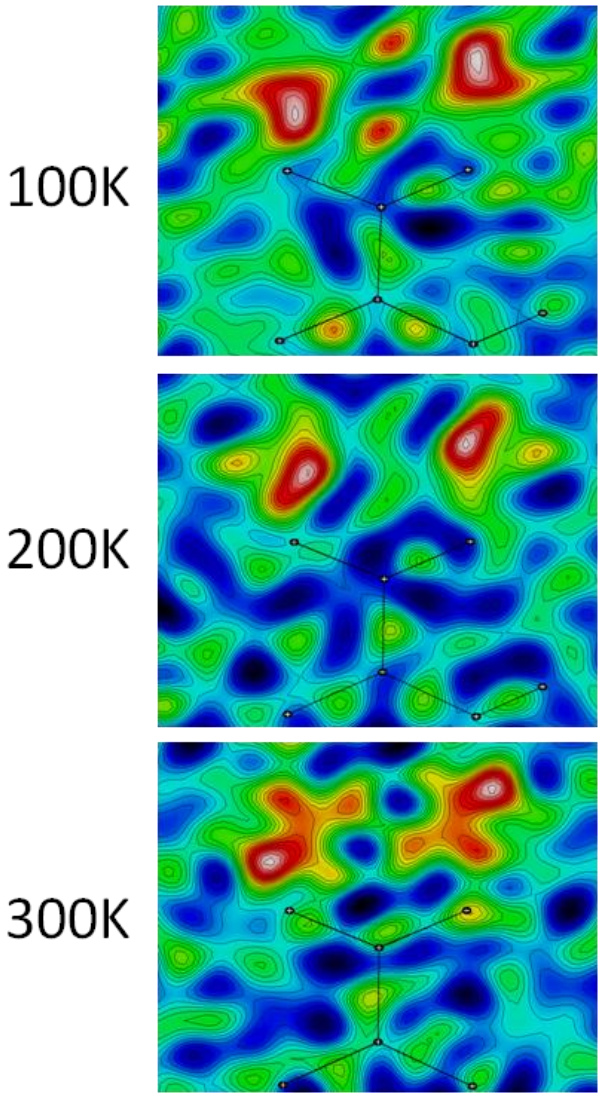

Figure 6.11 *Fourier difference maps showing the electron density of the hydrogen atom within the hydrogen bond linking the 3,5-DNBA dimers in the $P2_1/c$ polymorph.*

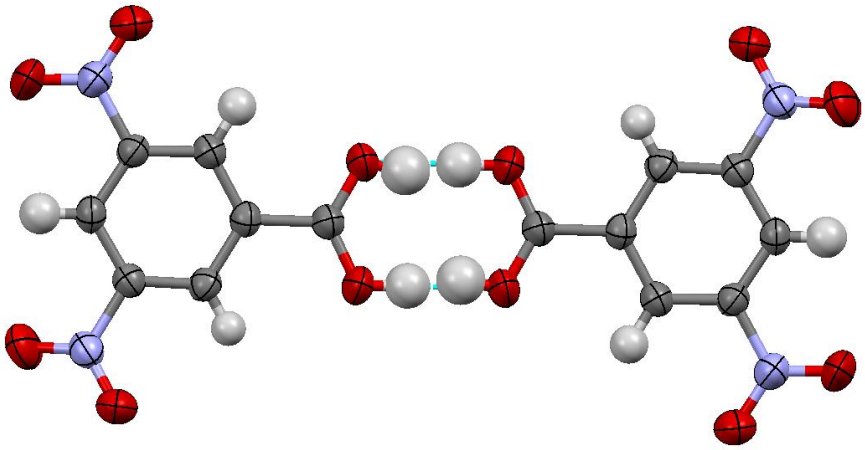

Figure 6.12 *The 3,5-DNBA dimer in the $P2_1/c$ polymorph with the hydrogen atom modelled as disordered over two positions at 300 K.*

Fourier difference maps directly imaging the hydrogen atom electron density within this hydrogen bond show a slight smearing out of the density along the hydrogen bond at 100 and 200 K while at 300 K an obvious second peak appears in the map (**Figure 6.11**) suggesting the hydrogen atom position can be described by a dual occupancy model across two sites. Disorder can be included in the model at 300 K and the relative occupancies of the two positions refined to 64:36 (**Figure 6.12** and **Table 6.7**). This is consistent with the values that were previously reported at RT.[180] Modelling the structure as disordered is a better representation of the electron density informed by the Fourier difference maps whilst the R-factor remains invariant (5.17% without disorder modelled and 5.16% with disorder modelled). The O-H distances in the disordered model at 300 K then take shorter values of 0.88(5) Å for the major site and 0.84(10) Å for the minor site (**Table 6.5**) while the distance between the two hydrogen atom sites is 0.96(8) Å. Whilst neutron data would be required to definitively show that proton disorder is present in this hydrogen bond, the X-ray data strongly support this interpretation of the behaviour of the hydrogen atom electron density.

6.4 3,5-Dinitrobenzoic Acid (*C*2/*c* Polymorph)

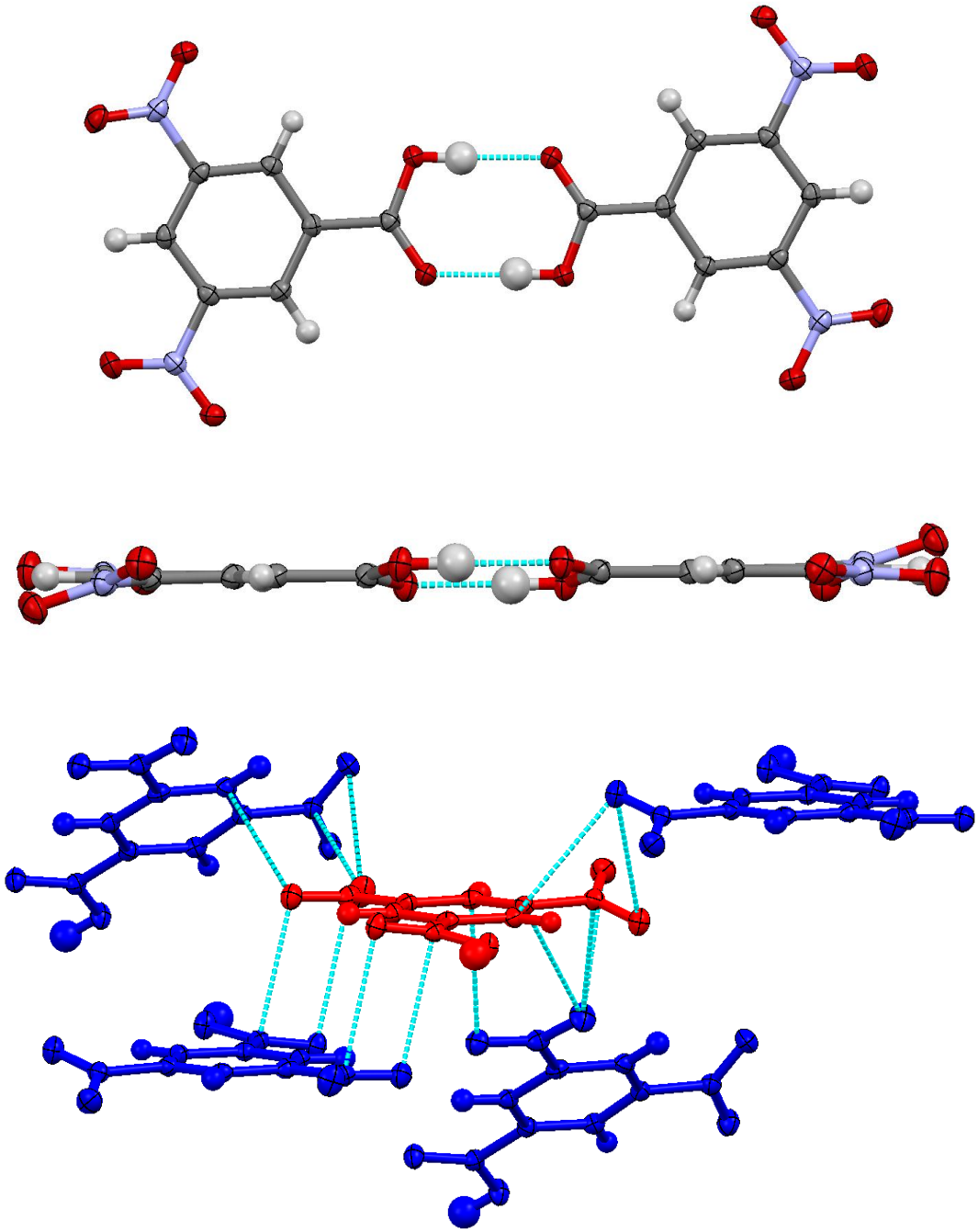

Figure 6.13 *A dimer of 3,5-DNBA (top), a side-on view of a dimer showing the nitro and acid groups out of the plane of the benzene ring (middle) and short contacts between a 3,5-DNBA molecule (red) and surrounding molecules showing layers of dimers (bottom) all from the structure of the C2/c polymorph at 100 K.*

The second polymorph of 3,5-DNBA belongs to the *C*2/*c* space group and also has one molecule in the asymmetric unit. This has been studied previously at 100 K[181] and RT[182,183] but no disorder was reported in either structure determination. The molecules

form dimers held together by moderate strength O-H···O (2.6314(11) Å at 100 K, **Table 6.6**) hydrogen bonds between the acid groups (**Figure 6.13**, top). The molecules in the dimers are again related by an inversion centre at the centre of a $R_2^2(8)$ hydrogen bonded ring. The nitro and acid groups are tilted slightly out of the plane of the ring with angles of 4.14(9)° and 19.32(10)° for the nitro groups and 9.04(12)° for the acid group, relative to the plane of the benzene ring in the 100 K X-ray structure (**Figure 6.13**, middle). Neighbouring dimers are rotated at ~37° to each other and these two sets of dimers form a two-dimensional layer structure as in the $P2_1/c$ polymorph (**Figure 6.13**, bottom). In the $C2/c$ form, the dimers in neighbouring layers overlap more than those in the $P2_1/c$ polymorph. There are several short contacts between each molecule and those in the neighbouring environment (**Figure 6.13**, bottom). These include N···O interactions between nitro groups ranging in distance from 2.799(1) to 2.969(1) Å and O···O interactions between nitro groups with distances from 2.945(1) to 3.016(1) Å at 100 K. There also contacts between nitro oxygens and ring carbons with distances ranging from 3.168(1) to 3.205(1) Å at 100 K. The final group of short contacts is between the acid group oxygens to a C-H ring proton with a distance of 3.508(1) Å and to a nitro group with at distances of 2.927(1) and 3.026(1) Å at 100 K.

Table 6.6 *Lengths of hydrogen bonds linking the 3,5-DNBA dimers in the C2/c polymorph from X-ray and neutron data. Where disorder is modelled in 3,5-DNBA dimers two values are given, (a) represents the major site and (b) the minor.*

T/K	r(O-H)/Å		r(H···O)/Å		r(O-H···O)/Å	
	X-ray	Neutron	X-ray	Neutron	X-ray	Neutron
20	-	1.006(3)	-	1.607(3)	-	2.613 (2)
50	-	1.007(3)	-	1.617(3)	-	2.624(2)
100	0.91(2)	1.008(2)	1.73(2)	1.621(2)	2.6314(11)	2.630(2)
150	-	1.007(2)	-	1.622(2)	-	2.629(2)
200 (a)	0.86(3)	1.004(3)	1.78(3)	1.629(3)	2.6345(12)	2.633(2)
(b)	0.96(9)	-	1.72(9)	-	2.6345(12)	-
250 (a)	-	0.996(4)	-	1.620(5)	-	2.616(2)
(b)	-	0.75(3)	-	1.87(3)	-	2.616(2)
300 (a)	0.85(3)	0.982(6)	1.79(3)	1.642(6)	2.6385(14)	2.623(3)
(b)	0.90(8)	0.85(3)	1.77(8)	1.77(3)	2.6385(14)	2.623(3)

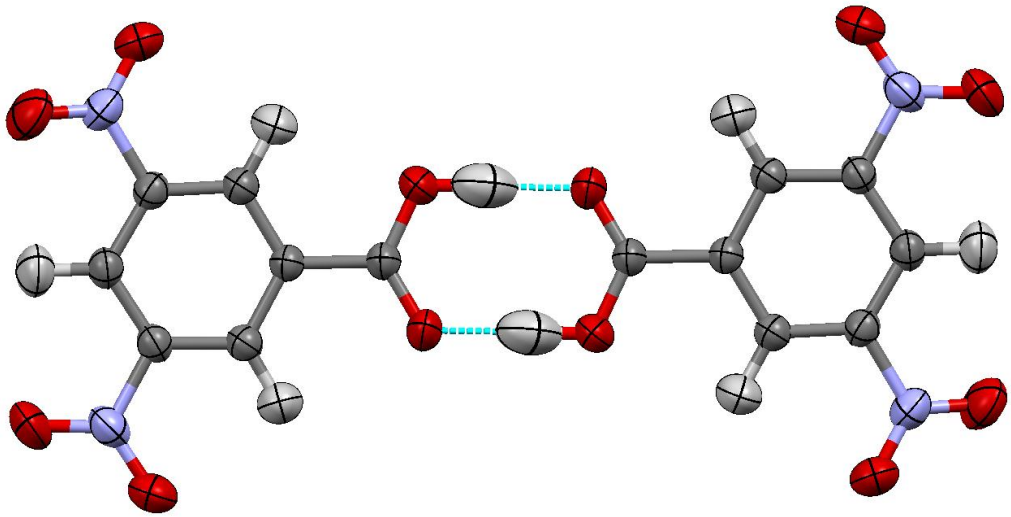

Figure 6.14 *A dimer of 3,5-DNBA taken from the C2/c polymorph neutron structure at 300 K.*

In the X-ray structure at 300 K, the isotropic displacement parameter of the hydrogen atom located in the hydrogen bond in the dimer is significantly larger than those of the other hydrogens in the structure and the refined atomic position has moved towards the centre of the bond; the O-H distance at 100 K is 0.91(2) Å, while it is 1.00(2) Å at 300 K. The C-O distances also vary with temperature with values of 1.2278(12) and 1.3075(12) Å at 100 K and 1.238(2) and 1.282(2) Å at 300 K. This is again an indicator of possible disorder within the moderate strength hydrogen bond and neutron data were therefore collected at several temperatures to probe this further (**Figure 6.14**). The neutron structures are in good agreement with those determined by X-ray diffraction and it was possible to refine fully all hydrogen positional and anisotropic displacement parameters. The anisotropic displacement parameters of the hydrogen atom of interest are also larger than those of the other hydrogen atoms in the structure and appear elongated along the direction of the hydrogen bond at 300 K (**Figure 6.14**). However the position of the atom does not shift towards the centre of the bond to the extent found from the X-ray data (O-H distances of 1.006(3) and 1.011(6) Å at 20 and 300 K, respectively). In both the X-ray and neutron structures the O···O distance is invariant over the temperature range studied (2.613(2) and 2.622(3) Å from the 20 and 300K neutron data, respectively).

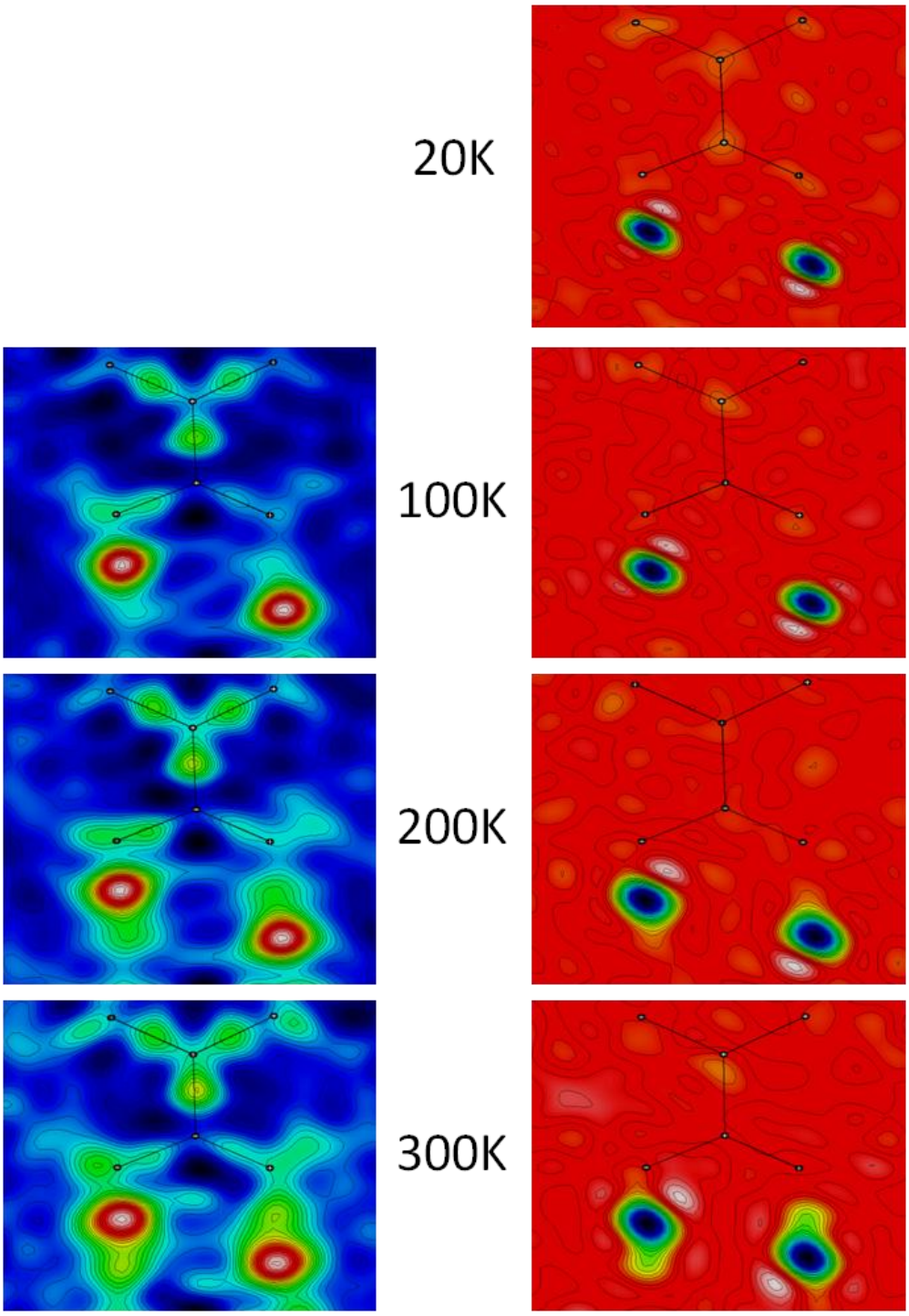

Figure 6.15 *Fourier difference maps showing the electron (left) and nuclear (right) density of the hydrogen atom in the hydrogen bond linking the 3,5-DNBA dimers in the C2/c polymorph.*

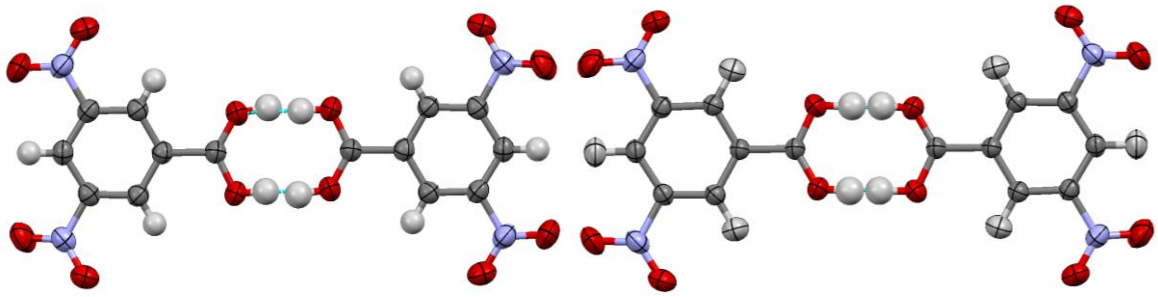

Figure 6.16 *Disordered 3,5-DNBA dimers in the C2/c polymorph from the X-ray (left) and neutron (right) data at 300 K.*

Fourier difference maps of the electronic and nuclear density show the emergence of a second site in both the X-ray and neutron data as the temperature is increased (**Figure 6.15**). The Fourier difference maps derived from X-ray data show a potential second electron density peak at 200 and 300 K (**Figure 6.15**, left); those derived from neutron data only show a slight elongation of the nuclear density at 200 K with two clear positions identifiable at 300 K (**Figure 6.15**, right). A disordered model can be refined for the X-ray data at 200 and 300 K with site occupancies of 78:22 and 72:28, respectively, and at 250 and 300 K for the neutron data with site occupancies of 86:14 and 81:19, respectively (**Figure 6.16** and **Table 6.7**). Again the distance between the two positions is larger for the X-ray data than for the neutron data reflecting the bonding nature of electron density compared to that of the nuclear density. Modelling the data this way shortens the observed O-H distances in the disordered model at 300 K to 0.85(3) Å from the X-ray data and 0.982(6) Å (**Table 6.6**) from the neutron data, compared with 1.011(6) Å in the model without disorder. Models refined against both the X-ray and neutron data follow the same trend of the second site occupancy increasing with temperature, though the occupancy values differ slightly again, possibly due to the uncertainty in the X-ray determined values. An increase in the occupancy of the second site with increasing temperature is expected in the case of a double-well potential hydrogen bond with two minima that are close in energy, as the minor position represents a slightly higher energy configuration of the dimers that is essentially unoccupied at low temperatures and a greater population of the two sites is obtained on increasing the temperature due to either an increase in thermal energy or a change in shape of the potential well.

The model for two, partially occupied, hydrogen atoms sites provides a better structural model than a single hydrogen atom position, particularly at higher temperatures, reflected in a drop in the R-factor. This reduction is very small in the X-ray data (3.49% to 3.45% for R1 at 300 K) but slightly larger in the neutron data (4.55% to 4.31% at 300 K) where scattering from the hydrogen atoms is much stronger.

Table 6.7 *Relative occupancies of the major and minor disordered proton sites in homodimers of 3,5-DNBA in the pure $P2_1/c$ and C2/c polymorphs, the binary complex[a], 4-DABA in the ternary complex and benzoic acid in its native structure from X-ray and neutron diffraction data.*

	3,5-DNBA (*P*2$_1$/*c*) X-ray		**3,5-DNBA (*C*2/*c*) X-ray**		**3,5-DNBA (*C*2/*c*) neutron**		**Binary X-ray[8]**		**Binary neutron**		**BA neutron [77]**		**Ternary neutron[175]**	
***T*/K**	**major %**	**minor %**	**major %**	**minor %**	**major %**	**minor %**	**major %**	**minor %**	**major %**	**minor %**	**major %**	**minor %**	**major %**	**minor %**
20	-	-	-	-	100	0	-	-	-	-	87	13	-	-
30	-	-	-	-	-	-	-	-	100	0	-	-	-	-
40	-	-	-	-	-	-	-	-	-	-	-	-	100	0
50	-	-	-	-	100	0	-	-	-	-	79	21	-	-
100	100	0	100	0	100	0	66	34	62	38	67	33	75	25
150	-	-	-	-	100	0	-	-	55	45	-	-	-	-
160	-	-	-	-	-	-	63	38	-	-	-	-	-	-
175	-	-	-	-	-	-	55	45	-	-	62	38	-	-
190	-	-	-	-	-	-	54	46	-	-	-	-	-	-
200	100	0	78	22	100	0	52	48	51	49	-	-	60	40
210	-	-	-	-	-	-	52	48	-	-	-	-	-	-
225	-	-	-	-	-	-	56	44	-	-	-	-	-	-
250	-	-	-	-	86	14	59	41	49	51	-	-	-	-
300	64	36	72	28	81	19	47	53	50	50	-	-	50	50

Errors on occupancies derived from X-ray data are estimated at approximately 10%. [a] *Relative occupancies from the 300 K neutron data for the binary complex are estimated from the position and shape of the nuclear density in a model without disorder due to the overlapping nuclear density of the two positions.*

6.5 Disorder in Benzoic Acid Dimers

The proportion of disorder identified at a given temperature in the homodimers of 3,5-DNBA shows some variation in all of the structures discussed so far. Polymorphs are an ideal route for producing subtle differences in local packing environments and examining their effect; in this case, the two polymorphs show different packing but similar proportions of disorder (**Table 6.7**). A more significant proportion of disorder is observed in the 3,5-DNBA dimers in the 2:2 molecular complex with 4-DABA where approximately 50:50 disorder is obtained by 200 K, as determined from the neutron diffraction data (**Table 6.7**). All of these disordered systems present non-planar 3,5-DNBA molecules with twists in both the carboxylic acid and nitro groups from the plane of the benzene ring. These geometric changes do not appear to eliminate proton disorder from the 3,5-DNBA dimers in a similar manner to that proposed by the pyrimidalisation of the nitrogen atom in the 4-DABA dimers[76], although the 3,5-DNBA homodimers in the binary complex do become more planar as the temperature is increased. The other common feature amongst these disordered systems is the change in the acid C-O distances, which become closer to being equal as the temperature is increased and disorder becomes more pronounced.

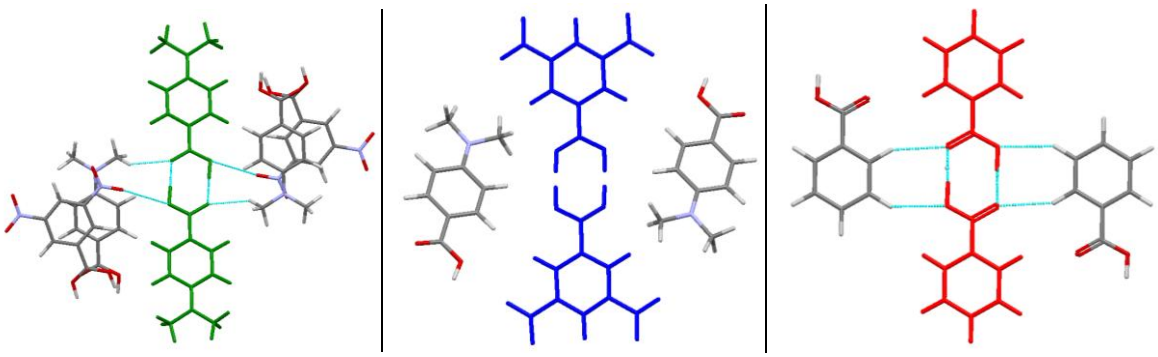

Figure 6.17 *A dimer of 4-DABA (left, green) involved in asymmetric weak interactions and an isolated dimer of 3,5-DNBA (centre, blue) from the binary complex with a benzoic acid dimer (right, red) involved in symmetric weak interactions,[80] all at 100 K.*

Another factor which may contribute to the absence of disorder in the 4-DABA dimers of the complex is the disposition of weak interactions around the acid hydrogen bonds, which can create an asymmetric environment for the two possible proton positions (**Figure 6.17**, left). The 3,5-DNBA dimers in the complex are not involved in weaker interactions to the acid groups so the local environment of the proton positions is more symmetric and disorder is observed (**Figure 6.17**, centre). Further, 4-DABA dimers are stacked on top of 3,5-DNBA dimers; these 4-DABA dimers represent a far less electron rich system and

thus the π - π interactions to the 3,5-DNBA dimers may be weaker. The spacing of these layers is thus increased to approximately 3.3 Å in the complex compared with 2.8 - 2.9 Å in the polymorphs where the proportion of disorder is lower. The weak C-H···O hydrogen bonds and nitro group interactions with the hydrogen bonded acid groups of the homodimers in the 3,5-DNBA polymorphs, which range in length from ~2.80 to 3.41 Å, again create an asymmetric local environment for the two possible proton positions, perhaps explaining the significantly increased energy barrier for the disorder evidenced by the higher onset temperature and lower occupancy for this disorder when compared with the molecular complex (**Figure 6.18**). The dimer in the molecular complex is far more isolated suggesting that the level of disorder is significantly influenced by the local interactions around the dimer linking hydrogen bonds.

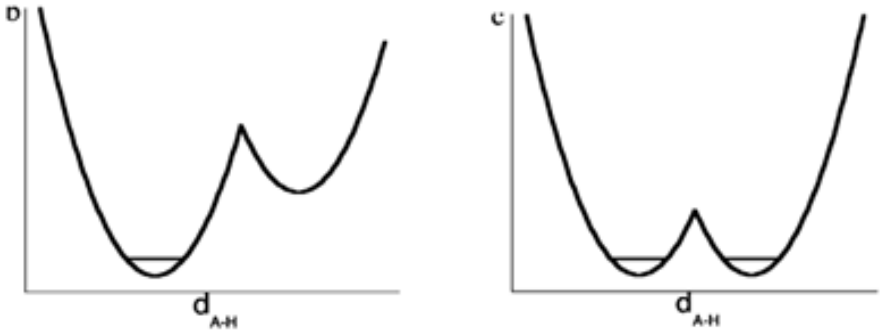

Figure 6.18 *Schematic representations of the hydrogen bond double-well potentials for the 3,5-DNBA dimers in the polymorphs where the energy difference between the two possible position is significant (left), and in the complex with 4-DABA, where the two possible positions are close in energy (right).*[6]

Comparisons can be made with the proton disorder exhibited in the 4-DABA dimers in its native form I[76] and in the ternary complex with 3,5-DNBA and BIPY[175] (**Table 6.7**). In form I of 4-DABA, the disorder determined from the X-ray data is present at 100 K and increases to a similar level as that observed in the 3,5-DNBA polymorphs at 300 K, while the disorder assigned in the dimers of 4-DABA from the ternary complex neutron data is more pronounced and of a similar level to the disorder in the binary complex (**Table 6.7**). Both these sets of dimers also have no weak interactions to the hydrogen bonded acid groups and can be described as relatively isolated in terms of their local environment which may account for the low onset temperature of disorder at temperatures as low as 100 K.

A further comparison can be made with benzoic acid (BA),[77] one of the most studied systems showing proton disorder, which shows an even greater proportion of disorder at lower temperatures than the other examples presented here (**Table 6.7**). It too has a relatively isolated dimer unit when considering the layers above and below with an approximate spacing of 3.2 - 3.3 Å, but it is involved in weak C-H···O hydrogen bonds (~3.5 - 3.6 Å in length) on either side of the acid dimer indicating that the presence of weak interactions is not necessarily a hindrance to disorder (**Figure 6.17**, right). However, it is important to note that these weak interactions are symmetric across the hydrogen bond and therefore have a similar effect on both the possible proton positions. This perhaps explains the lower energy difference between the two positions evidenced by the higher proportion of disorder at lower temperatures.

A CSD search was carried out to further investigate other occurrences of disordered structures containing the 3,5-DNBA homodimer motif. In total, nine other structures were found which contain 3,5-DNBA homodimers where the hydrogen atoms in the hydrogen bonds between the dimers have been located. Of these nine, four have proton disorder modelled within the hydrogen bonds while three others display elongated O-H distances which could be associated with the presence of disorder.

The four structures with disorder modelled within the dimers are complexes of 3,5-DNBA with *N*-methylcarbazole, *N*-isopropylcarbazole, *N*-butylcarbazole and *N*-isobutylcarbazole (CSD codes KIZQIT, KIZQOZ, KIZQUF and KIZREQ, respectively).[185] These structures report the disordered site occupancies as 50:50 at RT; this would suggest a small difference in energy between the two possible positions as in the 3,5-DNBA dimers in the binary complex. However, it is not clear that these occupancy values were allowed to refine freely and therefore the 50:50 levels of disorder may not be accurate. The O-H distances presented in these structures provide further evidence that the occupancies may not have been allowed to refine freely, or that the refinement is not completely reliable, with values as low as 0.638 Å observed. The fact that disorder was modelled implies that there was enough evidence that disorder is present even if the occupancy values are not accurate. If the local environment around the acid dimer can affect the energetics of the hydrogen bond, as suggested from the polymorphs of 3,5-DNBA and the binary complex, it would be expected that the dimers in these four other disordered dimers are relatively isolated, or at least have symmetric environments around either side of the acid group as in the case of BA. This proves to be the case; the dimers are relatively isolated with the acid groups taking part in only very weak C-H···O interactions at a distance of ~3.6 - 3.9 Å and layers are separated by ~3.3 - 3.4 Å in the four structures.

The same is also true of the three complexes with elongated O-H distances where disorder was not modelled. These are complexes of 3,5-DNBA with hexahelicene,[186] indole-3-acetic acid[187] and 3-aminobenzonitrile[188] (CSD codes ABUNOA, VOCHOK and YAFVOS, respectively; all studied at RT). The structures have relatively large layer spacings of 3.2 - 3.3 Å and the environments around the acid group dimers are fairly symmetrical with only very weak interactions to the surrounding molecules. In the complex with hexahelicene there are symmetric weak C-H···O interactions of ~3.4 - 3.6 Å in length. The complex with indole-3-acetic acid contains fairly symmetric weak interactions to a carboxyl group at a distance of 3.2 - 3.4 Å while the complex with 3-aminobenzonitrile has symmetric C-H···O interactions to both acid oxygens at a distance of 3.4 - 3.6 Å. These environments around the acid dimers may make the onset temperature of any disorder potentially below RT which may explain the elongated O-H distances.

This leaves two complexes with no evidence of disorder, these are a binary complex of 3,5-DNBA with 4-(phenyldiazenyl)aniline[189] and a ternary complex with anthracene and benzene[190] (CSD codes AJIXOH and ZUPJOJ, respectively). The complex with 4-(phenyldiazenyl)aniline has shorter interlayer distances of ~3.0 Å and an asymmetric environment around the acid groups with interactions to nitro groups of molecules in the layers above and below at ~3.0 Å. This could affect the energetics of the hydrogen bond in such a way that the onset temperature of any possible disorder is raised above 200 K (the temperature at which the complex was studied), possibly accounting for the absence of evidence for disorder. The other structure showing no evidence of disorder at RT (the complex with anthracene and benzene) has larger layer spacings of 3.3 - 3.4 Å with a fairly symmetric environment around the acid group which is involved in only weak C-H···O interactions at a distance of 3.4 - 3.5 Å. This would suggest that disorder should perhaps be present at RT, however it is not stated in the literature[190] how the hydrogen atoms were located so it is not possible to definitively say whether disorder is present or not. Further investigations of complexes containing 3,5-DNBA dimers are certainly required to test the effect the environment plays on the presence of disorder and how much the weaker interactions around the acid groups could affect the hydrogen bond potential energy surface.

6.6 Evolution of the 3,5-Dinitrobenzoic Acid Unit Cells with Temperature

Table 6.8 *Evolution of the unit cell parameters of the two polymorphs of 3,5-DNBA with temperature showing the contraction of the b-axes with increasing temperature.*

	$P2_1/c$			$C2/c$		
	100 K	**200 K**	**300 K**	**100 K**	**200 K**	**300 K**
***a* / Å**	9.7845(15)	9.9026(10)	10.0486(12)	20.3727(12)	20.6923(18)	21.042(3)
***b* / Å**	**8.9435(13)**	**8.9085(8)**	**8.8884(9)**	**8.7522(4)**	**8.7492(6)**	**8.7285(9)**
***c* / Å**	9.4500(12)	9.4714(7)	9.5167(8)	9.6991(6)	9.7407(9)	9.7693(10)
***β* / Å**	82.423(5)	83.467(3)	84.366(3)	110.093(2)	110.570(3)	111.118(4)
***Volume* / Å^3**	819.73(6)	830.12(3)	845.89(3)	1624.15(13)	1651.0(2)	1673.8(3)

The multi-condition studies presented here were conducted with the aim of investigating the temperature dependence of any observed proton disorder. Collecting data at multiple temperatures allows other aspects of the material to be studied; one such aspect is the change in the unit cell parameters and volume with temperature. This can be a field of study in its own right, in particular materials which exhibit negative thermal expansion (NTE).[191] In this context, the two polymorphs of 3,5-DNBA show unusual evolution of the unit cell parameters though they are not NTE materials. Only unit cell parameters derived from X-ray data are discussed here due to the inaccuracies of the parameters used in the neutron experiments. In both structures, as the temperature is increased the *b*-axis contracts, while the *a*- and *c*-axes and volume all increase (**Table 6.8**). The increase in the *a*-axis is more rapid than that seen for the *c*-axis in both examples. This behaviour is similar to that found in a complex of *N,N'*-dimethylurea and oxalic acid presented in **Chapter 4** and several of the complexes discussed in **Chapter 5**.

In both forms of 3,5-DNBA, the shift of a molecule in the dimer on increasing temperature is the cause of the unusual cell behaviour. In **Figure 6.19** the molecules on the left of each dimer are overlayed and a shift can be seen in the molecule on the right on changing the temperature. This shift occurs in the *ab* direction accounting for the contraction in the *b*-axis and the more rapid expansion of the *a*-axis.

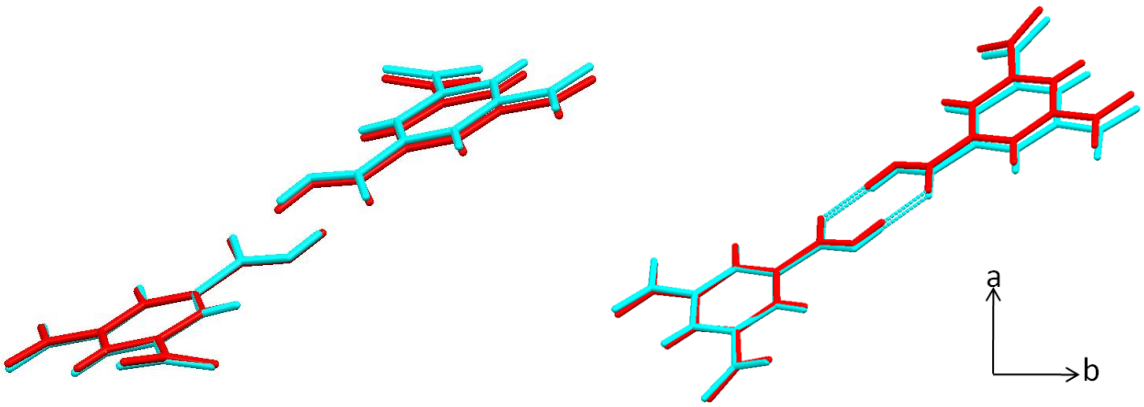

Figure 6.19 *Overlayed dimers of 3,5-DNBA looking approximately along the c-axis in the P21/c (left) and C2/c (right) forms in cyan and red from the 100 and 300 K X-ray data, respectively.*

6.7 Conclusions

Three structures containing 3,5-DNBA dimers have been presented; the two polymorphs and a binary complex with 4-DABA. All of these 3,5-DNBA dimers exhibit temperature dependent proton disorder which has been quantified by X-ray and neutron diffraction in the cases of the *C*2/*c* polymorph and binary complex[76] and only by X-ray diffraction in the case of the $P2_1/c$ polymorph. The disorder in the binary complex was previously determined from high quality X-ray data and this shows a remarkable agreement with the values obtained from the neutron data presented here. This shows the potential for identification and quantification of proton disorder without necessarily needing neutron diffraction data as long as high quality data is available and direct imaging of the electron density through Fourier difference maps is used. At higher temperatures, the X-ray data is in fact better at resolving the two possible proton positions due to X-rays visualising the further separated bonding, electronic density as opposed to the hydrogen atom nuclear density.

In the binary complex of 3,5-DNBA and 4-DABA, no disorder was observed in the 4-DABA dimers from the neutron data, in agreement with the previously determined X-ray data.[76] The absence of disorder was previously related to the increased pyramidalisation of the 4-DABA nitrogen atom due to close contacts with nitro groups from a 3,5-DNBA molecule. While this is still observed in the neutron structures, a further possible contributing factor to the absence of disorder, the local environment of the acid dimers, has also been investigated here. This clearly plays a role in the degree of disorder observed, evidenced by the differing amount of disorder observed in the 3,5-DNBA polymorphs. The

environment around the 4-DABA dimers in the complex showed weak interactions to surrounding molecules, causing the environment to be asymmetric in relation to the two possible proton positions, which may affect the energetics of the two sites causing one to be significantly favoured over the other. In contrast, the dimers of 3,5-DNBA in the binary complex are involved in no weaker interactions, implying a more symmetric environment, and disorder is present above 100 K. The two 3,5-DNBA polymorphs, on the other hand, also have weak intermolecular interactions to surrounding molecules which may explain the higher onset temperature for disorder, implying a larger energy difference between the two sites and the presence of an asymmetric environment. Comparisons have also been made to the disordered 4-DABA dimers in a ternary complex and the most well known system showing proton disorder, pure benzoic acid. In the ternary complex the 4-DABA dimers are fairly isolated and the disorder has a low onset temperature (100 K) in the implied symmetric environment.[175]

In the case of unsubstituted benzoic acid itself, the dimers show disorder at much lower temperatures than any of the other systems studied (20 K) even though the dimer units are involved in weak interactions.[77] Although this is an apparent argument against the rationale advanced here, the situation in the parent material can be rationalised by the symmetric environment of the two sites in the unsubstituted benzoic acid. The symmetry of the BA molecule lends symmetry to its weak intermolecular interactions and hence means that the two possible disordered configurations are closer in energy.

The effect of the local environment on proton disorder was investigated further through a literature search of other compounds containing 3,5-DNBA dimers using the CSD. In cases where disorder was modelled, the dimers appeared to be fairly isolated, in agreement with the data presented here. However, a lack of knowledge of how occupancies were refined and how hydrogen atoms were located means that it is difficult to draw any conclusions from these structures. The limited data available and small numbers of disordered structures studied using neutron diffraction adds to the difficulties of drawing firm conclusions regarding the presence and significance of any disorder. It does however seem plausible that either having fewer weaker interactions to the dimer units or a symmetric environment of weaker interactions for the two possible proton positions could make the sites closer in energy and disorder more likely at lower temperatures.

The neutron data presented here show one potential high throughput approach to single crystal neutron diffraction, made possible by the rapid data collection times on VIVALDI,

which can be used to study samples at multiple temperatures over a short period of time. This approach, which was also used to study the complexes in **Chapter 4** and **Chapter 5**, allows the evolution of the disorder to be accurately followed with temperature which is essential to understand how these materials could potentially be used as charge transfer systems.

Chapter 7

7. Neutron Studies of Complexes of the Proton Sponge DMAN

This work has so far focused on investigations of molecular complexes aimed at finding reliable approaches to tuning the properties of short (**Chapter 4** and **Chapter 5**) and moderate (**Chapter 6**) hydrogen bonds with a view to controlling the physical and chemical properties of molecular materials through dynamic proton transfer effects such as proton migration and proton disorder. In this chapter, the focus shifts to the study of static proton transfer between molecules, the ways in which this induces predictable hydrogen bonding motifs, and in particular the effect weak hydrogen bonds can have on the crystal structure.

To investigate these weaker interactions, it is desirable to find a system in which weak hydrogen bonds play a significant role in the crystal packing and where the lengths of the weak interactions can be tuned whilst maintaining a robust structural framework to allow systematic comparisons to be made. A set of structures which meet the requirements for this investigation are the proton transfer molecular complexes of the proton sponge, 1,8-bis(dimethylamino)napthalene (DMAN) (see **Section 1.10**), with organic acids (**Figure 7.1**). DMAN is a very strong, basic compound which readily accepts a proton when complexed with an acid, creating $DMANH^+$ and $ACID^-$ components, where the acid has been deprotonated, represented in the general case by the symbol $ACID^-$. Given the wide utility of the DMAN proton sponge to form molecular complexes with organic acids, previous single crystal X-ray diffraction studies have been conducted,[123,124] including on those complexes presented here,[125] from which reliable and reproducible strongly hydrogen bonded motifs have been identified; these are discussed below.

When DMAN accepts a hydrogen atom from an acid, it forms an intramolecular N-H···N hydrogen bond (see **Section 1.10**); this is often a short, strong hydrogen bond (**Figure 7.1**, left). In the case of the complexes presented in this chapter, another common feature is the motif of an acid molecule located above the N-H···N hydrogen bond in DMAN where an acid oxygen interacts with the methyl groups on the DMAN and possibly with the proton within the N-H···N hydrogen bond (**Figure 7.1**, right); these are weak interactions whose potential tuning will be investigated across a series of complexes. The third interesting structural feature is the tendency of a neutral and a deprotonated acid in the family of 1:2 (DMAN:acid) complexes with monosubstituted halobenzoic acids to form a charge-assisted O-H···O^- short, strong hydrogen bond (SSHB), linking acid molecules to form a negatively charged dimer (**Figure 7.1**, right). From the X-ray determined structures

of these complexes,[125] the N-H···N intramolecular hydrogen bonds appear mostly asymmetric, with accurate location of the hydrogen atom difficult due to the hydrogen atom electron density being spread across the hydrogen bond and shared between the two nitrogen atoms when visualised through Fourier difference maps. In the case of the charge-assisted O-H···O^- hydrogen bonds linking the carboxylic acid molecules into dimers, the hydrogen atom electron density within the hydrogen bonds is again found to be elongated, making accurate location of the hydrogen atom difficult. In addition to the 1:2 DMAN complexes with monosubstituted halobenzoic acids discussed above, complexes of DMAN with other organic acids may form with a 1:1 ratio. In such cases, each acid moiety in the structure is negatively charged and $ACID^{2-}$ dimers are formed. However, these dimers do not always contain the charge-assisted SSHBs observed in the complexes containing monosubstituted halobenzoic acids; two such examples are presented in this chapter.

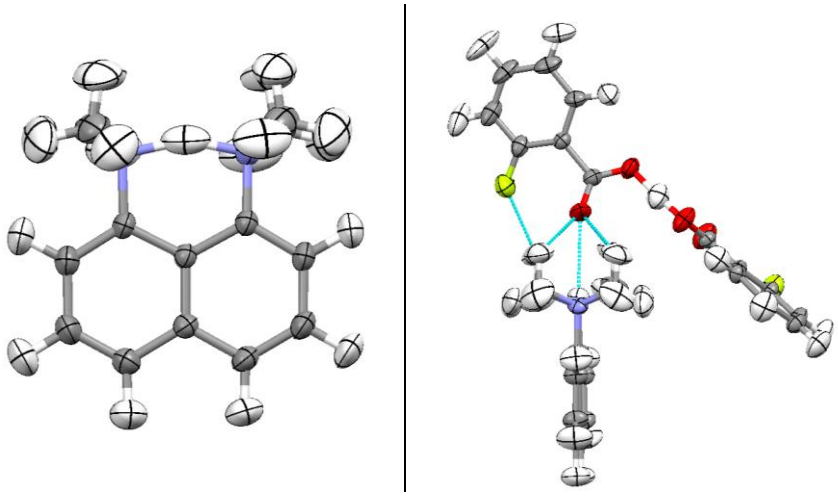

Figure 7.1 *A protonated $DMANH^+$ showing the intramolecular N-H···N hydrogen bond (left) and a benzoic acid dimer containing a charge-assisted short, strong hydrogen bond where a dimer oxygen is positioned above a $DMANH^+$ (right).*

To investigate these structural aspects further, single crystal neutron diffraction data were collected on complexes of DMAN with 2-fluorobenzoic acid (2-FBA), 2-iodobenzoic acid (2-IBA), 4-iodobenzoic acid (4-IBA), chloranilic acid (CLA) and 2,3-dihydroxybenzoic acid (2,3-DOHBA) (**Figure 7.2**). The complexes with CLA and 2,3-DOHBA do not form charge-assisted hydrogen bonds between acid molecules, instead forming complexes with a 1:1 stoichiometric ratio. The availability of neutron data means that the hydrogen atoms within the N-H···N and O-H···O hydrogen bonds of DMAN and the halobenzoic acid dimers can be located accurately and the effect of weak interactions on their location within the hydrogen bonds investigated; this may allow additional information on the

significance of any interactions to be inferred. It also means that the hydrogen atom thermal displacement parameters can be refined anisotropically and any possible correlation between the position of the acid oxygen above the N-H···N hydrogen bond, the hydrogen atom located within the bond and the orientation of the DMAN methyl groups investigated. As the structures present a range of distances between the acid molecule above the DMAN and the protons within the relevant DMAN groups (**Figure 7.1**), it is possible that this could provide a means to assess the length scale over which an electronegative atom has an effect on the behaviour of a hydrogen atom within a weak hydrogen bond. In this case, single temperature measurements (200 K) were collected for all complexes apart from DMAN:2-IBA, for which data were collected at several temperatures. The availability of neutron data from multiple related complexes utilises the possibilities offered by high-throughput neutron diffraction in a different way to those presented earlier.

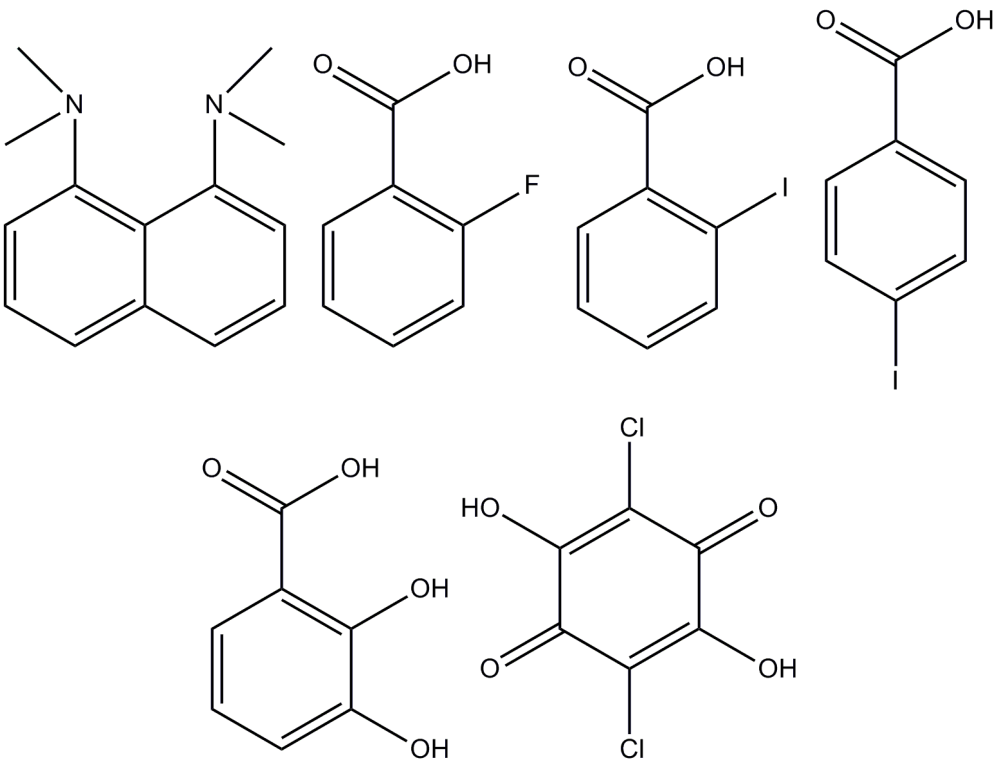

Figure 7.2 *Clockwise from top left: molecular structures of DMAN, 2-fluorobenzoic acid, 2-iodobenzoic acid, 4-iodobenzoic acid, chloranilic acid and 2,3-dihydroxybenzoic acid.*

7.1 Experimental

1:2 Complex of DMAN and 2-fluorobenzoic acid

Large, colourless crystals of the 1:2 complex of DMAN and 2-FBA were grown by slow evaporation from acetonitrile at 50°C. Single crystal neutron diffraction data were collected on VIVALDI at the ILL at 200 K. Structures were refined using SHELXL-97[138] within WinGX[140] taking the X-ray atomic coordinates as a starting model. Crystallographic data are given in **Table 7.1**.

1:2 Complex of DMAN and 2-iodobenzoic acid

Large, colourless crystals of the 1:2 complex of DMAN and 2-IBA were grown by slow evaporation from acetone at room temperature (RT). Single crystal neutron diffraction data were collected on VIVALDI at the ILL at 30, 100, 200 and 300 K. Structures were refined using SHELXL-97[138] within WinGX[140] taking the X-ray atomic coordinates as a starting model. Crystallographic data are given in **Table 7.1**.

1:2 Complex of DMAN and 4-iodobenzoic acid

Large, purple crystals of the 1:2 complex of DMAN and 4-IBA were grown by slow evaporation from acetonitrile at RT. Single crystal neutron diffraction data were collected on VIVALDI at the ILL at 200 K. Structures were refined using SHELXL-97[138] within WinGX[140] taking the X-ray atomic coordinates as a starting model. Crystallographic data are given in **Table 7.1**.

1:1 Complex of DMAN and chloranilic acid

Large, dark red crystals of the 1:1 complex of DMAN and CLA were grown by slow evaporation from methanol at 4°C. Single crystal neutron diffraction data were collected on VIVALDI at the ILL at 200 K. Structures were refined using SHELXL-97[138] within WinGX[140] taking the X-ray atomic coordinates as a starting model. Crystallographic data are given in **Table 7.1**.

1:1 Complex of DMAN and 2,3-dihydroxybenzoic acid

Large, colourless crystals of the 1:1 complex of DMAN and 2,3-DOHBA were grown by slow evaporation from methanol at RT. Single crystal neutron diffraction data were collected on VIVALDI at the ILL at 200 K. Structures were refined using SHELXL-97[138] within WinGX[140] taking the X-ray atomic coordinates as a starting model. Crystallographic data are given in **Table 7.1**.

Table 7.1 *Neutron data collection and refinement information for the DMAN-acid complexes.*[a]

Compound	**1:2 DMAN : 2-FBA**	**1:2 DMAN : 2-IBA**				**1:2 DMAN : 4-IBA**	**1:1 DMAN : CLA**	**1:1 DMAN : 2,3-DOHBA**
Diffractometer	VIVALDI	VIVALDI	VIVALDI	VIVALDI	VIVALDI	VIVALDI	VIVALDI	VIVALDI
Formula	$C_{28}H_{28}F_2N_2O_4$	$C_{28}H_{28}I_2N_2O_4$	$C_{28}H_{28}I_2N_2O_4$	$C_{28}H_{28}I_2N_2O_4$	$C_{28}H_{28}I_2N_2O_4$	$C_{28}H_{28}I_2N_2O_4$	$C_{20}H_{20}Cl_2N_2O_4$	$C_{21}H_{24}N_2O_4$
Molecular weight (g mol^{-1})	494.00	709.80	709.80	709.80	709.80	710.10	422.91	368.00
T (K)	200	30	100	200	300	200	200	200
Space group	*P*-1	*P*-1	*P*-1	*P*-1	*P*-1	$P2_1/n$	*P*-1	*P*-1
***a* (Å)**	10.24	10.41	10.44	10.49	10.53	11.42	9.79	9.89
***b* (Å)**	10.89	11.04	11.08	11.15	11.25	7.75	10.98	9.97
***c* (Å)**	12.68	12.64	12.70	12.79	12.89	30.76	11.09	10.81
***α* (°)**	72.20	68.49	68.47	68.43	68.42	90	111.32	67.53
***β* (°)**	68.80	88.00	88.31	88.69	89.20	96.82	98.30	81.82
***γ* (°)**	89.44	79.61	79.67	79.58	79.50	90	113.52	72.10
Volume (Å^3)	1266.6	1328.6	1343.4	1366.7	1393.8	2703.0	957.53	936.9
Z	2	2	2	2	2	4	2	2
Reflections collected	17110	17180	13238	9879	10143	14102	22901	10773
Independent	3979	5430	4013	2981	2615	2626	5034	2370
Observed > 2σ(I)	2747	4165	3057	2155	1822	2013	3572	1469
Parameters	576	578	578	578	578	578	434	461
GooF	1.09	1.19	1.39	1.31	1.23	1.15	1.09	0.99*
R_1 (observed)	0.0508	0.0400	0.0439	0.0451	0.0444	0.0370	0.0403	0.0463
R_1 (all)	0.0941	0.0675	0.0705	0.0795	0.0822	0.0661	0.0788	0.1053
wR_2 (all)	0.1062	0.0756	0.0868	0.0846	0.0792	0.0675	0.0730	0.0823
Δρ (max, min) / fm/Å^3	0.07, -0.08	0.06, -0.06	0.06, -0.05	0.04, -0.05	0.03, -0.03	0.03, -0.03	0.05, -0.05	0.04, -0.04

[a] *It is not possible to accurately determine unit cell parameters from a Laue experiment at a continuous neutron source so no errors are listed. X-ray determined values are used where available. * GooF values of <1 may arise from the neutron data due to the method of refinement.*

7.2 Molecular Complexes of DMAN and Halobenzoic Acids

7.2.1 DMAN 2-Fluorobenzoic Acid (1:2)

The molecular complex of DMAN and 2-FBA crystallises in the $P\bar{1}$ space group and contains one protonated $DMANH^+$ and a negatively charged 2-FBA dimer in the asymmetric unit (**Figure 7.3**). The $ACID^-$ dimer is located above the N-H···N hydrogen bond of the $DMANH^+$ with interactions between one of the acid oxygens and both the methyl groups and bound proton of $DMANH^+$ (**Figure 7.4**). The proton within the $DMANH^+$ is approximately centred in the N-H···N intramolecular hydrogen bond, while the 2-FBA molecules form an $ACID^-$ dimer through a charge-assisted O-H···O SSHB (**Table 7.2**). The position of the proton in the charge-assisted SSHB of the $ACID^-$ dimer is not centred, being located closer to the 2-FBA molecule which is not directly above the $DMANH^+$ N-H···N hydrogen bond. In both of the 2-FBA molecules the acid groups are twisted out of the plane of the benzene ring at angles of 32.0(3)° for the 2-FBA directly above the $DMANH^+$ and 6.2(5)° for the other acid molecule. The 2-FBA molecules in the $ACID^-$ dimer are not coplanar and are twisted around the short strong hydrogen bond with a torsion angle between the rings of ~86.7° while there are weak, C-H···π (3.622(4) - 3.816(5) Å in length) and C-H···O (3.659(4) Å in length) interactions linking $ACID^-$ dimer units (**Figure 7.5**, left). $DMANH^+$ molecules stack in pairs with π···π interactions between the molecules and a distance of ~3.74 Å between the ring systems (**Figure 7.5**, right). The two molecules are in different orientations, with the methyl groups pointing out from opposite ends of the molecular pair in a head-to-tail motif.

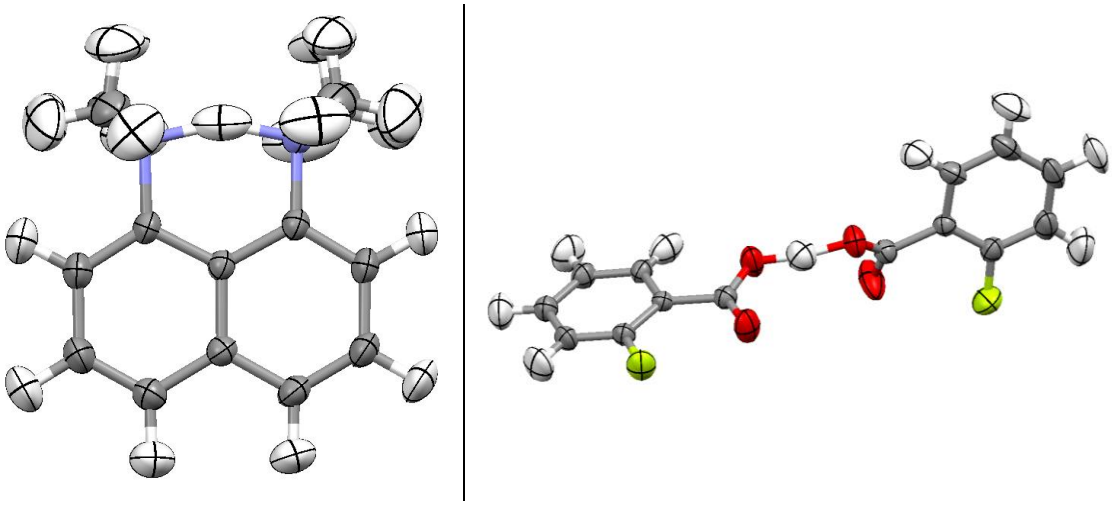

Figure 7.3 *A protonated $DMANH^+$ molecule (left) and the $ACID^-$ dimer containing a charge-assisted, short strong hydrogen bond (right). Taken from the 200 K neutron structure of the 1:2 DMAN 2-FBA complex.*

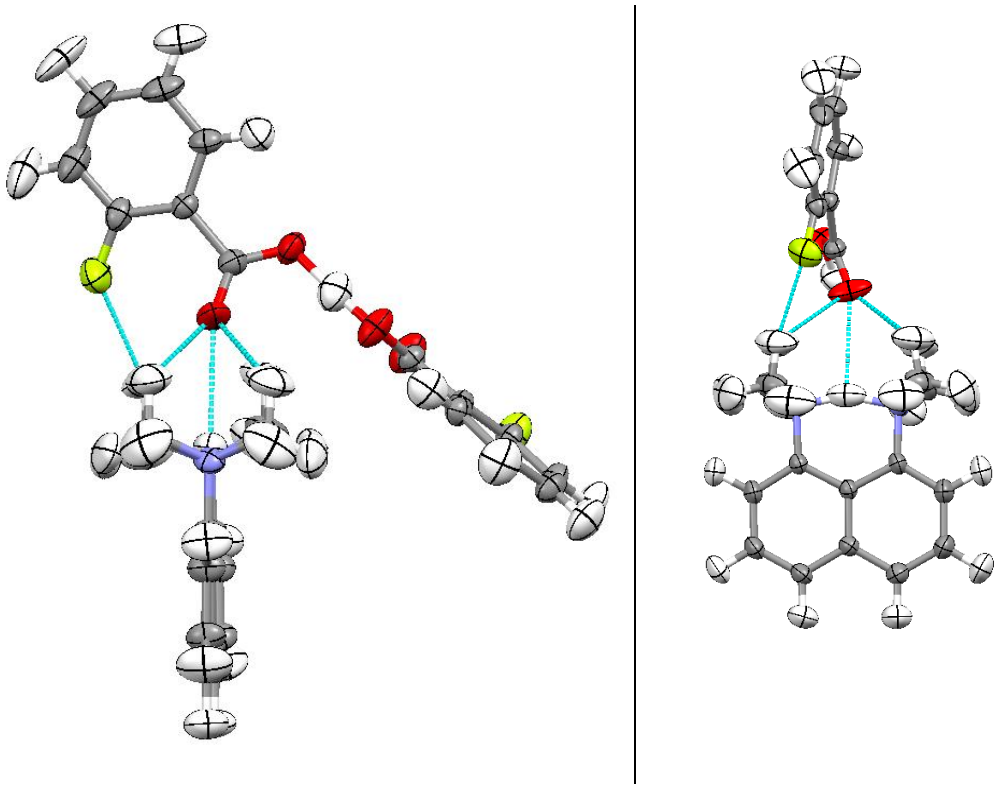

Figure 7.4 *Weak interactions between $DMANH^+$ and a 2-FBA molecule viewed in two orientations. Taken from the 200 K neutron structure of the 1:2 DMAN 2-FBA complex.*

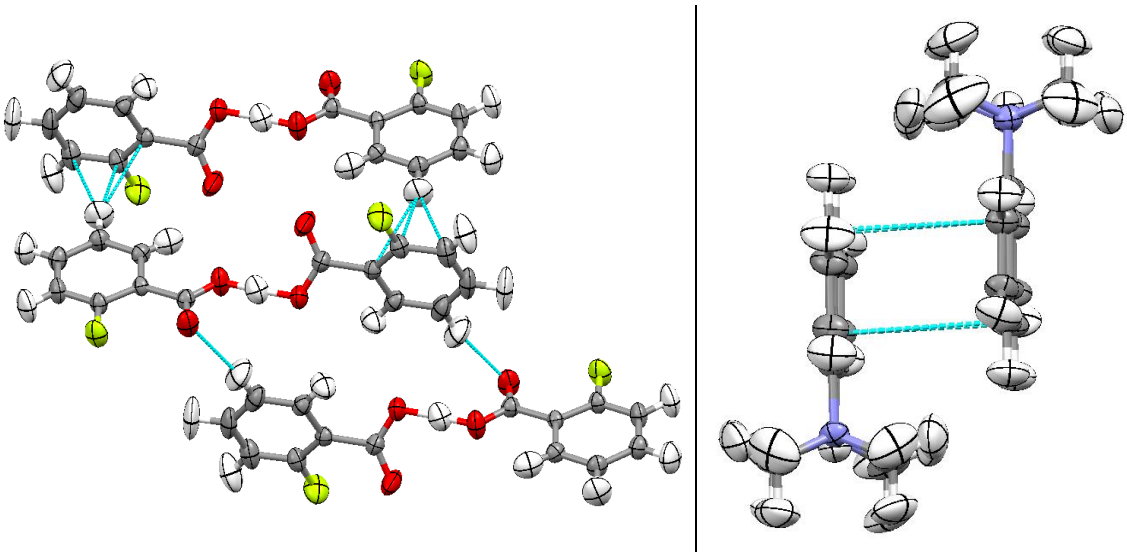

Figure 7.5 *Weak interactions between $ACID^-$ dimers (left) and stacked $DMANH^+$ molecules (right) in the 200 K neutron structure of the 1:2 DMAN 2-FBA complex.*

Table 7.2 *Lengths of the intramolecular and intermolecular hydrogen bonds in $DMANH^+$ and linking the $ACID^-$ dimers in the 1:2 complex of DMAN and 2-FBA at 200 K from the X-ray[125] and neutron data.*

Hydrogen bond	D-H / Å		H···A / Å		D-H···A / Å	
	X-ray	Neutron	X-ray	Neutron	X-ray	Neutron
N-H···N	1.30(3)	1.310(6)	1.35(3)	1.342(6)	2.584(3)	2.595(2)
O-H···O	1.18(3)	1.170(7)	1.27(3)	1.290(7)	2.445(2)	2.453(5)

There are several weak interactions linking the $DMANH^+$ molecules with the $ACID^-$ dimers. A number of these are C-H···π interactions from the ring hydrogen atoms on both $DMANH^+$ and 2-FBA to π electrons of the rings of the other moiety in the complex; these range in length (C···π) from 3.598(4) to 3.966(4) Å. The most important interactions in the context of this investigation are those from the methyl groups and bound proton in the $DMANH^+$ molecule to the 2-FBA molecule located above the N-H···N hydrogen bond in $DMANH^+$. The four C-H···O hydrogen bonds between the methyl groups and acid oxygen above have C···O lengths ranging from 3.230(5) to 3.434(6) Å while the O···H distance between the acid oxygen and the bound proton in the $DMANH^+$ is 2.666(6) Å. The acid oxygen is not located centrally above the N-H···N hydrogen bond, with N···O distances of 3.164(4) and 3.258(4) Å between the nitrogen atoms and the acid oxygen. The longer N···O distance corresponds to the nitrogen atom to which the proton in $DMANH^+$ is more closely associated. In the vicinity of these interactions there is also a methyl C-H···F hydrogen bond with a C···F length of 3.563(4) Å.

7.2.2 DMAN 2-Iodobenzoic Acid (1:2)

The molecular complex of DMAN and 2-IBA also crystallises in the $P\bar{1}$ space group and contains one protonated $DMANH^+$ and a negatively charged 2-IBA dimer in the asymmetric unit (**Figure 7.6**). The $ACID^-$ dimer is again situated above the $DMANH^+$ N-H···N hydrogen bond with interactions between an acid oxygen atom and the methyl groups and bound proton of $DMANH^+$. The N-H···N intramolecular hydrogen bond in $DMANH^+$ is more asymmetric than in the 2-FBA complex with the proton clearly located closer to one side while the 2-IBA molecules form an $ACID^-$ dimer through a charge-assisted SSHB (**Table 7.3**). The proton in the charge-assisted SSHB of the $ACID^-$ dimer is more centred than in the 2-FBA complex and on this occasion lies closer to the acid molecule which is located directly above the N-H···N hydrogen bond of the $DMANH^+$. The

tilt of the acid groups of the 2-IBA molecules is increased compared with those in the 2-FBA complex with angles of 41.5(2)° and 53.6(2)° from the plane of the ring. The rings of the two 2-IBA molecules in the dimer are again not coplanar and the torsion angle around the short strong hydrogen bond is ~114°. $ACID^-$ dimers interact mainly through I···π interactions at distances of 3.562(4) and 3.609(5) Å while there is also a C-H···π interaction with a C···π distance of 3.491(4) Å (**Figure 7.7**, left). Unlike the situation in the 2-FBA complex, the $DMANH^+$ molecules do not interact with one another directly and instead only have interactions to the $ACID^-$ dimer, through C-H···π interactions ranging in distance from 3.528(3) to 3.853(4) Å and weak C-H···O hydrogen bonds between the methyl hydrogen atoms on DMAN and surrounding acid oxygens at distances ranging from 3.254(5) to 3.646(5) Å (**Figure 7.7**, right).

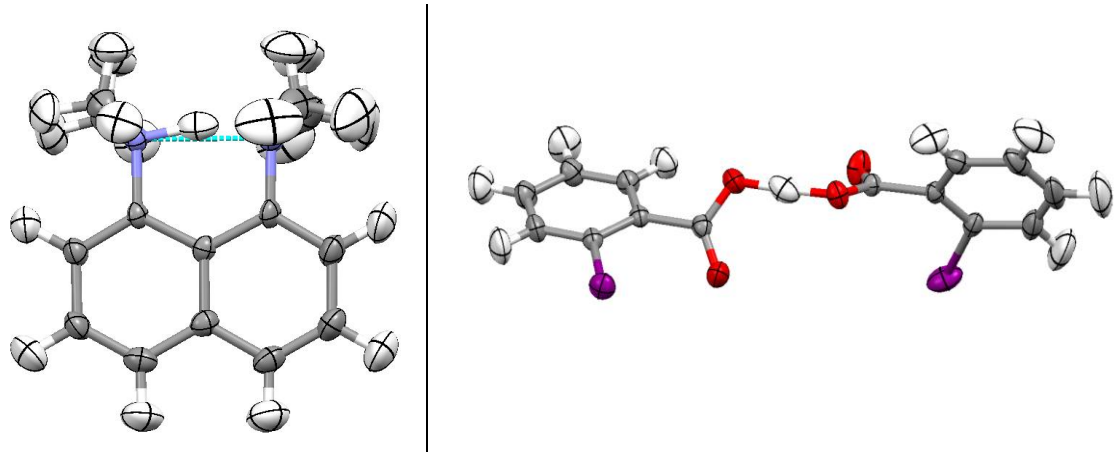

Figure 7.6 *A protonated $DMANH^+$ molecule (left) and the $ACID^-$dimer containing a charge-assisted, short strong hydrogen bond (right). Taken from the 200 K neutron structure of the 1:2 DMAN 2-IBA complex.*

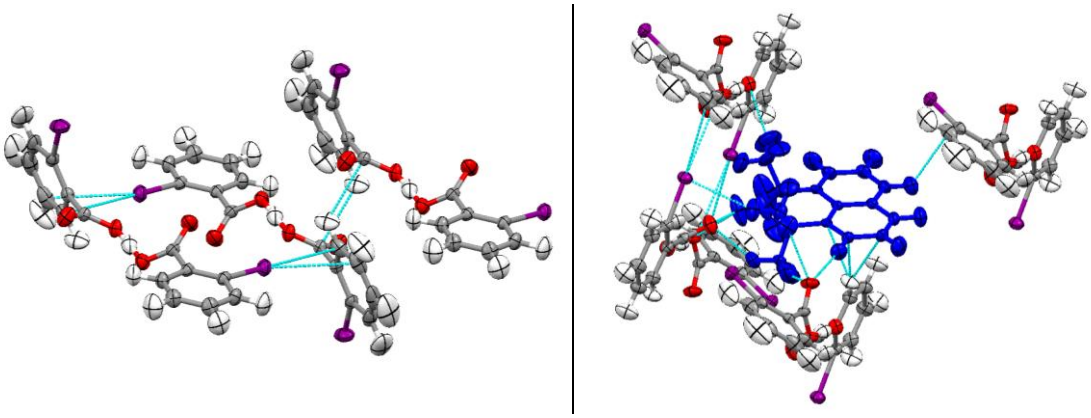

Figure 7.7 *Weak interactions between $ACID^-$dimers (left) and weak interactions between a $DMANH^+$ molecule (blue) and surrounding $ACID^-$ dimers (right). Taken from the 200 K neutron structure of the 1:2 DMAN 2-IBA complex.*

Table 7.3 *Lengths of the intramolecular and intermolecular hydrogen bonds in $DMANH^+$ and linking the $ACID^-$ dimers in the 1:2 complex of DMAN and 2-IBA at 200 K from the X-ray[125] and neutron data.*

Hydrogen bond	D-H / Å		H···A / Å		D-H···A / Å	
	X-ray	Neutron	X-ray	Neutron	X-ray	Neutron
N-H···N	1.13(4)	1.200(7)	1.48(3)	1.417(6)	2.552(4)	2.570(3)
O-H···O	1.13(5)	1.201(5)	1.33(5)	1.265(6)	2.459(3)	2.465(4)

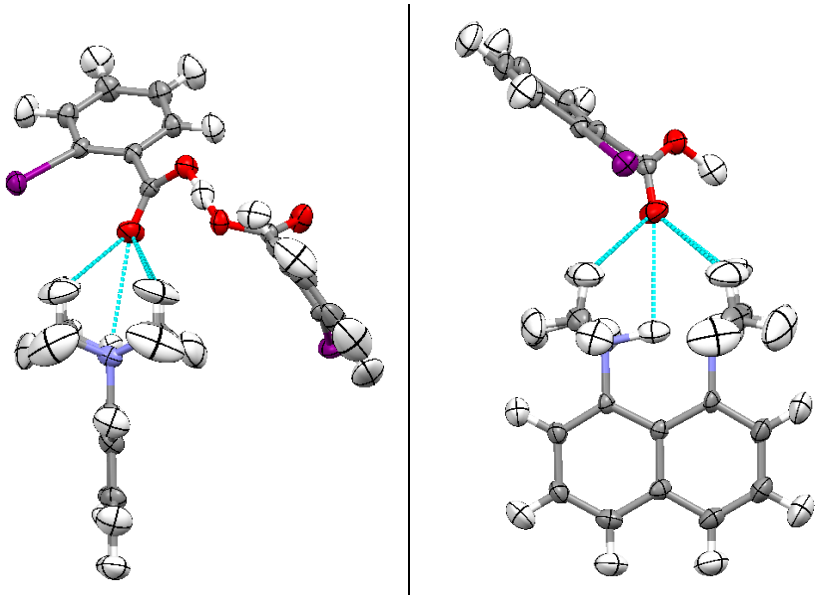

Figure 7.8 *Weak interactions between $DMANH^+$ and a 2-IBA molecule viewed in two orientations in the 200 K neutron structure of the 1:2 complex of DMAN and 2-IBA.*

The $ACID^-$ dimer is located above the N-H···N hydrogen bond in $DMANH^+$ at a distance of 2.912(5) Å between the bound proton and closest acid oxygen, considerably larger than that observed in the 2-FBA complex (**Figure 7.8**). The methyl groups also interact with the same oxygen with four C-H···O contacts with distances ranging from 3.254(5) to 3.646(5) Å. The oxygen atom is located approximately centrally above the $DMANH^+$ molecule with distances of 3.385(3) and 3.434(3) Å between the nitrogens and the acid oxygen. The shorter N···O distance corresponds to the nitrogen atom to which the proton in $DMANH^+$ is more strongly bound.

Variable temperature neutron data were collected for this complex at 30, 100, 200 and 300 K with the 200 K structure being discussed here for comparison with the other

complexes. The only point worth noting from the variable temperature data is the movement of the bound proton in $DMANH^+$ as the temperature is increased. Between 30 and 200 K the position is invariant, but between 200 and 300 K there is a shift of 0.038(11) Å towards a more central position with D-H and H···A distances of 1.200(7) and 1.417(6) Å at 200 K and 1.238(8) and 1.392(7) Å at 300 K while the N···N distance remains invariant. Possible implications of this shift are discussed in **Section 7.5**.

7.2.3 DMAN 4-Iodobenzoic Acid (1:2)

The molecular complex of DMAN and 4-IBA crystallises in the $P2_1/n$ space group and contains one protonated $DMANH^+$ and a negatively charged 4-IBA dimer in the asymmetric unit **Figure 7.9**, left). As in the 2-FBA and 2-IBA complexes, the $ACID^-$ dimer is located above the $DMANH^+$ molecule with interactions between the methyl groups and bound proton of $DMANH^+$ to an acid oxygen atom. The intramolecular N-H···N hydrogen bond of $DMANH^+$ is significantly asymmetric with the proton residing closer to one nitrogen atom than the other (**Table 7.4**). The acid molecules are linked through a charge-assisted O-H···O SSHB where the proton is located closer to the acid molecule that does not interact with the bound proton of $DMANH^+$ (**Table 7.4**). The acid groups of both 4-IBA molecules are tilted out of the plane of the parent rings, at angles of 8.0(6)° and 26.1(2)°. The two molecules in the $ACID^-$ dimer are tilted with respect to each other at an angle of 74.33(8)° measured from the angle between the planes of the two rings (**Figure 7.9**). $ACID^-$ dimers interact with one another through I···I contacts with a length of 3.881(5) Å, forming zigzag chains (**Figure 7.10**, top), while $DMANH^+$ molecules interact with each other through C-H···π interactions with a C···π distance of 3.770(4) Å, between methyl hydrogens and ring electrons of adjacent $DMANH^+$ molecules (**Figure 7.10**, bottom).

Table 7.4 *Lengths of the intramolecular and intermolecular hydrogen bonds in DMAN and linking the 4-IBA dimers in the 1:2 complex of DMAN and 4-IBA at 200 K from the X-ray[125] and neutron data.*

Hydrogen bond	D-H / Å		H···A / Å		D-H···A / Å	
	X-ray	Neutron	X-ray	Neutron	X-ray	Neutron
N-H···N	1.08(3)	1.102(6)	1.57(3)	1.562(6)	2.582(4)	2.602(3)
O-H···O	0.90(7)	1.108(6)	1.57(7)	1.360(5)	2.463(3)	2.465(4)

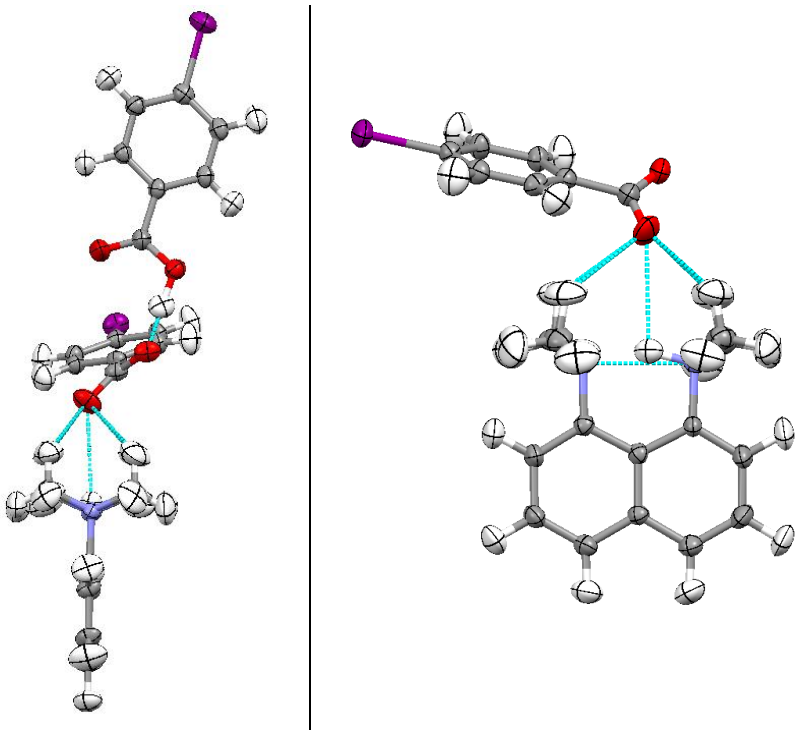

Figure 7.9 *The DMANH+ and ACID⁻ dimer viewed from two orientations showing weak interactions to the bound proton and methyl groups of DMANH+ in the 200 K neutron structure of the 1:2 complex of DMAN and 4-IBA.*

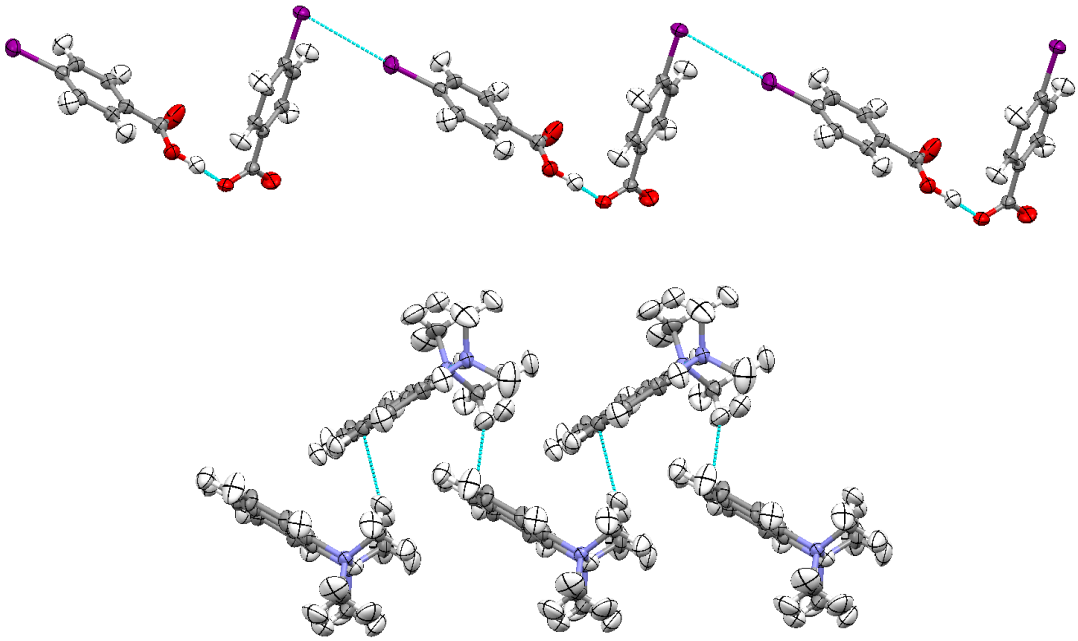

Figure 7.10 *A zigzag chain of ACID⁻ dimers (top) and interactions between DMANH⁺ molecules (bottom) in the 200 K neutron structure of the 1:2 complex of DMAN and 4-IBA.*

.

The interactions between the $DMANH^+$ methyl groups and bound proton to the acid positioned above the $DMANH^+$ moiety are similar to those in the other complexes discussed above. There are four C-H···O interactions between the methyl groups and acid oxygen with C···O distances ranging from 3.235(5) to 3.554(5) Å while the distance between the acid oxygen and bound proton is 2.809(6) Å (**Figure 7.9**, right). The acid oxygen atom is located 3.287(4) and 3.425(4) Å from the two nitrogen atoms, with the shorter distance corresponding to the nitrogen atom to which the bound proton is closer. There are also C-H···π interactions nearby between the methyl hydrogens and the 4-IBA ring electrons at a distance of 3.700(4) and 3.802(4) Å.

7.3 DMAN Chloranilic Acid (1:1)

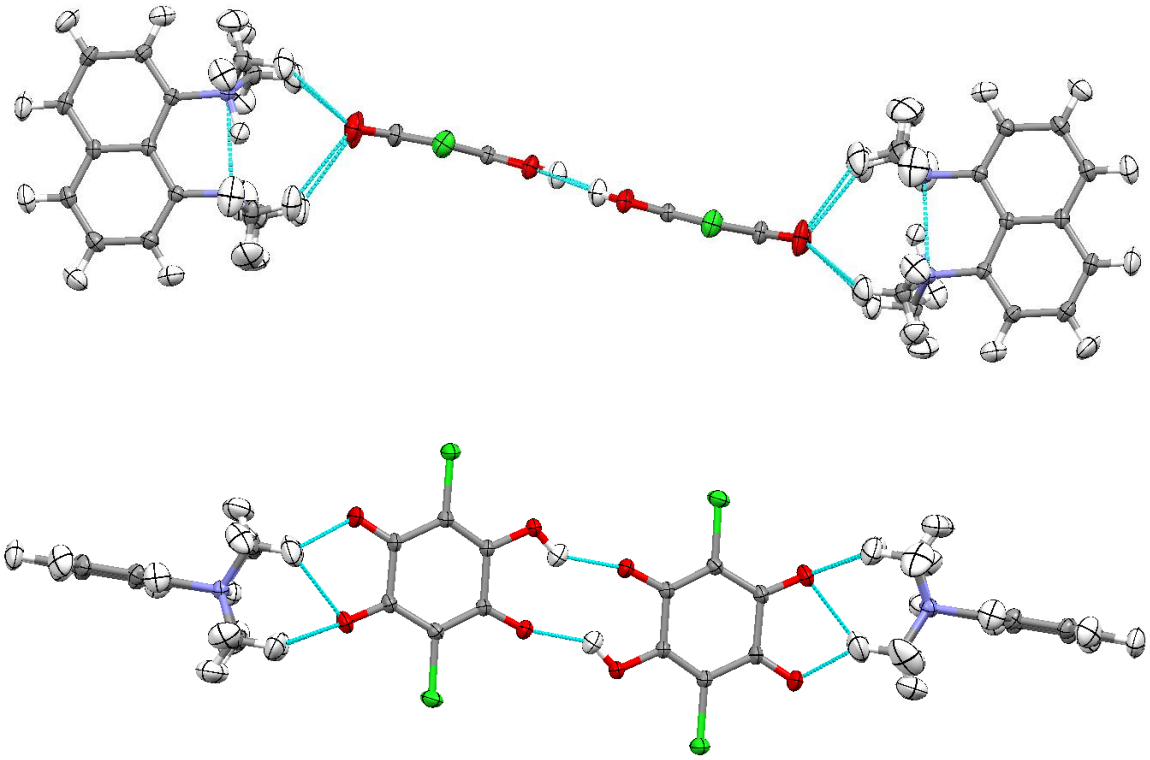

Figure 7.11 *Interactions between protonated $DMANH^+$ molecules and a $ACID^{2-}$ dimer viewed in two orientations in the 200 K neutron structure of the 1:1 complex of DMAN and CLA.*

The molecular complex of DMAN and CLA crystallises in the $P\bar{1}$ space group and contains one protonated $DMANH^+$ and one CLA^- molecule in the asymmetric unit (**Figure 7.11**). The CLA^- molecules form $ACID^{2-}$ dimers held in place by two symmetry equivalent, moderate strength O-H···O hydrogen bonds forming a $R_2^2(10)$ hydrogen bonded ring in a similar manner to that found in other complexes containing singly deprotonated CLA^-

molecules (**Table 7.5**).[18] The molecules in the dimers are approximately coplanar and each CLA^- molecule is located above the N-H···N intramolecular hydrogen bond of $DMANH^+$, interacting with the $DMANH^+$ through the two acid oxygens which are not involved in the O-H···O bonds that link the dimer. The N-H···N hydrogen bond in the $DMANH^+$ molecule is asymmetric, with the proton clearly located closer to one nitrogen atom and away from the centre of the bond.

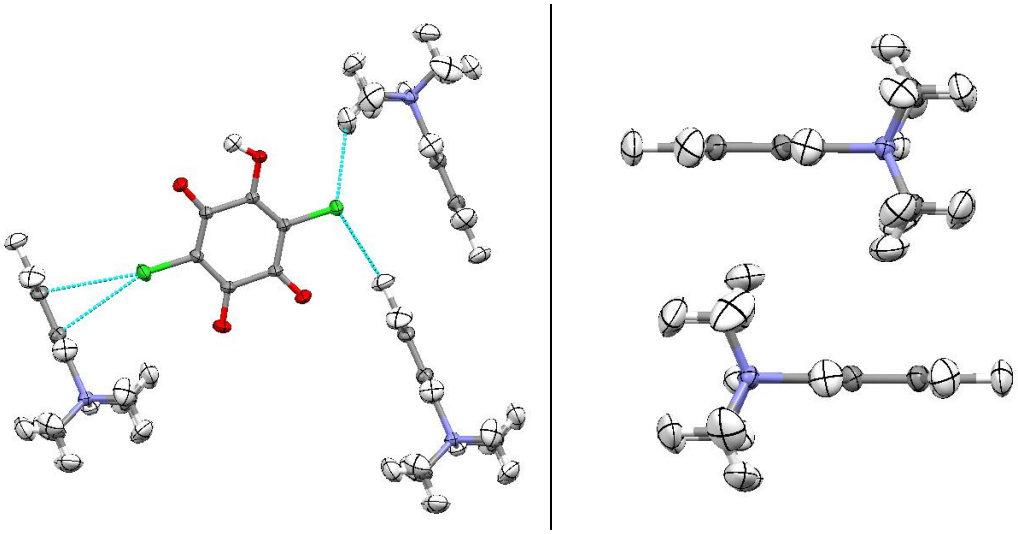

Figure 7.12 *Weak interactions between a CLA^- molecule and surrounding $DMANH^+$ molecules (left) and stacked $DMANH^+$ molecules (right) in the 200 K neutron structure of the 1:1 complex of DMAN and CLA.*

Table 7.5 *Lengths of the intramolecular and intermolecular hydrogen bonds in $DMANH^+$ and linking the $ACID^{2-}$ dimers in the 1:1 complex of DMAN and CLA from the X-ray[125] and neutron data.*[a]

Hydrogen bond	D-H / Å		H···A / Å		D-H···A / Å	
	X-ray	Neutron	X-ray	Neutron	X-ray	Neutron
N-H···N	1.02(2)	1.115(7)	1.64(2)	1.565(2)	2.610(2)	2.6209(10)
O-H···O	0.88(2)	0.968(8)	1.98(2)	1.800(8)	2.748(1)	2.681(5)

[a] *X-ray values were taken from the structure determined at 100 K, neutron values are from the 200 K structure.*

The $ACID^{2-}$ dimers do not interact with each other but are involved in weak interactions to several $DMANH^+$ molecules. These include the interaction to the bound proton in $DMANH^+$ from the two oxygen molecules above the N-H···N hydrogen bond, with one

interacting more strongly than the other, represented by O···H distances of 2.985(3) and 3.716(3) Å. The acid oxygens are also involved in C-H···O interactions with the methyl groups, with C···O distances ranging from 3.129(2) to 3.737(2) Å. The two oxygens are 3.443(2) and 4.001(2) Å from one nitrogen atom (N1) and 3.595(2) and 4.261(2) Å from the other (N2), with the proton in the N-H···N hydrogen bond located on the nitrogen which is closer to the acid oxygens (N1). The CLA^- molecules are also involved in weak C-H···Cl (distances 3.704(2) and 3.944(2) Å) and Cl···π (distances 3.297(1) and 3.3159(9) Å) interactions (**Figure 7.12**, left). $DMANH^+$ molecules are stacked in displaced pairs with a separation of ~4.86 Å (**Figure 7.12**, right) and are also involved in C-H···π interactions to a CLA^- molecule with lengths of 3.537(2) and 3.629(2) Å.

7.4 DMAN 2,3-Dihydroxybenzoic Acid (1:1)

The molecular complex of DMAN and 2,3-DOHBA crystallises in the $P\bar{1}$ space group and contains one protonated $DMANH^+$ and a $2,3\text{-}DOHBA^-$ molecule in the asymmetric unit (**Figure 7.13**). The deprotonated $2,3\text{-}DOHBA^-$ molecule contains an intramolecular O-H···O hydrogen bond and also forms an $ACID^{2-}$ dimer through two symmetry equivalent, moderate strength O-H···O hydrogen bonds which form an $R_2^2(10)$ hydrogen bonded ring in which the two acid molecules are approximately coplanar (**Table 7.6** and **Figure 7.13**, right). The intramolecular N-H···N hydrogen bond in the $DMANH^+$ is asymmetric. An acid molecule is situated above this hydrogen bond, with two oxygens from the acid interacting with the bound proton (H···O distances of 3.053(8) and 3.335(9) Å) and the $DMANH^+$ methyl groups (distances ranging from 3.293(6) to 3.561(7) Å). The distances between the nitrogen atoms of $DMANH^+$ and the acid oxygens are 3.589(5) and 3.745(5) Å for the nitrogen atom closer to the bound proton (N3) and 3.523(5) and 3.929(6) Å for the other (N4). The acid molecule above the $DMANH^+$ also takes part in C-H···O (lengths 3.508(5), 3.560(4), 3.583(4) and 3.591(6) Å) and C-H···π interactions (length 3.722(5) Å) to surrounding $DMANH^+$ molecules. The $DMANH^+$ molecules themselves are again stacked head-to-tail in displaced pairs with a separation of ~4.43 Å between the rings (**Figure 7.14**).

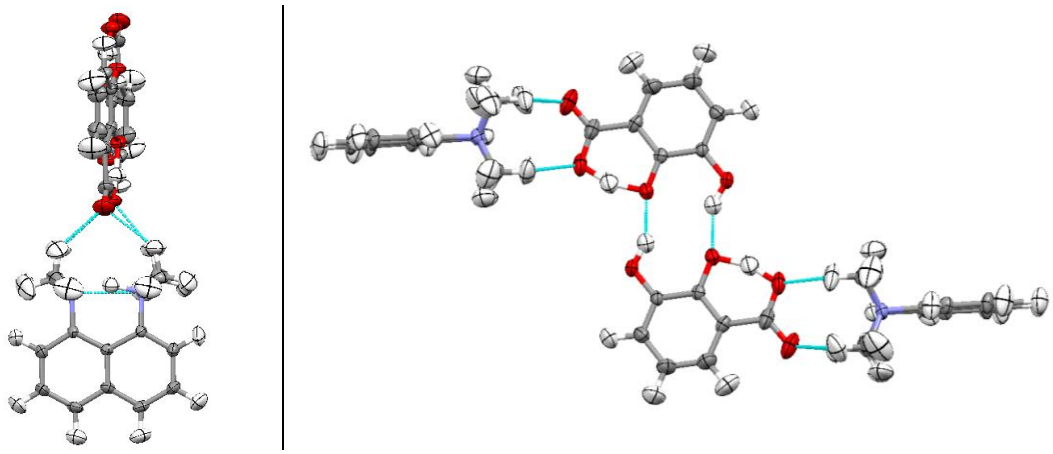

Figure 7.13 *A protonated DMANH^{+} with an ACID^{2-} dimer above viewed in two orientations in the 200 K neutron structure of the 1:1 complex of DMAN and 2,3-DOHBA.*

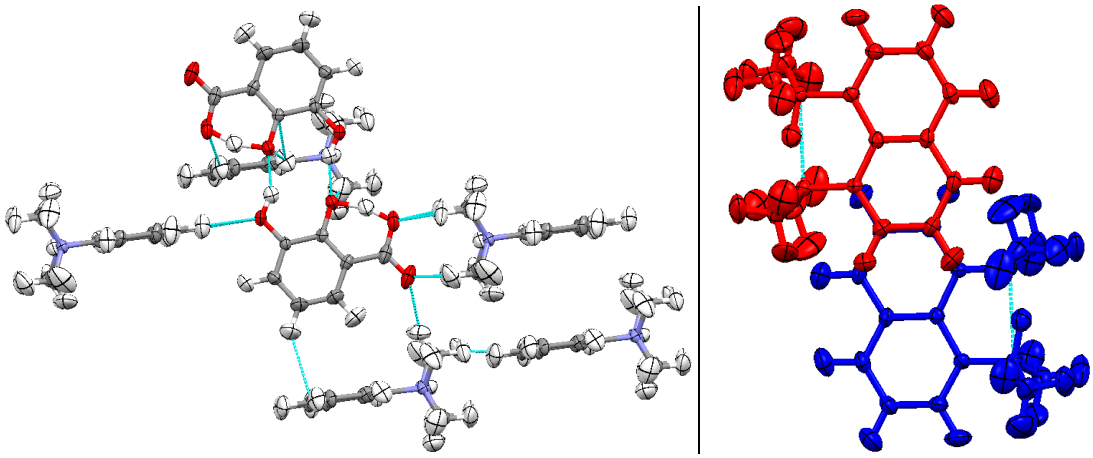

Figure 7.14 *Weak interactions between 2,3-DOHBA^{-} and DMANH^{+} molecules (left) and the displaced stacking of DMANH^{+} molecules in red and blue (right) in the 200 K neutron structure of the 1:1 complex of DMAN and 2,3-DOHBA.*

Table 7.6 *Lengths of the intramolecular and intermolecular hydrogen bonds in the 1:1 complex of DMAN and 2,3-DOHBA at 200 K from the X-ray and neutron data.*

Hydrogen bond	D-H / Å		H···A / Å		D-H···A / Å	
	X-ray	Neutron	X-ray	Neutron	X-ray	Neutron
N-H···N	1.11(2)	1.172(6)	1.53(2)	1.485(6)	2.590(1)	2.600(3)
O-H···O (intra)	1.14(3)	1.173(8)	1.30(2)	1.291(7)	2.422(2)	2.427(5)
O-H···O (inter)	0.88(2)	0.968(8)	1.88(2)	1.800(8)	2.687(1)	2.681(5)

7.5 Hydrogen Atom Behaviour in DMAN-Acid Complexes

The use of neutron data to study these DMAN complexes allows several elements of the structures related to the hydrogen atom behaviour to be studied in detail. These are:

- The level of interaction between the acid oxygens positioned above the N-H···N hydrogen bond in $DMANH^+$ and the bound proton in this interaction; i.e. can a limit be determined at which there is no longer a significant effect on the behaviour of a hydrogen atom resulting from the proximity of an electronegative atom?;
- How the position of the proton in the N-H···N hydrogen bond of the protonated $DMANH^+$ molecules can be related to other elements of the structure;
- Whether the position of the proton in the charge-assisted, short strong O-H···O hydrogen bonds linking halobenzoic acid molecules can be related to other elements of the structure.

The investigation of these properties is only possible through the unambiguous and accurate hydrogen positions which can be determined from the single crystal neutron diffraction data.

7.5.1 Over What Range is a Weak Hydrogen Bond Significant?

From the five complexes presented here, the three complexes of DMAN with halobenzoic acids have one oxygen atom interacting with the bound proton in $DMANH^+$, while the complexes with CLA and 2,3-DOHBA have two oxygens involved in the interaction. The interactions between the bound proton and the acid oxygens occur with different lengths in each complex, with O···H distances ranging from 2.666(6) Å in the 2-FBA complex to 3.716(3) Å in the CLA complex. This range of values means that the level of interaction between the oxygen and hydrogen can be assessed in each complex and it may be possible to define a limit where, in the case of these complexes at least, there is no longer a significant interaction between the oxygen atom and bound hydrogen. This is effectively investigating the maximum range over which a weak hydrogen bond is significant. The observation that the acid oxygen atom interacts with the methyl groups and bound proton of the $DMANH^+$ may be related to the fact that the two species are charged. The overall positive and negative charges on the $DMANH^+$ and acid molecules, respectively, leads to a strong interaction between the two species which leads to the formation of the close contact between the acid oxygen and $DMANH^+$.

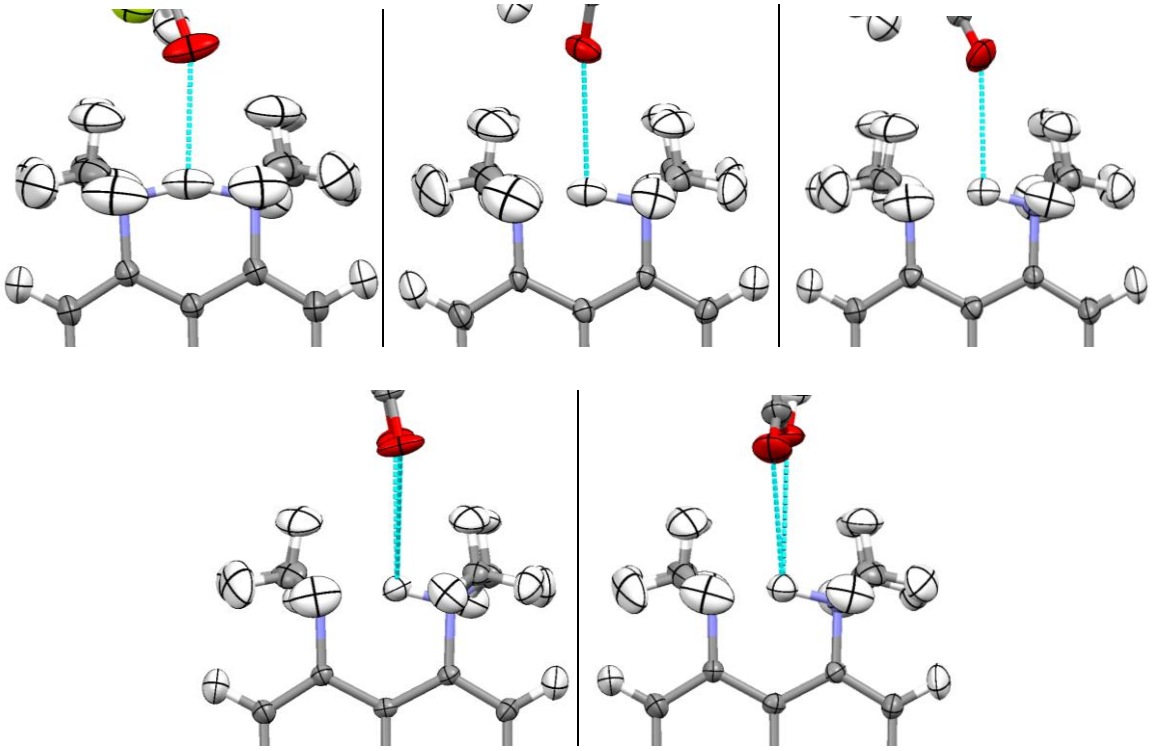

Figure 7.15 *Interactions between the bound protons in $DMANH^+$ and the acid oxygens. Clockwise from top left: DMAN complexes with 2-FBA, 2-IBA, 4-IBA, 2,3-DOHBA and CLA.*

Theoretical studies of the potential energy surfaces in which the bound protons of proton sponges reside suggests that for an N-H···N hydrogen bond with a short N···N distance, the potential is either a flat, single minimum or a double-well potential with a very low energy barrier between the two positions.[192] In both of these cases the potential is quite flat, meaning that the proton can readily move along the bond with only minimal energy input required. In the five DMAN complexes presented here, the N···N distances in the protonated $DMANH^+$ are very short for N-H···N hydrogen bonds, with distances ranging from 2.570(3) to 2.6209(10) Å. As these structures have been determined at 200 K, the thermal displacement parameters of the hydrogen atom within the hydrogen bond should be well defined and the expected elongation of the density along the direction of the hydrogen bond may be observed; in fact a range of values is observed for the size of the thermal ellipsoids, and of the corresponding anisotropic displacement parameters, of the hydrogen atom (**Table 7.7** and **Figure 7.15**).

Table 7.7 *Distances between the bound protons in $DMANH^+$ and the acid oxygens above the N-H···N hydrogen bond listed with the largest principal thermal parameters of the bound proton. The two values for the CLA and 2,3-DOHBA complexes correspond to the two oxygens which interact with the bound proton.*

Complex	O···H / Å	U_1 hydrogen / Å^2
2-FBA	2.666(6)	0.1087
4-IBA	2.809(6)	0.0477
2-IBA	2.912(5)	0.0647
CLA	2.985(3)	0.0388
	3.716(3)	-
2,3-DOHBA	3.053(8)	0.0467
	3.355(9)	-

Of all the structures, the complex of DMAN with 2-FBA has the largest anisotropic displacement parameter for the bound proton. This complex also has the shortest O···H distance and the oxygen has a significantly anisotropic displacement parameter, elongated along the direction of the hydrogen bond (**Table 7.7** and **Figure 7.15**). It appears that the relatively short distance between the bound proton and the acid oxygen leads to a significant interaction between the two and results in a correlated movement along the direction of the N-H···N hydrogen bond. It is not possible to determine if the movement of the proton within the flat potential causes the oxygen to move or if the movement of the oxygen causes the proton to move, but the behaviour of the two atoms appears to follow the same trend.

The next closest interaction is in the complex with 4-IBA; here the displacement parameters – representative of the possible movement – of the proton are much smaller and the equivalent parameters of the oxygen, whilst still significantly elongated, is no longer along the direction of the N-H···N hydrogen bond. This would suggest that in the case of the complex with 2-FBA, the movement of the bound proton is perhaps more a consequence of the movement of the oxygen than the other way round. A similar observation is made in the complex with 2-IBA which has the next longest interaction. There is still a significant elongation of the oxygen atom displacement ellipsoid, though again not along the direction of the bond, but a reduced effect on the bound proton in $DMANH^+$ (though this is greater than in the complex with 4-IBA). It may be that the longer distance between the bound proton and acid oxygen in this complex is now too large for

the oxygen atom to have a significant influence on the behaviour of the bound proton. If this is the case the distance limit within which the oxygen atom can have a significant effect on the behaviour of a proton may be in the region of ~2.67 - 2.81 Å.

In the complexes with CLA and 2,3-DOHBA, the situation is slightly different due to the presence of a second oxygen atom interacting with the $DMANH^+$. In both cases the proton has smaller anisotropic displacement parameters than found in the complexes with 2-FBA and 2-IBA. This could potentially be the result of the additional interaction stabilising the proton in the SSHB. However, in both of these complexes, the two oxygen atoms are located much further from the bound proton than in the other complexes and this distance may be too great for the oxygens to have a significant influence on the behaviour of the bound proton.

Although this study represents one of the most comprehensive neutron diffraction investigations of DMAN acid complexes, the effects are subtle and with the limited number of examples investigated it is not possible to draw any definitive conclusions from these results. What does appear clear is that in the 2-FBA complex, where the acid molecule is closest to the $DMANH^+$, the anisotropic displacement parameters of both the bound proton and the acid oxygen are largest and elongated in the same direction, suggesting an interaction between the two. In the other complexes, where the distance between the $DMANH^+$ and the acid is greater, the behaviour of the oxygens and bound protons is no longer obviously correlated. It is probable that the behaviour of the bound proton would be influenced by the oxygen atom above the N-H···N hydrogen bond if close enough (e.g. in the complex with 2-FBA), but the behaviour will also be significantly affected by the shape of the potential energy surface in which it resides (which is also affected by the presence of the oxygen atom) and also by other weak interactions in the neighbouring electronic environment. As these N-H···N hydrogen bonds are very short, the potentials should be quite flat so the proton should be able to move along the bond fairly easily and therefore any interactions in the local environment can play a role in determining the behaviour of the hydrogen atom.

7.5.2 The Position of the Proton in the N-H···N Hydrogen Bond of $DMANH^+$

In the X-ray determinations of the five complexes presented here, locating the hydrogen atom within the intramolecular N-H···N hydrogen bond of the protonated $DMANH^+$ proved difficult. This is due to the elongation of the hydrogen atom electron density in the bond and, in the cases of some complexes with halobenzoic acids, the presence of heavy atoms in the structure (**Tables 7.2 - 7.6**).[125] This shows the importance of using neutron

diffraction when studying these structures and with the hydrogen atoms accurately located in the neutron structures, it is now possible to examine the possible causes of the common asymmetry of the N-H···N hydrogen bond (**Figure 7.16**). In an isolated $DMANH^+$ molecule, it would be expected that the hydrogen atom within the N-H···N hydrogen bond would appear to be located centrally.[192] However, a close to centred proton is only found in the complex of DMAN with 2-FBA (**Table 7.8**). It is therefore likely that other interactions are playing a role in determining the lowest energy position of the proton within the hydrogen bond, similar to the effects discussed in the proton disorder systems of **Chapter 6**.

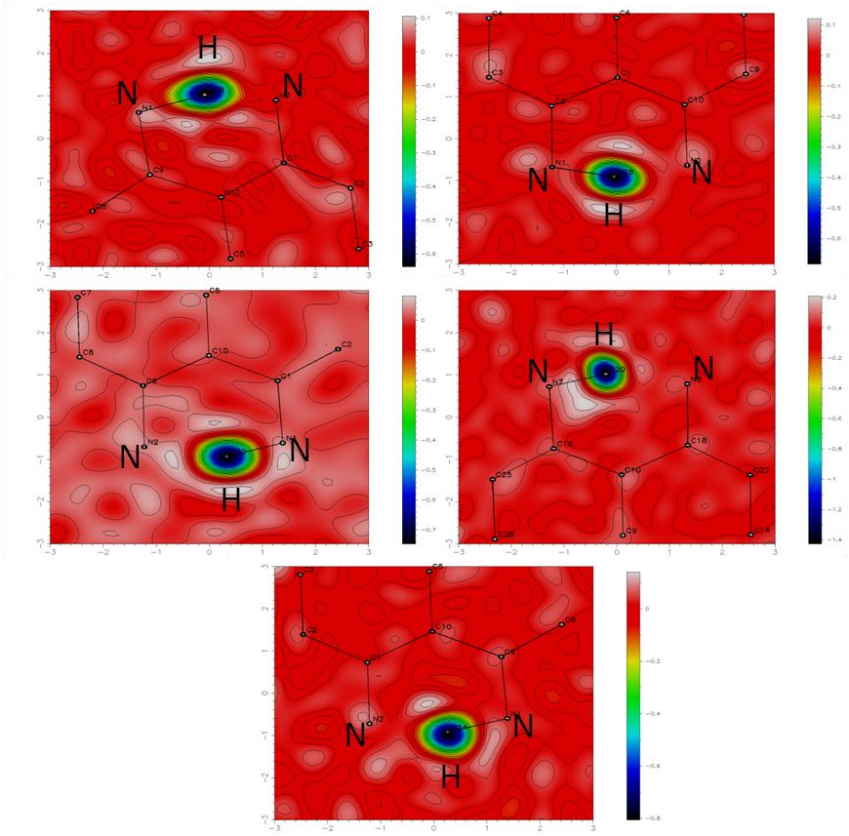

Figure 7.16 *Fourier difference maps of the DMANH+ N-H···N intramolecular hydrogen bond showing the hydrogen atom nuclear density in the complexes of DMAN with 2-FBA (top left), 2-IBA (top right), 4-IBA (centre left), CLA (centre right) and 2,3-DOHBA (bottom), taken from the 200 K neutron structures.*

Table 7.8 *Hydrogen bond distances for the intramolecular N-H···N bond in the $DMANH^+$ molecule in the DMAN acid complexes from the 200 K neutron structures.*

Complex	N-H / Å	H···N / Å	N-H···N / Å
2-FBA	1.310(6)	1.342(6)	2.595(2)
2-IBA	1.200(7)	1.417(6)	2.570(3)
4-IBA	1.102(6)	1.562(6)	2.602(3)
CLA	1.115(7)	1.565(2)	2.6209(10)
2,3-DOHBA	1.172(6)	1.485(6)	2.600(3)

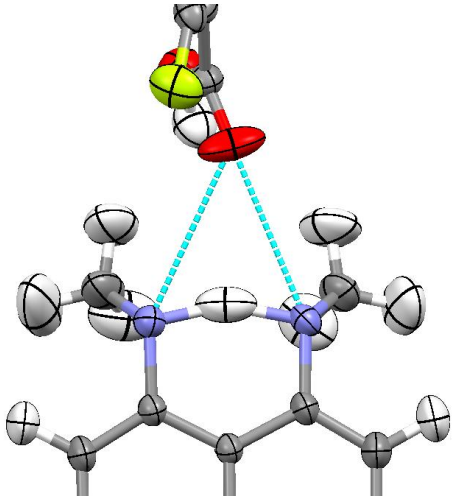

Figure 7.17 *The distances between the $DMANH^+$ nitrogen atoms and the acid oxygen positioned above the $DMANH^+$ in the DMAN 2-FBA complex. Methyl groups have been removed for clarity.*

The most obvious interaction which may affect the behaviour of the hydrogen atom in the N-H···N hydrogen bond is that with the acid oxygen located above the hydrogen bond, as discussed in **Section 7.5.1**. While in all the complexes the acid molecules are located above the $DMANH^+$, this does not mean they are located centrally. An estimate of how centrally the acid molecule is located above the $DMANH^+$ can be made by measuring the distances between the nitrogen atoms and the acid oxygens which interact with the bound proton (**Figure 7.17**). In the case of 2-FBA, where the proton is close to the centre of the bond, the distances between the two nitrogen atoms and the acid oxygen are 3.164(4) and 3.258(4) Å, with the hydrogen atom found closer to the nitrogen which is further from the oxygen. It might be expected that the proton would instead be located closer to the

nitrogen nearest the oxygen due to the attractive interaction to the oxygen affecting the shape of the potential energy surface of the intramolecular hydrogen bond and hence the location of the hydrogen atom. This is not, however, the case in the 2-FBA complex, and contributions from other weak interactions may also play a part. In particular, the interactions to each of the fused rings of the $DMANH^+$ molecule are asymmetric and this could lead to one side of the N-H···N hydrogen bond being favoured over the other.

The asymmetry of the weak interactions to the two sides of the DMAN molecule is a feature in the structures of all five DMAN complexes presented here. While these interactions could play a role in determining the energetics of the N-H···N hydrogen bond in the complexes, the interaction between the bound proton and the oxygens above the hydrogen bond also plays a part. This may be evidenced by the fact that, in the four other complexes, the hydrogen atom within the N-H···N hydrogen bond is located closer to the nitrogen atom nearest to the oxygen above. In the 2-IBA complex the distances between the two nitrogen atoms and the acid oxygen are 3.385(3) and 3.434(3) Å, while in the complex with 4-IBA the distances are much more asymmetric with distances of 3.287(4) and 3.425(4) Å; in both cases the hydrogen atom in the N-H···N hydrogen bond is located closer to the nitrogen nearest the oxygen atom.

In the complex with CLA, where there are two oxygen atoms from the acid molecule interacting with the bound proton of $DMANH^+$, the distances between the nitrogens and oxygens are 3.443(2) and 4.001(2) Å for one nitrogen (N1) and 3.595(2) and 4.261(2) Å for the other (N2). In this case the proton is more strongly bound to N1, which is closer to both the oxygen atoms than N2. In the complex with 2,3-DOHBA, where there are again two oxygens above the $DMANH^+$, the distances between the nitrogen atoms and the acid oxygens are 3.589(5) and 3.745(5) Å for one nitrogen (N3) and 3.523(5) and 3.929(6) Å for the other (N4); the proton within the N-H···N hydrogen bond is closer to N3. While the shortest distance between a nitrogen and oxygen in the structure is found for N4, the fact that the distance between the second oxygen and N3 is considerably longer than for N4 (3.929(6) Å compared to 3.745(5) Å) could play a role in determining on which side of the N-H···N hydrogen bond the proton resides.

It is worth noting here that in the variable temperature neutron structures of the complex with 2-IBA, the one structural feature which displays potentially interesting behaviour on changing the temperature is the behaviour of the N-H···N hydrogen bond in $DMANH^+$. Between 30 and 200 K, the position of the proton within the hydrogen bond is invariant. However, between 200 and 300 K the proton appears to shift towards the centre of the

bond, with the D-H distance changing from 1.195(7) to 1.238(8) Å and the H···A distances changing from 1.412(6) to 1.392(7) Å, while the D···A distance remains invariant. As this shift is only seen in one of the structural determinations it is difficult to confirm its significance, though the amount of migration does appear to be large. However, this could also be the result of changes in the weak interactions which occur on the expansion of the system with increasing temperature changing the shape of the potential energy surface of the N-H···N hydrogen bond.

While it is difficult to draw definitive conclusions from this limited data set, the fact that the hydrogen atom within the N-H···N intramolecular hydrogen bond of $DMANH^+$ is not centred in the majority of the complexes must be a consequence of weak interactions affecting the hydrogen bond energetics. The position of the proton is likely affected by interactions to the hydrogen bond from the acid molecule above and also interactions to the $DMANH^+$ molecule itself.

7.5.3 The Position of the Proton in the Charge-Assisted Hydrogen Bonds

In the three 1:2 complexes of DMAN with halobenzoic acids, the acid molecules form dimers with an overall negative charge. The charge on the dimers is stabilised through interactions with other molecules in the crystal structure and through the formation of charge-assisted O-H···O SSHBs linking the acid molecules in the dimers. In the absence of other interactions to the acid molecules, one of the lower energy structures may involve the hydrogen atom being shared equally between the two acids to give the greatest stabilisation to each molecule, in effect having half a negative charge on each acid molecule. However, the hydrogen is not observed to be shared centrally between the two acid molecules, with the hydrogen atom position being closest to the centre of the hydrogen bond in the dimer in the complex of DMAN with 2-IBA (**Table 7.9**). This may be evidenced by the hydrogen atom position and also potentially from the nominal C-O and C=O distances of the acid groups, where values for the two bond distances which are close in length would indicate the presence of a delocalised negative charge and hence less bonding with the hydrogen atom. The fact that these hydrogens atoms are not shared equally between the two molecules shows the effect of the weak interactions on the acid dimer. In this section, the acid molecules in the dimers are denoted ***x*** and ***y***. Acid ***x*** is the acid molecule located above the $DMANH^+$ N-H···N intramolecular hydrogen bond that interacts directly with the $DMANH^+$ methyl groups and bound proton. Acid ***y*** is the other acid molecule in the dimer that does not interact directly with the $DMANH^+$ methyl groups and bound proton (**Figure 7.18**).

Table 7.9 *Hydrogen bond distances for the charge-assisted short, strong hydrogen bonds in the halobenzoic acid dimers from the 200K neutron structures. (a) represents the oxygen of the acid molecules interacting with the bound proton of $DMANH^+$ while (b) is the other acid molecule of the dimer which is not positioned above the $DMANH^+$.*

Complex	O···H / Å (a)	O···H / Å (b)	O-H···O / Å
2-FBA	1.290(7)	1.170(7)	2.453(5)
2-IBA	1.201(5)	1.265(6)	2.465(4)
4-IBA	1.360(5)	1.108(6)	2.465(4)

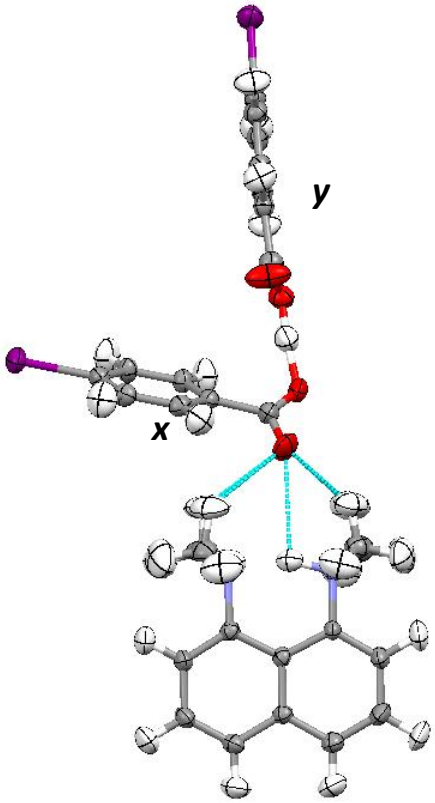

Figure 7.18 *A $DMANH^+$ molecule and a 4-IBA dimer containing a short, strong charge-assisted hydrogen bond with the **x** and **y** acid molecules labelled.*

Of the weak interactions discussed so far in this chapter, among the most important have been the interactions between the acid oxygen above the $DMANH^+$ N-H···N intramolecular hydrogen bond and the bound proton and $DMANH^+$ methyl groups. The complex of DMAN with 2-FBA has the acid ***x*** located closest to the $DMANH^+$, with a distance of 2.666(6) Å between the oxygen atom and bound proton of $DMANH^+$. The C-O distances for acid ***x*** are 1.219(4) and 1.270(4) Å, while they are 1.208(5) and 1.282(4) Å for acid ***y***,

showing no significant difference in C-O distances for the two acids. In this complex both acid molecules in the dimer are involved in C-H···O and C-H···π interactions, while the acid ***x*** closest to the $DMANH^+$ molecule has increased stabilisation from its interactions with the $DMANH^+$ methyl groups and the bound proton. This increased stabilisation of the acid molecule interacting with $DMANH^+$ plays a role in the observation that the hydrogen atom of the charge-assisted SSHB linking the dimers is located closer to the acid ***y*** which does not have the added stabilisation of the interactions with $DMANH^+$ (**Table 7.9**).

In the DMAN complex with 4-IBA, the $DMANH^+$ molecule is located further from acid ***x*** than in the complex with 2-FBA, though closer than in the complex with 2-IBA, with a distance of 2.809(6) Å between the acid oxygen and bound proton in $DMANH^+$. The stabilisation due to interactions with the $DMANH^+$ is therefore reduced when compared with the DMAN complex with 2-FBA. The C-O distances for acid ***x*** are 1.230(4) and 1.271(3) Å, while they are 1.209(5) and 1.291(3) Å for acid ***y***, supporting the observation that the hydrogen atom interacts more strongly with acid ***y***. In the complex with 4-IBA, the acid ***x*** located above the $DMANH^+$ N-H···N hydrogen bond is involved in C-H···O, C-H···π and I···I interactions while the acid ***y*** in the dimer is involved in C-H···O and C-H···π interactions. The increased stabilisation through the interaction with $DMANH^+$ again plays a role in the hydrogen atom in the charge-assisted SSHB being located closer to the acid ***y*** which does not interact with the $DMANH^+$ (**Table 7.9**).

The complex of DMAN with 2-IBA is the only complex where the hydrogen atom in the charge-assisted SSHB is located closer to the acid ***x*** which is directly above the $DMANH^+$ N-H···N hydrogen bond (**Table 7.9**). The distance between the acid ***x*** and $DMANH^+$ is longer than in the other complexes, at 2.912(5) Å, and the amount of stabilisation gained from the interactions with $DMANH^+$ is reduced compared with the two other complexes. The C-O distances for acid ***x*** are 1.224(3) and 1.284(3) Å, while they are 1.215(4) and 1.272(4) Å for acid ***y***, again showing no significant difference between the two acids. Both acid molecules are involved in C-H···π and I···π interactions, with the weaker interactions from the $DMANH^+$ to the acid ***x*** playing a role in the location of the hydrogen atom of the charge-assisted SSHB with respect to the neighbouring molecules.

The complexes of DMAN with acids presented here contain only two hydrogen bonds which could be classed as strong or moderate, the intramolecular N-H···N hydrogen bond in $DMANH^+$ and the O-H···O hydrogen bond linking the acid dimers; in some cases the latter is a charge-assisted SSHB. All other interactions within these complexes fall into the category of “weak” and these systems represent a useful way to investigate the effect

of these weak interactions on certain aspects of the crystal structure. While in **7.5.1** and **7.5.2** the effect of the acid oxygens on the bound proton within the $DMANH^+$ molecules was investigated; here it is shown that the weak interactions to the acid molecules also play a role in the location of the proton within the charge-assisted hydrogen bonds that link the acid molecules in the dimers. Were only X-ray data to be collected on these complexes, the only method for gauging which acid molecule the hydrogen atom is located closest to would be through analysis of C-O bonds in the acids, due to the difficulties in accurately locating hydrogen atoms from X-ray data. The results here show that in many cases the differences in C-O bond lengths are too small to be considered significant, therefore highlighting the importance of the neutron studies.

7.6 Conclusions

Five complexes of DMAN with organic acids have been studied using single crystal neutron diffraction. The complexes have either a 1:1 or 1:2 DMAN:acid stoichiometry and in all structures a proton is transferred from an acid to DMAN to form a strong N-H···N intramolecular hydrogen bond within the anticipated $DMANH^+$ molecule. The acid molecules form dimers in which an acid molecule is located above the N-H···N hydrogen bond in $DMANH^+$, interacting with the $DMANH^+$ methyl groups and the bound proton. The accurate hydrogen positional and thermal displacement parameters determined from the neutron diffraction data have allowed the effect of weak interactions on the behaviour of hydrogen atoms within the structure to be investigated.

The thermal motion of the bound proton in $DMANH^+$ and the nearest acid oxygen were found to correlated in the complex of DMAN with 2-FBA, which has the shortest distance between the $DMANH^+$ N-H···N hydrogen bond and the acid oxygen. In the other complexes the distance was greater and no obvious correlation was found. It seems likely that the thermal behaviour of the hydrogen atom within the intramolecular N-H···N hydrogen bond will be most significantly affected by two factors. The first is the shape of the potential in which the hydrogen atom resides; as these hydrogen bonds are very short, this is most likely to be either a single flat minimum or a double-well minimum with a low energy barrier between the positions.[192] These potentials are both fairly flat and the hydrogen atom should be able to move relatively freely within the hydrogen bond. The other factor that may influence the behaviour is the interaction with the acid oxygen, when it is sufficiently close. An obvious correlation is only observed in the complex with 2-FBA so it may be that above a distance of ~2.67 Å, the effect of the oxygen on the hydrogen atom thermal behaviour is no longer significant. However, the fact that the thermal motion

of the oxygen atoms in the other complexes is not along the direction of the N-H···N hydrogen bond affects this conclusion and may also have an effect.

The effect of weak interactions on the location of the hydrogen atom within the N-H···N hydrogen bond has also been investigated. These hydrogen bonds are often asymmetric, with only the complex with 2-FBA showing an approximately symmetric hydrogen bond. The acid molecules interacting with this bond are not centred over the bond and the interactions between the two may play a role in determining if the position of the proton in the intramolecular hydrogen bond is favoured towards one nitrogen atom. Interactions to each side of the $DMANH^+$ molecules were also found to be asymmetric and these could also play a role in determining the lowest energy position of the hydrogen atom within the N-H···N hydrogen bond by subtly affecting the energetics of the $DMANH^+$ molecules themselves.

Finally, weak interactions also appear to play a role in the position of the proton in the charge-assisted short strong O-H···O hydrogen bonds formed between acid molecules in the complexes of DMAN with halobenzoic acids. The hydrogen atoms within these bonds were not found to be equally shared between the two molecules, with the weak interactions perhaps acting to stabilise one acid molecule more than the other therefore causing the proton in the charge-assisted hydrogen bond to reside closer one acid molecule.

While there are only five examples presented here, analysing various aspects of the structures show that weak interactions may subtly affect the energetics of molecules within the solid-state and could have an effect of various aspects of the crystal structures, continuing on from the work presented in previous chapters. With a greater number of examples where neutron data has been collected, and by possibly supplementing these results with theoretical calculations, it may be possible to quantify the effect of the weak interactions and therefore produce more reliable methods for predicting the subtle properties of solid-state complexes.

Chapter 8

8. Other Complexes of Urea and Substituted Ureas with Organic Acids

This chapter deals with a range of complexes of urea and substituted ureas with organic acids that have been synthesised and structurally characterised. The structures presented again underline the versatility of ureas as a tool in crystal engineering, showing a variety of crystal packing motifs and hydrogen bond architectures.

Urea, *N*-methylurea and *N*,*N*-dimethylurea have been complexed with picolinic acid, 4-hydroxybenzoic acid (4-OHBA), 2,4-dihydroxybenzoic acid (2,4-DOHBA), chloranilic acid (CLA) and bromanilic acid (BRA) (**Figure 8.1**).

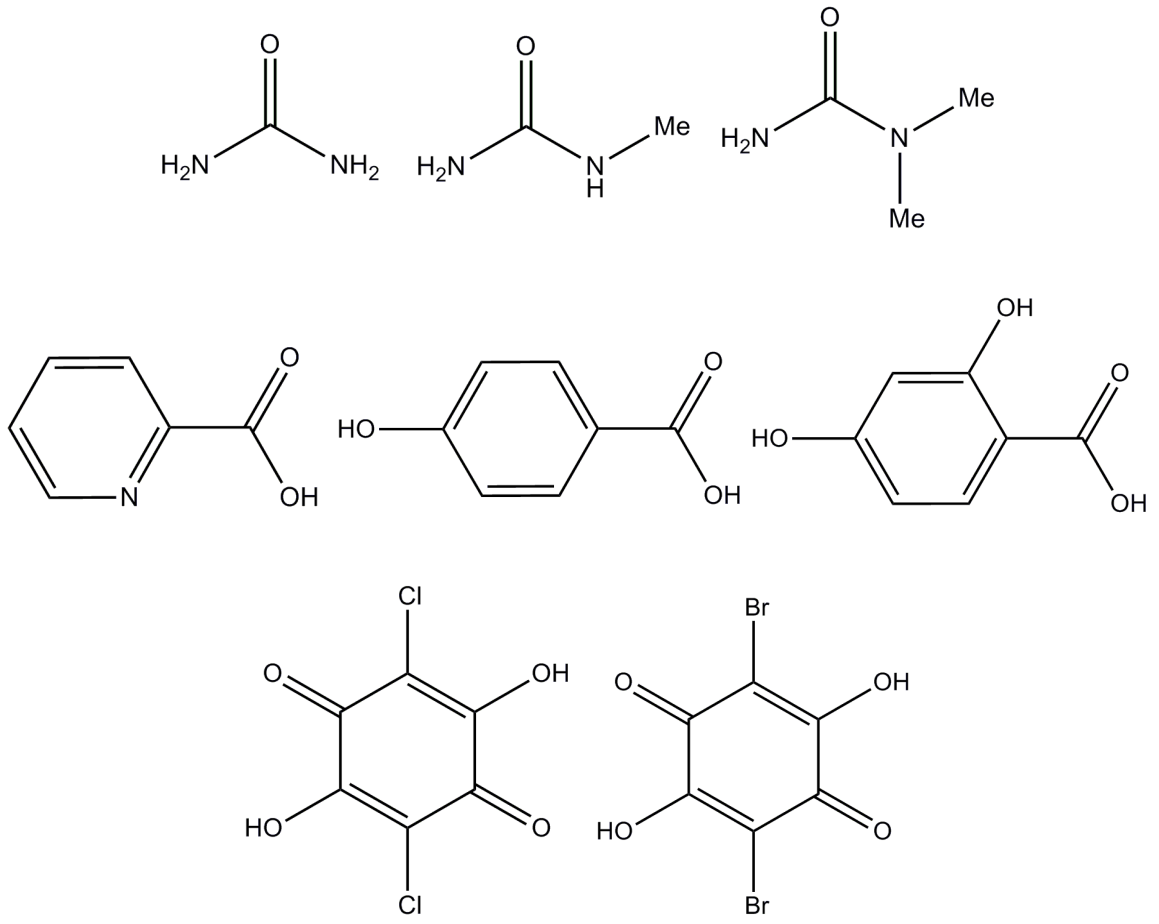

Figure 8.1 *Top to bottom and left to right: urea, N-methylurea, N,N-dimethylurea, picolinic acid, 4-hydroxybenzoic acid, 2,3-dihydroxybenzoic acid, chloranilic acid and bromanilic acid.*

8.1 Experimental

2:1 Complex of urea and picolinic acid monohydrate

Crystals of the 2:1 molecular complex of urea and picolinic acid monohydrate were grown by slow evaporation from isopropanol at room temperature (RT). Large block shaped crystals of a pale yellow colour were obtained. Single crystal X-ray diffraction data were collected on a Rigaku R-AXIS / RAPID diffractometer at 100, 200 and 300 K. The structure was solved using SHELXS-97[138] and refined with SHELXL-97[138] within the WinGX package.[140] Neutron data were collected on VIVALDI at the ILL at 10, 50, 100, 150, 200, 250 and 290 K. The neutron structures were refined using SHELXL-97[138] taking the X-ray atomic coordinates as a starting position. Crystallographic data are given in **Table 8.1**.

2:1 Complex of urea and 4-hydroxybenzoic acid

Colourless block shaped crystals of the 2:1 molecular complex of urea and 4-OHBA were grown by slow evaporation from ethanol at RT. Single crystal X-ray diffraction data were collected on a Bruker Nonius Kappa CCD diffractometer at 100 K. The structure was solved using SHELXS-97[138] and refined with SHELXL-97[138] within the WinGX package.[140] Crystallographic data are given in **Table 8.2**.

7:4 Complex of urea and bromanilic acid monohydrate

Deep red crystals of the 7:4:1 complex of urea, bromanilic acid and water were grown by slow evaporation from ethanol at 4 °C. Single crystal X-ray diffraction data were collected on a Bruker Nonius Kappa CCD diffractometer at 100 K. The structure was solved using SHELXS-97[138] and refined with SHELXL-97[138] within the WinGX package.[140] Crystallographic data are given in **Table 8.2**.

1:1 Complex of *N*-methylurea and picolinic acid

Colourless block shaped crystals with a pale yellow colour of the 1:1 molecular complex of *N*-methylurea and picolinic acid were grown by slow evaporation from acetonitrile at RT. Single crystal X-ray diffraction data were collected on a Bruker Nonius Kappa CCD diffractometer at 100 K. The structure was solved using SHELXS-97[138] and refined with SHELXL-97[138] within the WinGX package.[140] Crystallographic data are given in **Table 8.2**.

2:1 Complex of *N*-methylurea and 2,4-dihydroxybenzoic acid

Colourless block shaped crystals of the 2:1 molecular complex of *N*-methylurea and 2,4-DOHBA were grown by slow evaporation from ethanol at RT. Single crystal X-ray diffraction data were collected on a Rigaku R-AXIS / RAPID diffractometer at 300 K. The structure was solved using SHELXS-97[138] and refined with SHELXL-97[138] within the WinGX package.[140] Crystallographic data are given in **Table 8.2**.

1:1 Complex of *N*,*N*-dimethylurea and chloranilic acid monohydrate

Dark red block shaped crystals of the 1:1 molecular complex of *N*,*N*-dimethylurea and CLA monohydrate were grown by slow evaporation from methanol at RT. Single crystal X-ray diffraction data were collected on a Rigaku R-AXIS / RAPID diffractometer at 100, 200 and 300 K. The structure was solved using SHELXS-97[138] and refined with SHELXL-97[138] within the WinGX package.[140] Crystallographic data are given in **Table 8.3**.

2:1 Complex of *N*,*N*-dimethylurea and bromanilic acid

Crystals of the 1:1 molecular complex of *N*,*N*-dimethylurea and BRA were grown by slow evaporation from ethanol at RT. Large block shaped crystals of a dark red colour were obtained. Single crystal X-ray diffraction data were collected on a Rigaku R-AXIS / RAPID diffractometer at 100, 200 and 300 K. The structure was solved using SHELXS-97[138] and refined with SHELXL-97[138] within the WinGX package.[140] Neutron data were collected on VIVALDI at the ILL at 20, 100, 200, and 300 K. The neutron structures were refined using SHELXL-97[138] taking the X-ray atomic coordinates as a starting position. Crystallographic data are given in **Table 8.4**.

Table 8.1 *X-ray and neutron data collection and refinement information for the 2:1 complex of urea picolinic acid monohydrate.*[a]

Compound	**2:1 Urea : Picolinic acid monohydrate**									
Diffractometer	VIVALDI	VIVALDI	Rigaku R-AXIS RAPID	VIVALDI	VIVALDI	Rigaku R-AXIS RAPID	VIVALDI	VIVALDI	VIVALDI	Rigaku R-AXIS RAPID
Radiation	Neutron	Neutron	X-ray	Neutron	Neutron	X-ray	Neutron	Neutron	Neutron	X-ray
Formula	$C_8H_{15}N_5O_5$	$C_8H_{15}N_5O_5$	$C_8H_{15}N_5O_5$	$C_8H_{15}N_5O_5$	$C_8H_{15}N_5O_5$	$C_8H_{15}N_5O_5$	$C_8H_{15}N_5O_5$	$C_8H_{15}N_5O_5$	$C_8H_{15}N_5O_5$	$C_8H_{15}N_5O_5$
Molecular weight (g mol^{-1})	261.25	261.25	261.25	261.25	261.25	261.25	261.25	261.25	261.25	261.25
T (K)	10	50	100	100	150	200	200	250	290	300
Space group	*P*2$_1$/*n*	*P*2$_1$/*n*	*P*2$_1$/*n*	*P*2$_1$/*n*	*P*2$_1$/*n*	*P*2$_1$/*n*	*P*2$_1$/*n*	*P*2$_1$/*n*	*P*2$_1$/*n*	*P*2$_1$/*n*
***a* (Å)**	7.04	7.065	7.100(5)	7.10	7.102	7.1048(5)	7.105	7.11	7.12	7.120(5)
***b* (Å)**	22.44	22.54	22.691(5)	22.69	22.76	22.8469(14)	22.85	22.94	23.03	23.030(5)
***c* (Å)**	7.76	7.79	7.835(5)	7.84	7.855	7.8754(4)	7.88	7.91	7.93	7.933(5)
***β* (°)**	107.49	107.45	107.486(5)	107.49	107.41	107.327(2)	107.34	107.28	107.22	107.220(5)
Volume (Å^3)	1169.2	1183.4	1203.9(12)	1204.6	1211.5	1220.34(13)	1221.2	1231.9	1242.0	1242.5(12)
Z	4	4	4	4	4	4	4	4	4	4
Reflections collected	8738	16483	14928	9342	8742	14746	7577	6721	6989	14965
Independent	2351	2780	2767	1833	1715	2801	1505	1373	1328	2840
Observed > 2σ(I)	1747	2037	2346	1347	1224	2103	1038	922	885	1611
R_{int}	-	-	0.027	-	-	0.027	-	-	-	0.033
Parameters	299	298	223	299	299	223	299	299	299	223
GooF	1.30	1.33	1.04	1.17	1.12	1.11	1.11	1.18	1.11	1.10
R_1 (observed)	0.0569	0.0611	0.0305	0.0477	0.0518	0.0328	0.0514	0.0506	0.0505	0.0380
R_1 (all)	0.0909	0.1014	0.0388	0.0808	0.0920	0.0476	0.0938	0.1024	0.1045	0.0813
wR_2 (all)	0.1014	0.1000	0.0791	0.0876	0.0864	0.0893	0.0879	0.0931	0.0908	0.1121
Δρ (max, min) / e$^-$/Å^3 or fm/Å^3	0.10, -0.10	0.11, -0.09	0.25, -0.16	0.06, -0.05	0.05, -0.05	0.18, -0.17	0.04, -0.05	0.04, -0.05	0.04, -0.04	0.18, -0.23

[a] *It is not possible to accurately determine unit cell parameters from a Laue experiment at a continuous neutron source so no errors are listed. X-ray determined values are used where available.*

Table 8.2 *X-ray data collection and refinement information for the 2:1 complex of urea and 4-OHBA, the 7:4 complex of urea and BRA monohydrate, the 1:1 complex of N-methylurea and picolinic acid and the 2:1 complex of N-methylurea and 2,4-DOHBA.*

Compound	**2:1 Urea : 4-OHBA**	**7:4 Urea : BRA monohydrate**	**1:1 *N*-Methylurea : Picolinic acid**	**2:1 *N*-Methylurea : 2,4-DOHBA**
Diffractometer	Bruker Nonius Kappa CCD	Bruker Nonius Kappa CCD	Bruker Nonius Kappa CCD	Rigaku R-AXIS RAPID
Formula	$C_9H_{14}N_4O_5$	$C_{31}H_{38}Br_8N_{14}O_{24}$	$C_8H_{11}N_3O_3$	$C_{11}H_{18}N_4O_6$
Molecular weight (g mol^{-1})	258.24	1630.03	197.20	302.29
T (K)	100	100	100	300
Space group	*P*-1	*P*-1	*Pnma*	*P*-1
***a* (Å)**	6.3846(2)	10.5363(2)	13.1253(4)	10.0166(14)
***b* (Å)**	7.1582(2)	13.5954(2)	6.3876(2)	11.681(2)
***c* (Å)**	12.8496(4)	18.1649(3)	11.1016(3)	13.739(2)
***α*(°)**	87.709(2)	90.847(1)	90	88.917(4)
***β* (°)**	82.814(2)	103.925(1)	90	77.790(4)
***γ* (°)**	89.215(2)	93.524(1)	90	71.994(4)
Volume (Å^3)	582.15(3)	2519.61(7)	930.75(5)	1492.2(4)
Z	2	2	4	4
Reflections collected	14207	77327	14215	19442
Independent	2673	11596	1530	6794
Observed > 2σ(I)	2251	9426	1329	3770
R_{int}	0.046	0.052	0.038	0.028
Parameters	219	846	116	524
GooF	1.07	1.08	1.13	1.03
R_1 (observed)	0.0429	0.0341	0.0454	0.0409
R_1 (all)	0.0529	0.0510	0.0522	0.0824
wR_2 (all)	0.1199	0.0666	0.1282	0.1286
Δρ (max, min) / e$^-$/Å^3	0.41, -0.31	0.80, -0.57	0.57, -0.35	0.16, -0.15

Table 8.3 *X-ray data collection and refinement information for the 1:1 complex of N,N-dimethylurea and CLA monohydrate.*

Compound	**1:1 *N,N*-Dimethylurea : CLA Monohydrate**		
Diffractometer	Rigaku R-AXIS RAPID	Rigaku R-AXIS RAPID	Rigaku R-AXIS RAPID
Formula	$C_9H_{12}Cl_2N_2O_6$	$C_9H_{12}Cl_2N_2O_6$	$C_9H_{12}Cl_2N_2O_6$
Molecular weight (g mol^{-1})	315.11	315.11	315.11
T (K)	100	200	300
Space group	$P2_1/n$	$P2_1/n$	$P2_1/n$
***a* (Å)**	10.3952(8)	10.4378(10)	10.4773(11)
***b* (Å)**	9.1438(5)	9.1802(6)	9.2328(7)
***c* (Å)**	13.4248(8)	13.4918(10)	13.5671(11)
***β* (°)**	90.948(3)	90.443(4)	90.062(4)
Volume (Å^3)	1275.87(14)	1292.8(2)	1312.4(2)
Z	4	4	4
Reflections collected	16462	16711	17001
Independent	2914	2949	3006
Observed > 2σ(I)	2764	2527	2561
R_{int}	0.017	0.023	0.019
Parameters	220	220	220
GooF	1.05	1.08	1.07
R_1 (observed)	0.0232	0.0290	0.0321
R_1 (all)	0.0244	0.0345	0.0377
wR_2 (all)	0.0655	0.0790	0.0934
Δρ (max, min) / e$^-$/Å^3	0.39, -0.19	0.32, -0.25	0.49, -0.39

Table 8.4 *X-ray and neutron data collection and refinement information for the 2:1 complex of N,N-dimethylurea and BRA.*[a]

Compound	**2:1 *N,N*-Dimethylurea : BRA**						
Diffractometer	VIVALDI	Rigaku R-AXIS RAPID	VIVALDI	Rigaku R-AXIS RAPID	VIVALDI	Rigaku R-AXIS RAPID	VIVALDI
Radiation	Neutron	X-ray	Neutron	X-ray	Neutron	X-ray	Neutron
Formula	$C_{12}H_{18}Br_2N_4O_6$	$C_{12}H_{18}Br_2N_4O_6$	$C_{12}H_{18}Br_2N_4O_6$	$C_{12}H_{18}Br_2N_4O_6$	$C_{12}H_{18}Br_2N_4O_6$	$C_{12}H_{18}Br_2N_4O_6$	$C_{12}H_{18}Br_2N_4O_6$
Molecular weight (g mol^{-1})	474.12	474.12	474.12	474.12	474.12	474.12	474.12
T (K)	20	100	100	200	200	300	300
Space group	*P2$_1$/c*	*P2$_1$/c*	*P2$_1$/c*	*P2$_1$/c*	*P2$_1$/c*	*P2$_1$/c*	*P2$_1$/c*
***a* (Å)**	4.58	4.6294(2)	4.63	4.6758(2)	4.68	4.7246(4)	4.72
***b* (Å)**	9.16	9.2153(6)	9.22	9.2643(4)	9.26	9.3222(6)	9.32
***c* (Å)**	20.53	20.6213(10)	20.62	20.5526(11)	20.55	20.573(2)	20.57
***β* (°)**	92.61	92.637(2)	92.64	92.629(2)	92.63	92.659(3)	92.66
Volume (Å^3)	860.4	878.80(8)	879.3	889.36(7)	889.6	905.12(12)	903.9
Z	2	2	2	2	2	2	2
Reflections collected	15005	18535	14432	19965	10930	18835	8876
Independent	3535	1995	2857	2020	1986	2069	1428
Observed > 2σ(I)	2619	1881	2016	1858	1440	1813	1112
R_{int}	-	0.020	-	0.026	-	0.030	-
Parameters	191	145	191	145	191	145	191
GooF	1.23	1.07	1.22	1.06	1.41	1.03	1.58
R_1 (observed)	0.0516	0.0162	0.0502	0.0210	0.0535	0.0290	0.0496
R_1 (all)	0.0938	0.0178	0.0953	0.0237	0.0905	0.0350	0.0713
wR_2 (all)	0.0894	0.0414	0.0867	0.0533	0.0961	0.0730	0.0913
Δρ (max, min) / e$^-$/Å^3 or fm/Å^3	0.11, -0.12	0.36, -0.28	0.08, -0.08	0.50, -0.58	0.06, -0.08	0.77, -0.73	0.04, -0.05

[a] *It is not possible to accurately determine unit cell parameters from a Laue experiment at a continuous neutron source so no errors are listed. X-ray determined values are used where available.*

8.2 2:1 Molecular Complex of Urea and Picolinic Acid Monohydrate

The 2:1 complex of urea and picolinic acid monohydrate crystallises in the $P2_1/n$ space group with two urea molecules, one picolinic acid and one water molecule in the asymmetric unit. Picolinic acid in its native form exists with the acid hydrogen disordered over two positions with occupancies of 50:50; the hydrogen resides either on the acid group or on the pyridine nitrogen.[193] In the complex the picolinic acid molecule exists in a zwitterionic form with the acid hydrogen being transferred completely to the pyridine nitrogen atom; the charge is delocalised over the carboxylate group with C-O bond lengths of 1.244(2) and 1.255(1) Å in the 100 K X-ray structure. The urea, picolinic acid and water molecules form chains containing two urea moieties, one picolinic acid and one water moiety (**Figure 8.2**, top). Urea molecules in the chain are linked to one another through two $R_2^2(8)$ hydrogen bonded rings with N-H···O distances of 2.913(2) and 2.926(2) Å in one ring and 2.907(2) and 2.939(2) Å in the other (**Figure 8.2**, top). The two urea moieties in the chain are not coplanar and there is a tilt of 31.63(7)° between the planes of the molecules. One urea molecule in the chain is involved in a *DDHHA* bifurcated hydrogen bond to the oxygen of a picolinic acid in the chain through two N-H···O hydrogen bonds with lengths of 2.934(1) and 3.022(1) Å to the same oxygen (**Figure 8.2**, top). The same urea molecule is also involved in an N-H···O hydrogen bond to the second urea moiety in an adjacent chain with an N···O distance of 2.937(2) Å (**Figure 8.2**, bottom).

The picolinic acid molecules, whilst involved in a bifurcated hydrogen bond to a urea in the chain, also form hydrogen bonds to the water molecules in the chain (**Figure 8.2**, top). This occurs through a charge-assisted O-H···O hydrogen bond (2.726(2) Å in length) to a water from a carboxylate oxygen and an N-H···O hydrogen bond (2.734(2) Å in length) from the pyridine nitrogen to the water oxygen. The urea-picolinic acid-water chains are stacked on top of other chains flipped by 180° above and below (i.e. the urea segment of the chain stacked on top of a picolinic acid-water segment) linked through an O-H···O hydrogen bond from a water molecule to the carboxylate oxygen involved in the bifurcated hydrogen bond, at a distance of 2.803(2) Å (**Figure 8.2**, bottom). Adjacent stacks of layered chains are tilted at ~82.0° as already described by the tilt between adjacent urea chains (**Figure 8.2**, bottom).

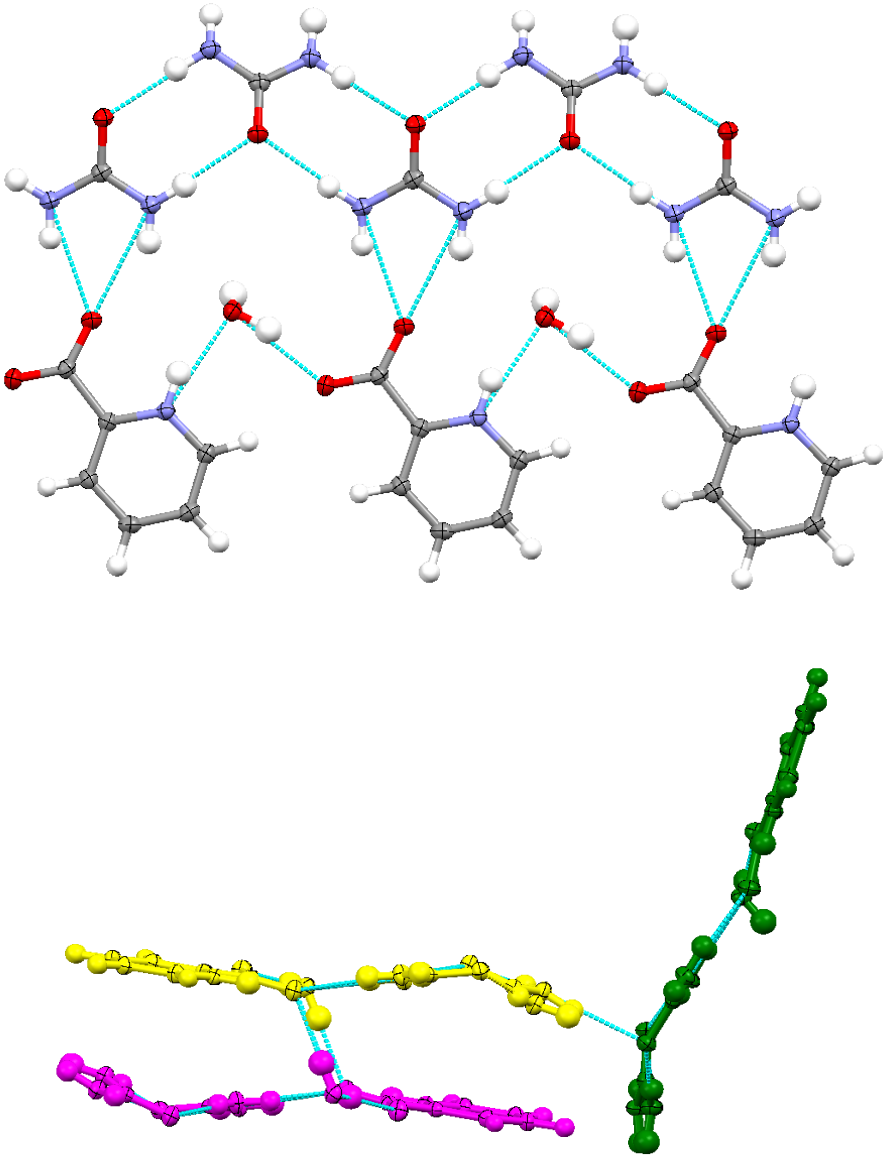

Figure 8.2 *Urea-picolinic acid-water chains (top) and three sets of chains (yellow, magenta and green) showing stacked sets of chains (yellow and magenta) and the tilted orientation of adjacent sets of chains (yellow/magenta vs. green) (bottom) in the 2:1 urea picolinic acid monohydrate complex at 100 K (X-ray).*

The complex shows no significant temperature dependent behaviour in the variable temperature X-ray and neutron structures. At all temperatures, the neutron structures show the effect of the hydrogen bonds on the behaviour of the hydrogen atoms in the urea molecules. Urea molecules in the native crystal structure are planar, whilst here they are involved in hydrogen bonds to molecules which are not coplanar resulting in the hydrogen atoms bending towards the acceptor atoms (**Figure 8.3**). This shows the strength and directionality of the hydrogen bonds and how they can affect the behaviour of the

hydrogen atoms in this subtle manner, clearly visible through the neutron diffraction data where the hydrogen atom behaviour can be modelled more accurately.

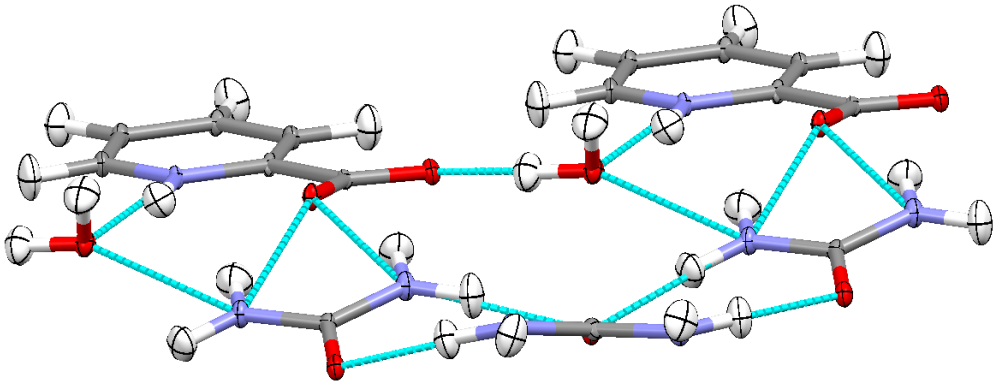

Figure 8.3 *The neutron structure of the 2:1 complex of urea picolinic acid monohydrate at 10 K, showing the hydrogen atoms of the urea molecules bent towards the hydrogen bond acceptor atoms.*

8.3 2:1 Molecular Complex of Urea and 4-Hydroxybenzoic Acid

The 2:1 complex of urea and 4-OHBA (**Figure 8.4**, top) crystallises in the $P\bar{1}$ space group with two urea molecules and one 4-OHBA molecule in the asymmetric unit. One of the urea moieties in the asymmetric unit forms a one-dimensional chain with equivalent urea molecules through two $R_2^2(8)$ hydrogen bonded rings (**Figure 8.4**, bottom left), each made up of two equivalent N-H···O hydrogen bonds (distances 2.8888(15) and 2.8928(15) Å at 100 K). The urea molecules in the chains are not coplanar but instead form a corrugated chain with urea molecules in two parallel planes separated by a distance of ~0.65 Å (**Figure 8.4**, bottom right). This separation results in the -NH_2 groups of the urea bending towards the next urea molecule in the chain; the urea molecules are therefore not planar. This behaviour is similar to that observed in the urea picolinic acid monohydrate complex. Each urea molecule in the chain is also involved in a *DDHHA* bifurcated hydrogen bond to the other urea moiety through two amide hydrogens (**Figure 8.4**, bottom left), interacting with the carbonyl oxygen of the other urea with N-H···O distances of 2.8738(15) and 2.9035(15) Å.

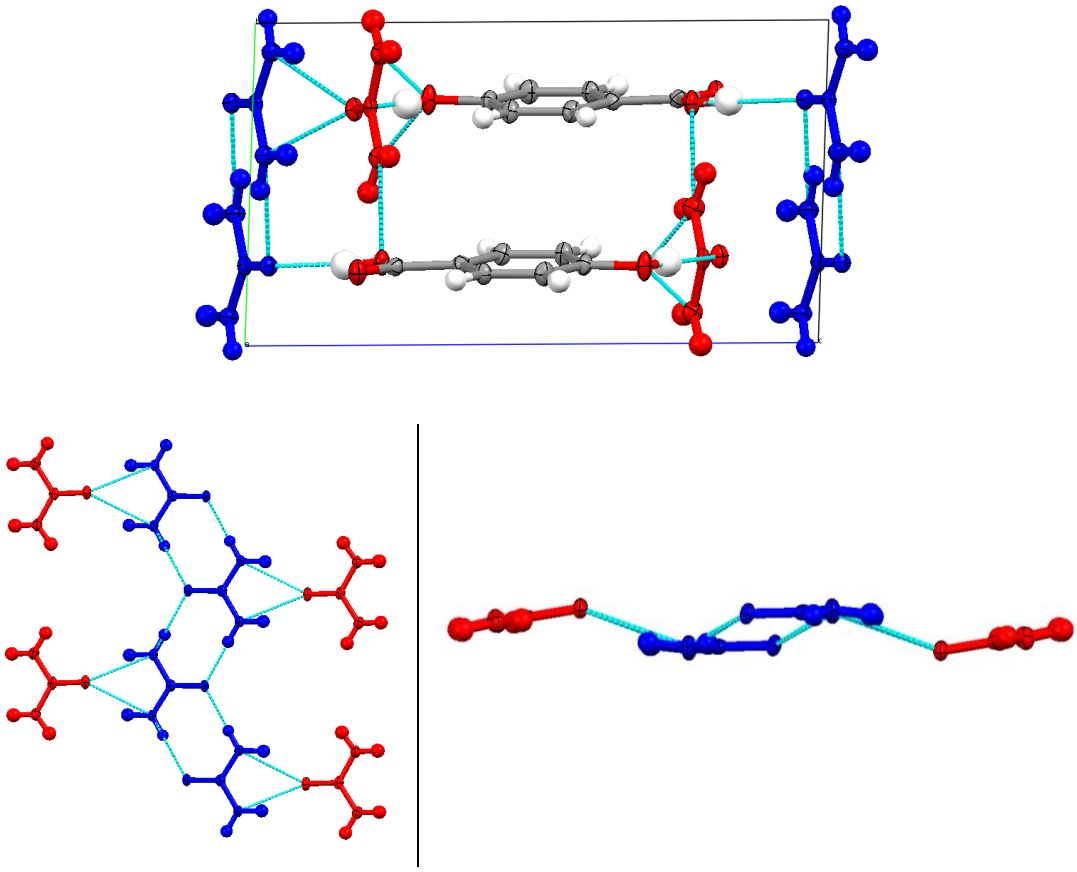

Figure 8.4 *Packing of urea and 4-OHBA molecules in a unit cell (top), hydrogen bonds between urea moieties (red and blue), showing the one-dimensional chain (blue) and bifurcated hydrogen bonds to other ureas (bottom left) and the two parallel planes of urea molecules in the chain (bottom right) in the 2:1 complex of urea and 4-OHBA at 100 K (from the X-ray determination).*

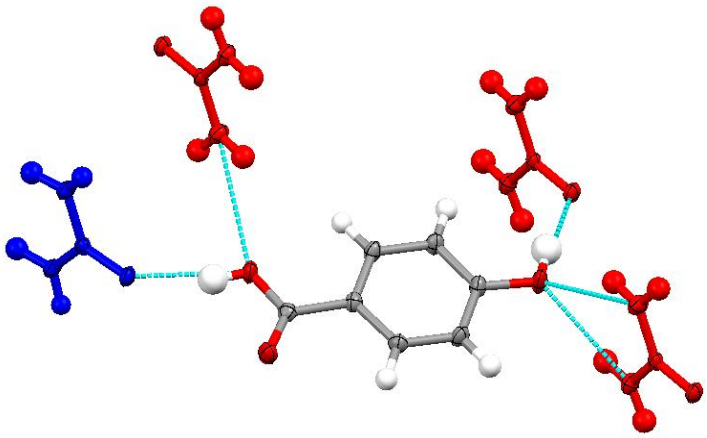

Figure 8.5 *Hydrogen bonds between urea moieties (red and blue) and the 4-OHBA molecule in the 100 K X-ray structure of the 2:1 complex of urea and 4-OHBA.*

Each urea moiety is also hydrogen bonded to the 4-OHBA molecules (**Figure 8.5**). The -OH of the carboxylic acid group of 4-OHBA interacts with the urea in the chain through an O-H···O interaction to the urea carbonyl oxygen with an O···O distance of 2.6602(14) Å. The other urea moiety is involved in three hydrogen bonds to the 4-OHBA. One of these is an O-H···O hydrogen bond to the hydroxyl group on the ring with an O···O distance of 2.6133(14) Å. The second is a symmetric *DDHHA* bifurcated hydrogen bond from two amide hydrogens to the ring hydroxyl oxygen of another 4-OHBA with N-H···O distances of 2.977(2) and 3.006(2) Å. The final interaction is an N-H···O hydrogen bond to the acid hydroxyl oxygen with an N···O distance of 3.068(2) Å. 4-OHBA molecules are also involved in top to tail displaced π···π stacks with a layer separation of ~3.39 Å (**Figure 8.4**, top).

One slightly unusual feature of this structure is that there is not an $R_2^2(8)$ hydrogen bonded ring formed through an acid···amide dimer as there has been in all the other urea-acid complexes presented so far. While the -OH of the acid group is involved in a moderate strength O-H···O hydrogen bond to a urea carbonyl oxygen, the carbonyl oxygen of the acid is only involved in two weak N-H···O hydrogen bonds with lengths of 3.211(2) and 3.407(2) Å (**Figure 8.6**). This complex shows a preference for amide···amide homodimers over more the common acid···amide heterodimers, with the acid molecule instead involved in multiple weaker interactions. The absence of the acid···amide heterodimer motif may be a consequence of the additional hydrogen bond donor group on the acid molecule in the form of the hydroxyl group.

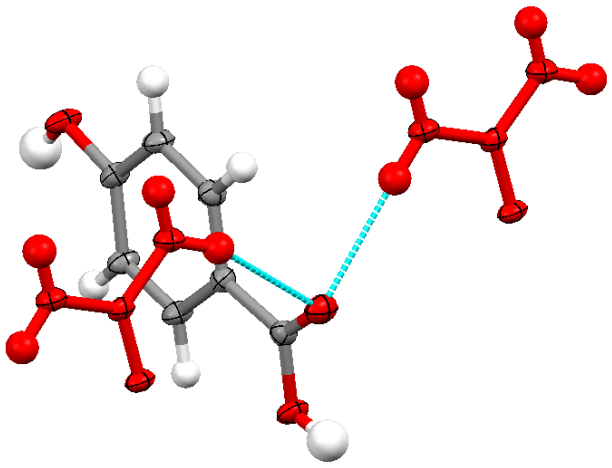

Figure 8.6 *Weak hydrogen bonds involving the acid carbonyl oxygen in the 100 K X-ray structure of the 2:1 complex of urea and 4-OHBA.*

8.4 7:4 Molecular Complex of Urea and Bromanilic Acid Monohydrate

The 7:4 complex of urea-BRA monohydrate crystallises in the $P\bar{1}$ space group with seven urea molecules, four BRA molecules and one water molecule in the asymmetric unit, forming a very complex structure containing one short, strong hydrogen bond. Despite repeated crystallisation attempts, only complex crystal structures were found to form containing these components (see also the urea-BRA complex in **Chapter 4**). Protons have transferred to three of the urea molecules in the asymmetric unit, leaving three singly deprotonated BRA molecules. The structure consists of two unique non-planar layers of molecules (***a*** and ***b***) in the *ac* plane, and has some common features with the 2:1 urea-BRA complex described in **Chapter 4**. The layers repeat with an ***aa-bb-aa-bb*** motif, where each layer is inverted relative to the adjacent equivalent layer.

Both layers can be split into two subunits. In layer ***a***, the first subunit contains a singly deprotonated BRA molecule (orange), one urea molecule (light blue) and one protonated urea molecule (grey) (**Figure 8.7**). The two urea molecules are tilted with respect to the BRA (orange) ring, at angles of 70.90(12)° (light blue) and 75.30(12)° (grey) at 100 K. The deprotonated BRA oxygen (orange) is involved in a short, strong charge-assisted O-H···O hydrogen bond to the protonated urea (O···O distance of 2.474(3) Å), with the hydrogen atom transferred across the hydrogen bond to the urea molecule. The same oxygen of the BRA molecule (orange) also interacts with a urea molecule from the other subunit (brown) in layer ***a*** through an N-H···O hydrogen bond (N···O distance of 2.972(4) Å). The other oxygen on the same side of the BRA molecule (orange) takes part in a *DDHHA* bifurcated hydrogen bond with two urea amide group hydrogens (light blue) (N···O distances of 3.140(4) and 3.218(4) Å). The hydroxyl group on the other side of the BRA molecule (orange) is involved in an O-H···O hydrogen bond to one urea moiety (light blue) (O···O distance of 2.526(3) Å), and also an N-H···O hydrogen bond to a urea molecule (purple) in the other subunit of layer ***a*** (N···O distance of 2.970(4) Å). The other oxygen on this side of the BRA molecule (orange) takes part in a *DDHHA* bifurcated hydrogen bond to two amide group hydrogen atoms of the protonated urea molecule (grey) (N···O distances of 3.001(4) and 3.257(4) Å). One of the urea molecules (light blue) forms an amide···amide dimer through two equivalent N-H···O hydrogen bonds, with the equivalent (light blue) urea molecule in the next, inverted, layer ***a*** (N···O distance of 2.930(4) Å). The other urea moiety in this subunit (grey), is then involved in an N-H···O hydrogen bond to a urea moiety (purple) in the adjacent, inverted, layer ***a*** (N···O distance of 3.134(4) Å), and another N-H···O hydrogen bond to a urea moiety (light green) in layer ***b*** (N···O distance of 2.956(4) Å). There are also two Br···Br interactions between the two

BRA molecules in layer ***a***, at distances of 3.5373(4) and 3.5455(4) Å (shorter than the sum of the van der Waals radii of 3.70 Å)

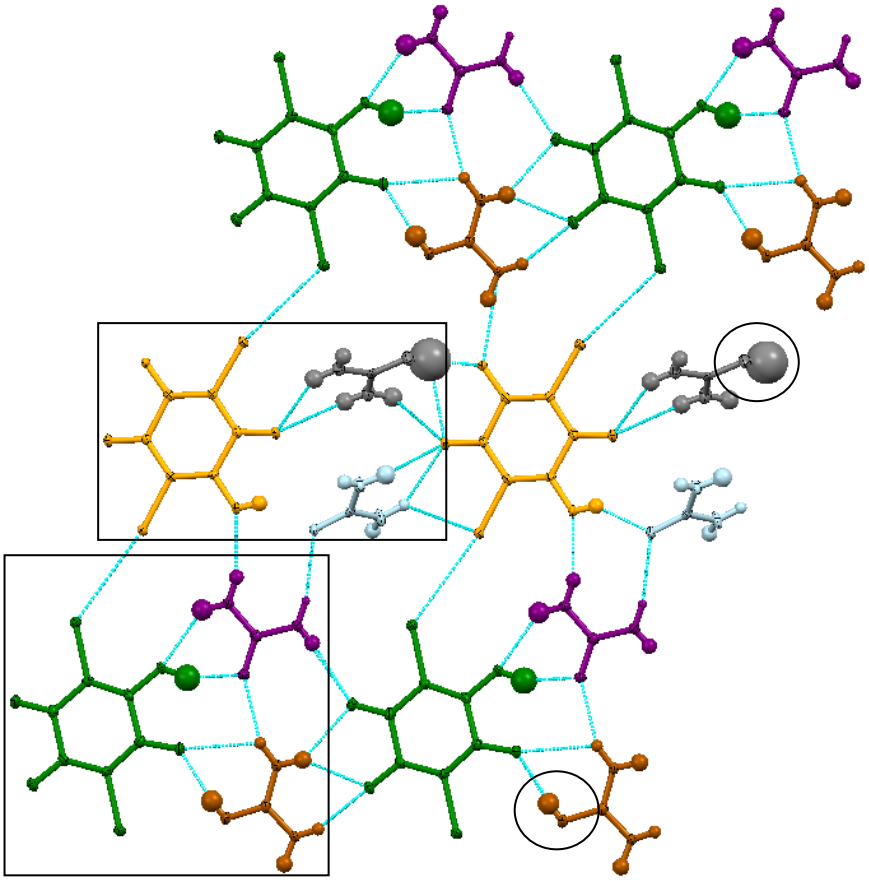

Figure 8.7 *Interactions in layer* ***a****, showing the subunits in boxes and the protonated urea molecules circled, in the 100 K X-ray structure of the 7:4 complex of urea and BRA monohydrate.*

The other subunit of layer ***a*** contains a singly deprotonated BRA molecule (dark green), one urea molecule (purple) and one protonated urea molecule (brown) (**Figure 8.7**). This subunit is much flatter than the other, with the two urea moieties only tilted with respect to the BRA ring (dark green), at angles of 4.24(3)° (purple) and 7.80(5)° (brown). The hydroxyl group of the BRA molecule (dark green) takes part in O-H···O and N-H···O hydrogen bonds to a urea molecule (purple), with O···O and N···O distances of 2.618(3) and 2.914(4) Å, respectively. The other oxygen on the same side of the BRA molecule (dark green) is involved in a *DDHHA* bifurcated hydrogen bond, consisting of a charge-assisted O-H···O hydrogen bond to a protonated urea (brown) (O···O distance of 2.590(3) Å, considerably longer than the equivalent hydrogen bond in the first subunit), and an N-H···O hydrogen bond to the same urea molecule (brown) (N···O distance of

3.071(4) Å). Both of the oxygen atoms on the other side of the BRA molecule (dark green) and involved in *DDHHA* bifurcated hydrogen bonds. One shows two N-H···O hydrogen bonds to the same urea molecule (brown) (N···O distances of 2.849(4) and 3.016(4) Å), whilst the other interacts with two urea moieties through N-H···O hydrogen bonds, with N···O distances of 2.979(4) Å (purple) and 3.025(4) Å (brown). Finally, there is an N-H···O hydrogen bond between an amide group hydrogen of one urea molecule (brown) and the carbonyl oxygen of the other (purple) (N···O distance of 3.005(4) Å). It should be noted that the proton transfer in this subunit has not simply occurred across the hydrogen bond as in the previous subunit, and the protonated urea (brown) does not interact with the deprotonated side of the BRA molecule (dark green); this may explain the longer O-H···O hydrogen bond in this subunit.

In layer ***b***, the first subunit contains a singly deprotonated BRA molecule (red), a protonated urea molecule (pink) and a water molecule (**Figure 8.8**). In this subunit, the protonated urea molecule (pink) is tilted slightly out of the plane of the BRA molecule (red), at an angle of 7.64(4)° to the plane of the BRA ring. The hydroxyl group of the BRA molecule (red) is involved in an O-H···O hydrogen bond to a urea carbonyl oxygen in the other subunit of layer ***a*** (yellow), with an O···O distance of 2.560(3) Å. The same BRA oxygen also takes part in an N-H···O hydrogen bond to the same urea molecule (yellow) (N···O distance of 2.824(4) Å). The other oxygen on the same side of BRA molecule (red) is involved in a *DDHHA* bifurcated hydrogen bond; both interactions are to the same protonated urea molecule (pink), to the protonated urea carbonyl (O···O distance of 2.520(3) Å) and to an amide group hydrogen (N···O distance of 3.052(4) Å). On the other (deprotonated) side of the BRA molecule (red), both oxygens are involved in *DDHHA* bifurcated hydrogen bonds. One oxygen has two N-H···O hydrogen bonds to the same urea molecule (pink) (N···O distances of 2.765(4) and 3.055(4) Å). The other oxygen interacts with two urea moieties through N-H···O hydrogen bonds, with N···O distances of 2.956(4) Å (pink) and 3.019(4) Å (yellow). The urea molecule in this subunit (pink) interacts with another urea carbonyl oxygen (yellow), through an N-H···O hydrogen bond with an N···O distance of 2.895 (4) Å. The protonated urea molecule (pink) interacts with the BRA of the other subunit in layer ***b*** (dark blue), through an N-H···O hydrogen bond to the BRA hydroxyl group (N···O distance of 2.952(4) Å), and also with the water molecule through an O-H···O hydrogen bond (O···O distance of 2.997(4) Å). The water molecule interacts with a urea molecule in layer ***a*** (purple) through an O-H···O hydrogen bond (O···O distance of 2.926(4) Å), a urea molecule (light green) in the next equivalent layer through an N-H···O hydrogen bond (N···O distance of 3.123(5) Å) and the hydroxyl group

of the BRA of the other subunit in layer ***a*** (dark blue) through an O-H···O hydrogen bond (O···O distance of 2.635(5) Å). Finally in this subunit, there are two Br···Br interactions between the BRA molecules in layer ***a***, with distances of 3.5152(4) and 3.5495(4) Å (shorter than the sum of the van der Waals radii of 3.70 Å). It should be noted that the proton transfer within this subunit has not simply occurred across a hydrogen bond, with the protonated urea oxygen (pink) not interacting with the deprotonated side of the BRA (red) molecule.

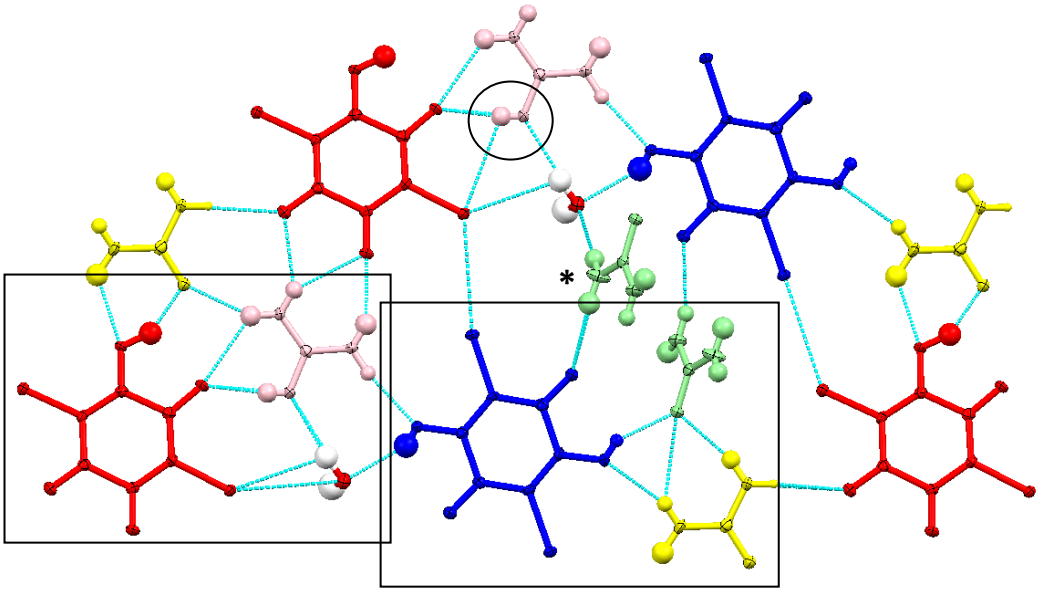

Figure 8.8 *Interactions in layer **b**, showing the subunits in boxes and the protonated urea circled, in the 100 K X-ray structure of the 7:4 complex of urea and BRA monohydrate. Note: the light green urea molecule marked with an asterisk (*) is in the next layer **a**, in the layer above the rest of the molecules in the figure.*

The second subunit within layer ***b*** contains entirely neutral components: a BRA molecule (dark blue) and two urea molecules (yellow and light green) (**Figure 8.8**). The urea molecules are again tilted with respect to the BRA ring, at angles of 9.13(7)° (yellow) and 59.73(15)° (light green). One of the hydroxyl groups of the BRA molecule (dark blue) interacts with the water and urea (pink) molecules through hydrogen bonds which have been described above. The other oxygen on the same side of the BRA molecule (dark blue) takes part in an N-H···O hydrogen bond with the urea molecule (light green) which is significantly tilted out of the plane of the BRA ring in this subunit, with an N···O distance of 3.043(4) Å. The hydroxyl group on the other side of the BRA molecule (dark blue) is involved in an O-H···O hydrogen bond to a urea moiety (light green) (O···O distance of 2.521(4) Å), and an N-H···O hydrogen bond with the other urea moiety (yellow) of the

subunit (N···O distance of 2.914(4) Å). The other oxygen on the same side of the BRA molecule (dark blue) is then involved in an N-H···O hydrogen bond to one of the urea moieties (light green) in the adjacent, inverted, layer ***b*** (N···O distance of 3.025(4) Å). The two urea molecules of the subunit interact with one another through an asymmetric *DDHHA* bifurcated hydrogen bond, with two N-H···O hydrogen bond components, to one of the urea carbonyls (light green) (N···O distances of 2.921(4) and 3.327(3) Å). One of the urea moieties (light green) also interacts with a urea molecule in layer ***b*** (grey) through an N-H···O hydrogen bond (N···O distance of 2.956(4) Å).

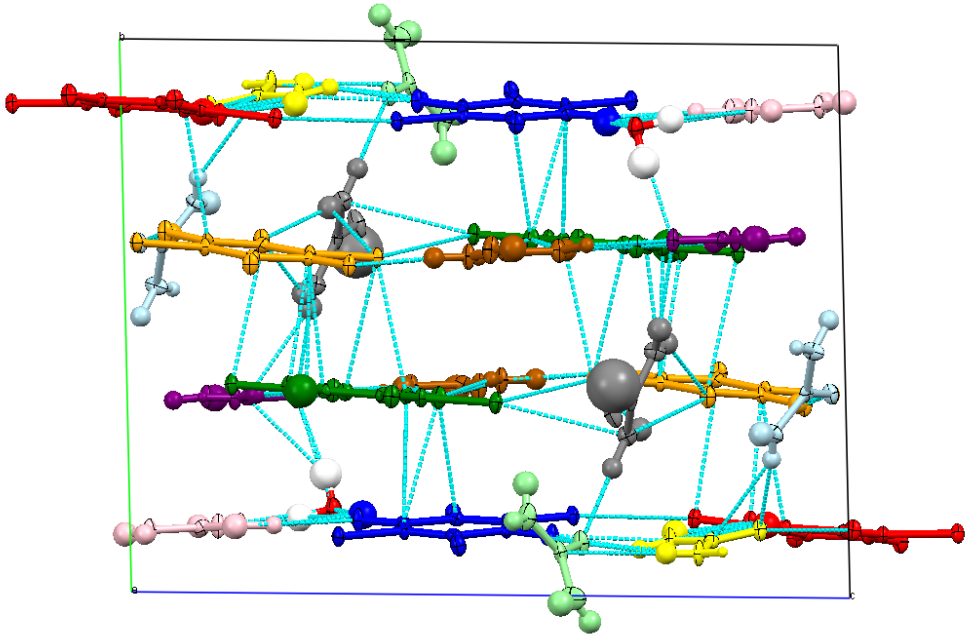

Figure 8.9 *Interactions between layers in the 100 K X-ray structure of the 7:4 complex of urea and BRA monohydrate, viewed along the a-axis.*

As well as the interactions between layers already described, there are also parallel-displaced π interactions between the BRA molecules in neighbouring layers (**Figure 8.9**). The approximate ***a***-***a***, ***b***-***b*** and ***a***-***b*** layer separations are 4.1, 3.3 and 3.4 Å, respectively.

The O-H distance (0.92(10) Å) of the short, strong hydrogen bond (O···O distance of 2.474(3) Å) in this complex is not elongated, though the hydrogen atom does have a large isotropic thermal displacement parameter. Analysis of the electron density in the hydrogen bond from a Fourier difference map does not show a distinct peak corresponding to the hydrogen atom electron density as would be expected (**Figure 8.10**). This is due to the quality of data and the large number of heavy atoms in the unit cell adding to the background of the map. With data only collected at 100 K, it is difficult to find any evidence of proton migration within this complex, even though the hydrogen bond

is <2.50 Å length (see **Chapter 4**). As in the case of all the complexes presented in this thesis, neutron diffraction data would be required to state definitively whether proton migration is present or not.

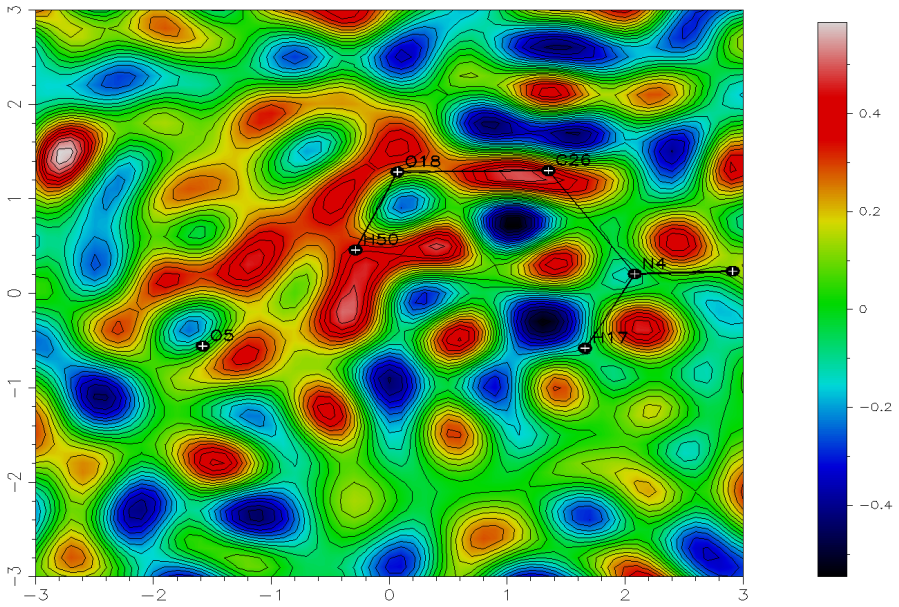

Figure 8.10 *Fourier difference map of the short, strong O-H···O hydrogen bond in the 7:4 complex of urea and BRA, from the X-ray data at 100 K.*

8.5 1:1 Molecular Complex of *N*-Methylurea and Picolinic Acid

The 1:1 complex of *N*-methylurea and picolinic acid crystallises in the *Pnma* space group with half an *N*-methylurea and half a picolinic acid molecule in the asymmetric unit (**Figure 8.11**). The methyl group of the *N*-methylurea is located in the *syn* position, on the same side of the molecule as the carbonyl. The acid group of the picolinic acid is protonated in this complex, in contrast to the complex containing urea and water, and molecules form acid···amide dimers through $R_2^2(8)$ hydrogen bonded rings with O-H···O and N-H···O distances of 2.5070(13) and 3.0636(15) Å, respectively (**Table 8.5**). The first of these is a short, strong hydrogen bond. The structure is layered and dimer units interact with others in the same layer through N-H···O and N-H···N hydrogen bonds from a methylurea to the acid carbonyl oxygen and the acid nitrogen with lengths of 2.8299(15) and 3.161(2) Å, respectively (**Figure 8.11**). There are also C-H···O hydrogen bonds between acid ring hydrogen atoms and the two oxygen atoms involved in the O-H···O hydrogen bond of the dimer with C···O lengths of 3.284(2) and 3.408(2) Å. There are π···π interactions between layers with a separation of ~3.19 Å, with picolinic acid rings centred over the carbonyl oxygens of the acid in layers above and below.

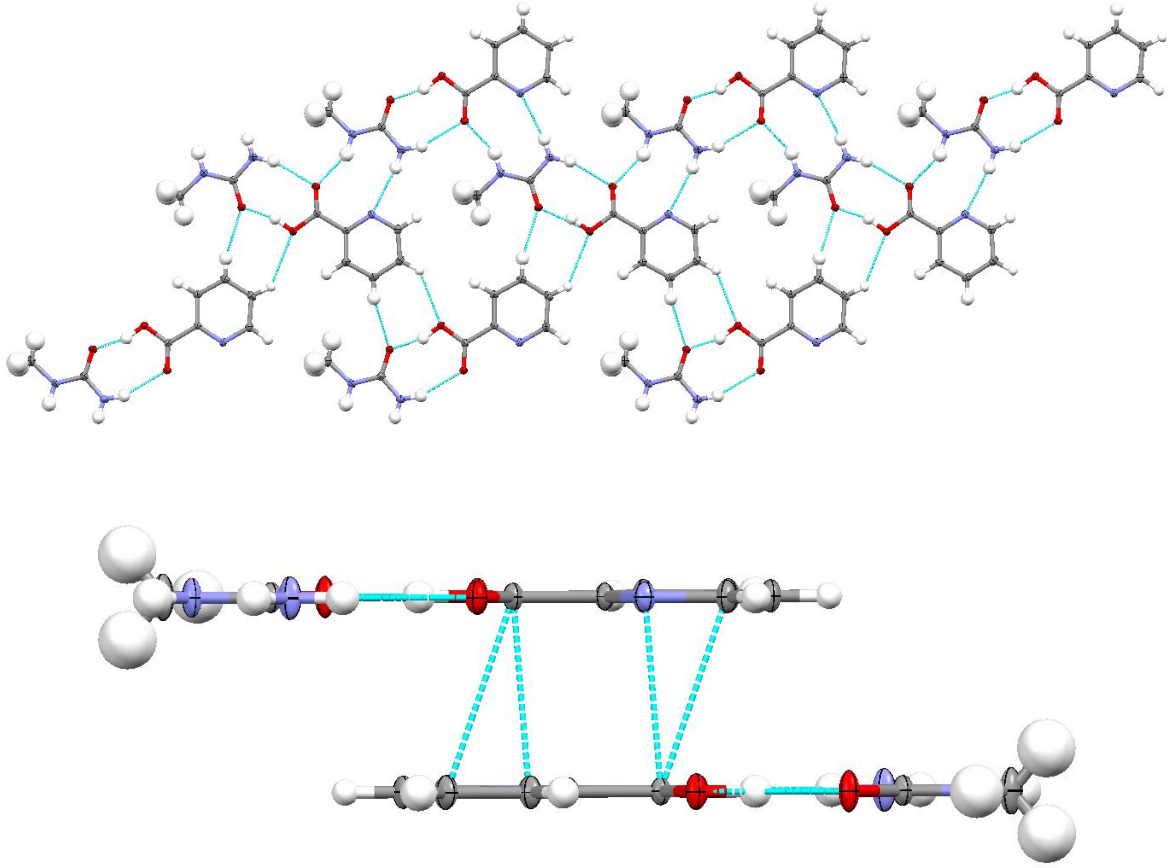

Figure 8.11 *A layer of dimers (top) and interactions between dimers in different layers (bottom) in the 1:1 complex of N-methylurea and picolinic acid, from the 100 K X-ray data.*

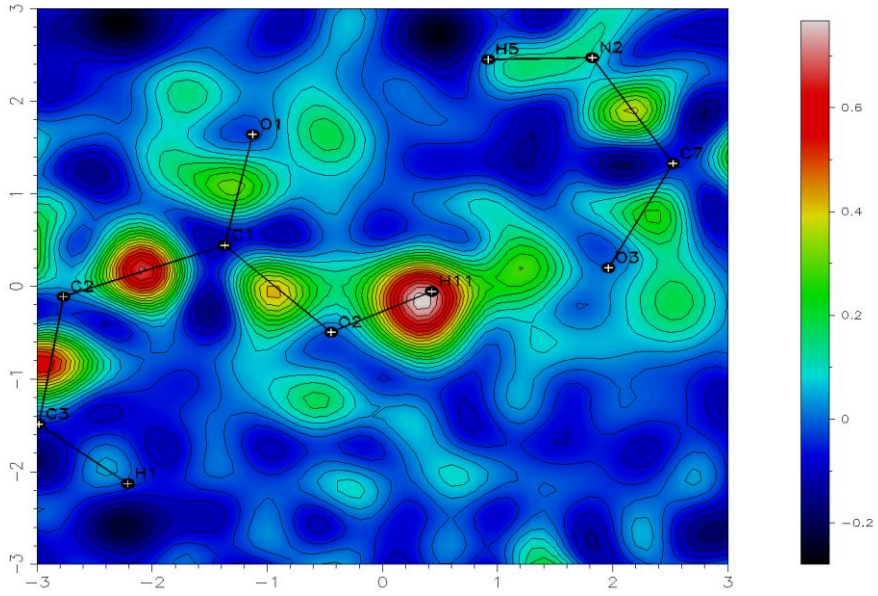

Figure 8.12 *Fourier difference map of the short, strong O-H···O hydrogen bond in the 1:1 complex of N-methylurea and picolinic acid, from the X-ray data at 100 K.*

Table 8.5 *Lengths of hydrogen bonds linking the acid···amide dimer in the 1:1 complex of N-methylurea and picolinic acid, from the 100 K X-ray data.*

Bond	r(D-H) / Å	r(H···A) / Å	r(D-H···A) / Å
O-H···O	0.98(2)	1.56(2)	2.5070(13)
N-H···O	0.91(2)	2.20(2)	3.0636(15)

The O-H distance in the short, strong O-H···O hydrogen bond of the dimer is slightly elongated with an X-ray determined length of 0.98(2) Å at 100 K (**Table 8.5**). Visualisation of the hydrogen atom electron density using a Fourier difference map shows that it is slightly spread out along the hydrogen bond, with the hydrogen atom shared more between the two oxygen atoms and the bond being more covalent in nature; the refined hydrogen atom position is close to the peak of the electron density. While this hydrogen bond is classed as short and strong, it is not as short as the hydrogen bonds in which migration has been observed (**Chapter 4**) while additionally the hydrogen atom is not centred in the bond, as is often seen in migration complexes. It therefore seems unlikely that this complex would exhibit proton migration and for this reason, as well as time constraints, this complex was only investigated at one temperature with X-ray diffraction.

8.6 2:1 Molecular Complex of *N*-Methylurea and 2,4-Dihydroxybenzoic Acid

The 2:1 complex of N-methylurea and 2,4-DOHBA crystallises in the $P\bar{1}$ space group with four urea and two 2,4-DOHBA molecules in the asymmetric unit at 300 K. The methyl group of the *N*-methylurea is in the *syn* position, on the same side of the molecule as the carbonyl group. Two acid and two methylurea moieties form layers of one-dimensional chains in the *ab* plane with a repeating U-A-U-A motif and an approximate layer separation of 3.4 Å (**Figure 8.13**). The two other methylurea moieties are titled with respect to the chains and reside between layers; chains in the same layer are linked by the tilted methylurea molecules.

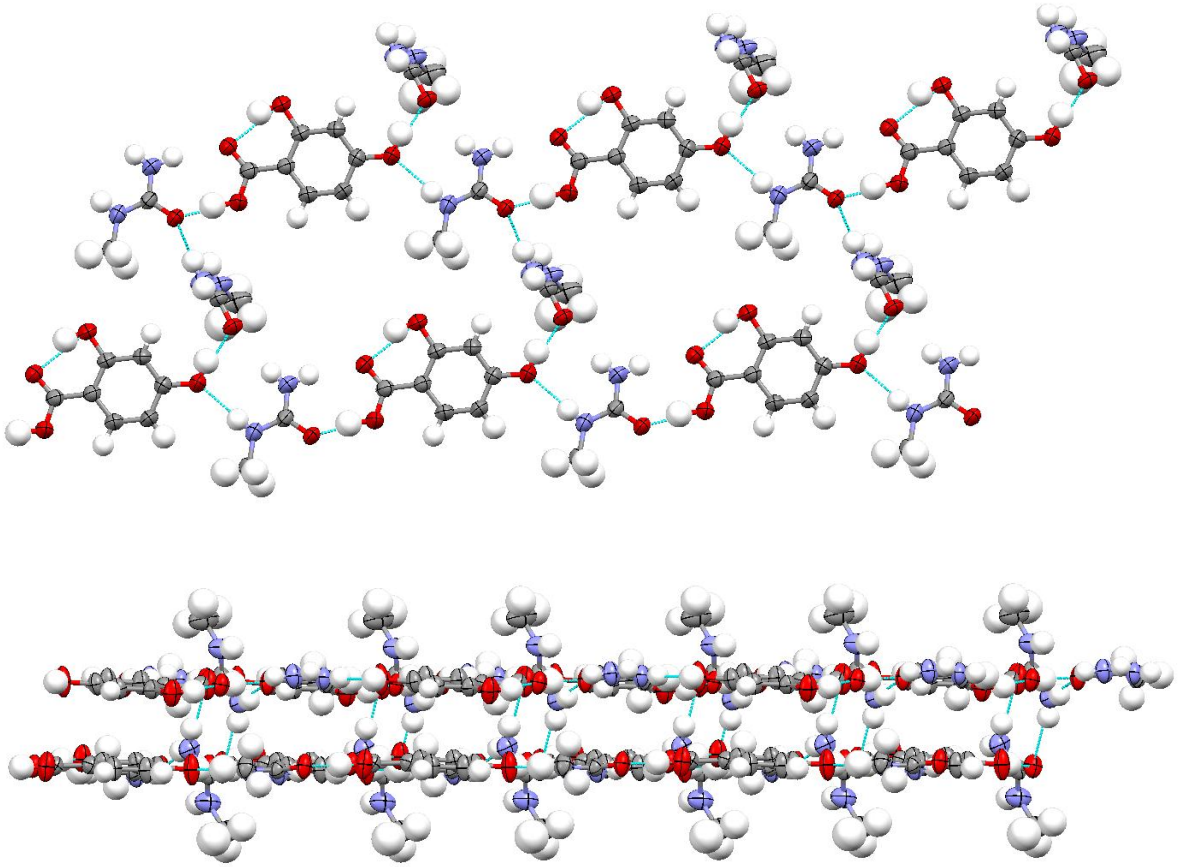

Figure 8.13 *One-dimensional acid-N-methylurea chains linked by tilted N-methylureas (top) and two layers of chains (bottom) in the 1:1 complex of N-methylurea and 2,4-DOHBA from the 300 K X-ray data.*

The two acid molecules are in near-identical environments. Both have an intramolecular O-H···O hydrogen bond between the hydroxyl group in the ortho- position and the acid carbonyl oxygen (with O···O lengths of 2.616(2) and 2.629(2) Å for the two environments), while the acid groups form acid···amide dimers to coplanar methylureas through $R_2^2(8)$ hydrogen bonded rings with O-H···O and N-H···O bond distances of 2.516(2) and 3.083(2) Å, respectively, for one acid and 2.535(2) and 3.081(2) Å, respectively, for the other (**Table 8.6**). The hydroxyl groups in the para- positions take part in two hydrogen bonds; one is an O-H···O hydrogen bond to the methylurea carbonyl with lengths of 2.615(2) Å for one acid and 2.587(2) Å for the other; the methylurea carbonyls are tilted to the planes of the acid rings at angles of ~71.8° and ~68.3°. The other hydrogen bond is to the methyl substituted amide nitrogen of a methylurea with N-H···O distances of 2.905(2) Å for one acid environment and 2.996(2) Å for the other; these N-H···O hydrogen bonds and the $R_2^2(8)$ hydrogen bonded rings of the acid···amide dimers form the basis of the one-dimensional hydrogen bonded chains. The tilted methylureas form amide···amide

homodimers through an $R_2^2(8)$ hydrogen bonded ring made up of two equivalent N-H···O hydrogen bonds with lengths of 3.035(2) Å. Between layers, there are short C-H···O contacts from a methylurea in the chain to an ortho hydroxyl oxygen of an acid at a distance of 3.556(3) Å, while there are other C-H···O contacts between the titled methylureas and the carbonyl of the acid with a C···O distance of 3.249(4) Å. Other short contacts include a C-H···N interaction from an acid to a tilted methylurea (3.594(3) Å in length) and an N-H···O interaction between a methylurea in the chain and the carbonyl of a tilted methylurea (3.100(2) Å in length).

Table 8.6 *Lengths of hydrogen bonds linking the acid···amide dimers in the 1:1 complex of N-methylurea and 2,4-DOHBA, from the 300 K X-ray data. (a) represents one dimer environment and (b) the other.*

Bond	r(D-H) / Å	r(H···A) / Å	r(D-H···A) / Å
O-H···O (a)	1.02(2)	1.51(2)	2.516(2)
N-H···O (a)	0.90(2)	2.21(2)	3.083(2)
O-H···O (b)	0.99(3)	1.57(3)	2.535(2)
N-H···O (b)	0.91(2)	2.19(2)	3.081(2)

The O-H distances in the two short strong O-H···O hydrogen bonds of the acid···amide dimers are slightly elongated, with lengths of 1.02(2) and 0.99(3) Å from the X-ray data (**Table 8.6**). Visualising the hydrogen atom electron density in the short strong hydrogen bonds through Fourier difference maps shows a slight smearing out of the electron density (**Figure 8.14**), though in both cases the refined hydrogen atom position is close to the peak of the electron density. As in the case of the 1:1 complex of *N*-methylurea with picolinic acid discussed in **Section 8.5**, these hydrogen bonds are longer than those in which migration has been confirmed (**Chapter 4**) with the hydrogen atoms again not centred in the bonds. Therefore, in both of these hydrogen bonds it seems unlikely that migration is present and data were consequently only collected using X-rays at one temperature.

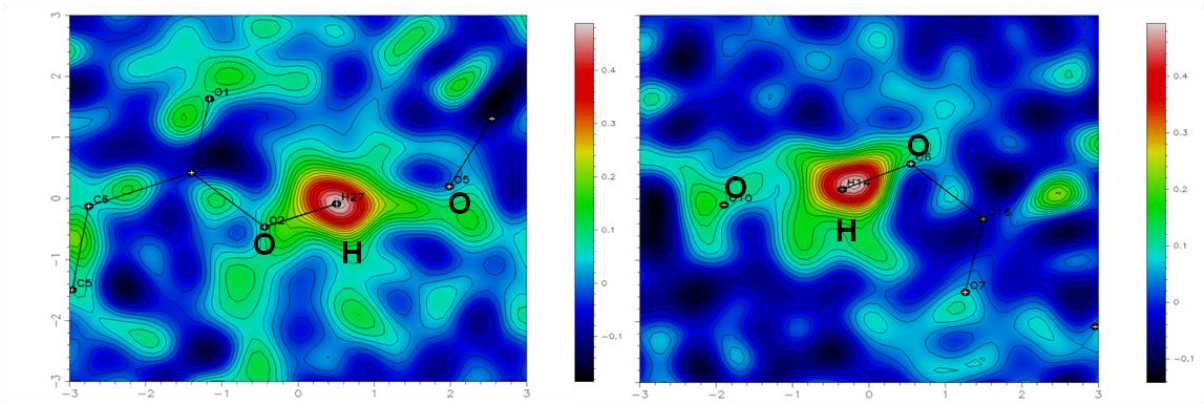

Figure 8.14 *Fourier difference maps of the short strong O-H···O hydrogen bonds linking the acid···amide dimers in the 1:1 complex of N-methylurea and 2,4-DOHBA, from the 300 K X-ray data.*

8.7 1:1 Molecular Complex of *N*,*N*-Dimethylurea and Chloranilic Acid Monohydrate

The 1:1 complex of *N*,*N*-dimethylurea and CLA monohydrate crystallises in the $P2_1/n$ space group with one dimethylurea, one CLA and one water molecule in the asymmetric unit. A proton has been transferred from the CLA to the dimethylurea, with the protonated dimethylurea carbonyl oxygen involved in a charge-assisted, short strong O-H···O hydrogen bond to a coplanar CLA oxygen with a hydrogen bond length of 2.4939(12) Å in the 100 K X-ray structure (**Table 8.7**). The two molecules involved in the short strong hydrogen bond are coplanar, with other dimethylurea-CLA units tilted approximately perpendicularly (~87.5°); units are linked together through hydrogen bonds to each other and the water molecules. Units are stacked on top of one another with a layer separation of ~3.24 Å (**Figure 8.15**).

The deprotonation of the CLA has affected the C-O bond distances; on the protonated side of the acid the C-O distances are 1.2326(13) and 1.3174(13) Å for the carbonyl and hydroxyl oxygens, respectively, whilst on the deprotonated side of the molecule the C-O distances are more equalised, with lengths of 1.2232(13) and 1.2682(13) Å. The CLA molecule takes part in several other hydrogen bonds; the acid oxygen involved in the charge-assisted, short strong O-H···O bond also takes part in an N-H···O hydrogen bond (2.9306(13) Å in length) to the coplanar dimethylurea. The other oxygen on the same side of the CLA molecule is involved in a charge-assisted O-H···O hydrogen bond to a water (2.7961(12) Å in length) and an N-H···O hydrogen bond to a dimethylurea in a tilted orientation (2.8859(13) Å in length). The hydroxyl of the CLA molecule takes part in an O-H···O hydrogen bond to a water molecule, with a distance of 2.5763(12) Å, while the other oxygen on the same side of the CLA molecule also takes part in an O-H···O

hydrogen bond to another water with an O···O distance of 2.8496(12) Å. The dimethylurea forms an N-H···O hydrogen bond to a water molecule with a length of 3.0289(13) Å.

Table 8.7 *Lengths of the short strong O-H···O hydrogen bond in the 1:1 complex of N,N-dimethylurea and CLA monohydrate from the variable temperature X-ray data.*

T/ K	r(O-H) / Å	r(H···O) / Å	r(O-H···O) / Å
100	0.85(2)	1.64(2)	2.4939(12)
200	0.91(3)	1.59(3)	2.495(2)
300	0.85(3)	1.65(3)	2.498(2)

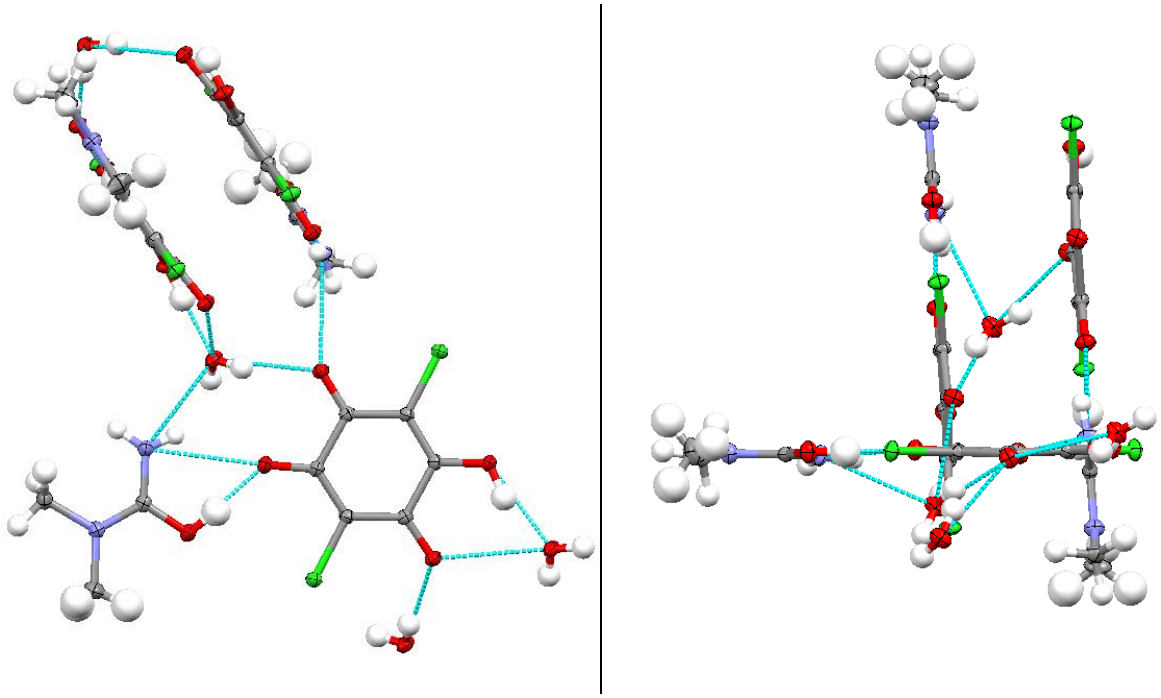

Figure 8.15 *Hydrogen bonds linking dimethylurea-CLA units showing the stacked units in the 100 K X-ray structure of the 1:1 complex of N,N-dimethylurea and CLA monohydrate.*

Variable temperature X-ray data were collected which show no significant temperature dependent effects. The short strong O-H···O hydrogen bond is longer than the majority of those in which migration has been observed in this work, and close to the suggested threshold of 2.50 Å (see **Chapter 4**), with the hydrogen atom appearing to be well

localised on the donor atom at all temperatures (**Table 8.7**). This suggests proton migration does not occur in this short strong hydrogen bond.

8.8 2:1 Molecular Complex of *N*,*N*-Dimethylurea and Bromanilic Acid

The 2:1 complex of *N*,*N*-dimethylurea and BRA crystallises in the $P2_1/c$ space group with one dimethylurea and half a BRA molecule in the asymmetric unit. In contrast to the previous structure containing CLA (see **Section 8.7**), there is no proton transfer from the acid molecule to the dimethylurea. The dimethylurea and BRA molecules form U-A-U units held together by a short strong O-H···O hydrogen bond (length of 2.4911(15) Å in the 100 K X-ray structure) between the acid hydroxyl groups and the dimethylurea carbonyl oxygens (**Figure 8.16** and **Table 8.8**); dimethylurea molecules are tilted at 80.6(1)° to the plane of the acid rings. BRA molecules are involved in parallel-displaced π interactions with a separation of ~3.30 Å between the rings; stacked U-A-U units also interact through N-H···O hydrogen bonds (2.976(2) Å in length) between dimethylureas in one unit and the acid carbonyl oxygens of another (**Figure 8.16**, bottom). The dimethylurea molecules also take part in another N-H···O hydrogen bond to the carbonyl oxygen of a dimethylurea in an adjacent unit. This unit is tilted, with respect to the original unit, at ~83.7° as measured by the angle between the planes of the aromatic rings in the two units (**Figure 8.16**, top). There are also weak C-H···O hydrogen bonds between the dimethylurea methyl groups and the acid oxygens with C···O distances of 3.208(2) and 3.352 (2) Å.

Table 8.8 *Lengths of the short strong O-H···O hydrogen bond in the 2:1 complex of N,N-dimethylurea and BRA from the variable temperature X-ray and neutron data.*

T/K	r(O-H) / Å		r(H···O) / Å		r(O-H···O) / Å	
	X-ray	Neutron	X-ray	Neutron	X-ray	Neutron
20	-	1.055(2)	-	1.469(2)	-	2.476(3)
100	0.80(3)	1.059(2)	1.72(3)	1.483(3)	2.4911(15)	2.493(3)
200	0.76(3)	1.051(4)	1.77(3)	1.492(4)	2.495(2)	2.492(3)
300	0.80(4)	1.038(4)	1.74(4)	1.515(4)	2.505(2)	2.501(4)

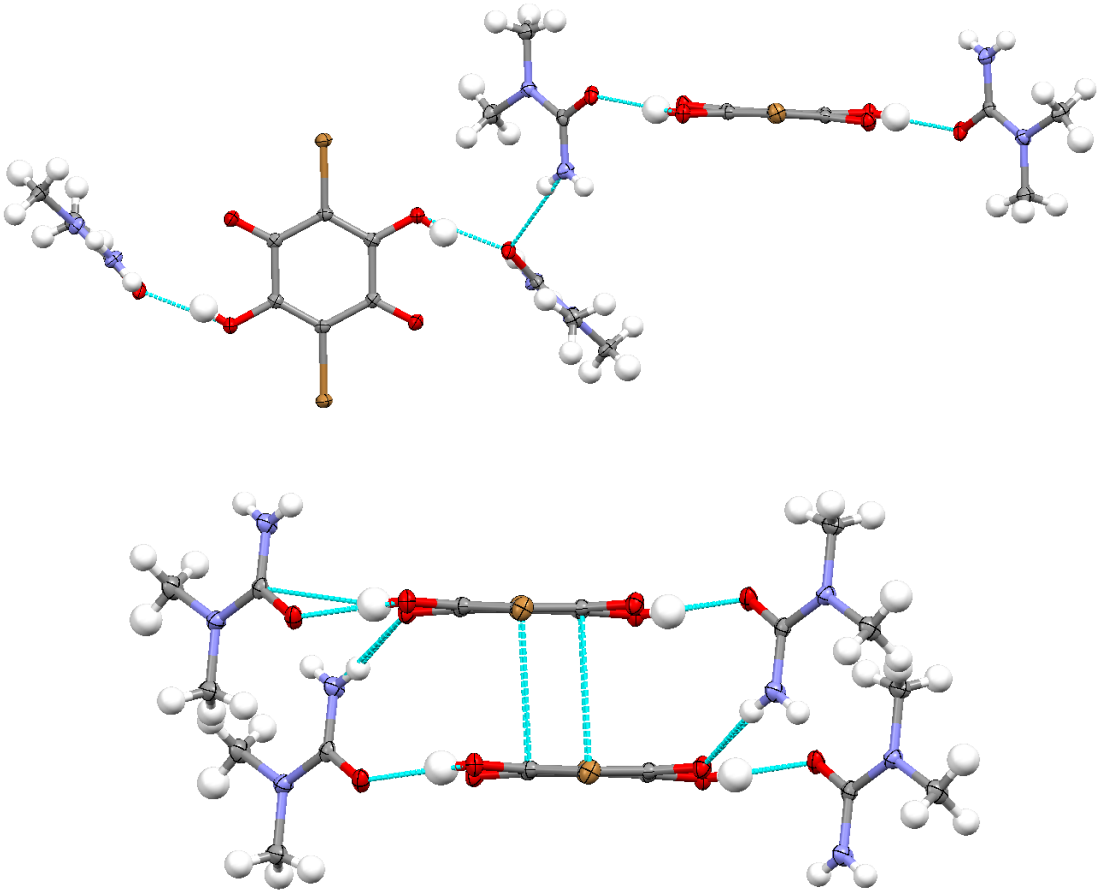

Figure 8.16 *Weak interactions linking adjacent molecular units (top) and layered units (bottom) in the 100 K (X-ray) structure of the 2:1 complex of N,N-dimethylurea and BRA.*

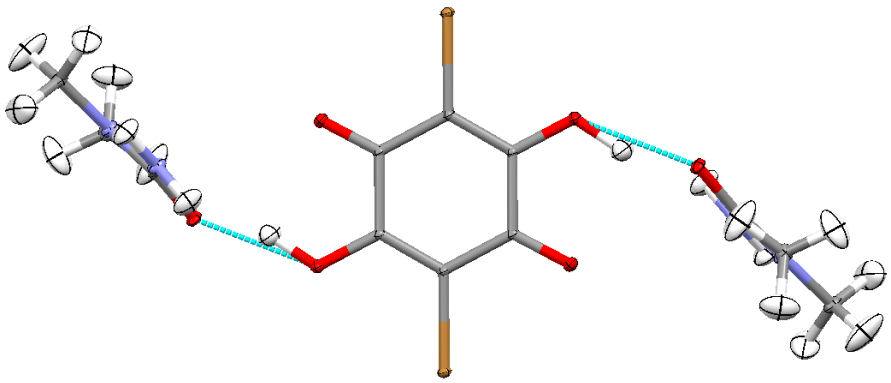

Figure 8.17 *A molecular unit of the 2:1 complex of N,N-dimethylurea and BRA in the 20 K neutron structure.*

Variable temperature X-ray and neutron data (**Figure 8.17** and **Figure 8.18**) were collected to investigate whether proton migration occurs within the short strong O-H···O hydrogen bond of the complex. The neutron data show that between 20 and 200 K there

is no movement of the proton within the short strong hydrogen bond. However, between 200 and 300 K the proton appears to shift 0.013(6) Å towards the donor oxygen (**Table 8.8**). The migration is not significant with respect to the size of the error and as it only occurs at one temperature, there is no trend of migration which can be established within this complex. Therefore, while the O-H···O hydrogen bond in this complex is short and strong (with a D···A distance below the 2.50 Å boundary suggested in **Chapter 4**), no significant migration is observed and the behaviour of the hydrogen bond with temperature is different to those where migration is observed.

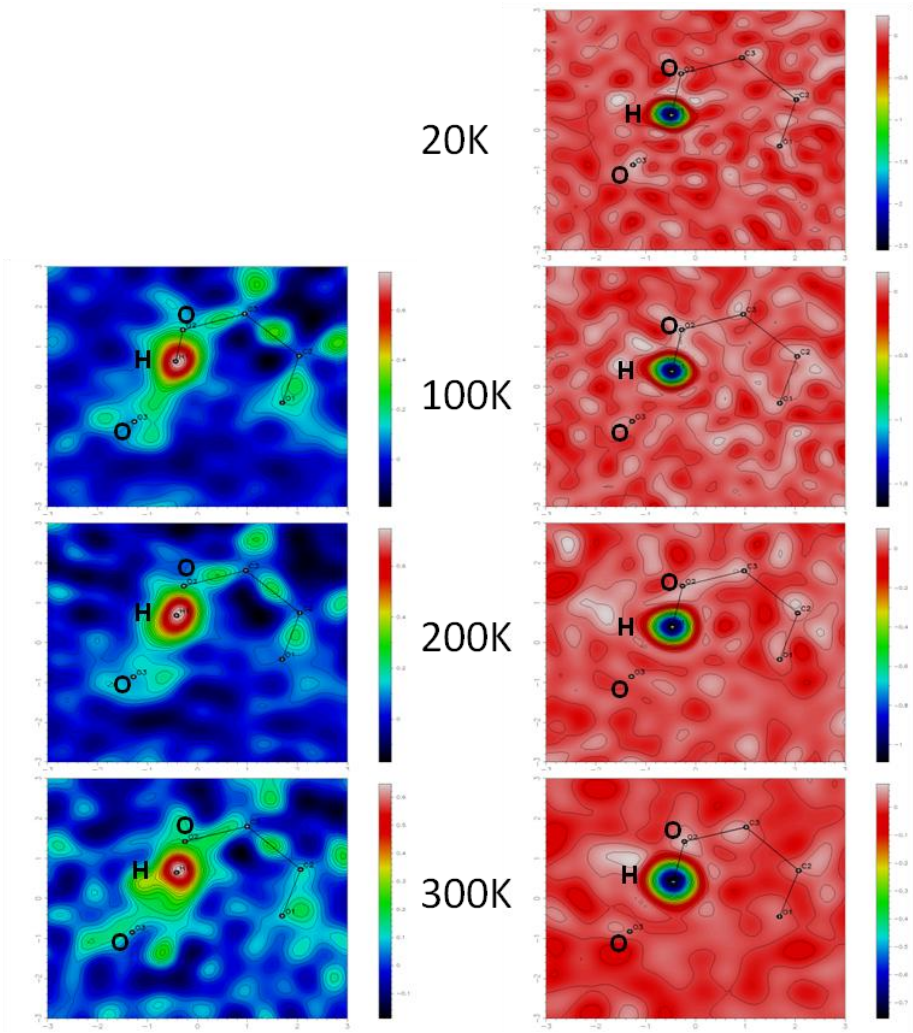

Figure 8.18 *Fourier difference maps of the short strong O-H···O hydrogen bond in the 2:1 complex of N,N-dimethylurea and BRA from the X-ray and neutron data.*

8.9 Conclusions

Seven complexes have been presented in this chapter, studied using a combination of X-ray and neutron diffraction. While these structures show an interesting variation of hydrogen bonding and crystal packing architectures, they do not show any significant temperature dependent behaviour. These results underline the conclusions drawn in earlier chapters with regards to short strong hydrogen bonds and the possible presence of a boundary length below which migration may occur. Three of the complexes in this chapter contain short, strong O-H···O hydrogen bonds, all of which are below, or close to, the suggested 2.50 Å boundary for the O···O separation, though there is little significant evidence of migration. These results further support the theory that whilst 2.50 Å is a sensible distance for the boundary, proton migration is by no means present in all hydrogen bonds below this boundary.

The complexes containing picolinic acid show how the contents of the crystal and the hydrogen bonded network can affect the proton positions. In native picolinic acid the acid proton is disordered over two sites within the molecule forming a zwitterion. The complexes presented here show the proton located either 100% on the acid or 100% on the pyridine nitrogen with no disorder evident; it is therefore evident that the component molecules affect the protonation state of the picolinic acid, further underlining the role played by the crystalline environment on the properties of the crystal structure.

The complexes containing haloanilic acids also showed a variation in the protonation states of the component molecules. In particular, the urea-BRA monohydrate complex showed transfer of three protons to the urea moieties within a very complex crystal structure. In the *N*,*N*-dimethylurea CLA monohydrate complex, a proton has been transferred from the CLA to the dimethylurea whilst proton transfer is not observed in the complex of *N*,*N*-dimethylurea and BRA. The presence of a water molecule in the complexes with CLA and BRA plays a role in determining a crystal packing and this may have an influence on whether proton transfer takes place.

Chapter 9

9. Conclusions and Future Work

9.1 Strong Hydrogen Bonds

One of the primary aims at the outset of this work was to produce molecular complexes that contain short, strong hydrogen bonds (SSHBs), within which the hydrogen atom undergoes temperature dependent proton migration. This objective was achieved, with proton migration confirmed in three new systems using neutron diffraction data, with strong evidence for proton migration observed in the X-ray diffraction data of two other complexes (presented in **Chapter 4**). The three systems in which proton migration is confirmed are a complex of *N*-methylurea and chloranilic acid (CLA), a complex of *N,N*-dimethylurea and oxalic acid and a complex of *N,N'*-dimethylurea and oxalic acid (**Table 9.1** and **Figure 9.1**).[167] The two complexes in which strong evidence is observed from the X-ray diffraction data (but for which no neutron diffraction data are available) are a complex of urea and bromanilic acid (BRA) and a complex of *N*-methylurea and BRA. Migration in the complex of *N*-methylurea and BRA can also be inferred due to the presence of migration in the isostructural *N*-methylurea-CLA complex.

Other systems containing SSHBs have been synthesised and characterised by diffraction techniques, in which there is no evidence of significant temperature dependent proton migration from neutron diffraction studies. In addition, several complexes containing SSHBs were synthesised and characterised only by X-ray diffraction, with no evidence to suggest the presence of proton migration. However, in the case of these complexes, variable temperature neutron diffraction studies would be required to confirm the absence of migration and it cannot be ruled out in this work.

Table 9.1 *Selected properties and experimental details of some of the urea-acid complexes presented in this work. A key is below the table.*

Acid Co-Molecule in Complex	Urea	*N*-Methylurea	N,N-Dimethylurea	N,N'-Dimethylurea
Succinic	No migration 2.5149(10) Å X, n -4.14	No migration 2.5340(11) Å X, n -4.43	No migration 2.5249(11) Å X, n -4.42	-
Fumaric	No migration 2.496(2) Å X, n -3.05	No migration 2.5291(12) Å X -3.34	No migration 2.5000(15) Å X, n -3.33	-
Oxalic	-	No migration 2.458(2) Å X -1.57	Migration 2.4398(15) Å X, n -1.56	Migration 2.4469(9) Å X, n -1.94
CLA	-	Migration 2.459(2) Å X, n -1.57	-	-
CLA Hydrate	-	-	No migration 2.4939(12) Å X -1.56	-
BRA	Migration 2.425(2) Å[a] X -1.24	Migration 2.455(3) Å X -1.53	No migration 2.4911(15) Å X, n -1.52	-
BRA Hydrate	No migration 2.474(3) Å X (100 K only) -1.24	-	-	-

[a] *X-ray structure determination at 110 K.*

Key for table cells (top to bottom of each cell) -	*Evidence of migration; shortest O-H···O hydrogen bond (from 100 K X-ray data unless stated); X-ray (X) or neutron (n) data collected (variable temperature unless stated); ΔpK_a value.*

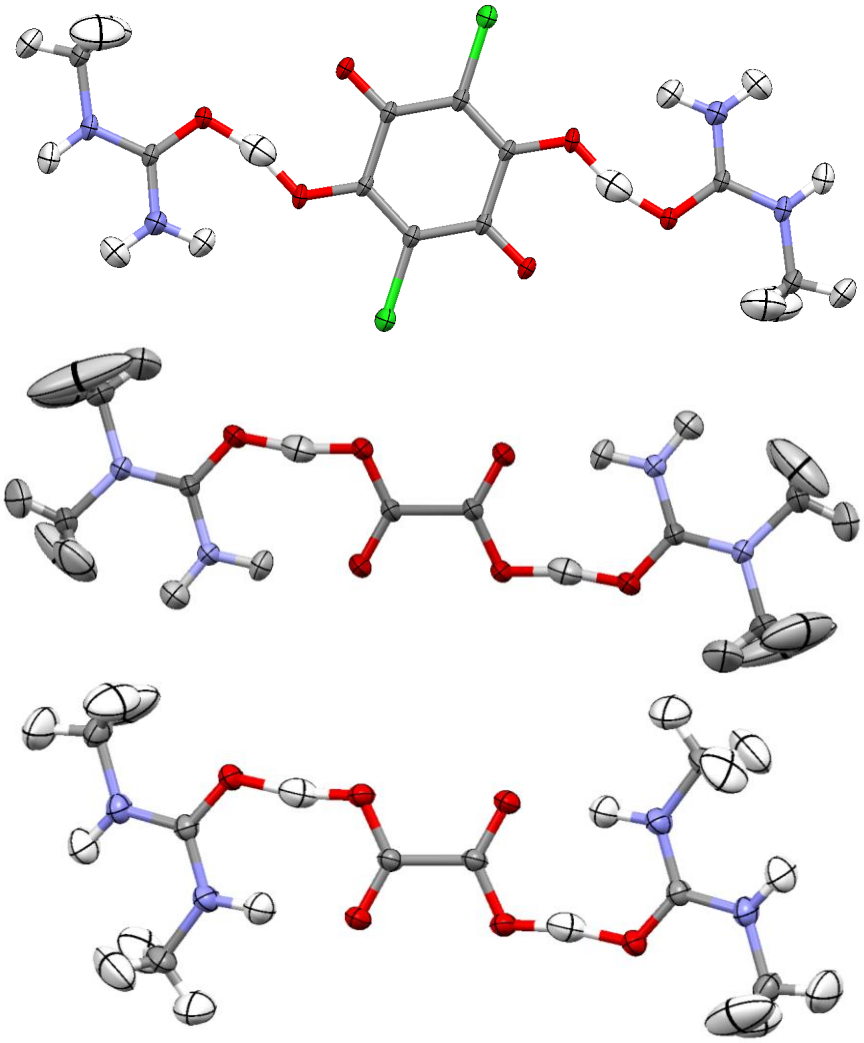

Figure 9.1 *The short, strong hydrogen bonds in which protons undergo temperature dependent proton migration from the neutron diffraction data, showing the hydrogen bonded units in the complexes of N-methylurea and CLA (top), N,N-dimethylurea and oxalic acid (middle) and N,N'-dimethylurea and oxalic acid (bottom).*

The key structural feature required for proton migration to take place is that a sufficiently short hydrogen bond must be formed within the complex. Based on the known examples of proton migration complexes, a D···A distance of <2.50 Å appears to be an appropriate threshold to postulate; it may be possible for temperature dependent proton migration to occur in O-H···O hydrogen bonds with a length below this threshold value. However, it may be the case that there are in fact two types of system in which proton migration can occur: those where the D···A distance increases with temperature (such as *N*-methylurea-CLA) and those where the D···A distance remains invariant as the temperature is varied (such as *N,N*-dimethylurea-oxalic acid). In urea-dicarboxylic acid complexes, migration is only observed in hydrogen bonds with a SSHB D···A distance below ~2.45 Å, whilst there is little evidence of migration in complexes with SSHB D···A distances above this, such as

in the complex of *N*-methylurea-oxalic acid (D···A = 2.458(2) Å at 100 K). In this type of migration system, 2.45 Å may then be a sensible threshold to postulate. In contrast, the urea-haloanilic acids have SSHB D···A distances which increase up to ~2.50 Å at higher temperatures, whilst migration is not observed in some complexes with D···A distances close to this potential boundary value (such as the complex of *N,N*-dimethylurea and BRA).

What does appear clear from the data presented in this work is that the shorter a hydrogen bond is, the more likely migration is to occur. Further examples studied using neutron diffraction are needed to support this hypothesis, however, and care should be taken when making use of this suggested boundary, as it is unlikely that migration is present in all O-H···O hydrogen bonds with a D···A distance below the suggested boundaries. Having such boundaries, however, enables a more targeted approach to the analysis of systems which may display proton migration. As neutron diffraction data is required to confirm the presence of migration, this targeting may mean that less, expensive neutron beam time is allocated to materials which are unlikely to display migration.

The magnitude of the migration of the proton within the SSHB is found to differ depending on the complex. This is of particular in interest in the case of the complexes of two isomers of dimethylurea with oxalic acid. These complexes differ only in the conformation of the urea component, and both complexes display different crystal packing motifs. The SSHB lengths in the two complexes are, however, similar. The differences in the magnitude of migration can therefore be considered as resulting from changes in the local environment and the weak interactions involving the molecular units in which migration is observed. The importance of these effects should not be underestimated, and if control of these interactions enables more accurate tuning of the charge transfer behaviour, these effects must be understood and accounted for. The results presented here are a starting point in this endeavour and further examples are needed to develop a better understanding of the relevant factors.

Theoretical data have also been presented in this work to complement the crystallographic data of the proton migration complexes. There was a degree of agreement between theory and experiment in some of the key features of the complexes studied. All of the theoretical data supported the presence of temperature dependent proton migration and also showed the same direction of migration of the proton (always towards the original donor atom). The theoretical potential energy surfaces (PESs) were

found to be broad, generally asymmetric, single wells as would be expected in such short hydrogen bonds. The PESs were also found to be temperature dependent, which could be a factor facilitating the observed migration in a similar manner to that found in the complex of urea and phosphoric acid.[68,69] The magnitude of the migration and the position of the hydrogen atom within the SSHB found in the theoretical models, however, were not in agreement with the experimental data. These differences show the difficulties in modelling subtle structural features, such as proton migration, with current methods. There are certain aspects of the simulations which could have been improved fairly easily, such as fixing unit cell parameters for each temperature to the experimental values. However, it is not clear why, for example, the hydrogen atom position within the SSHB, was not in agreement with the neutron data, and it seems unlikely that simply altering the unit cell parameters slightly would change this. In this work, it was not possible to analyse the theoretical phonon spectra, which may have given additional insight into the processes governing the proton migration. This is another area of investigation that could be pursued as part of the future work of this project to develop the current understanding of proton migration systems.

The synthesis of the proton migration complexes presented in this work has been achieved through rational design, utilising techniques based on simple crystal engineering principles. The main building block that has been used as the basis of the proton migration materials studied here is urea, which has been utilised based on its potential to form hydrogen bonds showing varying degrees of proton transfer across the hydrogen bond and its proven capability to form a proton migration complex when co-crystallised with phosphoric acid.[62,63] Methyl substituted ureas were also used in an effort to promote the formation of shorter hydrogen bonds which would favour proton migration. Both of these tactics proved successful, with complexes containing urea, *N*-methylurea and dimethylurea all displaying temperature dependent proton migration. The dimethylurea complexes with oxalic acid also contained SSHBs shorter than those observed in the urea and methylurea complexes with oxalic acid, proving the validity of the approach taken.[108,109,112]

Haloanilic acids have also shown their potential to form proton migration complexes with the urea and substituted urea compounds. These acids were chosen as a molecular component due to their strong proton donation properties and their known ability to form complexes with varying degrees of charge transfer across hydrogen bonds. The complex of urea with BRA produced the shortest hydrogen bond of any of the complexes presented in this work (O···O distance of 2.425(2) Å at 110 K). This SSHB was contained

within a complex crystal structure which also showed transfer of a proton to a urea molecule, showing the potential of these components to form interesting hydrogen bonded motifs. Complexes of CLA and BRA with *N*-methylurea displayed proton migration as well as the urea-BRA complex, further showcasing the design of materials showing proton migration from the simple rational design principles advanced above.

The results presented in this work have also shown that ΔpK_a values may be used as a guide when designing systems containing SSHBs and also potentially to predict the magnitude of migration within an SSHB. Despite the difficulties in applying pK_a values to solid-state molecular complexes, there is some, though limited, evidence to suggest that less negative ΔpK_a values may indicate that proton migration is more likely to occur within any SSHB formed as this would favour the formation of a complex which is intermediate between a salt and co-crystal, as found in many proton migration materials. There is also a correlation found between ΔpK_a values and the magnitude of migration in three migration complexes which have been studied extensively by neutron diffraction (urea-phosphoric acid from previous studies, *N,N*-dimethylurea-oxalic acid and *N,N'*-dimethylurea-oxalic acid from this work). These values should, however, only be used as a guide, as the SSHB length is not found to correlate directly with the ΔpK_a value.

Variable temperature methods and the imaging of hydrogen atom electronic and nuclear density within the SSHBs using Fourier difference maps are found to be key to the study of proton migration materials. These non-routine methods allow the migration to be observed clearly and, in the case of the Fourier difference maps, can show that the migration is not an artefact of large thermal displacement of the hydrogen atom. The work presented here shows that by applying these methods, it is possible to observe phenomena which would normally be missed in a typical X-ray structural determination conducted at one temperature, even if this is an accurate study.

9.2 Moderate Hydrogen Bonds

Moderate strength hydrogen bonds are the most common class of hydrogen bonds in the solid-state. However, they can also show interesting temperature dependent behaviour, similar to SSHBs, through proton disorder (see **Chapter 6**). The results presented in this work follow on from an X-ray characterisation of proton disorder in 3,5-dinitrobenzoic acid (3,5-DNBA) dimers in a molecular complex with 4-dimethylaminobenzoic acid (4-DABA).[16,76] Neutron diffraction data for this complex have been presented, along with structural analysis of the two polymorphs of 3,5-DNBA; one characterised by variable temperature X-ray diffraction (the $P2_1/c$ form), the other by variable temperature X-ray and

neutron diffraction (the *C*2/*c* form). Temperature dependent proton disorder was found in the 3,5-DNBA dimer in all three structures (**Figure 9.2**), allowing comparisons of the behaviour to be made which may aid in the understanding and deign of other proton disorder systems.

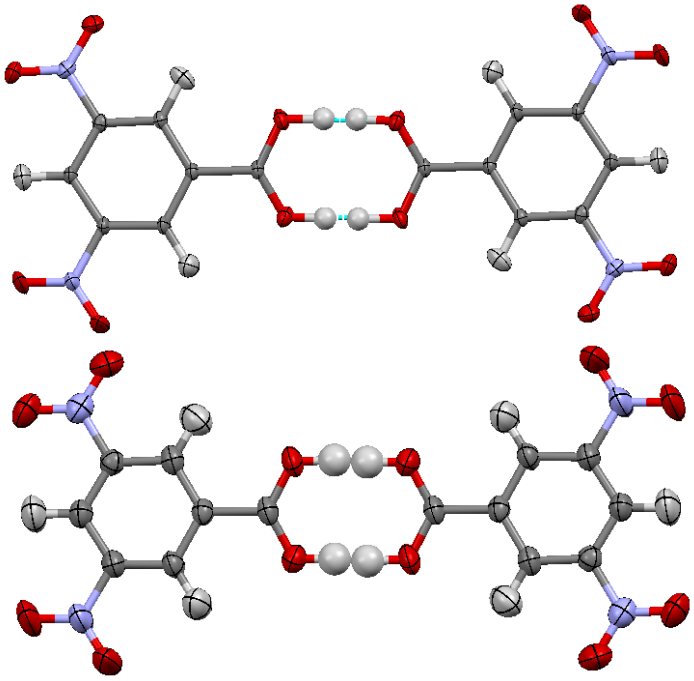

Figure 9.2 *Disordered dimers of 3,5-DNBA in the molecular complex with 4-DABA at 100 K and 250 K (top and bottom, respectively).*

The systematic investigation into 3,5-DNBA dimers in general has indicated that the local environment plays a role in the presence of disorder. The 3,5-DNBA dimers in the complex with 4-DABA are isolated and do not have weak interactions to the acid dimer, leading to the environment of the two potential hydrogen atom positions being symmetric. This could result in a much smaller energy difference between the two configurations corresponding to the two possible proton sites, hence resulting in proton disorder being observed even at the low temperature of 100 K. Analysis of the environment of the 3,5-DNBA dimers in the two polymorphs shows that, in this case, there are significant weak interactions to other acid dimers; this could account for the higher onset temperatures of the disorder (300 K in the $P2_1/c$ form and 250 K in the *C*2/*c* form) as the energy difference between the configurations corresponding to the two potential proton positions is increased.

These may help to explain the absence of disorder in the 4-DABA dimers of the binary complex. No disorder is present in the 4-DABA dimers from the neutron data, in

agreement with the previous X-ray study. As disorder had been observed in pure 4-DABA, the absence of disorder in the complex has previously been attributed to the increased pyramidalisation of the nitrogen atom due to close contacts with 3,5-DNBA nitro groups.[76] The increased pyramidalisation of the nitrogen atom was confirmed in the neutron data presented here; however, it is proposed here that the local environment also plays a role. The environment around the 4-DABA dimers in the binary complex with 3,5-DNBA showed asymmetric weak interactions to other molecules, potentially affecting the relative energies of the two configurations corresponding to the two possible proton positions, making these more unequal and causing one position to be favoured over the other and eliminating disorder.

The possible impact of the presence of weak interactions on proton disorder can be investigated further through comparisons with benzoic acid dimers from the literature. 4-DABA dimers in a ternary complex with 3,5-DNBA and 4,4'-bipyridine, show a low onset temperature (100 K) for proton disorder, with the dimers being fairly isolated with few interactions to surrounding molecules.[175] This supports the other findings in this work. Benzoic acid dimers also show a low onset temperature for disorder in the pure material (20 K).[77] The dimers are found to have weak interactions to surrounding molecules; however, in this case the interactions are symmetric across the hydrogen bond. This suggests the configurations corresponding to the two potential hydrogen atom positions would again be close in energy, supported by the low onset temperature observed for the disorder.

A CSD search of structures containing 3,5-DNBA dimers showed similar results to those already reported. When weak interactions to the acid groups in the dimers cause the environment to be asymmetric, disorder is either not present or only manifests at higher temperature, indicating a significant difference in the relative energies of the two hydrogen atom positions. However, if there are few weak interactions to the dimer, or the interactions are symmetric across the hydrogen bond, disorder is present at lower temperatures and the configurations corresponding to the two positions are closer in energy.

These findings on the temperature dependent properties of moderate strength hydrogen bonds which display proton disorder, support the conclusions drawn in the analysis of SSHBs, that the local environment around the hydrogen bond can have a significant effect on the behaviour of the hydrogen atom within it. This knowledge of how the weak interactions affect the proton behaviour means that if these interactions can be controlled

then so can the dynamic charge transfer properties of the hydrogen bond. For example, if it were possible to induce a symmetric environment around hydrogen bonds with the potential to display proton disorder, then proton disorder effects could effectively be "switched on", and *vice versa*. Therefore, studies such as those presented here, which further the understanding of these charge transfer processes, can aid in the design of future systems and help to make the most of these properties.

Variable temperature methods and imaging of the hydrogen atom electronic and nuclear density within the hydrogen bonds using Fourier difference maps are again shown to be vital to this type of study. The variable temperature data are necessary to observe the evolution of the hydrogen atom occupancy factors, while Fourier difference maps of the scattering density in the important regions representing the proton locations give clear indications of whether proton disorder is present from both the X-ray and neutron data. This study has also shown that high resolution X-ray data can be used to quantify the proton disorder within the moderate strength hydrogen bonds, showing good agreement with the neutron determined occupancy values. It should also be noted that at higher temperatures where larger thermal parameters can make the disorder more difficult to distinguish, X-ray diffraction data can offer a clearer image of the disorder than the neutron data in the Fourier difference maps. This is due to the bonding electronic density being observed in the X-ray data, which is pulled in towards the donor oxygen atom so there is a greater separation of the electron density peaks than the nuclear density peaks in the neutron Fourier difference maps. This is an example of the complementarity of the X-ray and neutron diffraction, showing that more insight can be gained from using the two techniques in tandem.

9.3 Weak Hydrogen Bonds

With weak interactions playing a significant role in the behaviour of hydrogen atoms undergoing dynamic charge transfer effects such as proton migration and proton disorder, the ability to understand and control these weak interactions becomes of great importance. Complexes of the proton sponge, 1,8-bis(dimethylamino)napthalene (DMAN), with organic acids provide a robust structural framework where the lengths of the weak interactions can be tuned and comparisons made to develop understanding of these weak interactions (see **Chapter 7**).

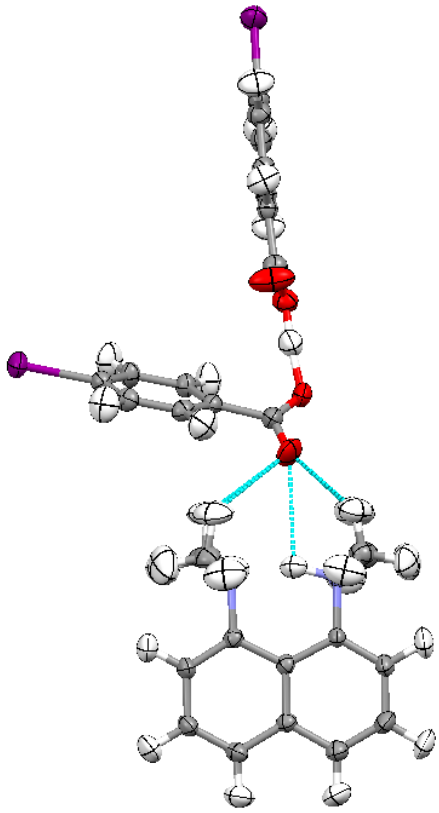

Figure 9.3 *A $DMANH^+$ molecule and a 4-IBA dimer containing a short, strong charge-assisted hydrogen bond.*

All of the DMAN complexes presented in this work had previously been studied by single crystal X-ray diffraction.[125] The structures show the transfer of a proton to DMAN, forming an intramolecular N-H···N SSHB, with an acid oxygen located above this hydrogen bond (**Figure 9.3**). This oxygen atom interacts with the methyl group hydrogen atoms of $DMANH^+$, and also with the hydrogen atom within the intramolecular N-H···N hydrogen bond. By analysing neutron diffraction data of these structures, insight can be gained into any correlation between the behaviour of the acid oxygen atom and the hydrogen atom within the N-H···N hydrogen bond.

Five DMAN complexes have been studied by neutron diffraction allowing analysis of the hydrogen atom anisotropic displacement parameters, with a correlation found between the thermal displacement of the acid oxygen atom and the hydrogen atom in the N-H···N hydrogen bond in the complex of DMAN with 2-fluorobenzoic acid. In this complex the distance between the oxygen and hydrogen is the shortest of the studied complexes, and the principal direction of thermal displacement of the oxygen atom is in the direction of the N-H···N hydrogen bond. In the other complexes, where the O···H separations are larger, there is no obvious correlation between the behaviour of the two atoms. This suggests

that at O···H distances above ~2.67 Å, the effect of the oxygen on the hydrogen atom thermal behaviour may no longer be significant. The fact that the principal direction of thermal displacement of the oxygen atoms in these complexes is not along the direction of the N-H···N hydrogen bond may also play a role.

The hydrogen atom position within the intramolecular N-H···N hydrogen bond formed on the protonation of DMAN was often found to be asymmetric. The acid oxygen atom located above the N-H···N hydrogen bond is not centred, and may play a role in determining the hydrogen atom position with the $DMANH^+$ molecule. Weak interactions to each of the fused rings of DMAN were also found to be asymmetric and could also affect the hydrogen atom position within the N-H···N hydrogen bond.

In the structures of the DMAN-halobenzoic acid complexes, the acid molecules were found to form $ACID^-$ dimers involving one protonated and one deprotonated halobenzoic acid molecule linked by a charge-assisted O-H···O SSHB. The position of the hydrogen atom within these SSHBs was also found to be affected by asymmetric weak interactions to the molecules in the $ACID^-$ dimer. The hydrogen atoms were not centred within the charge-assisted SSHBs. In two of the DMAN complexes (with 2-fluorobenzoic acid and 4-iodobenzoic acid), the hydrogen atom was located closer to the acid molecule which does not interact directly with the $DMANH^+$, suggesting the weak interactions with $DMANH^+$ assist in stabilising the charge on the acid molecule closest to the $DMANH^+$. In the complex with 2-iodobenzoic acid, where the acid molecule above the $DMANH^+$ is located further away than in the other two complexes, the hydrogen atom in the charge-assisted SSHB is found to be closer to the acid molecule directly above the $DMANH^+$. This would suggest that, as the distance has increased, the interactions to the $DMANH^+$ no longer have the same stabilisation effect, and this affects the hydrogen position within the charge-assisted SSHB.

The study of this set of DMAN-acid complexes again shows the importance weaker interactions can have on structural properties when analysed in detail. It also provides a potential length range over which an electronegative atom may significantly affect the behaviour of a hydrogen atom within a hydrogen bond. As in the case of the investigations into the properties of strong and moderate strength hydrogen bonds, further examples are needed to test these findings. However, these first results show that the effect of weaker interactions should not be underestimated.

9.4 Crystal Engineering of Urea-Acid Complexes

The urea (and methyl substituted urea) complexes with organic acids presented in this work have not only shown their potential to form SSHBs displaying temperature dependent behaviour, but also that robust and reproducible structural motifs can be formed in which varying degrees of proton transfer may occur between the acid and urea moieties (see **Chapter 4** and **Chapter 5**).

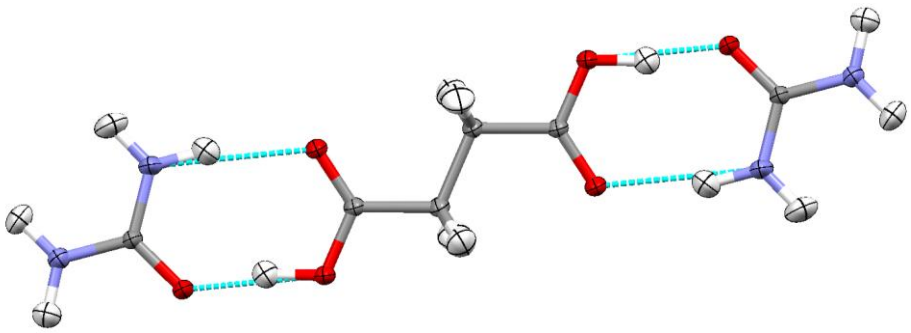

Figure 9.4 *A "U-A-U" hydrogen bonded unit in the complex of urea and succinic acid. This motif is observed in the structures of all urea-dicarboxylic acid complexes presented in this work.*

The complexes of ureas with dicarboxylic acids all formed in a 2:1 (urea:acid) ratio, and all formed acid···amide heterodimers with a urea-acid-urea (U-A-U) motif (**Figure 9.4**). Amide···amide homodimers are also formed in urea- and *N*-methylurea-dicarboxylic acid complexes, with the acid···amide heterodimer motif formed preferentially while the presence of the methyl groups in dimethylurea-dicarboxylic acid complexes means that both hetero- and homodimer motifs cannot form in the same system. This shows the robustness of this structural motif, which is to be expected, with the best proton donor hydrogen bonding to the best proton acceptor.[37]

Whilst the formation of the acid···amide heterodimer may be expected, the similarity in the overall crystal structures of the urea and substituted urea complexes with succinic and fumaric acid is unexpected; the complexes show one-dimensional chains of hydrogen bonded units in two orientations. This is particularly unexpected in the case of the complex of *N,N*-dimethylurea-succinic acid, where the presence of the urea methyl groups may be expected to perturb the packing motif. On the other hand, the complex of *N,N*-dimethylurea and fumaric acid showed a packing motif different to that of the *N,N*-dimethylurea-succinic acid complex, and it is not apparent why this is the case. Other structural motifs, such as layered structures in the complexes of *N*-methylurea-oxalic acid and *N,N'*-dimethylurea-oxalic acid, have also been observed, further showing

the flexibility of packing motifs that may be found containing the “U-A-U” units found in these crystal structures.

The complexes of haloanilic acids with urea also show acid···urea interactions as the primary hydrogen bonded motifs, though a wide variety of packing motifs is found. Proton transfer between the acid and urea moieties is also observed in some cases within complex crystal structures, such as those of the 2:1 urea-BRA complex and 7:4 urea-BRA monohydrate, where a water molecule replaces a urea molecule and the structures have some similar properties. Whilst these packing motifs are not as predictable as those of the urea-dicarboxylic acid complexes, they do display many interesting features (such as proton migration), and the unpredictable and complex structures are interesting in their own right.

9.5 Variable Temperature Measurements

The routine application of variable temperature measurements in this work has proved an important component of the study of the evolution of the structures studied. When investigating dynamic charge transfer processes such as proton migration and proton disorder, variable temperature measurements are vital to establish the presence of the phenomena and to analyse their temperature dependence. Variable temperature measurements have also revealed interesting thermal expansion behaviour in some complexes which do not display disorder or migration, related to a shift in the molecular units on changing the temperature, and also a phase transition in the complex of *N,N*-dimethylurea and oxalic acid. If the structural characterisation of this complex had only been carried out at 100 K, as is common, then the different structure at higher temperatures would not have been observed. This shows that greater insight into the properties of these materials can be gained through such non-routine measurements, and though variable temperature measurements take more time, the rewards more than balance this out.

9.6 Complementarity of X-ray and Neutron Diffraction

Throughout this work X-ray and neutron diffraction have been used in tandem to characterise a large number of organic molecular complexes. Each technique gives access to different structural information, and utilising the two techniques together enables a greater understanding of the systems under study. With regards to hydrogen atoms, X-ray diffraction gives information of the electron density, which is normally drawn into covalent bonds, while the nuclear density will be located further from the donor atoms. This can be important, such as in systems displaying proton disorder, where it may be

easier to resolve the two positions from the X-ray data in spite of the inherent difficulties in locating hydrogen atoms with this technique. In addition, the electronic and nuclear density do not always follow the same behavioural trend, as the nuclear positions and electron density associated with the hydrogen bond may evolve slightly differently. Dynamic effects, such as proton migration and proton disorder, require neutron diffraction studies for the effects to be quantified accurately. However, X-ray studies also play a key role in the identification of potential systems for study using neutron diffraction. With neutron diffraction being a difficult and expensive technique, the full exploitation of the potential of laboratory based X-ray diffraction techniques in initial studies of a system is essential as a precursor to applying for time at a neutron facility.

9.7 High Throughput Neutron Diffraction

Many of the results presented in this work have been obtained from high throughput neutron diffraction experiments made possible by the availability of VIVALDI and the neutron Laue technique. The rapid data collections that are possible with the high throughput capabilities have been utilised in two ways:

- To collect multiple temperature data sets of a given complex quickly during one experiment, e.g. for the proton migration and proton disorder systems, and;
- To collect data on many samples quickly during one experimental allocation period, e.g. for the DMAN-acid complexes.

These experiments have shown that it is possible to collect neutron diffraction data within a similar time scale to X-ray diffraction data. The vast majority of data sets were collected in under a day, with the most rapid data collection taking less than two hours per temperature, with 10 minute exposures for collection of an image plate frame. In this experiment, it was actually the time taken to change the sample temperature which became the limiting step, in terms of speed of data collection, and not the required exposure time.

Processing neutron Laue data remains a difficult task, and the high demands on sample quality means that the approach may not be suitable for all systems. However, the data presented here show that, in favourable circumstances, the neutron Laue technique is a powerful method which enables not only rapid data collection, but also small samples ($<1mm^3$) to be utilised. This is an important feature of the technique, as the growth of large, high quality single crystals of a material is often challenging.

9.8 Future Work

The common theme running through much of this work is the importance of weak interactions, and the role they can play in altering the behaviour of hydrogen atoms within strong and moderate hydrogen bonds; this work represents only a starting point in the understanding of these effects.

In the case of proton migration materials, one of the key issues is that there are still very few examples known and extensively characterised. This work shows that it is possible for such systems to be designed utilising crystal engineering principles and potentially by consideration of ΔpK_a values, and the next step would be to synthesise more of these materials. Neutron diffraction studies would be required to quantify the results experimentally, while there is also scope to develop the understanding of the processes further through theoretical studies. The theoretical data presented in this work show that there is currently some disagreement between experiment and theory, and finding a computational modelling technique that mimics experiment more accurately is desirable. In this work, it was not possible to analyse the theoretical phonon spectra of the materials studied, and this would be a sensible next step, whilst this goal could also be achieved through inelastic neutron scattering studies. Finding a common process by which migration occurs in all of the known materials would be an important step in furthering the understanding of how to make use of such systems. Accurately quantifying the effects of weak interactions in the local environment around the SSHBs would also be desirable, in order that their influence on the migration process may be understood better. However, current computational techniques do not allow this to be carried out in an accurate and efficient manner, and further development of the technique is required.

Proton disorder systems also suffer from the problem of there currently being few known examples of materials in which the effect has been well studied. This is no doubt partly due to potential disorder being missed during structural characterisation; analysis of bond lengths within carboxylic acid groups of benzoic acid dimers (e.g. C-O, C=O and O-H) would provide a relatively simple route to identifying systems in which potential proton disorder was either not noticed or not deemed worthy of comment in more routine determinations. This could be carried out alongside the synthesis of new materials which may display proton disorder, so that a greater number of systems may be characterised. Understanding the effects of weak interactions to the acid dimers is important and theoretical studies could again play a role in this. These studies may also provide access to the PESs (to quantify the differences in energy of the configurations corresponding to

the two potential hydrogen atom sites) and theoretical phonon spectra of disordered systems, to further the understanding the underlying processes.

As part of future investigations into how weak interactions affect the behaviour of hydrogen atoms within hydrogen bonds, further analysis could also be conducted of the DMAN-acid systems. Only a small number of these have been studied by neutron diffraction, and further studies of similar complexes would allow a wider range of weaker interactions, and their effects, to be analysed. Several other systems have already been characterised using X-ray diffraction and could, in the future, be characterised by neutron diffraction, while there is also scope to synthesise new DMAN-acid complexes.

10. References

(1) Pauling, L. *The Nature of the Chemical Bond*; Cornell University Press: New York, 1960.

(2) Jeffrey, G. A. *An Introduction to Hydrogen Bonding*; Oxford University Press: New York, 1997.

(3) Arunan, E.; Desiraju, G. R.; Klein, R. A.; Sadlej, J.; Scheiner, S.; Alkorta, I.; Clary, D. C.; Crabtree, R. H.; Dannenberg, J. J.; Hobza, P.; Kjaergaard, H. G.; Legon, A. C.; Mennucci, B.; Nesbitt, D. J. *Pure Appl. Chem.* **2011**, *83*, 1637.

(4) Desiraju, G. R. *Angew. Chem. Int. Ed.* **2011**, *50*, 52.

(5) McNaught, A. D.; Wilkinson, A. *IUPAC Compendium of Chemical Terminology, 2nd ed. (the "Gold Book")*; Blackwell Scientific Publications: Oxford, 1997.

(6) Perrin, C. L. *Acc. Chem. Res.* **2010**, *43*, 1550.

(7) Gilli, P.; Bertolasi, V.; Ferretti, V.; Gilli, G. *J. Am. Chem. Soc.* **1994**, *116*, 909.

(8) Wilson, C. C. *Single Crystal Neutron Diffraction from Molecular Materials*; World Scientific: Singapore, 2000.

(9) Ward, M. D. *Chem. Commun.* **2005**, 5838.

(10) Fillaux, F.; Leygue, N.; Tomkinson, J.; Cousson, A.; Paulus, W. *Chem. Phys. Lett.* **1999**, *244*, 387.

(11) Wilson, C. C.; Thomas, L. H.; Morrison, C. A. *Chem. Phys. Lett.* **2003**, *381*, 102.

(12) Fleck, M.; Bohaty, L. *Z. Naturforsch., B: Chem. Sci.* **2009**, *64*, 517.

(13) Gilli, G.; Gilli, P. *J. Mol. Struct.* **2000**, *552*, 1.

(14) Desiraju, G. R. *Acc. Chem. Res.* **2002**, *35*, 565.

(15) Desiraju, G. R. *Acc. Chem. Res.* **1991**, *24*, 290.

(16) Sharma, C. V. K.; Panneerselvam, K.; Pilati, T.; Desirajui, G. R. J. *J. Chem. Soc., Perkin Trans. 2* **1993**, 2209.

(17) Meyer, M.; Brandl, M.; Sühnel, J. *J. Phys. Chem. A* **2001**, *105*, 8223.

(18) Adam, M. S.; Parkin, A.; Thomas, L. H.; Wilson, C. C. *CrystEngComm* **2010**, *12*, 917.

(19) Metrangolo, P.; Meyer, F.; Pilati, T.; Resnati, G.; Terraneo, G. *Angew. Chem. Int. Ed.* **2008**, *47*, 6114.

(20) Walsh, R. B.; Padgett, C. W.; Metrangolo, P.; Resnati, G.; Hanks, T. W.; Pennington, W. T. *Cryst. Growth Des.* **2001**, *1*, 165.

(21) Metrangolo, P.; Resnati, G. *Science* **2008**, *321*, 918.

(22) Desiraju, G. R.; Parthasarathy, R. *J. Am. Chem. Soc.* **1989**, *111*, 8725.

(23) Hunter, C. A.; Sanders, J. K. M. *J. Am. Chem. Soc.* **1990**, *112*, 5525.

(24) Dougherty, D. A. *Science* **1996**, *271*, 163.

(25) Gallivan, J. P.; Dougherty, D. A. *Proc. Natl. Acad. Sci. USA* **1999**, *96*, 9459.
(26) Braga, D. *Chem. Commun.* **2003**, 2751.
(27) Desiraju, G. R. *Angew. Chem. Int. Ed.* **2007**, *46*, 8342.
(28) Aakeröy, C. B.; Champness, N. R.; Janiak, C. *CrystEngComm* **2010**, *12*, 22.
(29) Desiraju, G. R. *CrystEngComm* **2003**, *5*, 466.
(30) Dunitz, J. D. *CrystEngComm* **2003**, *5*, 506.
(31) Bond, A. D. *CrystEngComm* **2007**, *9*, 833.
(32) Parkin, A.; Gilmore, C. J.; Wilson, C. C. *Z. Kristallogr.* **2008**, *223*, 430.
(33) Desiraju, G. R. *Angew. Chem. Int. Ed.* **1995**, *34*, 2311.
(34) Allen, F. H. *Acta Crystallogr.* **2002**, *B58*, 380.
(35) Desiraju, G. R. *Chem. Commun.* **2005**, 2995.
(36) Nishio, M. *CrystEngComm* **2004**, *6*, 130.
(37) Etter, M. C. *Acc. Chem. Res.* **1990**, *23*, 120.
(38) Aakeröy, C. B.; Salmon, D. J. *CrystEngComm* **2005**, *7*, 439.
(39) Feld, R.; Lehmann, M. S.; Muir, K. W.; Speakman, J. C. *Z. Kristallogr.* **1981**, *157*, 215.
(40) Glidewell, C.; Ferguson, G.; Gregson, R. M.; Lough, A. J. *Acta Crystallogr.* **1999**, *C55*, 2133.
(41) Aakeröy, C. B.; Beatty, A. M.; Helfrich, B. A. *J. Am. Chem. Soc.* **2002**, *124*, 14425.
(42) Fleischman, S. G.; Kuduva, S. S.; McMahon, J. A.; Moulton, B.; Bailey Walsh, R. D.; Rodríguez-Hornedo, N.; Zaworotko, M. J. *Cryst. Growth Des.* **2003**, *3*, 909.
(43) Chae, H. K.; Siberio-Perez, D. Y.; Kim, J.; Go, Y.; Eddaoudi, M.; Matzger, A. J.; O'Keeffe, M.; Yaghi, O. M. *Nature* **2004**, *427*, 523.
(44) Rowsell, J. L. C.; Yaghi, O. M. *Angew. Chem. Int. Ed.* **2005**, *44*, 4670.
(45) Millward, A. R.; Yaghi, O. M. *J. Am. Chem. Soc.* **2005**, *127*, 17998.
(46) Li, J.-R.; Kuppler, R. J.; Zhou, H.-C. *Chem. Soc. Rev.* **2009**, *38*, 1477.
(47) Lee, J.; Farha, O. K.; Roberts, J.; Scheidt, K. A.; Nguyen, S. T.; Hupp, J. T. *Chem. Soc. Rev.* **2009**, *38*, 1450.
(48) Moulton, B.; Zaworotko, M. J. *Chem. Rev.* **2001**, *101*, 1629.
(49) Brittain, H. G. *J. Pharm. Sci.* **2007**, *96*, 705.
(50) - -
Hornedo, N. r. *Adv. Drug Deliv. Rev.* **2004**, *56*, 241.
(51) Vishweshwar, P.; McMahon, J. A.; Bis, J. A.; Zaworotko, M. J. *J. Pharm. Sci.* **2006**, *95*, 499.
(52) Beckmann, W. *Org. Proc. Res. Dev.* **2000**, *4*, 372.
(53) Trask, A. V.; Motherwell, W. D. S.; Jones, W. *Chem. Commun.* **2004**, 890.

(54) Bauer, J.; Spanton, S.; Henry, R.; Quick, J.; Dziki, W.; Porter, W.; Morris, J. *Pharm. Res.* **2001**, *18*, 859.

(55) Zundel, G. *Adv. Chem. Phys.* **2000**, *111*, 1.

(56) Childs, S. L.; Stahly, G. P.; Park, A. *Mol. Pharm.* **2007**, *4*, 323.

(57) Huang, K.-S.; Britton, D.; late Margaret C. Etter, t.; Byrn, S. R. *J. Mater. Chem.* **1997**, *7*, 713.

(58) Bhogala, B. R.; Basavoju, S.; Nangia, A. *CrystEngComm* **2005**, *7*, 551.

(59) Schmidtmann, M.; Wilson, C. C. *CrystEngComm* **2008**, *10*, 177.

(60) Steiner, T.; Majerz, I.; Wilson, C. C. *Angew. Chem. Int. Ed.* **2001**, *40*, 2651.

(61) Martins, D. M. S.; Middlemiss, D. S.; Pulham, C. R.; Wilson, C. C.; Weller, M. T.; Henry, P. F.; Shankland, N.; Shankland, K.; Marshall, W. G.; Ibberson, R. M.; Knight, K.; Moggach, S.; Brunelli, M.; Morrison, C. A. *J. Am. Chem. Soc.* **2009**, *131*, 3884.

(62) Wilson, C. C. *Acta Crystallogr.* **2001**, *B57*, 435.

(63) Wilson, C. C.; Shankland, K.; Shankland, N. *Z. Kristallogr.* **2001**, *216*, 303.

(64) Cowan, J. A.; Howard, J. A. K.; McIntyre, G. J.; Lo, S. M. F.; Williams, I. D. *Acta Crystallogr.* **2003**, *B59*, 794.

(65) Cowan, J. A.; Howard, J. A. K.; McIntyre, G. J.; Lo, S. M. F.; Williams, I. D. *Acta Crystallogr.* **2005**, *B61*, 724.

(66) Parkin, A.; Harte, S. M.; Goeta, A. E.; Wilson, C. C. *New J. Chem.* **2004**, *28*, 718.

(67) Wilson, C. C.; Morrison, C. A. *Chem. Phys. Lett.* **2002**, *362*, 85.

(68) Morrison, C. A.; Siddick, M. M.; Camp, P. J.; Wilson, C. C. *J. Am. Chem. Soc.* **2005**, *127*, 4042.

(69) Fontaine-Vive, F.; Johnson, M. R.; Kearley, G. J.; Howard, J. A. K.; Parker, S. F. *J. Am. Chem. Soc.* **2006**, *128*.

(70) Kostansek, E. C.; Busing, W. R. *Acta Crystallogr.* **1972**, *B28*, 2454.

(71) Sundera-Rao, R. V. G.; Turley, J. W.; Pepinsky, R. *Acta Crystallogr.* **1957**, *10*, 435.

(72) Wolfram, W.; Artunian, E. G.; Antishkina, A. S.; Porai-Koshits, M. A. *Bull. Acad. Polonaise Sci. Ser. Sci. Chim.* **1967**, *15*, 83.

(73) Harkema, S.; Unpublished work, presented in ISIS Annual Report 1993, p. 18. Rutherford Appleton Laboratory Report RAL-93-050, Oxfordshire, England., 1993.

(74) Ilczyszyn, M. M.; Ratajczak, H.; Barnes, A. J. *J. Raman. Spec.* **1992**, *23*, 1.

(75) Ford, S. J.; Delamore, O. J.; Evans, J. S. O.; McIntyre, G. J.; Johnson, M. R.; Radosavljević Evans, I. *Chem. Eur. J.* **2011**, *17*, 14942.

(76) Parkin, A.; Seaton, C. C.; Blagden, N.; Wilson, C. C. *Cryst. Growth Des.* **2007**, *7*, 531.
(77) Wilson, C. C.; Shankland, N.; Florence, A. J. *Chem. Phys. Lett.* **1996**, *253*, 103.
(78) Sim, G. A.; Robertson, J. M.; Goodwin, T. H. *Acta Crystallogr.* **1955**, *8*, 157.
(79) Bruno, G.; Randaccio, L. *Acta Crystallogr.* **1980**, *B36*, 1711.
(80) Wilson, C. C.; Shankland, N.; Florence, A. J. *J. Chem. Soc., Faraday Trans.* **1996**, *92*, 5051.
(81) Cai, W.; Katrusiak, A. *CrystEngComm* **2012**, *14*, 4420.
(82) Neumann, M.; Brougham, D. F.; McGloin, C. J.; Johnson, M. R.; Horsewill, A. J.; Trommsdorff, H. P. *J. Chem. Phys.* **1998**, *109*, 7300.
(83) Brougham, D. F.; Horsewill, A. J.; Trommsdorff, H. P. *Chem. Phys.* **1999**, *243*, 189.
(84) Fillaux, F.; Limage, M. H.; Romain, F. *Chem. Phys.* **2002**, *276*, 181.
(85) Jenkinson, R. I.; Ikram, A.; Horsewill, A. J.; Trommsdorff, H. P. *Chem. Phys.* **2003**, *294*, 95.
(86) Wu, W.; Noble, D. L.; Owers-Bradley, J. R.; Horsewill, A. J. *J. Mag. Res.* **2005**, *175*, 210.
(87) Fillaux, F.; Romain, F.; Limage, M.-H.; Leygue, N. *Phys. Chem. Chem. Phys.* **2006**, *8*, 4327.
(88) Plazanet, M.; Fukushima, N.; Johnson, M. R.; Horsewill, A. J.; Trommsdorff, H. P. *J. Chem. Phys.* **2001**, *115*, 3241.
(89) Johnson, M. R.; Trommsdorff, H. P. *Chem. Phys. Lett.* **2002**, *364*, 34.
(90) Smedarchina, Z.; Fernandez-Ramos, A.; Siebrand, W. *J. Chem. Phys.* **2005**, *122*, 134309.
(91) Middlemiss, D. S.; Facchini, M.; Morrison, C. A.; Wilson, C. C. *CrystEngComm* **2007**, *9*, 777.
(92) Kanters, J. A.; Roelofsen, G.; Kroon, J. *Nature* **1975**, *257*, 625.
(93) Fischer, P.; Zolliker, P.; Meier, B. H.; Ernst, R. R.; Hewat, A. W.; Jorgensen, J. D.; Rotella, F. J. *J. Solid State Chem.* **1986**, *61*, 109.
(94) Destro, R. *Chem. Phys. Lett.* **1991**, *181*, 232.
(95) Wilson, C. C.; Goeta, A. E. *Angew. Chem. Int. Ed.* **2004**, *43*, 2095.
(96) Wilson, C. C.; Xu, X.; Florence, A. J.; Shankland, N. *New J. Chem.* **2006**, *30*, 979.
(97) Moré, R.; Scholz, M.; Busse, G.; Busse, L.; Paulmann, C.; Tolkiehn, M.; Techert, S. *Phys. Chem. Chem. Phys.* **2012**, *14*, 10187.
(98) Adam, M. S.; Gutmann, M. J.; Leech, C. K.; Middlemiss, D. S.; Parkin, A.; Thomas, L. H.; Wilson, C. C. *New J. Chem.* **2010**, *34*, 85.

(99) Vaughan, P.; Donohue, J. *Acta Crystallogr.* **1952**, *5*, 530.
(100) Videnova-Adrabinska, V. *J. Mol. Struct.* **1996**, *374*, 199.
(101) Videnova-Adrabinska, V. *Acta Crystallogr.* **1996**, *B52*, 1048.
(102) Smith, G.; Kennard, C. H. L.; Byriel, K. A. *Aust. J. Chem.* **1997**, *50*, 1021.
(103) Thaimattam, R.; Shekhar Reddy, D.; Xue, F.; C. W. Mak, T.; Nangia, A.; R. Desiraju, G. *J. Chem. Soc., Perkin Trans. 2* **1998**, 1783.
(104) Custelcean, R. *Chem. Commun.* **2008**, 295.
(105) Alhalaweh, A.; George, S.; Boström, D.; Velaga, S. P. *Cryst. Growth Des.* **2010**, *10*, 4847.
(106) Worsham, J. E., Jnr; Busing, W. R. *Acta Crystallogr.* **1969**, *B25*, 572.
(107) Nelyubina, Y. V.; Lyssenko, K. A.; Golovanov, D. G.; Antipin, M. Y. *CrystEngComm* **2007**, *9*, 991.
(108) Harkema, S.; ter Brake, J. H. M.; Helmholdt, R. B. *Acta Crystallogr.* **1984**, *C40*, 1733.
(109) van Hummel, G. J.; Helmholdt, R. B. *Acta Crystallogr.* **1991**, *C47*, 213.
(110) Sklar, N.; Senko, M. E.; Post, B. *Acta Crystallogr.* **1961**, *14*, 716.
(111) Bryden, J. *Acta Crystallogr.* **1957**, *10*, 714.
(112) Harkema, S.; Ter Brake, J. H. M.; Meutstege, H. J. G. *Acta Crystallogr.* **1979**, *B35*, 2087.
(113) Huiszoon, C.; Tiemessen, G. W. M. *Acta Crystallogr.* **1976**, *B32*, 1604.
(114) Pathirana, H. M. K. K.; Weiss, T. J.; Reibenspies, J. H.; Zingaro, R. A.; Meyers, E. A. *Z. Kristallogr.* **1994**, *209*, 696.
(115) Perez-Folch, J.; Subirana, J. A.; Aymami, J. *J. Chem. Cryst.* **1997**, *27*, 367.
(116) Fairlie, D. P.; Woon, T. C.; Wickramasinghe, W. A.; Willis, A. C. *Inorg. Chem.* **1994**, *33*, 6425.
(117) Marsh, R. *Acta Crystallogr.* **2004**, *B60*, 252.
(118) Harris, K. D. M. *Chem. Soc. Rev.* **1997**, *26*, 279.
(119) Alder, R. W.; Bowman, P. S.; Steele, W. R. S.; Winterman, D. R. *Chem. Commun. (London)* **1968**, 723.
(120) Staab, H. A.; Saupe, T. *Angew. Chem. Int. Ed.* **1988**, *27*, 865.
(121) Kazheva, O.; Shilov, G.; Dyachenko, O.; Mehh, M.; Sorokin, V.; Ozeryanskii, V.; Pozharskii, A. F. *Russ. Chem. Bull.* **2005**, *54*, 2492.
(122) Pozharskii, A. F. *Russ. Chem. Rev.* **1998**, *67*, 1.
(123) Mallinson, P. R.; Smith, G. T.; Wilson, C. C.; Grech, E.; Wozniak, K. *J. Am. Chem. Soc.* **2003**, *125*, 4259.
(124) Parkin, A.; Wozniak, K.; Wilson, C. C. *Cryst. Growth Des.* **2007**, *7*, 1393.

(125) Kállay, A. A. *An X-ray and neutron diffraction investigation into engineering hydrogen bonding interactions in molecular complexes.*; PhD Thesis, University of Glasgow, 2012.
(126) Röntgen, W. C. *Nature* **1896**, *53*, 274.
(127) Sherwood, D. *Crystals X-rays and Proteins*; Longman Group Limited, 1976.
(128) Bragg, W. H.; Bragg, W. L. *Proc. Royal Soc. Lon. A* **1913**, *88*, 428.
(129) Dickinson, R. G.; Raymond, A. L. *J. Am. Chem. Soc.* **1923**, *45*, 22.
(130) Oszlányi, G.; Süto, A. *Acta Crystallogr.* **2004**, *A60*, 134.
(131) Oszlányi, G.; Süto, A. *Acta Crystallogr.* **2005**, *A61*, 147.
(132) Nonius Kappa-CCD Four Circle Diffractometer: Nonius BV, Delft, The Netherlands, http://www.nonius.nl/products/sms/kappa/.
(133) CRYSTALCLEAR, Rigaku Corporation, Tokyo, Japan.
(134) COLLECT, Nonius BV, Delft, The Netherlands.
(135) Otwinowski, Z.; Minor, W. *Macromolecular Crystallography. Part A. Methods in Enzymology*; New York: Academic Press, 1997; Vol. 276.
(136) SADABS, Bruker AXS Inc., Madison, Wisconsin, USA. 2001.
(137) Higashi, T. ABSCOR. Rigaku Corporation, Tokyo, Japan. 1995.
(138) Sheldrick, G. M. *Acta Crystallogr.* **2008**, *A64*, 112.
(139) Spek, A. L. *J. Appl. Cryst.* **2003**, *28*, 659.
(140) Farrugia, L. J. *J. Appl. Cryst.* **1999**, *32*, 837.
(141) Macrae, C. F.; Edgington, P. R.; McCabe, P.; Pidcock, E.; Shields, G. P.; Taylor, R.; Towler, M.; van de Streek, J. *J. Appl. Cryst.* **2006**, *39*, 453.
(142) Bruker D8 Powder Diffractometer, Bruker AXS Inc., Madison, Wisconsin, USA. http://www.bruker-axs.com/d8_advance.html.
(143) Keen, D. A.; Gutmann, M. J.; Wilson, C. C. *J. Appl. Cryst.* **2006**, *39*, 714.
(144) http://www.isis.stfc.ac.uk/.
(145) http://www.ansto.gov.au/research/bragg_institute/facilites/instruments/koala.
(146) http://www.ansto.gov.au/research/bragg_institute.
(147) McIntyre, G. J.; Lemée-Cailleau, M.-H.; Wilkinson, C. *Physica B* **2006**, *385-386*, 1055.
(148) http://www.ill.eu.
(149) D19A and B: design and construction of a 4-circle neutron diffractometer with two-dimensional PSDs; Thomas, M.; Stansfield, R. F. D.; Benerom, M.; Filhol, A.; Greenwood, G. *Position-sensitive detection of thermal neutrons*; Academic Press, 1983.
(150) http://neutrons.ornl.gov/facilities/SNS/.

(151) http://www.epn-campus.eu.

(152) Helliwell, J. R.; Habash, J.; Cruickshank, D. W.; Harding, M. M.; Greenhough, T. J.; Campbell, J. W.; Clifton, I. W.; Elder, M.; Machin, P. A.; Papiz, M. Z.; Zurek, S. *J. Appl. Cryst.* **1989**, *22*, 483.

(153) Cipriani, F.; Castagna, J. C.; Wilkinson, C.; Oleinik, P.; Lehmann, M. S. *J. Neutron Res.* **1996**, *4*, 79.

(154) Campbell, J. W.; Hao, Q.; Harding, M. M.; Nguti, N. D.; Wilkinson, C. *J. Appl. Cryst.* **1998**, *31*, 496.

(155) Wilkinson, C.; Khamis, H. W.; Stansfield, R. F. D.; McIntyre, G. J. *J. Appl. Cryst.* **1988**, *21*, 471.

(156) Campbell, J. W.; Habash, J.; Helliwell, J. R.; Moffat, K. *Daresbury Inf. Quart. Protein Crystallogr.* **1986**, *18*, 23.

(157) Piltz, R. O. *Acta Crystallogr.* **2011**, *A67*, C155.

(158) Lehmann, M. S.; Larsen, F. K. *Acta Crystallogr.* **1974**, *A30*, 580.

(159) LADIABS - A program to calculate attenuation factors and mean path lengths for reflections in Laue patterns from faceted crystal. Unpublished.

(160) Coppens, P.; Leiserowitz, L.; Rabinovich, D. *Acta Crystallogr.* **1965**, *18*, 1035.

(161) Howard, J. A. K.; Johnson, O.; Schultz, A. J.; Stringer, A. M. *J. Appl. Cryst.* **1987**, *20*, 120.

(162) Rodríguez-Carvajal, J. *Physica B* **1993**, *192*, 55.

(163) Larson, A. *Acta Crystallogr.* **1967**, *23*, 664.

(164) http://www.hector.ac.uk.

(165) VandeVondele, J.; Krack, M.; Mohamed, F.; Parrinello, M.; Chassaing, T.; Hutter, J. *Comp. Phys. Commun.* **2005**, *167*, 103.

(166) http://www.cp2k.org.

(167) Jones, A. O. F.; Lemée-Cailleau, M.-H.; Martins, D. M. S.; McIntyre, G. J.; Oswald, I. D. H.; Pulham, C. R.; Spanswick, C. K.; Thomas, L. H.; Wilson, C. C. *Phys. Chem. Chem. Phys.* **2012**, *DOI: 10.1039/C2CP41782K*.

(168) Molcanov, K.; Kojic-Prodic, B. *CrystEngComm* **2010**, *12*, 925.

(169) Horiuchi, S.; Kumai, R.; Tokura, Y. *J. Am. Chem. Soc.* **2005**, *127*, 5010.

(170) Gotoh, K.; Asaji, T.; Ishida, H. *Acta Crystallogr.* **2008**, *C64*, o550.

(171) Wilson, C. C. *Chem. Phys. Lett.* **2001**, *335*, 57.

(172) Wiedenfeld, H.; Knoch, F. *Acta Crystallogr.* **1990**, *C46*, 1038.

(173) Cruz-Cabeza, A. J.; Day, G. M.; Jones, W. *Chem. Eur. J.* **2008**, *14*, 8830.

(174) Aakeröy, C. B.; Desper, J.; Levin, B. *Acta Crystallogr.* **2005**, *C61*, o702.

(175) Thomas, L. H.; Blagden, N.; Gutmann, M. J.; Kallay, A. A.; Parkin, A.; Seaton, C. C.; Wilson, C. C. *Cryst. Growth Des.* **2010**, *10*, 2770.

(176) Aakeröy, C. B.; Desper, J.; Helfrich, B. A. *CrystEngComm* **2004**, *6*, 19.

(177) Aakeröy, C. B.; Beatty, A. M.; Helfrich, B. A. *Angew. Chem. Int. Ed.* **2001**, *40*, 3240.

(178) Aakeröy, C. B.; Schultheiss, N.; Desper, J.; Moore, C. *New J. Chem.* **2006**, *30*, 1452.

(179) Sharma, C. V. K.; Panneerselvam, K.; Pilati, T.; Desiraju, G. R. *J. Chem. Soc., Chem. Commun.* **1992**, 832.

(180) Kanters, J. A.; Kroon, J.; Hooft, R.; Schouten, A.; Schijndel, J. A. M. v.; Brandsen, J. *Croat. Chem. Acta* **1991**, *64*, 353.

(181) Prince, P.; Fronczek, F. R.; Gandour, R. D. *Acta Crystallogr.* **1991**, *C47*, 895.

(182) Colapietro, M.; Domenicano, A.; Marciante, C.; Portalone, G. *Eur. Cryst. Meeting* **1983**, *8*, 124.

(183) Domenicano, A.; Schultz, G.; Hargittai, I.; Colapietro, M.; Portalone, G.; George, P.; Bock, C. W. *Struct. Chem.* **1989**, *1*, 107.

(184) Paulini, R.; Müller, K.; Deiderich, F. *Angew. Chem. Int. Ed.* **2005**, *44*, 1788.

(185) Hosomi, H.; Ohba, S.; Ito, Y. *Acta Crystallogr.* **2000**, *C56*, e144.

(186) Ermer, O.; Neudörfl, A. *Helv. Chim. Acta.* **2001**, *84*, 1268.

(187) Lynch, D. E.; Smith, G.; Byriel, K. A.; Kennard, C. H. L. *Aust. J. Chem.* **1991**, *44*, 809.

(188) Ding, X.; Wang, S.; He, W.; Huang, W. *Acta Crystallogr.* **2011**, *E67*, o2833.

(189) Smith, G.; Wermuth, U. D.; Young, D. J.; White, J. M., , *Acta Crystallogr.* **2009**, *C65*, o543.

(190) Pedireddi, V. R.; Jones, W.; Chorlton, A. P.; Docherty, R. *Chem. Commun.* **1996**, 987.

(191) Miller, W.; Smith, C.; Mackenzie, D.; Evans, K. *J. Mater. Sci.* **2009**, *44*, 5441.

(192) Horbatenko, Y.; Vyboishchikov, S. F. *ChemPhysChem* **2011**, *12*, 1118.

(193) Hamazaki, H.; Hosomi, H.; Takeda, S.; Kataoka, H.; Ohba, S. *Acta Crystallogr.* **1998**, *C54*.